

**INSIGHTS INTO ELEMENTAL SULFUR METABOLISM AND
LOW-ENERGY ADAPTATIONS IN *CHLOROBACULUM TEPIDUM*
TO ENABLE BIOTECHNOLOGY-BASED PROCESSES
FOR WASTE SULFUR UTILIZATION**

by

Amalie Tuerk Levy

A dissertation submitted to the Faculty of the University of Delaware in partial fulfillment of the requirements for the degree of Doctor of Philosophy in Chemical Engineering

Fall 2016

© 2016 Amalie Tuerk Levy
All Rights Reserved

**INSIGHTS INTO ELEMENTAL SULFUR METABOLISM AND
LOW-ENERGY ADAPTATIONS IN *CHLOROBACULUM TEPIDUM*
TO ENABLE BIOTECHNOLOGY-BASED PROCESSES
FOR WASTE SULFUR UTILIZATION**

by

Amalie Tuerk Levy

Approved:

Abraham M. Lenhoff, Ph.D.
Chair of the Department of Chemical and Biomolecular Engineering

Approved:

Babatunde A. Ogunnaike, Ph.D.
Dean of the College of Engineering

Approved:

Ann L. Ardis, Ph.D.
Senior Vice Provost for Graduate and Professional Education

I certify that I have read this dissertation and that in my opinion it meets the academic and professional standard required by the University as a dissertation for the degree of Doctor of Philosophy.

Signed:

Kelvin H. Lee, Ph.D.
Professor in charge of dissertation

I certify that I have read this dissertation and that in my opinion it meets the academic and professional standard required by the University as a dissertation for the degree of Doctor of Philosophy.

Signed:

Wilfred Chen, Ph.D.
Member of dissertation committee

I certify that I have read this dissertation and that in my opinion it meets the academic and professional standard required by the University as a dissertation for the degree of Doctor of Philosophy.

Signed:

Thomas E. Hanson, Ph.D.
Member of dissertation committee

I certify that I have read this dissertation and that in my opinion it meets the academic and professional standard required by the University as a dissertation for the degree of Doctor of Philosophy.

Signed:

April Kloxin, Ph.D.
Member of dissertation committee

I certify that I have read this dissertation and that in my opinion it meets the academic and professional standard required by the University as a dissertation for the degree of Doctor of Philosophy.

Signed:

Eleftherios T. Papoutsakis, Ph.D.
Member of dissertation committee

ACKNOWLEDGMENTS

First I would like to thank my advisor Kelvin Lee for his guidance and support through my doctoral research. He both championed and challenged me, and I fully appreciated his encouragement to chart my own path through my dissertation research. I have greatly benefitted from his advice on all aspects of my graduate trajectory, from detailed technical discussions to career planning, as well as his ability to bring me back from the occasional brink of experimental or career-decision-making despair. I have fully enjoyed the stimulating and caring atmosphere that he has cultivated in his lab group, and I am so grateful for the opportunity to have worked in the Lee research group.

I also want to thank Thomas Hanson for his counsel and mentoring through my doctoral research, and for introducing me to the weird and fascinating bacterium *Chlorobaculum tepidum*. While not his official advisee, I still felt fully embedded in the Hanson research group and greatly benefitted from our weekly meetings to discuss my research progress; I hope I have absorbed at least a fraction of his wealth of knowledge. I am indebted to him for pulling me back out of research rabbit holes, providing invaluable career guidance, and teaching me how to take research failures in stride and with a sense of humor.

I am very grateful to the members of my dissertation committee, Wilfred Chen, April Kloxin, and Eleftherios Papoutsakis, for their insightful suggestions and thoughtful mentorship through my doctoral research. My research benefitted from

their probing questions, and their advice on topics ranging from journal selection to effective time management enhanced my professional development.

I am grateful to the National Science Foundation (grants GRFP-0750966, MCB-1244373, and EPS-0814251), Delaware INBRE (NIGMS grant P20 GM103446), and the University of Delaware Research Fund for providing the funds that enabled my doctoral research.

I gratefully acknowledge research and experimental assistance from many individuals; without their help this work would not have been possible. Leila Choe performed protein identifications by mass spectrometry analysis, and provided invaluable advice on all aspects of preparing samples for proteomic analysis along with Kristin Valente. Cassandra Marnocha provided training on and assistance with light and electron microscopy, and shared images and data from her own work that were essential to the interpretation of my own data. I am grateful to Clara Chan for the use of light microscopes, the Firesting oxygen meter, and other equipment in her laboratory. Deborah Powell and Chandran Sabanayagam provided assistance with scanning electron microscopy and energy dispersive X-ray spectroscopy. Casey Smith executed the culturing experiments that investigated the oxygen tolerance of *Chlorobaculum tepidum* and generated purified S⁰ from *C. tepidum*, helping to improve the purification procedure for S⁰. I received advice on various experimental techniques from Lie Min, Leila Choe, Kristin Valente, Benjamin Kremkow, Jennifer Mantle, Jongyoun Baik, Katie Kalis, Jennifer Hiras, Jacob Hilzinger, Brian Eddie, and Kevin Shuman. Madolyn MacDonald provided bioinformatics assistance in organizing and minimizing duplication in the *Chlorobaculum tepidum* protein database used for protein identifications. Amino acid analyses were performed by the Molecular

Structure Facility at the University of Davis. I am also incredibly thankful for the staff members at both the Delaware Biotechnology Institute and the Department of Chemical and Biomolecular Engineering; their assistance with items ranging from class scheduling to room reservations to equipment upkeep was absolutely essential to my graduate career and successful completion of my doctoral work.

I am incredibly fortunate to have worked in the company of many talented researchers in both the Lee and Hanson research groups. I have learned so much from their diverse research endeavors and creative approaches to problem solving, and my professional development was furthered by their valuable feedback on my abstracts, manuscripts, and presentations over the years. My work also benefitted from their excellent questions during group meeting and their technical advice. Equally important are the friendships I have formed with my labmates, and I have many cherished memories from ‘Hoho’ discussions, last minute dessert contest preparations, potluck picnics, conversation and companionship during hours of labwork, and ‘therapeutic’ lunches out on Main Street. I gratefully acknowledge current and former members of the Lee research group, Jongyoun Baik, Sansheng Chen, Josephine Chiu, Leila Choe, Michael Gallucci, Jing Guo, Stephanie Hammond, Shuyu Hou, Benjamin Kremkow, Madolyn MacDonald, Jennifer Mantle, Lie Min, John Ruano-Salguero, Jeff Swanberg, Kristin Valente, Diane Wuest, and Xiaolin Zhang, and current and former members of the Hanson Research group, Alexa Bennett, Brian Eddie, Jacob Hilzinger, Jennifer Hiras, Katie Kalis, Karen Rossmassler, and Kevin Shuman.

I am so thankful for the companionship of the graduate students in the Department of Chemical and Biomolecular Engineering; my graduate school experience was enriched by the ability to decompress with so many talented and fun

individuals over long bike rides with the ‘Riders of CHEG’, runs around the campus with the ‘Legs of CHEG’, trips to the Delaware beaches, hiking adventures, wine and painting nights, rides on SEPTA, and happy hour beers. I am also grateful for the love and support of my friends from my life ‘outside’ graduate school, who were tolerant and understanding of my odd schedule and (at times) infrequent contact; these friendships provided perspective and balance, as well as invaluable advice, during the times I needed it most.

Finally, I want to express my extreme gratitude to my family for their tireless patience, support, and love, both through my time at the University of Delaware and throughout my life. I am thankful to my crazy pup Abita for forcing me to take breaks from dissertation writing, and for the joy she brings me. I am truly blessed to have had Terrence and Anne Tuerk as my parents, who taught me the value of hard work and perseverance, and who gave me confidence to pursue my dreams. My sister Elissa Tuerk is a wealth of sound advice, a creative inspiration, and cherished friend, and provided essential support during some of the rougher periods of graduate school. My extended family - grandparents, aunts, uncles, and cousins - have been incredible role models for me through out my life, and my in-laws Peter and Rosemary Levy and my sister-in-law Julia Levy are the most supportive family I could have hoped to marry into. And finally, I am so thankful for the love and support of my husband, Nick Levy, whose unfailing confidence in me and countless nights of cooked dinners propelled me to the finish line, and whose love has enriched my life in ways I couldn’t have imagined.

TABLE OF CONTENTS

LIST OF TABLES	xvi
LIST OF FIGURES	xix
ABSTRACT	xxiii

Chapter

1	INTRODUCTION	1
1.1	Project Motivation: Challenges of Sulfur Contamination and Sulfur Management Facing Industry	1
1.2	Project Background	6
1.2.1	The biogeochemical sulfur cycle	6
1.2.2	Metabolic strategies of microbial sulfur oxidation	6
1.2.3	S ⁰ globule production and degradation are poorly understood	8
1.2.4	<i>Chlorobaculum tepidum</i> provides a model system for studying S ⁰ production and degradation	9
1.3	Project Aims and Scope of Work	14
1.3.1	Aim 1: Control and characterize the <i>Chlorobaculum tepidum</i> system	15
1.3.2	Aim 2: Identify proteins associated with <i>Chlorobaculum tepidum</i> S ⁰	16
	REFERENCES	18
2	<i>CHLOROBACULUM TEPIDUM</i> MODULATES AMINO ACID COMPOSITION IN RESPONSE TO ENERGY AVAILABILITY, AS REVEALED BY A SYSTEMATIC EXPLORATION OF THE ENERGY LANDSCAPE OF PHOTOTROPHIC SULFUR OXIDATION	27
2.1	Preface	27
2.1.1	Abstract	27
2.1.2	Importance	28

2.2	Introduction	28
2.3	Materials and Methods	32
2.3.1	Experimental design	32
2.3.2	Bacterial strains and growth conditions	35
2.3.3	Culture media	36
2.3.4	Quantification of sulfur compounds and acetate	36
2.3.5	Protein and bacteriochlorophyll <i>c</i> determinations	37
2.3.6	Amino acid analysis (AAA)	37
2.3.7	Microscopy and cell volume measurements.....	39
2.3.8	Cellular carbohydrate analysis	39
2.3.9	Statistical analysis	40
2.4	Results	41
2.4.1	Calibration of indirect protein assays provides accurate prediction of absolute biomass protein concentration	41
2.4.2	Comparisons of WH and EX protein measurements suggest characteristics of the internal metabolite pools of <i>C. tepidum</i>	45
2.4.3	<i>C. tepidum</i> cell size variations across the energy landscape are associated with the production of storage carbohydrates	48
2.4.4	<i>C. tepidum</i> amino acid composition varies across the energy landscape	51
2.4.5	Light flux affects biomass amino acid composition according to amino acid biosynthetic cost	54
2.5	Discussion.....	59
2.5.1	Prior extraction of biomass samples improves accuracy of indirect protein assays	59
2.5.2	Extractable pools inferred from protein analyses	59
2.5.3	<i>C. tepidum</i> cell size changes suggest the formation of storage compounds.....	61
2.5.4	Amino acid composition changes induced by energy landscape parameters suggest biosynthetic streamlining at low energy can be observed with bulk measurements	62
2.6	Concluding remarks.....	65
2.7	Acknowledgments	66
	REFERENCES	67
3	ANALYSIS OF <i>CHLOROBACULUM TEPIDUM</i> SULFUR METABOLISM BY A FACTORIAL APPROACH	75

3.1	Preface	75
3.1.1	Abstract.....	75
3.1.2	Importance.....	77
3.2	Introduction	78
3.3	Materials and Methods	80
3.3.1	Bacterial strains and growth conditions	80
3.3.2	Culture media	80
3.3.3	Quantification of sulfur compounds and acetate	81
3.3.4	Protein and bacteriochlorophyll <i>c</i> determinations	82
3.3.5	Cellular carbohydrate analysis	82
3.3.6	Experimental design and statistical analysis	82
3.3.7	Yield calculations	84
3.4	Results and Discussion	85
3.4.1	<i>C. tepidum</i> growth yield on an electron equivalent basis was highest with sulfide and lowest with thiosulfate as electron donor.....	85
3.4.1.1	Comparison of measured <i>C. tepidum</i> growth yields to values reported in the literature	90
3.4.1.2	Differential growth yields on sulfide, S ⁰ , and thiosulfate provide evidence that electrons from oxidation of S ⁰ do not enter the membrane-bound electron transport chain	92
3.4.1.3	Current state of knowledge on electron transport from oxidation of sulfur compounds in <i>C. tepidum</i>	97
3.4.1.3.1	Electron fate for oxidation of sulfide to S ⁰ ..	97
3.4.1.3.2	Electron fate for oxidation of S ⁰ to sulfite..	98
3.4.1.3.3	Electron fate for oxidation of sulfite to sulfate	99
3.4.1.3.4	Electron fate for oxidation of thiosulfate to S ⁰ and sulfate	99
3.4.2	Growth yield on acetate increased with increasing light flux but was reduced for growth on sulfide relative to growth on S ⁰ or thiosulfate.....	99
3.4.3	Discrepancies in the sulfur mass balance suggest intracellular storage of sulfur compounds by <i>C. tepidum</i>	103

3.4.4	Polysulfides accumulate extracellularly during early phases of sulfide oxidation and S ⁰ globule formation	107
3.4.5	During S ⁰ oxidation at low light, production of sulfate lagged behind S ⁰ oxidation.....	112
3.4.6	Polysulfides as dissolved intermediates involved in S ⁰ globule production and dissolution at a distance.....	114
3.4.7	Lack of thiosulfate oxidation at low light raises interesting questions about regulation of photosynthetic electron transport under stress conditions	117
3.5	Concluding Remarks	123
	REFERENCES	126
4	PROTEINS ASSOCIATED WITH <i>CHLOROBACULUM TEPIDUM</i> S ⁰ PROVIDE INSIGHT INTO MECHANISMS OF S ⁰ GENERATION	130
4.1	Preface	130
4.1.1	Abstract.....	130
4.1.2	Importance.....	132
4.2	Introduction	132
4.3	Materials and Methods	138
4.3.1	Strains and growth conditions	138
4.3.2	Light microscopy.....	138
4.3.3	Cryo-scanning electron microscopy and energy-dispersive x-ray spectroscopy	139
4.3.4	Generation of S ⁰ by repeated sulfide feeding and S ⁰ purification	139
4.3.5	Generation of S ⁰ by single sulfide feeding and S ⁰ purification ..	142
4.3.6	Protein measurements of <i>C. tepidum</i> cells and purified S ⁰	143
4.3.7	Extraction of S ⁰ -associated proteins for examination by one-dimensional sodium dodecyl sulfate polyacrylamide gel electrophoresis (SDS-PAGE)	143
4.3.8	One-dimensional SDS-PAGE	144
4.3.9	Protein identification from gels	145
4.3.10	Extraction of proteins from S ⁰ for shotgun proteomics.....	145
4.3.11	Sample pre-treatment and digestion for shotgun proteomics	146
4.3.12	LC and MALDI-TOF/TOF MS.....	147
4.3.13	Protein sequence analysis	148
4.4	Results and Discussion	150

4.4.1	S ⁰ globules are formed at the cell periphery and likely contain lipids	150
4.4.2	Proteins from purified S ⁰ appear to constitute an enriched subset of the <i>C. tepidum</i> proteome	157
4.4.3	Differentiation of proteins weakly and strongly associated with S ⁰	162
4.4.4	The protein profile of S ⁰ from wild type <i>C. tepidum</i> WT2321 exhibits subtle differences from that of S ⁰ from mutant strain C3	167
4.4.5	Development of methods for shotgun proteomic profiling of S ⁰ from <i>C. tepidum</i>	175
4.4.6	Shotgun proteomic exploration of WT S ⁰ identified proteins consistent with the protein profiles of outer membrane vesicles from gram negative bacteria	183
4.4.6.1	Commonalities between S ⁰ globule proteome and OMVs include cell envelope spanning transport complexes and cell division machinery	194
4.4.6.2	S ⁰ globule proteins not typically found in OMVs are involved in energy-dependent ion transport	202
4.4.6.3	S ⁰ biogenesis: originating from locally-energized sites of OM-IM connectivity?	206
4.4.6.4	S ⁰ proteins homologous to three periplasmic chaperones suggest the possibility that that S ⁰ production may be related to the σ^E envelope stress response	208
4.4.7	CT1305 and CT1320.1 are two proteins identified only in association with S ⁰ produced by strain C3	213
4.5	Concluding Remarks	220
	REFERENCES	222
5	CONCLUSIONS AND RECOMMENDATIONS FOR FUTURE WORK ..	231
5.1	Conclusions	231
5.2	Recommendations for Future Work	234
5.2.1	Investigate biased amino acid composition as a mechanism for energy conservation under light- and energy-limited conditions.	234
5.2.2	Identify constituents of intracellular sulfur pools and their dynamics	235

5.2.3	Protein expression differences between S ⁰ -attached and S ⁰ -unattached cells during S ⁰ production and degradation	236
5.2.4	Probing the roles of S ⁰ -associated proteins in S ⁰ production, degradation, and cell-S ⁰ attachment by mutagenesis studies	237

REFERENCES	241
------------------	-----

Appendix

A	REPRINT PERMISSIONS	243
B	COMPARISON OF ROTISSERIE OVEN AND STIRRED WATER BATH CULTURE.....	250
B.1	Results	250
B.2	Discussion.....	251
B.3	Methods	252
	References	254
C	DETAILS OF CALCULATIONS FOR CHAPTER 2.....	255
C.1	Calculating prediction accuracy of protein assays	255
C.2	Identifying amino acids depleted by methanol extraction.....	256
	References	257
D	<i>CHLOROBACULUM TEPIDUM</i> OXYGEN TOLERANCE STUDIES.....	258
D.1	Results and Discussion	258
D.1.1	Evidence for trace oxygen contamination as a root cause of culture failure.....	258
D.1.2	<i>C. tepidum</i> can recover from dissolved oxygen concentrations of approximately 10 µM.....	261
D.1.3	<i>C. tepidum</i> cells remove oxygen in light-dependent manner	264
D.2	Methods	267
D.2.1	Bacterial strains, growth conditions, and culture media.....	267
D.2.2	Oxygen measurements.....	268
D.2.3	Measurements of culture protein and thiosulfate	269
	References	270

E	LIST OF ALL PROTEIN IDENTIFICATIONS FROM GEL-BASED STUDIES OF S ⁰	271
F	SHOTGUN PROTEOMIC IDENTIFICATIONS FROM <i>C. TEPIDUM</i> S ⁰ ..	278
G	HOMOLOGS OF S ⁰ PROTEINS FOUND IN PROTEOMIC STUDIES OF OUTER MEMBRANE VESICLES	283

LIST OF TABLES

Table 2.1	Details of the of the 3×3 factorial design composing the energy landscape of phototrophic sulfur oxidation, including how treatments were distributed among the different culturing blocks.....	33
Table 2.2	Observed technical variation in protein-based assays for biomass determination.....	38
Table 2.3	Accuracy of Bradford and BCA (indirect) protein assay measurements in predicting protein determined by amino acid analysis (direct quantitation).....	43
Table 2.4	Changed abundance of amino acids in <i>C. tepidum</i> biomass did not contribute equally to the observed changes in $\sim P_{avg}$	56
Table 2.5	Effect of excluding individual amino acids from the calculation of $\sim P_{avg}$ on the light-effect parameter B_1 in the relationship between $\sim P_{avg}$ and light.	56
Table 3.1	Number of biological replicates for each treatment combination in the energy landscape experimental design.	83
Table 3.2	Significance of energy landscape parameter effects on <i>C. tepidum</i> growth yield based on Y_{eq} oxidized ($Yield_{eq-OxP}$) and parameter estimates used in Eq. 3.12 to calculate the yield values displayed in Fig. 3.1-B.....	87
Table 3.3	Previously reported yields for growth of <i>C. tepidum</i> on single electron donors and acetate and CO ₂ as carbon source.	91
Table 3.4	Summary of the electron fate from oxidation of sulfide, S ⁰ , and thiosulfate based on known electron transport pathways in <i>C. tepidum</i> .	94
Table 3.5	Breakdown of the experimentally observed <i>C. tepidum</i> growth yields into the Baseline (Y_B), membrane-bound electron transport-associated (Y_{MB}), and ‘Unknown’ (Y_U) components (see Fig. 3.2, Eq. 3.13, and Eq. 3.14).	96

Table 3.6	Significance of energy landscape effects on <i>C. tepidum</i> growth yield on acetate (Yield _{Acetate}) and parameter estimates used in Eq. 3.15 to calculate the yield values displayed in Fig. 3.3-B.	100
Table 4.1	List of S ⁰ batches used in Chapter 4 studies and details of their preparation.	140
Table 4.2	Elemental composition of <i>C. tepidum</i> S ⁰ as measured by SEM-EDX. .	154
Table 4.3	List of the proteins identified in Laemmli Tris-HCl SDS-PAGE gel comparing protein profiles of S ⁰ and <i>C. tepidum</i> (Fig. 4.4).	159
Table 4.4	Sequential treatments of S ⁰ to distinguish proteins that weakly and strongly associate with S ⁰	163
Table 4.5	List of proteins identified in bands from the Tris-Tricine SDS-PAGE gel shown in Figure 4.5 that are unique to SHD and AAP S ⁰ extracts.	165
Table 4.6	Sequential treatments of S ⁰ to distinguish proteins weakly and strongly associated with S ⁰	169
Table 4.7	List of protein identifications from bands with differences between S ⁰ produced by wildtype <i>C. tepidum</i> and S ⁰ produced by <i>C. tepidum</i> mutant strain C3, and additional proteins unique to S ⁰	172
Table 4.8	Formulations of buffers used in screening of shotgun-compatible extraction approaches for protein extraction from <i>C. tepidum</i> S ⁰	177
Table 4.9	List of proteins identified by shotgun proteomic analysis of S ⁰ from wild type <i>C. tepidum</i>	185
Table 4.10	Functional classification of proteins associated with S ⁰ based on COG categories, and portion of proteins within COG categories with homologs previously identified in proteomic studies of outer membrane vesicles.	193
Table 4.11	List of outer membrane vesicle proteomic studies included in the compilation of OMV proteins against which the <i>C. tepidum</i> S ⁰ protein identifications were compared.....	194
Table 4.12	Proteins identified in association with S ⁰ as well as in previous proteomic studies of OMVs that suggest involvement of outer membrane-inner membrane connectivity and cell envelope stress response in S ⁰ biogenesis.	195

Table 4.13	Results of a BLASTP search using CT1320.1 as the query sequence against the UniProt knowledge base (www.uniprot.org). Only homologs with an e-value < 1E-10 were considered significant. A version of this table originally appeared as Supplemental Table 1 in Hanson et al. 2016.	217
Table 5.1	List of high-priority S ⁰ -associated proteins for characterization by mutagenesis studies.	238
Table A.1	License agreement for Chapter 4.....	249
Table B.1	Measured growth rates for <i>C. tepidum</i> during exponential growth in each culturing system while oxidizing S ⁰ or thiosulfate.	250
Table E.1	List of all protein identifications from gel based studies of purified S ⁰ from <i>C. tepidum</i>	273
Table F.1	Shotgun proteomic protein identifications from wildtype <i>C. tepidum</i> S ⁰ , organized by number of total matched peptides per protein.....	278
Table G.1	List of S ⁰ proteins where homologs were found in proteomic studies of outer membrane vesicles	284
Table G.2	List of S ⁰ proteins with no homologs in OMV proteomes.	299

LIST OF FIGURES

Figure 2.1	Schematic of the ‘Energy Landscape’ of phototrophic sulfur oxidation.....	32
Figure 2.2	Calibration of indirect protein measurements against AAA. Values from BCA and Bradford assays are plotted versus direct protein quantitation by AAA for (A) WH samples and (B) EX samples along with the linear least squares regression.	44
Figure 2.3	Methanol extraction removed protein and preferentially extracted alanine, proline, and glutamine + glutamate.	46
Figure 2.4	Trends in the error of BCA-WH but not BCA-EX measurements suggest that <i>C. tepidum</i> accumulates intracellular pools of methanol-soluble, Cu(II)-reducing compounds during early phase growth on sulfide and S ⁰ , but not thiosulfate.....	47
Figure 2.5	Cell length and volume, but not diameter, correlate with growth rate. Culture means for log-transformed cell diameter, cell length, and cell volume are plotted versus observed culture growth rate.	49
Figure 2.6	Effect of electron donor and acetate depletion on cell volume and storage carbohydrate accumulation across cultures of different growth rates.	50
Figure 2.7	Variation of cell diameter (A) and length (B) with growth rate, electron donor, and acetate availability.	51
Figure 2.8	Average amino acid composition of unextracted, whole (WH) <i>C. tepidum</i> biomass.	52
Figure 2.9	The composition of certain amino acids varied in response to electron donor identity, light, and culture duration.	54
Figure 2.10	Light level affects variation in amino acid abundance according to biosynthetic cost.	55
Figure 2.11	Overall amino acid composition varied with BChl <i>c</i> content, but BChl <i>c</i> content did not correlate with ~P _{avg}	58

Figure 3.1	Effect of electron donor on <i>C. tepidum</i> growth yields based on electron equivalents oxidized.	89
Figure 3.2	Model for relationship of <i>C. tepidum</i> growth yield to electron transport pathways.	93
Figure 3.3	Effect of electron donor and light flux level on <i>C. tepidum</i> growth yields based on acetate uptake.	101
Figure 3.4	Sulfur mass balance closure across the energy landscape.	104
Figure 3.5	Breakdown of sulfur contained in the main intermediates of <i>C. tepidum</i> sulfur metabolism across the energy landscape.	105
Figure 3.6	Accumulation of polysulfides during <i>C. tepidum</i> growth on sulfide. ...	108
Figure 3.7	Timecourses showing electron donor oxidation, polysulfide presence, and <i>C. tepidum</i> growth for (A) sulfide oxidation/S ⁰ production and (B) S ⁰ degradation during growth at 20 $\mu\text{mol photon m}^{-2} \text{s}^{-1}$ light flux.	112
Figure 3.8	Polysulfides were present but did not accumulate during low light growth on S ⁰	113
Figure 3.9	Model of S ⁰ globule production and degradation in <i>C. tepidum</i>	116
Figure 3.10	Profiles of growth and substrate consumption for energy landscape cultures grown at low light and provided sulfide, S ⁰ , or thiosulfate as sole electron donor.	118
Figure 3.11	Profiles of growth and substrate consumption for cultures provided thiosulfate as sole electron donor at 5 $\mu\text{mol photon m}^{-2} \text{s}^{-1}$, compared to cultures provided no electron donor.	120
Figure 4.1	During the early phase of sulfide oxidation at (A) 20 $\mu\text{mol photons m}^{-2} \text{s}^{-1}$ and (B) 5 $\mu\text{mol photons m}^{-2} \text{s}^{-1}$, <i>C. tepidum</i> cells exhibit a ‘blebbed’, phase-bright outer surface that diminishes as sulfide is exhausted.	152
Figure 4.2	Scanning electron microscopic images and results of elemental composition by SEM-EDX of S ⁰ produced by <i>C. tepidum</i>	154
Figure 4.3	Images of unfixed S ⁰ produced by wildtype <i>C. tepidum</i> stained with FM® 1-43FX membrane stain, with phase contrast and DIC images for comparison.	156

Figure 4.4	Protein profiles of purified S ⁰ and <i>C. tepidum</i> cells compared by one-dimensional SDS-PAGE.	158
Figure 4.5	Protein profiles of differential extractions of S ⁰ and <i>C. tepidum</i> compared by one-dimensional gel electrophoresis.	164
Figure 4.6	Purified S ⁰ from wildtype cultures exhibited much lower cell contamination after the first purification procedure (left panel) relative to S ⁰ from mutant strain C3 (right panel).	168
Figure 4.7	Protein profiles of (A) WH and (B) SHD extracts from wildtype S ⁰ and C3 S ⁰ and <i>C. tepidum</i> cells compared by one-dimensional gel electrophoresis (4-20% acrylamide Tris-HCl gel).	171
Figure 4.8	Protein profiles of wildtype S ⁰ extracts obtained from shotgun-compatible protocols compared to S ⁰ proteins directly extracted into L(+) sample buffer by one-dimensional gel electrophoresis.	178
Figure 4.9	One-dimensional gel electrophoresis profiles of the proteins remaining in association with S ⁰ after extraction by shotgun-compatible protocols, compared to proteins from S ⁰ when directly extracted into L(+) sample buffer.	180
Figure 4.10	Extraction of S ⁰ with 2% CHAPS and DetergentOUT™ clean-up was found to extract the largest total amount of protein by BCA assay (A) and demonstrated the most protein bands by one-dimensional SDS-PAGE.	182
Figure 4.11	Breakdown of predicted subcellular location for proteins identified from wildeyp S ⁰ (A) versus the whole <i>C. tepidum</i> proteome (B).	192
Figure 4.12	Schematic of proposed process for extracellular S ⁰ globule formation by membrane vesicle-like mechanism.	211
Figure 4.13	Annotated schematic of the alignment of CT1320.1 and CT1305 homologs in the <i>Chlorobiaceae</i>	214
Figure A.1	Copyright information for Chapter 2.	244
Figure A.2	Microbiology Society License to Publish, pg. 1.	246
Figure A.2	Microbiology Society License to Publish, pg. 2.	247
Figure A.2	Microbiology Society License to Publish, pg. 3.	248

Figure D.1	Trace oxygen contamination in sulfide-free Pf-7 medium may contribute to failed <i>C. tepidum</i> cultures.	260
Figure D.2	Oxygen added to thiosulfate-only media induced lag in <i>C. tepidum</i> growth but did not affect overall growth yields except for highest O ₂ treatment.	263
Figure D.3	<i>C. tepidum</i> removed O ₂ from culture in a light-dependent manner.	265

ABSTRACT

The metabolic capabilities of environmental microbes, which enable them to thrive in niche environments and survive harsh conditions, can inspire novel solutions to challenging problems. One such problem is the enormous amount of waste elemental sulfur produced as a byproduct of crude oil and natural gas refining. The supply of waste sulfur greatly exceeds demand, and the ~7 million tons produced annually is landfilled or stored in open piles at refineries. As sulfur oxidizing bacteria use elemental sulfur (S^0) and other reduced sulfur compounds as substrates for growth, waste sulfur represents an untapped resource for fueling useful microbial processes.

The phototrophic sulfur oxidizing bacterium *Chlorobaculum tepidum* uses electrons obtained from the oxidation of reduced sulfur compounds for carbon dioxide fixation. *C. tepidum* oxidizes sulfide as the preferred electron donor, depositing S^0 into insoluble extracellular globules; once sulfide is depleted, *C. tepidum* oxidizes S^0 to sulfate. However, the mechanisms of S^0 production and degradation are poorly understood, as are the interactions that mediate cell- S^0 attachment. Thus the aim of this work was to improve understanding of S^0 metabolism in *C. tepidum* to facilitate alternative uses of waste sulfur *via* synthetic biology approaches.

Challenges with growth variability and a lack of reliable biomass quantitation methods in *C. tepidum* were initial obstacles to deriving meaningful information from quantitative systems-based studies. To address these issues, design of experiments methodology was used to evaluate the growth of *C. tepidum* across a 3×3 factorial space of S^0 -producing and S^0 -degrading states and a range of light fluxes: the ‘energy

landscape’ of sulfur oxidation. Protein measurements collected across the landscape were calibrated against amino acid analysis quantitation, providing improved measurement methods for assessing biomass growth. Unexpectedly, these results also revealed adaptations that increase *C. tepidum* fitness in low-energy environments. Comprehensive measurements of the various intermediates of sulfur metabolism across this factorial space revealed that electron donor, but not light flux, affected growth yields on an electron equivalent basis, providing insight into pathways of energy conservation in *C. tepidum*. This work also revealed the presence of soluble intermediates of S^0 production and degradation, providing a mechanism to explain time-lapse microscopic observations of S^0 globules growing and degrading at a distance from cells.

Towards characterizing the surface properties of S^0 to better understand cell- S^0 interactions, analysis of the S^0 ‘proteome’ revealed intriguing similarities with the proteomes of the outer membrane vesicles of other gram negative bacteria. Of particular interest was the observation of proteins involved in spatial localization of import/export machinery and cell division, inorganic ion transport and metabolism, and the envelope stress response, along with uncharacterized outer membrane proteins. Together, these data suggest a new model for S^0 generation in *C. tepidum*, and provide new protein targets for characterization in the context of S^0 metabolism and cell- S^0 interactions.

The comprehensive ‘landscape’ approach used in this work enabled new insights into S^0 metabolism and low-energy adaptations in *C. tepidum* that would not have been observed by single-factor experiments. Furthermore, these efforts form a basis for future quantitative, systems-based studies, and this approach is generalizable

to preparing for these types of studies in other systems. The specific insights into S^0 metabolism obtained from this work could be applied to improved waste sulfur management and the low-energy adaptations have implications for optimizing the efficiency of “designer microbes” used in industrial processing.

Chapter 1

INTRODUCTION

1.1 Project Motivation: Challenges of Sulfur Contamination and Sulfur Management Facing Industry

Hydrogen sulfide (H_2S), the most reduced form of sulfur, causes a range of issues in the petrochemical industry. As the remaining number of high-quality “sweet” oil and gas fields has diminished, lower quality “sour” fields rich in H_2S are coming online (Ziaei et al. 2013). These sulfidic oil and gas streams cause corrosion in stainless steel equipment of upstream processing facilities, where the reaction of steel and H_2S to form metal sulfides causes brittle fractures. Also known as sulfide stress cracking, this corrosion can cause catastrophic failure of pressurized vessels or pipes (Ogden 2005) or the failure of the bodies of wellhead flow control valves (Ziaei et al. 2013). The presence of H_2S and other organic sulfur species in raw oil and gas streams can also poison the precious metal catalysts used in hydrocarbon processing (Dunleavy 2006).

Sulfur can also cause issues at the combustion stage, where burning of sulfur-containing fuel leads to the formation of sulfur dioxides (SO_2). The abiotic oxidation of both H_2S and SO_2 in the atmosphere forms sulfuric acid, producing acid rain (Clarke & Radojevic 1987; Singh et al. 2016). The presence of sulfur in fuel can also cause problems in the engines themselves (“hot corrosion”), particularly in the gas turbine engines of modern aircraft when operated in the atmosphere above a marine environment. When the sulfur-containing fuel is mixed with intake air contaminated

with NaCl, combustion leads to the formation of molten Na₂SO₄ at the high operating temperatures of the engine. The condensation of Na₂SO₄ and other salt contaminants damages the protective surface oxides of the turbine components, and can eventually lead to catastrophic failure (Eliaz et al. 2002).

Sulfur compounds also cause issues in sewer corrosion and in wastewater processing. Wastewaters rich in H₂S, such as those from petrochemical plants, tanneries, and rayon manufactures (Janssen et al. 1999), can feed sulfur oxidizing bacteria that colonize concrete sewer surfaces. These bacteria produce sulfuric acid, which acidifies the concrete sewer surface and induces corrosion (Vollertsen et al. 2008). In 2013, it was estimated that the costs to replace damaged pipes across the U.S., along with other updates to infrastructure for wastewater treatment, was nearly \$300 billion dollars over the next 20 years (ASCE 2013; Wren 2014).

These issues have motivated the removal of sulfide from petrochemical and natural gas streams as well as from sulfidic wastewaters (Janssen et al. 1995; Janssen et al. 1999; Lens & Kuenen 2001). These processes are generating enormous amounts of waste sulfur, with the majority produced from petrochemical refining. Furthermore, the production of waste sulfur is increasing, particularly with the increased processing of sulfur-rich oil and gas streams (Lim et al. 2015). Approximately a half pound of sulfur is removed from every 19 gallons of gasoline refined (Ayre 2013), with annual production of about 1.8 million tons of sulfur recovered from oil and natural gas production in the United States, and over 13.5 million tons of total sulfur production worldwide (U.S. Geological Survey, 2016). While some of this waste sulfur is used in the production of sulfuric acid, there are few other uses or applications and the supply of waste sulfur far exceeds its demand. Thus sulfur accumulates and is stored

indefinitely in large piles at refineries or in remote areas (Chung et al. 2013; Lim et al. 2015).

The long-term effects of these open sulfur piles have not yet been assessed (Lim et al. 2015), but both abiotic and biological processes will likely play roles in the fate of the piles and downstream effects. Elemental sulfur and sulfide serve as electron donors for microbial respiration or phototrophy by sulfur oxidizing bacteria, and elemental sulfur can also serve as an electron acceptor for sulfur reducing bacteria, producing sulfide. Thus, the release of waste sulfur into the environment would likely cause disturbances in affected ecosystems. For example, the reduction of waste sulfur by sulfur reducing bacteria present in the environment would produce sulfide. This biological process could have effects ranging to nuisance smells, detectable at concentrations down to 8.1 ppb (Amoore & Hautala 1983), to more harmful effects in both humans and in wildlife: at gaseous concentrations above 600-800 ppm sulfide is lethal to humans (Kleinjan et al. 2003), and the production of sulfide by sulfide reducing bacteria in anoxic waters causes fish and invertebrate kills (Weeks et al. 2002; Lavik et al. 2009).

To avoid these detrimental effects, a more favorable scenario is to harness the waste sulfur (either the sulfur itself or the energy and electrons it contains) for useful purposes. Recent research efforts have focused on developing novel advanced materials that incorporate elemental sulfur, including composites for cathodes of lithium-sulfur batteries (Dirlam et al. 2016) and polymers with desirable properties (Chung et al. 2013; Griebel et al. 2015). However, a currently unexplored avenue is the use of waste elemental sulfur as an electron donor substrate that fuels the metabolism of microbes simultaneously producing a useful compound. For example,

the oxidation of sulfur could be coupled to carbon dioxide (CO₂) fixation to produce organic commodity chemical precursors, biofuel precursors, or even sulfur-containing compounds such as antibiotics.

The use of sulfur oxidizing bacteria in biotechnology-based processes has precedence, such as in various bioreactor configurations to remove sulfide from biogas (reviewed in Syed et al. 2006), where some processes have been deployed at commercial scales (Thiopaq® and Sulfothan™ processes; Pokorna & Zabranksa 2016). These approaches to sulfide removal provide energy savings and environmental benefits over conventional physicochemical methods of sulfide removal (Janssen et al. 1999; Kleinjan et al. 2003). As biogenic elemental sulfur (S⁰) is produced as an intermediate of sulfide oxidation by sulfur oxidizing bacteria, and is subsequently oxidized to sulfate, elemental sulfur is also a substrate to these processes. S⁰ has also been used as a substrate for the microbial communities involved in mineral bio-leaching processes (Kleinjan et al. 2003).

The processes described above have employed both aerobic chemolithotrophic and anaerobic photoautotrophic sulfur oxidizing bacteria, as single species as well as in natural consortia. However, in developing a process that uses waste sulfur as the substrate for the production of a useful compound, these naturally-competent sulfur oxidizing bacteria may not be ideal candidates due to slow growth rates, phototrophic requirements, and/or limited genetic tools for installation of product-synthesis pathways. Thus, a synthetic biology approach whereby a ‘designer’ microbe is constructed with desirable properties (metabolic modes enabling high growth and substrate oxidation rates, oxygen-tolerant, efficient product synthesis pathways, etc.)

could provide a substantial benefit. In the context of biotechnology-based processes for sulfur management in industry, this approach is unexplored.

The creation of ‘designer’ microbes is becoming more feasible thanks to advances in synthetic biology, which have enabled developments such as the creation of a fully-synthetic microbe containing less than 500 genes (Hutchinson et al. 2016), the development of synthetic scaffolds (Siu et al. 2015) and nanocages (Zhao et al. 2016) for localizing enzymes to increase reaction rates and stability, and the incorporation of heterologous pathways for the production of fuel precursors and commodity chemicals into a range of organisms (Keasling & Venter 2013). Efforts to engineer a ‘designer’ sulfur oxidizing microbe will require knowledge from a range of disciplines, such as metabolic engineering, biochemistry, and microbial physiology, among others. Furthermore, in the construction of a designer microbe many aspects beyond the sulfur metabolism will need to be incorporated, including product synthesis pathways, redox homeostasis, and cofactor balancing. However, a critical prerequisite to this synthetic biology approach is a comprehensive understanding of how naturally-competent microbes utilize S^0 as an electron donor.

Therefore the aim of this work was to characterize the biological systems for S^0 production and degradation employed by a sulfur oxidizing microbe, *Chlorobaculum tepidum*, to facilitate alternative uses of waste sulfur by synthetic biology approaches.

1.2 Project Background

1.2.1 The biogeochemical sulfur cycle

The chemical properties of sulfur, including its ability to exist in stable valence states ranging from -2 (sulfide, $\text{H}_2\text{S} \leftrightarrow \text{HS}^- \leftrightarrow \text{S}^{2-}$) to +6 (sulfate, SO_4^{2-}), enable this element to play a central role in biochemistry. In particular, its redox activity has established sulfur compounds as critical electron donors and acceptors for microbial respiration in the biosphere. Thus, the fate, transformation, and cycling of sulfur in the environment is dependent upon microbial activities (Klotz et al. 2011).

Sulfide, the most reduced form of sulfur, is formed by the metabolic activity of anaerobic chemotrophic sulfate-reducing bacteria that utilize sulfate as the electron acceptor in the oxidation of organic compounds or hydrogen (Sturman et al. 2008). Oxidation of sulfide in the biosphere back to sulfate occurs both by abiotic and microbial mechanisms; however the rates of microbial oxidation are almost always three or more orders of magnitude faster than abiotic processes (Luther et al. 2011) emphasizing the importance of microbially-catalyzed sulfur cycling in natural systems. During microbial sulfur oxidation, reduced sulfur compounds (sulfide, S^0 , thiosulfate, tetrathionate, and sulfite) supply the reducing equivalents for microbial respiration. In the context of a ‘designer’ microbe for biotechnology-based solutions for waste sulfur utilization, to avoid production of problematic sulfide, this work focused on the activities of sulfur oxidizing bacteria.

1.2.2 Metabolic strategies of microbial sulfur oxidation

In general, microbial sulfur oxidation proceeds in two steps. First, sulfide is oxidized incompletely to zero-valent (‘elemental’) sulfur (S^0), which is deposited into insoluble globules. Subsequently, under conditions of sulfide limitation, S^0 is oxidized

to SO_4^{2-} . Other sulfur compounds, including thiosulfate, tetrathionate, polythionates, and organic sulfur compounds, can also serve as electron donors for various sulfur oxidizing bacteria (Ghosh & Dam 2009). The biochemistry and physiology of these diverse bacteria have been extensively reviewed (Dahl & Prange 2006; Frigaard & Dahl 2009; Ghosh & Dam 2009); a brief summary is provided below.

The oxidization of reduced sulfur compounds supplies reducing equivalents for chemolithotrophic and phototrophic metabolism. Most well-studied chemotrophic sulfur oxidizing bacteria are aerobic, coupling sulfur oxidation to the reduction of oxygen as a terminal electron acceptor for fixation of CO_2 (Ghosh & Dam 2009). Classically known as the ‘colorless’ sulfur bacteria, these bacteria come from a range of genera from across the Proteobacteria (*Acidithiobacillus*, *Acidiphilium*, *Sulfobacillus*, *Beggiatoa*, and others) and from the Archaea (order Sulfolobales; Dahl & Prange 2006). The chemotrophic bacteria are quite metabolically diverse, both in terms of the reduced sulfur compounds used, the exact mechanisms of sulfur oxidation employed, whether they are obligate or facultative chemolithotrophs, and their optimal pH and temperature (Ghosh & Dam 2009). Under anoxic conditions, some chemotrophic bacteria use nitrate as an alternative electron donor (Syed et al. 2006). This type of respiration is performed facultatively by bacterial species from a range of genera (*Thiobacillus*, *Beggiatoa*, *Thioploca*, *Thioalkalivibrio*, *Thiohalomonas*, *Thiomicrospira* and *Sulfurimonas*) and where *Sulfurimonas denitrificans* is the most well-characterized member (Ghosh & Dam, 2009).

In contrast to the chemotrophic sulfur oxidizing bacteria, all phototrophic sulfur-oxidizers are anaerobes. Reducing equivalents from the oxidation of sulfur compounds are used in anoxygenic photosynthesis to reduce cellular electron carriers

used in CO₂ fixation. The phototrophic sulfur oxidizing bacteria are classified into two main groups: the purple sulfur bacteria (families *Chromatiaceae* and *Ectothiorhodospiraceae* in the Gammaproteobacteria) and the green sulfur bacteria (family *Chlorobiaceae* in the phylum Chlorobi) (Frigaard & Dahl 2009). In addition to these main groups, some other bacteria have limited abilities to oxidize sulfur under phototrophic conditions (e.g. Heliobacteria, *Chloroflexaceae*), but the physiology and biochemistry of these groups are not well understood (Ghosh & Dam 2009). The green and purple sulfur bacteria differ both in their primary photochemical processes and light harvesting structures (Ghosh & Dam 2009). They also differ in terms of the pathway used for CO₂ fixation, where the purple sulfur bacteria use the Calvin cycle and the green sulfur bacteria use the reductive tricarboxylic acid (rTCA) cycle (Brune 1995). Furthermore, the purple sulfur bacteria are more metabolically diverse, also capable of heterotrophic growth in the dark and facultative aerobic oxidization of sulfur (Frigaard & Dahl 2009; Ghosh & Dam 2009). By contrast the green sulfur bacteria are obligate photoautotrophs, although some can assimilate simple organic compounds such as pyruvate and acetate (Imhoff 2003; Chan et al. 2008; Feng et al. 2010).

1.2.3 S⁰ globule production and degradation are poorly understood

A major distinguishing factor of all the sulfur-oxidizing bacteria is where insoluble S⁰ is deposited during sulfide oxidation. Most chemotrophic sulfur oxidizing bacteria and the green sulfur bacteria deposit S⁰ into extracellular globules, whereas the purple sulfur bacteria and some chemotrophic members of the *Gammaproteobacteria* deposit S⁰ into protein-encapsulated intracellular inclusions (Brune, 1995; Dahl & Prange 2006; Frigaard & Dahl; 2009). A common feature is that

S⁰ accumulates during sulfide oxidation, and is not oxidized to sulfate until after the depletion of sulfide (Sturman et al. 2008; Chan et al. 2009).

The production and degradation of S⁰ is one of the most poorly understood aspects of sulfur oxidation (Dahl & Prange 2006). How cells attach to extracellular S⁰, degrade S⁰, and take up S⁰ or its intermediates, as well as how the products of sulfide oxidation are packaged into S⁰, are open questions. Even the nature of the “elemental sulfur” contained in S⁰ from different bacteria has been debated in the literature. Studies using X-ray absorption near-edge structure (XANES) spectroscopy to study sulfur speciation of S⁰ *in situ* have produced contradictory results: Dahl and Prange (2006) summarize studies suggesting that S⁰ produced by different types of sulfur oxidizing bacteria is composed of different forms of sulfur; whereas, George et al. (2008) contend that this conclusion is a result of uncorrected experimental artifacts associated with the spectroscopy method. Investigating the nature of sulfur allotropes contained in S⁰ was not a goal of the present work, but this debate serves as an illustrative example of the uncertainty around the chemistry, biochemistry, and metabolism of biogenic S⁰.

1.2.4 *Chlorobaculum tepidum* provides a model system for studying S⁰ production and degradation

The organism studied in this work is the model species of the phototrophic green sulfur bacteria, *Chlorobaculum tepidum*. *C. tepidum* produces insoluble, extracellular globules of S⁰ as a result of sulfide oxidation, and oxidizes S⁰ to sulfate upon depletion of sulfide (Chan et. al. 2009). *C. tepidum* also can utilize thiosulfate as an electron donor (Imhoff 2003; Chan et al. 2008; Sakurai et al. 2010). Electrons from these reduced sulfur compounds are donated to the photosynthetic electron transport

chain, where *C. tepidum* uses light energy to drive the reduction of the cellular electron carrier ferredoxin by the photosynthetic reaction center (Brune 1995). Ferredoxin subsequently reduces NAD(P)^+ via a ferredoxin-NAD(P)⁺ reductase (Seo & Sakurai 2002), and ferredoxin and NAD(P)H are used as the electron donors for fixation of carbon dioxide by the rTCA cycle (Brune 1995). *C. tepidum* also can assimilate the simple organic compounds acetate and pyruvate (Chan et al. 2008; Feng et al. 2010).

Like the other green sulfur bacteria, *C. tepidum* harvests light energy through specialized organelles called chlorosomes. These structures are highly efficient at capturing light energy, and *C. tepidum* and other members of the *Chlorobiaceae* are adapted to light intensities much lower than that required to support the growth of other phototrophs (Frigaard et al. 2002; Overmann 2006). On this basis, the chlorosomes of *C. tepidum* and other members of the *Chlorobiaceae* have been the subject of many studies to elucidate their organizational structure, mechanisms of excitation energy transfer, and the function of individual components (e.g. Frigaard et al. 1999; Pšenčík et al. 2002; Pšenčík et al. 2003; Li et al. 2006; Morgan-Kiss et al. 2008; Wen et al. 2009; Huang et al. 2012; Johnson et al. 2013; Li et al. 2013; Valleau et al. 2014; Günther et al. 2016; Nielsen et al. 2016; Saer et al. 2016). Based on their high efficiency, the chlorosomes have also been used as model systems for understanding the principles of light harvesting towards developing artificial photosynthetic chlorosome-based systems for converting light energy to electricity or fuel (Oostergetel 2010; Orf & Blankenship 2013).

In general, pathways for the oxidation of sulfide, thiosulfate, and sulfite are reasonably well established, as are some aspects of S^0 oxidation. *C. tepidum* oxidizes

sulfide (HS^-) by one of several sulfur-quinone oxidoreductases (SQR) encoded in the genome (CT0117, CT0876, CT1087; Chan et al. 2009; Shuman & Hanson 2016). While the fate of the products of SQR, disulfide and/or polysulfides, are not fully elucidated, it is predicted that these are oxidized further by the polysulfide reductase like complex (PSRLC1), encoded by *CT0496-CT0494*, based on an increase in the transcript level of these genes after a sulfide spike (Eddie & Hanson 2013). However, how these soluble polysulfides are converted into the insoluble form of sulfur present in S^0 , and how S^0 is packaged into globules and exported out of the cell is unknown.

The initial steps in the degradation and oxidation of S^0 are not clear. The dissimilatory sulfite reductase (Dsr) system is known to be essential for S^0 oxidation in *C. tepidum* (Holkenbrink et al. 2011), as in *Allochromatium vinosum* (Dahl et al. 2005; Weissgerber et al. 2014). Characterization of the roles of individual components of the Dsr system has been performed primarily in *A. vinosum* (Pott & Dahl 1998; Dahl et al. 2005; Dahl et al. 2006; Grein et al. 2010; Stockdreher et al. 2012; Stockdreher et al. 2014). However, Dsr-mediated oxidation of zero-valent sulfur substrates, possibly in a protein-bound form (Dahl 2015), is predicted to occur in the cytoplasm (Stockdreher et al. 2012; Stockdreher et al. 2014), and the oxidation of sulfite, the product of Dsr, is also oxidized in the cytoplasm (see below). Therefore, how the zero-valent sulfur in extracellular S^0 is extracted and transported back into the cytoplasm are unclear. Sakurai et al. (2010) proposed that CT1075, a homolog of the *E. coli* protein DsbD, and the periplasmic protein SoxW (CT1023) could be involved in transferring S^0 equivalents across the cytoplasmic membrane. However, whether this occurs has not been established in either *C. tepidum* or *A. vinosum*, and in other organisms

Sulfite is oxidized in the cytoplasm first by adenylylphosphosulfate reductase (ApsBA; CT0864-0865), where a quinone interacting membrane bound oxidoreductase (QmoABC; CT0866-0868) transfers electrons into the quinone pool, and then by ATP sulfurylase (Sat; CT0862) (Rodriguez et al. 2011). Thiosulfate ($\text{S}_2\text{O}_3^{2-}$) is oxidized in the periplasm by the Sox system (Sakurai et al. 2010; Chan et al. 2008), which is widely distributed among the sulfur oxidizing bacteria (Friedrich et al. 2001). Oxidation of thiosulfate by Sox yields one molecule of sulfate (SO_4^{2-}) and a persulfane sulfur attached to the carrier protein SoxY (CT1017); the fate of the persulfane sulfur in *C. tepidum* and in *A. vinosum* has not been determined, as the Sox systems in these bacteria are missing the sulfur dehydrogenase SoxCD, responsible for oxidative hydrolysis of the cysteinyl persulfide (Sakurai et al. 2010). The lack of SoxCD is expected to result in the accumulation of a polysulfide group on the sulfur carrier protein SoxY, which could be spontaneously liberated or transferred to a thiol forming the transient extracellular S^0 observed with thiosulfate oxidation (Sakurai et al. 2010). Again, the mechanism for packing and export of zero-valent sulfur produced by thiosulfate oxidation into the extracellular S^0 is unknown.

The genome of *C. tepidum* is fully sequenced (Eisen et al. 2002), which has enabled genomics-based insights into its metabolism (Frigaard et al. 2003; Frigaard & Bryant 2004). The sequenced genome has also enabled systems-based studies; Eddie & Hanson (2013) employed a global transcriptome analysis of *C. tepidum* using RNA-seq to evaluate gene expression changes in response to a sulfide spike, and found over 120 differentially expressed genes. Specific genes with altered expression implicated the polysulfide reductase-like complex in sulfide oxidation to S^0 and a potential sulfide-dependent regulator (Eddie & Hanson 2013). Using quantitative shotgun

proteomics, Falkenby et al. (2011) detected increased expression of the Sox system proteins and the periplasmic cytochrome c-555 in late-culture cells growing on thiosulfate as electron donor compared to early-culture cells growing on sulfide. The sequenced genome of *C. tepidum* has also enabled the use of deletion mutants for characterizing protein functions *via* a modest collection of genetic tools that have been developed for *Chlorobaculum tepidum*. These include the capacity for chromosomal gene inactivation (Chung et al. 1998; Frigaard & Bryant 2001), transposon mutagenesis (Chan et al. 2008), and conjugative gene transfer from *Escherichia coli* (Wahlund & Madigan 1995; Azai et al. 2013). These tools have enabled the characterization of a number of genes within the genome, including genes for the three sulfide-quinone oxidoreductases (Chan et al. 2009), a cluster of genes from CT0867-CT0876 (encoding QmoBC, the SQR-like protein CT0876, and a number of uncharacterized proteins; Chan et al. 2008), cytochrome c-554 (Tsukatani et al. 2006), and Sox B (Azai et al. 2009), among others.

As described above, many aspects of S⁰ metabolism in *C. tepidum* have remained elusive, including mechanisms by which cells attach to S⁰. However, the capacity for systems-based studies and targeted gene knockouts in *C. tepidum* provide many opportunities to obtain new insights. An improved understanding of the surface interactions governing microbe-S⁰ attachment, as well as mechanisms of S⁰ production and degradation, would help identify key systems that could be employed in biotechnology-based approaches to utilize waste sulfur or improve sulfide-remediating processes.

1.3 Project Aims and Scope of Work

Studying *C. tepidum* under conditions of S^0 production and degradation will provide new insight into mechanisms of S^0 production and degradation and of cell- S^0 attachment. In addition to applications in using waste sulfur, an improved understanding of these processes could also provide insight into the wide range of strategies that microbes use to interact with their extracellular environment, and could inform novel ways of functionalizing surfaces for biocompatibility. While focused studies, i.e. for characterizing the roles of individual gene products or the regulation of discrete systems, are obviously critical for developing new understanding of biological pathways, quantitative systems-based studies are extremely useful for observing organism-wide changes in response to imposed changes. The outcomes of these types of studies, including transcriptomic, proteomic, and metabolomic studies, can subsequently be used to identify new targets for focused, hypothesis-driven investigations. The utility of quantitative systems-based studies in obtaining an organism-wide view of gene and protein expression changes has been demonstrated for *C. tepidum* and other green sulfur bacteria (Wenter et al. 2010; Falkenby et al. 2011; Eddie & Hanson 2013), for *Allochromatium vinosum* (Weissgerber et al. 2013; Weissgerber et al. 2014), and other sulfur-oxidizing bacteria (e.g. Mangold et al. 2011; Kucera et al. 2013).

However, obtaining valid information from systems-based approaches requires a controlled experimental system and a well-characterized organism under the relevant conditions. These checkpoints are required to maximize the likelihood that observed changes in the measured responses are due to the experimental conditions under comparison, and not just biological noise. Thus, this work focused on first controlling and characterizing *C. tepidum* under the growth conditions most relevant for a better

understanding of the metabolic pathways and systems involved in S^0 metabolism, namely S^0 production during sulfide oxidation and S^0 degradation as sole electron donor. Subsequently, this work sought to identify proteins associated with S^0 from *C. tepidum* to provide insight into mechanisms of S^0 production, and potential routes for S^0 degradation.

These studies elucidated previously unknown aspects of *C. tepidum* physiology and have set the stage for future systems-based approaches to understanding S^0 metabolism, along with directed studies to probe hypotheses in mechanisms of sulfur production and degradation. Chapter 5 details suggested routes for these future studies.

1.3.1 Aim 1: Control and characterize the *Chlorobaculum tepidum* system

Variable growth of *C. tepidum*, particularly when S^0 or thiosulfate were provided as the sole electron donor in the absence of sulfide, posed challenges to detailed studies of this organism. Furthermore, the ability of indirect protein quantitation methods to accurately predict *C. tepidum* biomass across all growth conditions was not conclusively established. These challenges motivated the development of controlled culture conditions to provide reproducible growth under S^0 production, S^0 degrading, and thiosulfate oxidizing conditions, as well as the calibration of colorimetric protein methods (Bradford and bicinchoninic acid assays). Design of Experiments (DOE) methodology was used to construct a factorial space of varied electron donor type, light flux level, and batch culture duration. This space, the energy landscape of sulfur oxidation, spanned 27 unique conditions across 48 cultures and was used to calibrate *C. tepidum* protein measurements against protein measured by amino acid analysis. This large effort resulted in unexpected insights into the low

energy adaptations of *C. tepidum*. These studies and the associated outcomes are the subject of Chapter 2, and formed the publication Levy et al. 2016.

To characterize sulfur metabolism across varying conditions, measurements of sulfur compounds, including electron donors and oxidation products, collected across the energy landscape study were analyzed. These data were used to assess the effects of electron donor type and light flux on *C. tepidum* biomass yields, as well as to evaluate closure of the sulfur mass balance. This analysis revealed that electron donor type affected biomass yields on an electron equivalent basis, providing insight into energy conservation pathways in *C. tepidum*. Regions of the energy landscape where the mass balance did not close prompted additional studies that suggested roles for soluble polysulfide intermediates in S^0 production and degradation. These studies and the associated outcomes are the subject of Chapter 3, and portions were published in Marnocha et al. 2016.

1.3.2 Aim 2: Identify proteins associated with *Chlorobaculum tepidum* S^0

Studies of biogenic S^0 from *C. tepidum* suggested interesting surface properties, including the possibility for the association of proteins with the S^0 surface. These observations, combined with microscopic evidence for packaging of S^0 into vesicle-like particles, motivated exploratory proteomic studies to characterize the S^0 ‘proteome’. Through a combination of gel-based and shotgun proteomic approaches, a profile of the *C. tepidum* S^0 proteome emerged that shared intriguing similarities with the proteomes of outer membrane vesicles of other gram negative bacteria. In particular this work identified protein subunits of cell envelope spanning complexes, proteins involved with spatial control of cell division machinery, envelope stress response proteins, uncharacterized outer membrane proteins, subunits of inner-

membrane complexes responsible for proton motive force generation and ATP generation, and certain proteins involved with inorganic ion transport and energy metabolism. Together these data suggest a new model for S^0 generation in *C. tepidum*, and provide numerous targets for directed studies to test hypotheses about the roles of these proteins in S^0 metabolism and cell- S^0 interactions. These studies and the associated outcomes are the subject of Chapter 4, and portions were published in Hanson et al. 2016.

REFERENCES

- Amoore, J.E. & Hautala, E., 1983. Odor as an aid to chemical safety: odor thresholds compared with threshold limit values and volatilities for 214 industrial chemicals in air and water dilution. *Journal of Applied Toxicology*, 3(6), pp.272–90.
- ASCE, 2013. *2013 Report Card for America's Infrastructure*. American Society of Civil Engineers. Available at: www.infrastructurereportcard.org. [Accessed October 22, 2016].
- Ayre, J., 2013. New process turns common waste sulfur into material useful for EV batteries. *CleanTechnica*. Available at: <https://cleantechnica.com/2013/04/18/new-process-turns-common-waste-sulfur-into-material-useful-for-ev-batteries/> [Accessed October 22, 2016].
- Azai, C. et al., 2009. Sulfur oxidation in mutants of the photosynthetic green sulfur bacterium *Chlorobium tepidum* devoid of cytochrome c-554 and SoxB. *Photosynthesis Research*, 100(2), pp.57–65.
- Azai, C., Harada, J. & Oh-oka, H., 2013. Gene expression system in green sulfur bacteria by conjugative plasmid transfer. *PLoS ONE*, 8(11), e82345. doi:10.1371/journal.pone.0082345.
- Brune, D.C., 1995. Sulfur compounds as photosynthetic electron donors. In R. E. Blankenship, M. T. Madigan, & C. E. Bauer, eds. *Anoxygenic Photosynthetic Bacteria*. Dordrecht: Kluwer Academic Publishers, pp. 847–70.
- Chan, L.-K. et al., 2008. A genomic region required for phototrophic thiosulfate oxidation in the green sulfur bacterium *Chlorobium tepidum* (syn. *Chlorobaculum tepidum*). *Microbiology*, 154(3), pp.818–829.
- Chan, L.-K., Morgan-Kiss, R.M. & Hanson, T.E., 2009. Functional analysis of three sulfide:quinone oxidoreductase homologs in *Chlorobaculum tepidum*. *Journal of Bacteriology*, 191(3), pp.1026–1034.

- Chung, S. et al., 1998. Insertional inactivation studies of the *csmA* and *csmC* genes of the green sulfur bacterium *Chlorobium vibrioforme* 8327: The chlorosome protein CsmA is required for viability but CsmC is dispensable. *FEMS Microbiology Letters*, 164(2), pp.353–361.
- Chung, W.J. et al., 2013. The use of elemental sulfur as an alternative feedstock for polymeric materials. *Nature Chemistry*, 5(6), pp.518–524.
- Clarke, A.G. & Radojevic, M., 1987. Oxidation of SO₂ in rainwater and its role in acid rain chemistry. *Atmospheric Environment*, 21(5), pp.1115–1123.
- Dahl, C., 2015. Cytoplasmic sulfur trafficking in sulfur-oxidizing prokaryotes. *IUBMB Life*, 67(4), pp.268–274.
- Dahl, C. et al., 2005. Novel genes of the *dsr* gene cluster and evidence for close interaction of Dsr proteins during sulfur oxidation in the phototrophic sulfur bacterium *Allochromatium vinosum*. *Journal of Bacteriology*, 187(4), pp.1392–1404.
- Dahl, C. & Prange, A., 2006. Bacterial sulfur globules: occurrence, structure and metabolism. In J. M. Shivley, ed. *Inclusions in Prokaryotes*. Microbiology Monographs. Berlin: Springer-Verlag, pp. 21–51.
- Dirlam, P.T. et al., 2016. Elemental sulfur and molybdenum disulfide composites for Li-S batteries with long cycle life and high-rate capability. *ACS Applied Materials and Interfaces*, 8(21), pp.13437–13448.
- Dunleavy, J.K., 2006. Sulfur as a catalyst poison. *Platinum Metals Review*, 50(2), p.110.
- Eddie, B.J. & Hanson, T.E., 2013. *Chlorobaculum tepidum* TLS displays a complex transcriptional response to sulfide addition. *Journal of Bacteriology*, 195(2), pp.399–408.
- Eisen, J.A. et al., 2002. The complete genome sequence of *Chlorobium tepidum* TLS, a photosynthetic, anaerobic, green-sulfur bacterium. *Proceedings of the National Academy of Sciences of the United States of America*, 99(14), pp.9509–9514.
- Eliasz, N., Shemesh, G. & Latanision, R.M., 2002. Hot corrosion in gas turbine components. *Engineering Failure Analysis*, 9(1), pp.31–43.

- Falkenby, L.G. et al., 2011. Quantitative proteomics of *Chlorobaculum tepidum*: insights into the sulfur metabolism of a phototrophic green sulfur bacterium. *FEMS Microbiology Letters*, 323(2), pp.142–50.
- Feng, X. et al., 2010. Metabolic flux analysis of the mixotrophic metabolisms in the green sulfur bacterium *Chlorobaculum tepidum*. *The Journal of Biological Chemistry*, 285(50), pp.39544–39550.
- Friedrich, C.G. et al., 2001. Oxidation of reduced inorganic sulfur compounds by bacteria: emergence of a common mechanism? *Applied and Environmental Microbiology*, 67(7), pp.2873–2882.
- Frigaard, N.-U. et al., 2003. *Chlorobium tepidum*: Insights into the structure, physiology, and metabolism of a green sulfur bacterium derived from the complete genome sequence. *Photosynthesis Research*, 78(2), pp.93–117.
- Frigaard, N.-U. & Bryant, D.A., 2001. Chromosomal gene inactivation in the green sulfur bacterium *Chlorobium tepidum* by natural transformation. *Applied and Environmental Microbiology*, 67(6), pp.2538–2544.
- Frigaard, N.-U. & Dahl, C., 2009. Sulfur metabolism in phototrophic sulfur bacteria. In R. K. Poole, ed. *Advances in Microbial Physiology*, Vol. 54. Burlington, MA: Academic Press, pp. 103–200.
- Frigaard, N.-U. & Matsuura, K., 1999. Oxygen uncouples light absorption by the chlorosome antenna and photosynthetic electron transfer in the green sulfur bacterium *Chlorobium tepidum*. *Biochimica et Biophysica Acta - Bioenergetics*, 1412(2), pp.108–117.
- Frigaard, N.-U., Voigt, G.D. & Bryant, D.A., 2002. *Chlorobium tepidum* mutant lacking bacteriochlorophyll *c* made by inactivation of the *bchK* gene, encoding bacteriochlorophyll *c* synthase. *Journal of Bacteriology*, 184(12), pp.3368–3376.
- George, G.N. et al., 2008. X-ray absorption spectroscopy as a probe of microbial sulfur biochemistry: The nature of bacterial sulfur globules revisited. *Journal of Bacteriology*, 190(19), pp.6376–6383.
- Ghosh, W. & Dam, B., 2009. Biochemistry and molecular biology of lithotrophic sulfur oxidation by taxonomically and ecologically diverse bacteria and archaea. *FEMS Microbiology Reviews*, 33(6), pp.999–1043.

- Grein, F., Pereira, I.A.C. & Dahl, C., 2010. Biochemical characterization of individual components of the *Allochromatium vinosum* DsrMKJOP transmembrane complex aids understanding of complex function in vivo. *Journal of Bacteriology*, 192(24), pp.6369–6377.
- Günther, L.M. et al., 2016. Structure of light-harvesting aggregates in individual chlorosomes. *Journal of Physical Chemistry B*, 120(24), pp.5367–5376.
- Hanson, T.E. et al., 2016. *Chlorobaculum tepidum* growth on biogenic S(0) as the sole photosynthetic electron donor. *Environmental Microbiology*, 18(9), pp.2856–2867.
- Holkenbrink, C. et al., 2011. Sulfur globule oxidation in green sulfur bacteria is dependent on the dissimilatory sulfite reductase system. *Microbiology*, 157(Pt 4), pp.1229–1239.
- Huang, R.Y.-C. et al., 2012. Hydrogen-deuterium exchange mass spectrometry reveals the interaction of Fenna-Matthews-Olson protein and chlorosome CsmA protein. *Biochemistry*, 51(1), pp.187–93.
- Hutchison, C.A. et al., 2016. Design and synthesis of a minimal bacterial genome. *Science*, 351(6280), aad6253. doi:10.1126/science.aad6253.
- Imhoff, J.F., 2003. Phylogenetic taxonomy of the family *Chlorobiaceae* on the basis of 16S rRNA and fmo (Fenna-Matthews-Olson protein) gene sequences. *International Journal of Systematic and Evolutionary Microbiology*, 53(4), pp.941–951.
- Janssen, A.J.H. et al., 1995. Biological sulphide oxidation in a fed-batch reactor. *Biotechnology and Bioengineering*, 47(3), pp.327–333.
- Janssen, A.J.H., Lettinga, G. & de Keizer, A., 1999. Removal of hydrogen sulphide from wastewater and waste gases by biological conversion to elemental sulphur; Colloidal and interfacial aspects of biologically produced sulphur particles. *Colloids and Surfaces A: Physicochemical and Engineering Aspects*, 151, pp.389–397.
- Johnson, T.W. et al., 2013. [2Fe-2S] Proteins in chlorosomes: Redox properties of CsmI, CsmJ, CsmX of the chlorosome envelope of *Chlorobaculum tepidum*. *Biochemistry*, 52(8), pp.1331–1343.
- Keasling, J.D. & Venter, J.C., 2013. Applications of synthetic biology to enhance life. *The Bridge*, 43(3), pp.47–58.

- Kleinjan, W.E., de Keizer, A. & Janssen, A.J.H., 2003. Biologically produced sulfur. In R. Steudel, ed. *Elemental Sulfur and Sulfur-Rich Compounds I*. Topics in Current Chemistry. New York, NY: Springer-Verlag, pp. 167–188.
- Kucera, J. et al., 2013. Ferrous iron oxidation by sulfur-oxidizing *Acidithiobacillus ferrooxidans* and analysis of the process at the levels of transcription and protein synthesis. *Antonie van Leeuwenhoek*, 103(4), pp.905–919.
- Kutney, G., 2007. *Sulfur. History, Technology, Applications & Industry*, Toronto: ChemTec Pub. pp.1-232.
- Lavik, G. et al., 2009. Detoxification of sulphidic African shelf waters by blooming chemolithotrophs. *Nature*, 457(7229), pp.581–584.
- Lens, P.N.L. & Kuenen, J.G., 2001. The biological sulfur cycle: novel opportunities for environmental biotechnology. *Water science and technology*, 44(8), pp.57–66.
- Levy, A.T., Lee, K.H. & Hanson, T.E., 2016. *Chlorobaculum tepidum* modulates amino acid composition in response to energy availability, as revealed by a systematic exploration of the energy landscape of phototrophic sulfur oxidation. *Applied and Environmental Microbiology*, 82(21), pp.6431–6439.
- Li, H., Frigaard, N.-U. & Bryant, D.A., 2013. [2Fe-2S] Proteins in chlorosomes: CsmI and CsmJ participate in light-dependent control of energy transfer in chlorosomes of *Chlorobaculum tepidum*. *Biochemistry*, 52(8), pp.1321–1330.
- Li, H., Frigaard, N.-U. & Bryant, D.A., 2006. Molecular contacts for chlorosome envelope proteins revealed by cross-linking studies with chlorosomes from *Chlorobium tepidum*. *Biochemistry*, 45(30), pp.9095–9103.
- Lim, J., Pyun, J. & Char, K., 2015. Recent approaches for the direct use of elemental sulfur in the synthesis and processing of advanced materials. *Angewandte Chemie - International Edition*, 54(11), pp.3249–3258.
- Luther, G.W. et al., 2011. Thermodynamics and kinetics of sulfide oxidation by oxygen: a look at inorganically controlled reactions and biologically mediated processes in the environment. *Frontiers in Microbiology*, 2(April), 62. doi:10.3389/fmicb.2011.00062.
- Mangold, S. et al., 2011. Sulfur Metabolism in the Extreme Acidophile *Acidithiobacillus Caldus*. *Frontiers in Microbiology*, 2(February), pp.1–18.

- Maresca, J.A. et al., 2004. The *bchU* gene of *Chlorobium tepidum* encodes the C-20 methyltransferase in bacteriochlorophyll c biosynthesis. *Journal of Bacteriology*, 186(9), pp.2558–2566.
- Marnocha, C.L. et al., 2016. Mechanisms of extracellular S⁰ globule production and degradation in *Chlorobaculum tepidum* via dynamic cell–globule interactions. *Microbiology*, 162(7), pp.1125–1134.
- Morgan-Kiss, R.M. et al., 2009. *Chlorobaculum tepidum* regulates chlorosome structure and function in response to temperature and electron donor availability. *Photosynthesis Research*, 99(1), pp.11–21.
- Nielsen, J.T. et al., 2016. In situ high-resolution structure of the baseplate antenna complex in *Chlorobaculum tepidum*. *Nature Communications*, 7, 12454. doi: 10.1038/ncomms12454.
- Ogden, B.L., 2005. Sulfide stress cracking - practical application to the oil and gas industry. *Southwest Petroleum Short Course, Texas Tech University*. Available at: http://www.halliburton.com/public/multichem/contents/Papers_and_Articles/web/Sulfide-Stress-Cracking-SWPSC-2005.pdf. [Accessed October 21, 2016].
- Oostergetel, G.T., van Amerongen, H. & Boekema, E.J., 2010. The chlorosome: A prototype for efficient light harvesting in photosynthesis. *Photosynthesis Research*, 104(2), pp.245–255.
- Orf, G.S. & Blankenship, R.E., 2013. Chlorosome antenna complexes from green photosynthetic bacteria. *Photosynthesis Research*, 116(2–3), pp.315–331.
- Overmann, J., 2006. The Family *Chlorobiaceae*. In M. Dworkin et al., eds. *The Prokaryotes Volume 7: Proteobacteria: Delta and Epsilon Subclasses. Deeply Rooting Bacteria*. Singapore: Springer Science+Business Media, L.L.C., pp. 359–378.
- Pickering, I.J. et al., 2001. Analysis of sulfur biochemistry of sulfur bacteria using X-ray absorption spectroscopy. *Biochemistry*, 40(27), pp.8138–8145.
- Pokorna, D. & Zabranska, J., 2015. Sulfur-oxidizing bacteria in environmental technology. *Biotechnology Advances*, 33(6), pp.1246–1259.
- Pott, A.S. & Dahl, C., 1998. Sirohaem sulfite reductase and other proteins encoded by genes at the *dsr* locus of *Chromatium vinosum* are involved in the oxidation of intracellular sulfur. *Microbiology*, 144(7), pp.1881–1894.

- Prange, A. & Dahl, C., 2002. X-ray absorption spectroscopy of bacterial sulfur globules: a detailed reply. *Microbiology*, 148(8), pp.2267–2272.
- Pšenčík, J. et al., 2003. Excitation energy transfer dynamics and excited-state structure in chlorosomes of *Chlorobium phaeobacteroides*. *Biophysical Journal*, 84(2), pp.1161–1179.
- Pšenčík, J. et al., 2002. Excitation energy transfer in chlorosomes of *Chlorobium phaeobacteroides* strain CL 1401: The role of carotenoids. *Photosynthesis Research*, 71, pp.5–18.
- Rodriguez, J., Hiras, J. & Hanson, T.E., 2011. Sulfite oxidation in *Chlorobaculum tepidum*. *Frontiers in Microbiology*, 2(May), 112. doi:10.3389/fmicb.2011.00112.
- Saer, R.G. et al., 2016. Perturbation of bacteriochlorophyll molecules in Fenna-Matthews-Olson protein complexes through mutagenesis of cysteine residues. *Biochimica et Biophysica Acta - Bioenergetics*, 1857(9), pp.1455–1463.
- Sakurai, H. et al., 2010. Inorganic sulfur oxidizing system in green sulfur bacteria. *Photosynthesis Research*, 104(2–3), pp.163–176.
- Seo, D. & Sakurai, H., 2002. Purification and characterization of ferredoxin-NAD(P)(+) reductase from the green sulfur bacterium *Chlorobium tepidum*. *Biochimica et Biophysica Acta*, 1597(1), pp.123–132.
- Shuman, K.E. & Hanson, T.E., 2016. A sulfide:quinone oxidoreductase from *Chlorobaculum tepidum* displays unusual kinetic properties. *FEMS Microbiology Letters*, 363(12), fnw100. doi:10.1093/femsle/fnw100.
- Singh, S., Elumalai, S.P. & Pal, A.K., 2016. Rain pH estimation based on the particulate matter pollutants and wet deposition study. *Science of the Total Environment*, 563–564, pp.293–301.
- Siu, K.H. et al., 2015. Synthetic scaffolds for pathway enhancement. *Current Opinion in Biotechnology*, 36, pp.98–106.
- Stockdreher, Y. et al., 2012. Cytoplasmic sulfurtransferases in the purple sulfur bacterium *Allochromatium vinosum*: Evidence for sulfur transfer from DsrEFH to DsrC. *PLoS ONE*, 7(7), e40785. doi: 10.1371/journal.pone.0040785.
- Stockdreher, Y. et al., 2014. New proteins involved in sulfur trafficking in the cytoplasm of *Allochromatium vinosum*. *Journal of Biological Chemistry*, 289(18), pp.12390–12403.

- Sturman, P.J. et al., 2008. Sulfur cycling in constructed wetlands. In J. Vymazal, ed. *Wastewater Treatment, Plant Dynamics, and Management in Constructed and Natural Wetlands*. Berlin, Heidelberg: Springer Science + Business Media B.V., pp. 329–344.
- Syed, M. et al., 2006. Removal of hydrogen sulfide from gas streams using biological processes - a review. *Canadian Biosystems Engineering*, 48, p.2.1-2.14.
- Tsukatani, Y. et al., 2006. Soluble cytochrome c-554, CycA, is not essential for photosynthetic electron transfer in *Chlorobium tepidum*. *FEBS Letters*, 580(9), pp.2191–2194.
- U.S. Geological Survey, 2016. *Mineral Commodity Summaries 2016*, Reston, VA: U.S. Geological Survey., pp.162-163.
- Valleau, S. et al., 2014. Electromagnetic study of the chlorosome antenna complex of *Chlorobium tepidum*. *ACS Nano*, 8(4), pp.3884–3894.
- Vollertsen, J. et al., 2008. Corrosion of concrete sewers-The kinetics of hydrogen sulfide oxidation. *Science of the Total Environment*, 394(1), pp.162–170.
- Wahlund, T.M. & Madigan, M.T., 1995. Genetic transfer by conjugation in the thermophilic green sulfur bacterium *Chlorobium tepidum*. *Journal of Bacteriology*, 177(9), pp.2583–2588.
- Weeks, S.J., Currie, B. & Bakun, A., 2002. Massive emissions of toxic gas in atlantic. *Nature*, 415(6871), pp.493–494.
- Weissgerber, T. et al., 2014. A comparative quantitative proteomic study identifies new proteins relevant for sulfur oxidation in the purple sulfur bacterium *Allochromatium vinosum*. *Applied and Environmental Microbiology*, 80(7), pp.2279–2292.
- Weissgerber, T. et al., 2013. Genome-wide transcriptional profiling of the purple sulfur bacterium *Allochromatium vinosum* DSM 180T during growth on different reduced sulfur compounds. *Journal of Bacteriology*, 195(18), pp.4231–4245.
- Wen, J. et al., 2009. Membrane orientation of the FMO antenna protein from *Chlorobaculum tepidum* as determined by mass spectrometry-based footprinting. *Proceedings of the National Academy of Sciences of the United States of America*, 106(15), pp.6134–6139.

- Wenter, R. et al., 2010. Expression-based identification of genetic determinants of the bacterial symbiosis “*Chlorochromatium aggregatum*.” *Environmental Microbiology*, 12, pp.2259–2276.
- Wren, K., 2014. From sewers to streetlights, microbes are grabbing civil engineers’ attention. *AAAS News*. 16 April 2014. Available at: <https://www.aaas.org/news/sewers-streetlights-microbes-are-grabbing-civil-engineers-attention>. [Accessed October 22, 2016].
- Zhao, Z. et al., 2016. Nanocaged enzymes with enhanced catalytic activity and increased stability against protease digestion. *Nature Communications*, 7, 10619. doi:10.1038/ncomms10619.
- Ziaei, S.M.R., Kokabi, A.H. & Nasr-Esfehani, M., 2013. Sulfide stress corrosion cracking and hydrogen induced cracking of A216-WCC wellhead flow control valve body. *Case Studies in Engineering Failure Analysis*, 1(3), pp.223–234.

Chapter 2

***CHLOROBACULUM TEPIDUM* MODULATES AMINO ACID COMPOSITION IN RESPONSE TO ENERGY AVAILABILITY, AS REVEALED BY A SYSTEMATIC EXPLORATION OF THE ENERGY LANDSCAPE OF PHOTOTROPHIC SULFUR OXIDATION**

2.1 Preface

This chapter (including all text, figures, and tables) was adapted from [Levy, Lee, and Hanson \(2016\)](#) with permission (see Appendix A.1), and describes efforts to characterize *Chlorobaculum tepidum* across an experimental space relevant to studies of S⁰ production and degradation.

2.1.1 Abstract

Microbial sulfur metabolism, particularly the formation and consumption of insoluble elemental sulfur (S⁰), is an important biogeochemical engine that has been harnessed for applications ranging from bioleaching and biomining to remediation of waste streams. *Chlorobaculum tepidum*, a low-light adapted photoautolithotrophic sulfur oxidizing bacterium, oxidizes multiple sulfur species and displays a preference for more reduced electron donors: sulfide > S⁰ > thiosulfate. To understand this preference in the context of light energy availability, an ‘energy landscape’ of phototrophic sulfur oxidation was constructed by varying electron donor identity, light flux, and culture duration. Biomass and cellular parameters of *C. tepidum* cultures grown across this landscape were analyzed. From these data, a correction factor for colorimetric protein assays was developed, enabling more accurate biomass

measurements for *C. tepidum* as well as other organisms. *C. tepidum*'s bulk amino acid composition correlated with energy landscape parameters, including a tendency toward less energetically expensive amino acids under reduced light flux. This correlation, paired with an observation of increased cell size and storage carbon production under electron-rich growth conditions, suggests that *C. tepidum* has evolved to cope with changing energy availability by tuning its proteome for energetic efficiency and storing compounds for leaner times.

2.1.2 Importance

How microbes cope with and adapt to varying energy availability is an important factor in understanding microbial ecology and in designing efficient biotechnological processes. We explored the response of a model phototrophic organism, *Chlorobaculum tepidum*, across a factorial experimental design that enabled simultaneous variation and analysis of multiple growth conditions, what we term the 'energy landscape'. *C. tepidum* biomass composition shifted toward less energetically expensive amino acids at low light. This observation provides experimental evidence for evolved efficiencies in microbial proteomes and emphasizes the role that energy flux may play in the adaptive responses of organisms. From a practical standpoint, our data suggest that bulk biomass amino acid composition could provide a simple proxy to monitor and identify energy stress in microbial systems.

2.2 Introduction

Microbes that synthesize or degrade insoluble sulfur-minerals are instrumental in the biogeochemical sulfur cycle (Lavik et al. 2009), and have been applied for biomining (Johnson 2014; Rawlings 2005) and sulfide remediation (Fortuny et al.

2010; Janssen et al. 2001; Syed et al. 2006; Lens & Kuenen 2001). However, little is known about how these organisms respond to fluctuations in available energy due to shifts in electron donor identity, fixed carbon availability, or light in the case of phototrophic bacteria. A deeper understanding of microbial strategies for coping with energy fluctuations has the potential to improve microbe-catalyzed industrial processes (Sturman et al. 2008) and to impact our understanding of microbial ecology as shaped by energy availability (Macalady et al. 2013). Furthermore, a specific understanding of these adaptations among microbes capable of degrading elemental sulfur could inform new technologies for mitigating the effects of sulfur-metabolizing microbes on disturbed ecosystems (e.g. waste sulfur piles from petrochemical refining), particularly if coupled with recent advances in systems and synthetic biology.

Microbes that produce insoluble elemental sulfur (S^0) as an intermediate of reduced sulfur compound oxidation and subsequently oxidize S^0 to sulfate include both chemotrophs (genera *Acidothiobacillus*, *Beggiatoa*; order Sulfolobales) and phototrophs (families *Chromatiaceae*, *Chlorobiaceae*). S^0 may be deposited either extra- or intra-cellularly (Kleinjan et al. 2003; Dahl & Prange 2006). The *Chlorobiaceae* are obligate anaerobes that use sulfide and other reduced sulfur compounds as electron donors for anoxygenic photosynthesis, and transiently deposit S^0 as extracellular globules (Chan, Weber, et al. 2008; Holkenbrink et al. 2011; Hanson et al. 2016; Wahlund et al. 1991). Unlike the more metabolically versatile species of the *Chromatiaceae*, which are capable of dark, aerobic chemotrophic growth in addition to phototrophic sulfur oxidation (Imhoff 2006), all characterized *Chlorobiaceae* are obligate anaerobic photolithoautotrophs, although some

Chlorobiaceae assimilate simple organic carbon compounds (acetate, pyruvate) (Overmann 2006). *Chlorobaculum tepidum* produces and degrades insoluble extracellular S^0 as an obligate intermediate of sulfide oxidation, grows rapidly (Wahlund et al. 1991; Mukhopadhyay et al. 1999), is genetically tractable (Chan, Morgan-Kiss, et al. 2008; Wahlund & Madigan 1995; Frigaard & Bryant 2001; Hanson & Tabita 2001; Azai et al. 2013) and has a sequenced genome (Eisen et al. 2002), making it an ideal platform for studying S^0 metabolism by systems-based methods.

Systems-based methods require reproducible growth under controlled conditions and robust methods of biomass quantitation, both of which are challenging for *C. tepidum*. For example, consistent growth on S^0 as the sole electron donor has only recently been reported (Hanson et al. 2016). Extracellular S^0 complicates growth measurements by standard methods (i.e. optical density and dry weight) because S^0 adds turbidity (Mukhopadhyay et al. 1999; Frigaard et al. 2002) and mass. Therefore, colorimetric protein assays are the method of choice for biomass determinations of *C. tepidum* (Mukhopadhyay et al. 1999; Chan, Weber, et al. 2008; Frigaard et al. 2002). However, differences between the amino acid compositions of biomass and protein standards and interference from a range of compounds (Sapan et al. 1999), including photosynthetic pigments, mean that colorimetric protein assays often do not reflect absolute protein concentration. While pigment extraction prior to protein measurement is common (Mukhopadhyay et al. 1999; Chan, Weber, et al. 2008; Frigaard et al. 2002), the effects of extraction and of varying pigment content, induced by changes in light level (Morgan-Kiss et al. 2009; Borrego et al. 1999) and electron donor (Chan, Weber, et al. 2008), have not been investigated systematically.

Design of Experiments methodology (Mead et al. 2012; Ogunnaike 2010) was used to assess protein-based biomass quantitation methods and the response of *C. tepidum* across a factorial space defined by electron donor, light flux level, and culture duration. This space – the ‘energy landscape’ of phototrophic sulfur oxidation (Fig. 2.1) – was designed to alter pigment content by altering energy availability. *C. tepidum* displayed shifts in biomass amino acid composition, cell volume, and storage carbohydrate content across the energy landscape, suggesting that *C. tepidum* alters its physiology in response to energy availability to a greater extent than previously appreciated. While bias in the amino acid composition of highly-expressed proteins towards energetically inexpensive amino acids has been inferred by bioinformatic analyses for a range of organisms (Akashi & Gojobori 2002; Raiford et al. 2012; Heizer et al. 2006), this work reports an experimentally-measured shift in bulk amino acid composition for a single organism as a function of growth conditions. This observation implies that relatively simple bulk biomass measurements can be used to infer details about energy status and adaptation of microbes.

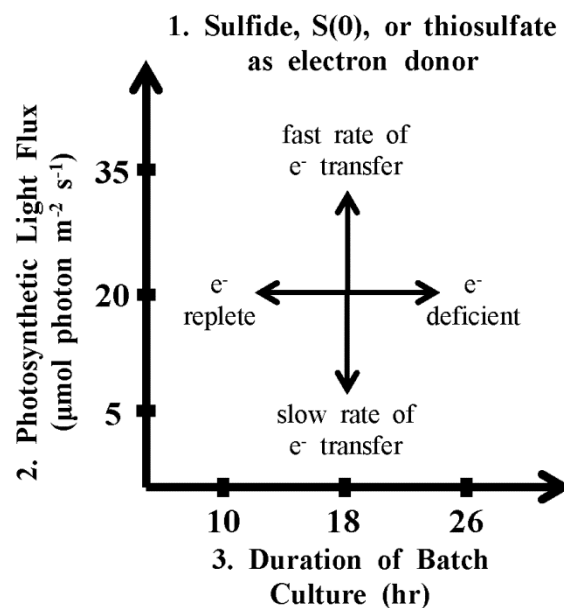


Figure 2.1 Schematic of the ‘Energy Landscape’ of phototrophic sulfur oxidation. The energy landscape of phototrophic sulfur oxidation is constructed from three factors at three levels: (1) electron donor identity (sulfide, S⁰, or thiosulfate), (2) light flux (5, 20, or 35 μmol photons m⁻² s⁻¹) and (3) duration of batch culture (10, 18, or 26 hours).

2.3 Materials and Methods

2.3.1 Experimental design

A 3×3 factorial experiment was employed to examine *C. tepidum* growth and characteristics as a function of electron donor type, light flux level, and culture duration at three levels per factor. The I-optimal design was created using JMP® Pro (SAS Institute Inc.) and contained 48 independent cultures performed in six culturing blocks (Table 2.1). This design enabled quantitative analysis of the effects of simultaneous changes in the energy landscape parameters on various measured

Table 2.1 Details of the of the 3×3 factorial design composing the energy landscape of phototrophic sulfur oxidation, including how treatments were distributed among the different culturing blocks. AAA, amino acid analysis; WH, whole unextracted samples; EX, extracted cell pellet samples (see 2.3.5).

Culturing Block	Culture		Light Flux ($\mu\text{mol photons m}^{-2} \text{s}^{-1}$)		Culture Duration (hrs)		AAA technical reps	
	Unit ID#	Electron Donor	Actual	Coded	Actual	Coded	WH	EX
1	1	Sulfide	5	-1	26	1	1	
	2	Sulfide	20	0	18	0		
	3	Sulfide	35	1	10	-1	1	1
	4	Thiosulfate	5	-1	10	-1		
	5	Thiosulfate	20	0	18	0	3	1
	6	Thiosulfate	35	1	26	1	1	1
	7	S ⁰	20	0	18	0		1
	8	S ⁰	20	0	18	0		
2	9	Sulfide	20	0	18	0	1	1
	10	Sulfide	20	0	18	0		
	11	Thiosulfate	5	-1	10	-1	1	1
	12	Thiosulfate	20	0	26	1	1	
	13	Thiosulfate	35	1	26	1		
	14	S ⁰	5	-1	18	0	1	
	15	S ⁰	5	-1	26	1	1	1
	16	S ⁰	35	1	10	-1		
3	17	Sulfide	5	-1	26	1		
	18	Sulfide	35	1	10	-1		
	19	Thiosulfate	20	0	18	0		
	20	Thiosulfate	20	0	18	0		
	21	Thiosulfate	35	1	10	-1	1	1
	22	S ⁰	5	-1	10	-1	1	1
	23	S ⁰	20	0	18	0	1	1
	24	S ⁰	35	1	26	1	1	1

Table 2.1 continued.

Culturing Block	Culture Unit ID#	Electron Donor	Light Flux ($\mu\text{mol photons m}^{-2} \text{s}^{-1}$)		Culture Duration (hrs)		AAA technical reps	
			Actual	Coded	Actual	Coded	WH	EX
4	25	Sulfide	5	-1	10	-1	1	
	26	Sulfide	0	0	18	0		
	27	Sulfide	5	1	26	1		1
	28	Thiosulfate	0	-1	18	0	1	
	29	Thiosulfate	0	0	10	-1	1	
	30	Thiosulfate	0	0	18	0	1	1
	31	S ⁰	0	-1	26	1		
	32	S ⁰	5	1	10	-1	1	1
5	33	Sulfide	5	-1	18	0	1	1
	34	Sulfide	0	0	10	-1	1	1
	35	Sulfide	5	1	26	1	1	
	36	Thiosulfate	0	-1	26	1	1	1
	37	Thiosulfate	5	1	10	-1		
	38	S ⁰	0	-1	10	-1		
	39	S ⁰	0	0	26	1	1	
	40	S ⁰	5	1	18	0	1	
6	41	Sulfide	5	-1	10	-1		
	42	Sulfide	0	0	26	1	1	1
	43	Sulfide	5	1	18	0	1	
	44	Thiosulfate	0	-1	26	1		
	45	Thiosulfate	5	1	18	0	1	
	46	S ⁰	0	-1	18	0	1	
	47	S ⁰	0	0	10	-1	1	
	48	S ⁰	5	1	26	1		

responses (cell size attributes, total carbohydrate, amino acid composition) by a second-order interaction polynomial model, where Y is the measured response, x_i are experimental factors, $\beta_{0,i,ij,ii}$ are coefficients determined from multiple regression, and ϵ represents random error. β_0 is the mean value of the response; main effect terms (β_i) represent a factor's direct effect, cross-interaction terms (β_{ij}) represent the synergistic impact of two factors, and polynomial terms (β_{ii}) represent non-linear effects (Equation 2.1).

$$Y = \beta_0 + \sum \beta_i x_i + \sum_{i < j} \beta_{ij} x_i x_j + \sum \beta_{ii} x_i x_i + \epsilon \quad 2.1$$

Culturing block was investigated as a factor except for analyses with amino acid analysis (AAA)-derived data as the dependent variable(s), which were conducted on a subset of the full design (Table 2.1).

2.3.2 Bacterial strains and growth conditions

Chlorobaculum tepidum strain WT2321, a plating strain derivative of the original TLS1 isolate (Wahlund et al. 1991; Wahlund & Madigan 1995), was grown in 20 ml cultures with a 10 psig (177 kPa) headspace composed of 95%:5% N₂:CO₂ passed through a heated copper scrubber. Experimental cultures were inoculated to 4 µg protein ml⁻¹ from pre-cultures derived from cryogenic stocks, and were grown at 45-46 °C in a heated rotisserie culturing system. This system provided improved culture-to-culture consistency in light exposure and mixing relative to stirred water bath cultures (see Appendix B for details). A light field of 35 µmol photons m⁻² s⁻¹ was provided from 100 W Reveal® incandescent bulbs (GE Lighting) measured with a quantum PAR sensor (LI-COR). To obtain 5 and 20 µmol photons m⁻² s⁻¹ light, individual cultures were shaded using printed transparency films. Culture durations

(Fig. 2.1) were selected to capture mid-exponential, late-exponential, and early stationary phase at $20 \mu\text{mol photons m}^{-2} \text{ s}^{-1}$ light flux.

2.3.3 Culture media

Sulfur-free Pf-7 medium (Wahlund et al. 1991) was prepared by omitting sulfide and thiosulfate from Pf-7 prepared as previously described (Chan, Weber, et al. 2008). Electron donors were added to individual tubes from concentrated, anoxic stock solutions. Sulfide stocks were pH-neutralized (Siefert & Pfennig 1984) and biogenic S^0 was purified as previously described (Hanson et al. 2016). The electron donor concentrations in uninoculated media were: sulfide: $3.4 \pm 0.2 \text{ mM}$; S^0 : $9.3 \pm 0.3 \text{ mM}$; thiosulfate: $10.2 \pm 0.1 \text{ mM}$. Acetate was provided at an initial concentration of $7.4 \pm 0.3 \text{ mM}$ to all cultures.

2.3.4 Quantification of sulfur compounds and acetate

Measurements were performed as described previously (Chan, Weber, et al. 2008; Rethmeier et al. 1997) with the following modifications. Elemental sulfur was extracted from cell pellets with 10:1 vol/vol chloroform:methanol prior to quantitation by reversed phase HPLC. Sulfate was quantified by ion chromatography with suppressed conductivity detection (Metrohm) using an A Supp 5 100 x 4 mm column eluted with $3.2 \text{ mM Na}_2\text{CO}_3 + 1.0 \text{ mM NaHCO}_3 + 6.5 \% \text{ v/v acetone}$ in ultrapure water. Standard curves were prepared from sodium sulfide nonahydrate (ACS, Fisher), elemental sulfur powder (USP, Fisher), sodium thiosulfate pentahydrate (>99.5%, Sigma-Aldrich), sodium sulfate (>99%, Sigma-Aldrich), and sodium acetate (>99%, EM Science).

2.3.5 Protein and bacteriochlorophyll *c* determinations

C. tepidum cells collected by centrifugation ($16,873 \times g$, 5 mins) were lysed with 0.25 M NaOH (10 mins), neutralized with an equal volume of 0.25 M HCl, centrifuged gently to pellet S^0 ($14 \times g$, 1 min), and diluted with 0.25 M NaCl prior to protein quantitation. Bradford assays were performed with Protein Assay Dye Reagent Concentrate (BioRad Laboratories) per manufacturer instructions using either the absorbance at 595 nm or the ratio of absorbance at 595 nm and 470 nm as the measured response (Ernst & Zor 2010; Zor & Selinger 1996). BCA assays were performed with the Pierce® BCA kit (Thermo Scientific) at 37 °C incubation; the ratio of sample to working reagent was increased to 1:2 vol/vol. The observed technical variation for all protein assays is reported in Table 2.2. Bovine serum albumin (> 98%, EM Science OmniPur®) was used as a protein standard. Pigments were removed from extracted (EX) samples by methanol extraction (-20° C, 10 mins) prior to lysis, whereas whole (WH) pigment-intact samples were analyzed without prior extraction; bacteriochlorophyll *c* (BChl *c*) in the extracts was determined by absorbance at 669 nm ($\epsilon = 86.0 \text{ l g}^{-1} \text{ cm}^{-1}$, (Stanier & Smith 1960)).

2.3.6 Amino acid analysis (AAA)

Lyophilized cell samples were hydrolyzed (1% v/v phenol in 6 N HCl, 110 °C, 24 hrs), and amino acids were separated by ion-exchange chromatography (Hitachi L-8800) with sodium citrate buffer as mobile phase. The hydrolysis destroys Cys, Met, and Trp, and converts the amide amino acids Asn and Gln to Asp and Glu, respectively. Biomass amino acid molar composition was calculated based on the molar quantities of individual amino acids measured in a sample.

Table 2.2 Observed technical variation in protein-based assays for biomass determination.

Type	Method	Data analysis method	Pellet status	Abbreviation	Observed Technical Variation		
					Pooled SD ^a ($\mu\text{g/ml}$)	Normalized Pooled SD ^b	Pooled CV ^c
Direct	AAA	---	WH	AAA-WH	4.6	5.6%	5.0%
Indirect	BCA	---	WH	BCA-WH	9.9	7.3%	9.2%
			EX	BCA-EX	10.3	9.1%	9.1%
	Bradford	Standard (A ₅₉₅ only)	WH	BrS-WH	15.0	18%	13%
			EX	BrS-EX	15.9	20%	14%
		Ratio (A ₅₉₅ / A ₄₇₀)	WH	BrR-WH	12.4	18%	14%
			EX	BrR-EX	13.2	17%	12%

^a Pooled standard deviation for technical replicates^b Pooled SD, normalized by mean of response^c Pooled coefficient of variation (CV) for technical replicates

2.3.7 Microscopy and cell volume measurements

Culture aliquots were fixed with 0.37% formaldehyde and stored in the dark (4 °C). At least three phase contrast images at 1000x total magnification were collected for each culture with an AxioImager Z1 light microscope and a 100x oil-immersion objective lens (Zeiss). Images were thresholded and masked using ImageJ (version 1.49t, <http://imagej.nih.gov/ij>) default settings and a 15.5 pixel μm^{-1} scale. The particle analyzer function in Fiji (<http://fiji.sc/Fiji>) was used to extract area and perimeter measurements of cell-like objects from the images using pre-determined area and circularity criteria. Extracted objects were validated as cells by cross-referencing with the original images. Dividing, clumped, or out of focus cells and other debris were manually excluded so that only well-resolved cells were retained in the final dataset. Cell images were modeled as the two-dimensional projection of a cylinder with hemispherical end-caps to calculate cell diameter, length, and volume from area and perimeter measurements. Diameter, length, and volume measurements displayed lognormal distributions across the dataset and within cultures, and were log-transformed and averaged by culture prior to analysis by least squares linear models.

2.3.8 Cellular carbohydrate analysis

Cellular carbohydrates were measured by the anthrone-sulfuric acid assay (Hanson & Phillips 1981) adapted to a 96-well format (Leyva et al. 2008; Zuroff et al. 2013). Cell pellets were extracted with acetone (10 mins, -20 °C) to remove interfering pigments (Turnbull et al. 2007). Extracellular carbohydrates were removed by resuspending in a solution of 0.85% NaCl, centrifuging ($16,873 \times g$, 5 mins), and removing the supernatant (Hanson & Phillips 1981). Pellets were re-suspended in

water and sample aliquots (45 μ l per well) were transferred to a polypropylene 96-well plate (VWR). Samples were mixed with 150 μ l anthrone reagent (2 g l⁻¹ anthrone (Acros Organics) in 98% sulfuric acid (EM Science)). For each sample, one aliquot was mixed with sulfuric acid without anthrone as a negative control, and one aliquot was spiked with 5 μ g glucose as a positive control. The covered plate was incubated at 4 °C for 10 minutes, at 95-105 °C for 20 minutes, and cooled at room temperature for 20 minutes. The absorbance at 620 nm was measured along with a glucose standard curve (0.5-10 μ g glucose per well).

2.3.9 Statistical analysis

JMP® Pro was used for all statistical analyses and preparation of box-and-whisker plots. In box-and-whisker plots used throughout, the middle line indicates the median value, boxes span the 25th to 75th quantiles, and the whiskers represent either $1.5 \times$ the inter-quantile range from the end of the box, or the upper and lower data points (excluding outliers).

The effect of the energy landscape on univariate responses was analyzed by least squares fitting of the data to the second-order interaction polynomial model described under Experimental Design. Log transformed and averaged cell dimensions were fit by weighted least squares analysis, using the inverse of the variance of the cell dimension measurement as the weighting variable, to account for the large range of cell sizes observed within each population. Analysis of variance (ANOVA) was used to assess overall model significance by F-test, which can assess multiple coefficients simultaneously, and to estimate parameter coefficient values, where the significance of individual parameters was determined by t-test. Insignificant parameters, defined as $p > 0.2$, were sequentially eliminated to improve model significance and parameter

estimates, and only parameters with t-test probabilities of $p < 0.01$ were considered to have a significant effect on the measured response. Light and culture duration factors were coded between -1 and 1 before model fitting. In some cases, using culture attributes (e.g. growth rate, etc.) as factors provided more meaningful relationships than the original energy landscape parameters, and the factors identified as producing significant effects are specified in the relevant sections below.

Amino acid composition data were fit by multivariate analysis of variance (MANOVA), which enabled analysis of the effects of the energy landscape on amino acid composition as a whole as well as on individual amino acids. The statistical significance of effects in MANOVA is determined by F-test, to enable the assessment of multiple coefficients simultaneously; approximated F ratios for categorical factors in MANOVA analysis were calculated by Wilk's lambda.

2.4 Results

2.4.1 Calibration of indirect protein assays provides accurate prediction of absolute biomass protein concentration

As intended in the experimental design, cultivation of *C. tepidum* across all 27 energy landscape treatments (Table 2.1) produced biomass with bacteriochlorophyll *c* contents spanning 0.10 to 0.24 $\mu\text{g BChl } c (\mu\text{g protein})^{-1}$. Photosynthetic pigment interference in indirect protein assays, specifically the Bradford (Br) and bicinchoninic acid (BCA) methods, was assessed by comparing protein measurements of whole (WH) and methanol-extracted (EX) samples. Two versions of the Bradford assay were used: standard (BrS), which measured A595, and ratio (BrR), which measured the ratio A595/A470 to provide increased sensitivity and linearity compared to the standard assay (Zor & Selinger 1996; Ernst & Zor 2010). The performance of the

indirect assays was benchmarked against direct quantitation of protein by amino acid analysis (AAA) measurements on WH samples, which displayed <5% error with bovine serum albumin as a standard (data not shown).

Indirect protein assays were highly correlated with AAA measurements (Table 2.3; Fig. 2.2), with the highest accuracy exhibited by BCA on EX samples (normalized root mean square error (nRMSE) = 16%; Table 2.3; see Appendix C for calculations of accuracy metrics). The BCA assay over-predicted protein in WH samples (nRMSE = 37%), particularly for early- to mid-exponential phase cultures (Fig. 2.2A inset). Both versions of the Bradford assay under-predicted protein (> 25% nRMSE) regardless of whether pigments were removed, with BrR-WH measurements the least accurate (nRMSE = 38%).

The accuracy for all assays except BCA-WH was improved by a linear correction function (Equation 2.2).

$$\text{corrected} = (\text{indirect} - \beta_0) \times \beta_1^{-1} \quad 2.2$$

Parameters β_0 and β_1 were obtained from the intercept and slope, respectively, of least squares linear regressions of indirect protein measurements against AAA measurements (Table 2.3). Although BCA-WH exhibited the smallest absolute RMSE when corrected by a linear correlation function, it had the highest nRMSE due to proportionally large deviations for low density cultures (Table 2.3; Fig. 2.2A inset). Corrected Bradford measurements on EX samples demonstrated the smallest nRMSE (13% for BrS and 12% for BrR), a slight improvement in prediction accuracy compared to the uncorrected BCA-EX measurements.

Thus, for routine usage in highly pigmented organisms like *C. tepidum*, BCA-EX measurements should provide the best results without the need for a correction

factor. For the subsequent experiments, however, we employed corrected BrR-Ex measurements based on the improvement in overall accuracy.

Table 2.3 Accuracy of Bradford and BCA (indirect) protein assay measurements in predicting protein determined by amino acid analysis (direct quantitation).

Assay correction, pigment status, and assay method	R^2	β_1	β_0	RMSE ($\mu\text{g/ml}$)	nRMSE (%)
Without correction					
WH cell pellet					
BCA	0.989			26	37%
BrS	0.966			38	25%
BrR	0.969			56	38%
EX cell pellet					
BCA	0.983			12	16%
BrS	0.971			40	29%
BrR	0.983			43	33%
After correction ¹					
WH cell pellet					
BCA		1.07	15.0	10	24%
BrS		0.734	2.61	18	15%
BrR		0.604	1.52	17	15%
EX cell pellet					
BCA		0.981	3.30	12	18%
BrS		0.734	-0.57	16	13%
BrR		0.714	-2.11	12	12%

¹ Corrected = (Indirect - β_0) $\times \beta_1^{-1}$

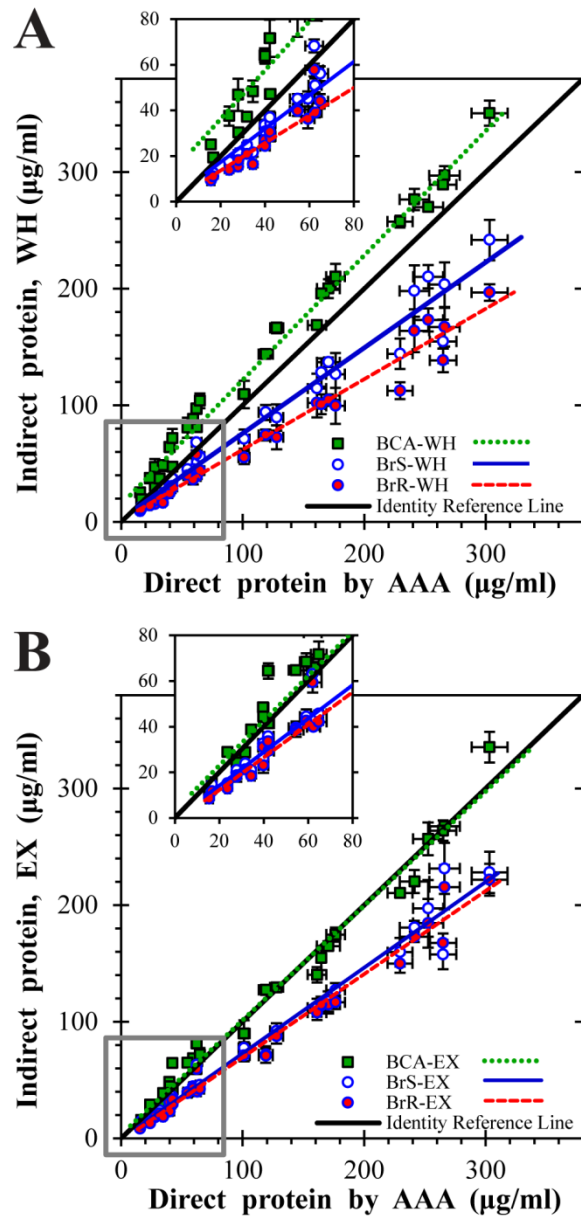


Figure 2.2 Calibration of indirect protein measurements against AAA. Values from BCA and Bradford assays are plotted versus direct protein quantitation by AAA for (A) WH samples and (B) EX samples along with the linear least squares regression. Insets show low concentration regions. The solid black identity reference line indicates equality between indirect and AAA protein determination. Vertical error bars for indirect assay measurements represent the standard error of triplicate determinations; horizontal error bars on AAA measurements represent propagation of the pooled standard error for four replicated AAA analyses.

2.4.2 Comparisons of WH and EX protein measurements suggest characteristics of the internal metabolite pools of *C. tepidum*

While methanol extraction improved the accuracy (i.e. lowered the nRMSE) of Bradford and BCA assays, this step could remove protein and/or soluble pools from biomass samples. Indeed, methanol extraction reduced measured protein mass by 9% on average (Fig. 2.3A; $p = 0.001$, 1-tailed test) as measured by AAA for 16 pairs of WH and EX samples (Table 2.1). Furthermore, the amino acid composition was altered between WH and EX samples, indicating that extraction preferentially removed Ala, Pro, and Glx (Fig. 2.3-B; see Appendix C for details). This observation was interpreted as the loss of soluble pools for these amino acids. However, there was no obvious relationship between the extent of depletion of Ala, Pro, or Glx and the energy landscape (data not shown).

Comparing BCA-WH and BCA-EX measurements revealed an interesting bias in BCA-WH error. While there was no relationship between BCA-EX error and energy landscape parameters, the tendency of BCA-WH to over-predict protein was greatest among samples from sulfide- and S^0 -grown cultures, at early durations or low light, but not with thiosulfate-grown cultures (Fig. 2.4). These observations suggest that *C. tepidum* possesses one or more internal pools of methanol-soluble metabolic reductants that artificially increase the signal of the BCA-WH assay, which is based on the reduction of Cu(II) to Cu(I).

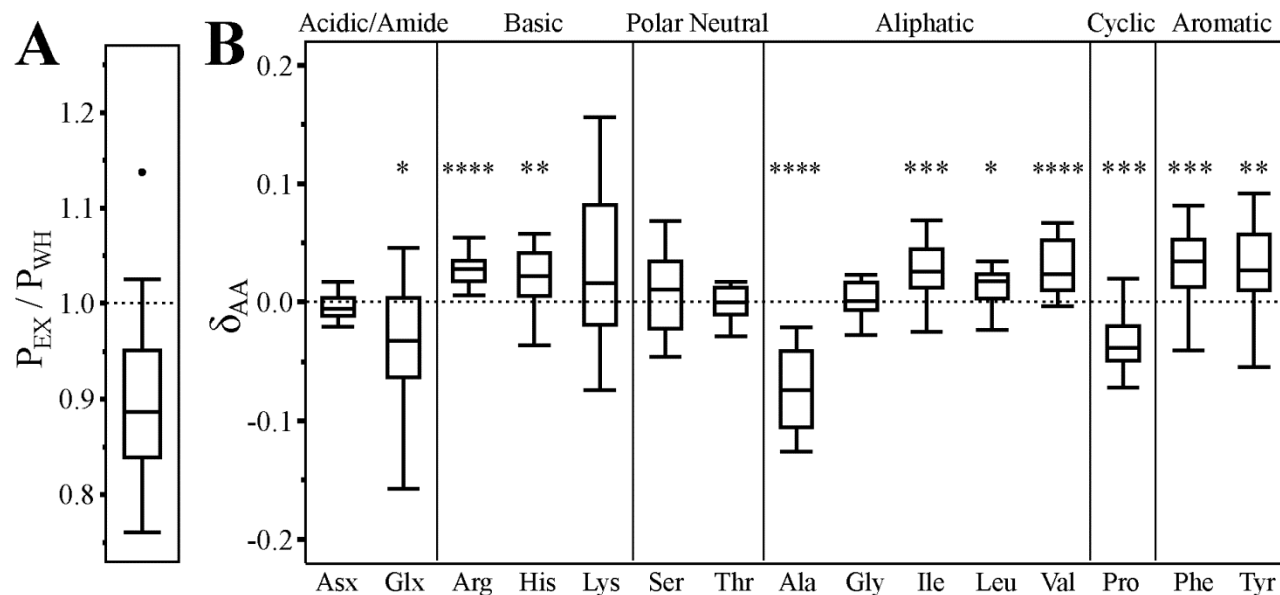


Figure 2.3 Methanol extraction removed protein and preferentially extracted alanine, proline, and glutamine + glutamate. (A) Standard box-and-whisker plot showing the distribution of P_{EX}/P_{WH} , the ratio of amino acid analysis-determined total protein masses, across 16 pairs of methanol-extracted (EX) and whole, unextracted (WH) samples. Amino acid analysis-determined protein in EX samples was less than in WH samples ($p = 0.0012$, 1-tailed matched pairs analysis) by 9% on average. (B) Standard box-and-whisker plot showing the distribution of δ_{AA} , a parameter that assesses whether amino acid AA was depleted or enriched by methanol extraction (see Supplemental Text C for details). $\delta_{AA} < 0$ indicates preferential depletion of amino acid AA by methanol extraction; $\delta_{AA} > 0$ indicates enrichment. Asterisks indicate the significance of two-tailed matched pairs analysis as described in Supplemental Text C. * $p < 0.05$; ** $p < 0.01$; *** $p < 0.001$; **** $p < 0.0001$.

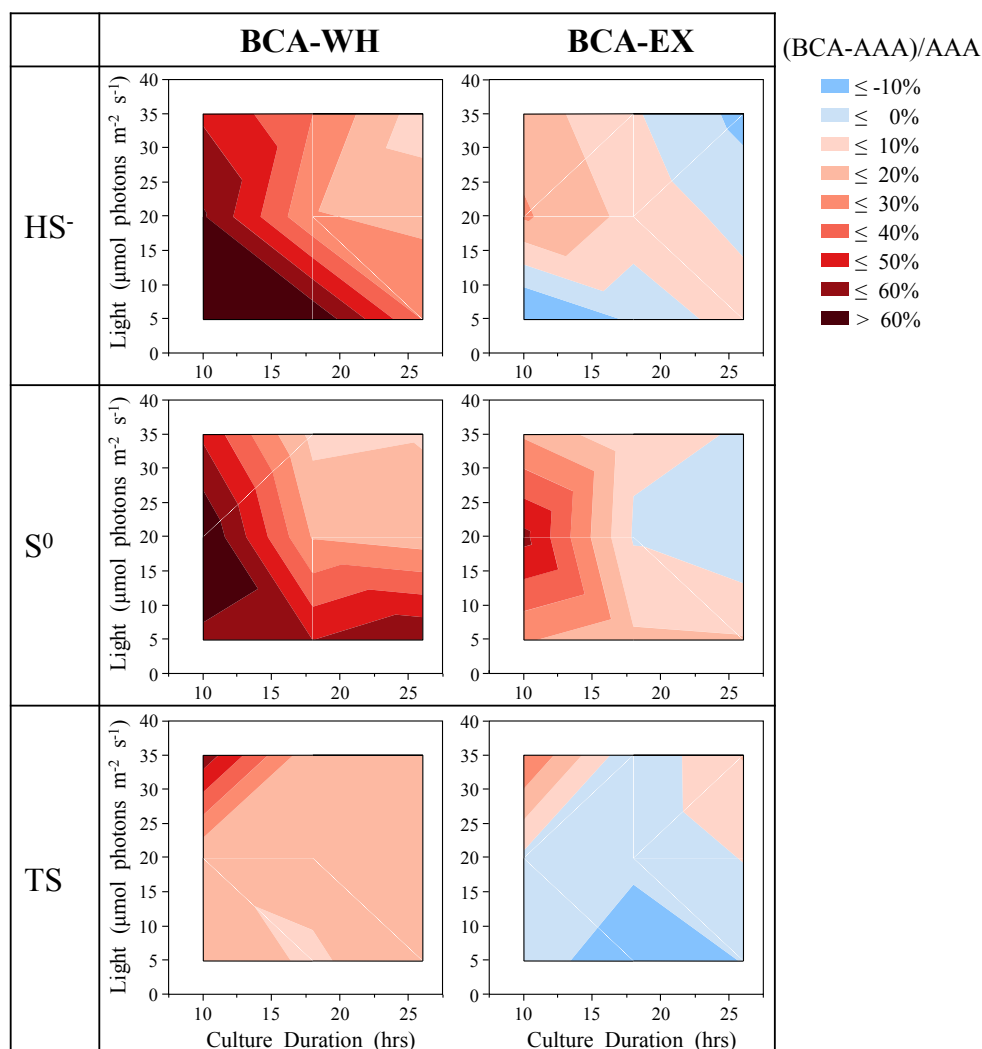


Figure 2.4 Trends in the error of BCA-WH but not BCA-EX measurements suggest that *C. tepidum* accumulates intracellular pools of methanol-soluble, Cu(II)-reducing compounds during early phase growth on sulfide and S^0 , but not thiosulfate. Contour plots depict the relative deviation between BCA-WH and AAA measurements (left panel) and BCA-EX and AAA measurements (right panel). For WH samples, the deviation between BCA and AAA was higher for early phase sulfide- and S^0 grown cells, but this pattern was eliminated by methanol extraction (EX samples) suggesting the presence of methanol-soluble pools of reductant. These pools could represent sulfide or polysulfides, and may comprise other compounds. HS^- = sulfide; TS = thiosulfate.

2.4.3 *C. tepidum* cell size variations across the energy landscape are associated with the production of storage carbohydrates

As cell size provides an indicator of the physiological state of microbes (Sánchez et al. 1998), we assessed changes in *C. tepidum* cell dimensions across the energy landscape and found that growth rate positively correlated with cell length ($R^2 = 0.38$; $p < 0.0001$) and cell volume ($R^2 = 0.34$; $p < 0.0001$), but did not correlate with cell diameter (Fig. 2.5). Increases in cell volume with faster growth rates is a well-established phenomenon (Neidhardt et al. 1990), but the large variability in cell volume at a particular growth rate suggested that additional factors were influencing cell size (Sánchez et al. 1998). Adding parameters for electron donor identity and acetate availability revealed that these factors affected cell size beyond the effect of growth rate (Fig. 2.6A). Growth on sulfide led to larger (21%, $p < 0.0001$) and longer (17%, $p < 0.0001$) cells relative to growth on S^0 and thiosulfate, but had a negligible effect on cell diameter (Fig 2.7). Acetate depletion decreased cell volume by 29% through a combined effect of decreased length (17%; $p < 0.001$) and decreased diameter (8%; $p < 0.0001$).

As the accumulation and depletion of storage carbohydrates is known to influence cell volume (Leyva et al. 2008; Hanson & Phillips 1981), total carbohydrate (TC) was measured in biomass samples from across the energy landscape. Growth on sulfide increased the ratio of TC:protein of *C. tepidum* by 72% on average ($p < 0.0001$). The corresponding increase in cell volume and TC:protein for sulfide-grown cultures (Fig. 2.6B) provides evidence that growth on sulfide leads to enhanced glycogen production relative to *C. tepidum* growth on S^0 or thiosulfate. Interestingly, TC:protein was not correlated with acetate depletion; thus, decreased cell volume for acetate-depleted cultures is not a result of storage carbohydrate degradation.

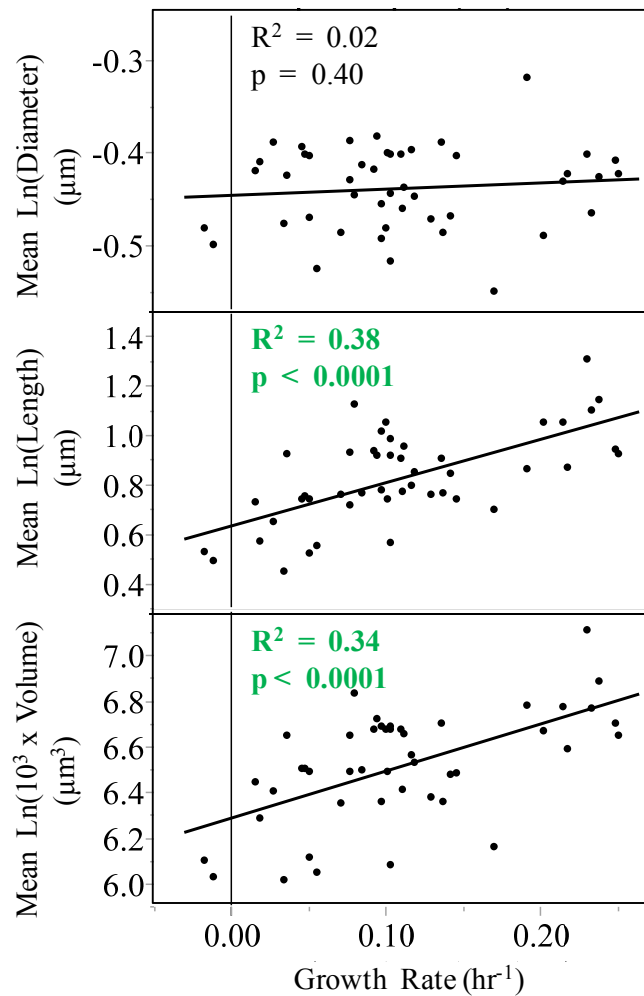


Figure 2.5 Cell length and volume, but not diameter, correlate with growth rate. Culture means for log-transformed cell diameter, cell length, and cell volume are plotted versus observed culture growth rate. Cell length and volume exhibit an increasing relationship with growth rate, while cell diameter is largely independent of growth rate. These trends indicate that *C. tepidum* largely mediates changes in cell size by changes in length and not diameter.

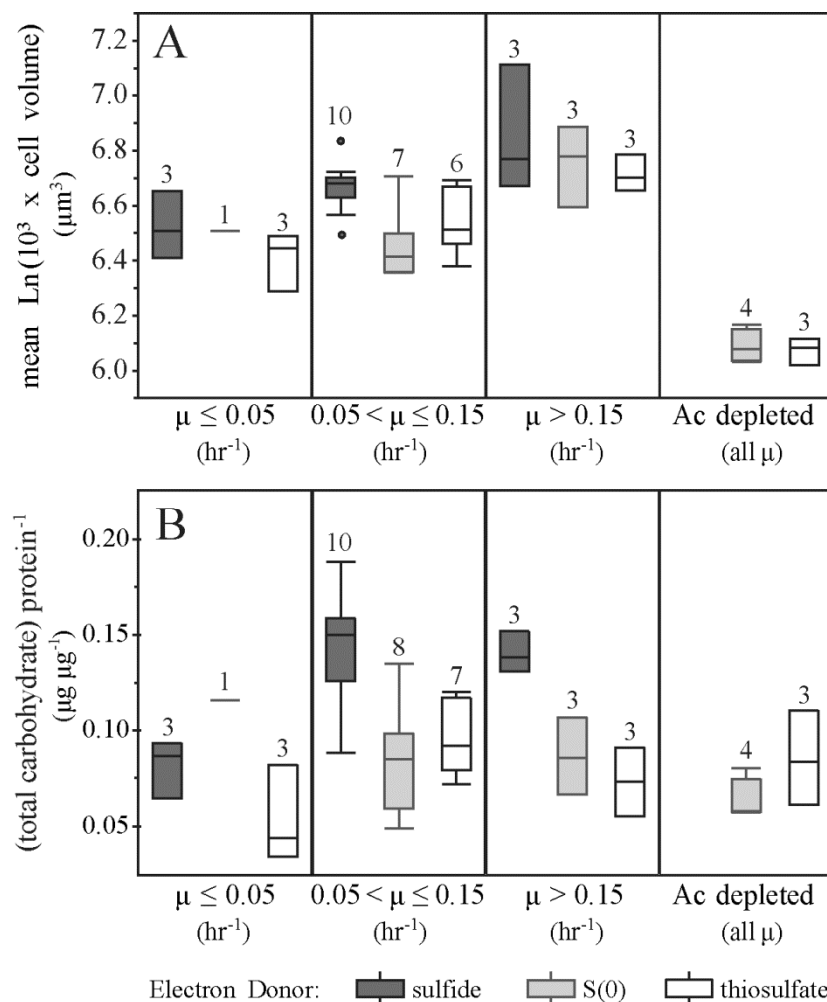


Figure 2.6 Effect of electron donor and acetate depletion on cell volume and storage carbohydrate accumulation across cultures of different growth rates. Box-and-whisker plots of (A) culture-averaged log-transformed cell volumes and (B) total culture carbohydrate normalized to culture protein binned by growth rate and classified by electron donor identity and acetate (Ac) availability. The number of cultures for each grouping is indicated above the box. Acetate was fully depleted by the 26 hour timepoint for S⁰- and thiosulfate-grown cultures at the middle (20 $\mu\text{mol photons m}^{-2} \text{s}^{-1}$) and high (35 $\mu\text{mol photons m}^{-2} \text{s}^{-1}$) light levels. S(0) = S⁰.

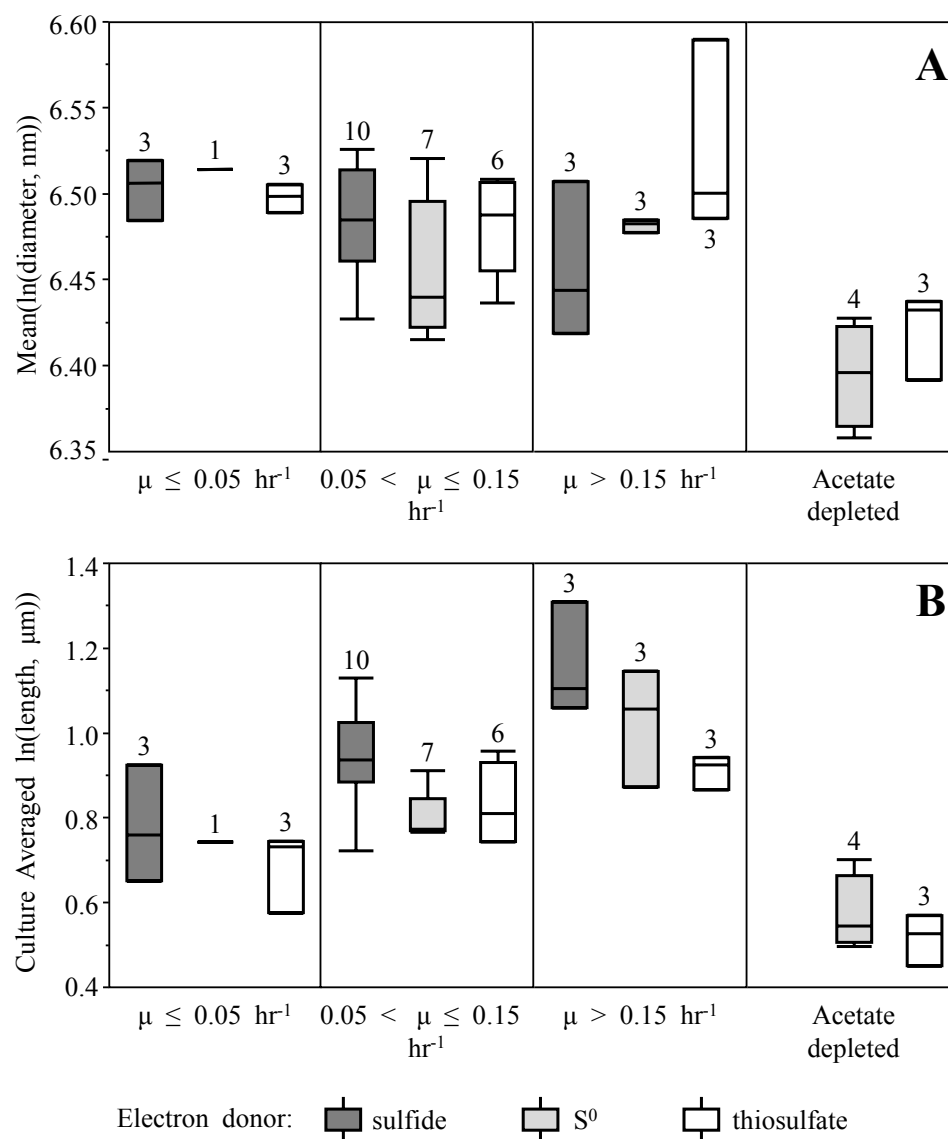


Figure 2.7 Variation of cell diameter (A) and length (B) with growth rate, electron donor, and acetate availability. Standard box-and-whisker plots showing the distribution of culture-averaged log-transformed dimension measurements.

2.4.4 *C. tepidum* amino acid composition varies across the energy landscape

The bulk amino acid composition of *C. tepidum* biomass as determined from the AAA measurements (Fig. 2.8) exhibited statistically significant changes across the

energy landscape. Multivariate analysis of variance (MANOVA) produced a highly significant ($p \leq 0.0001$) second-order interaction model (see methods), revealing that electron donor ($p = 0.0006$), light ($p < 0.0001$), and culture duration ($p = 0.002$) affected the abundance of specific amino acids (where the interaction of light and duration had a weak effect, $p = 0.04$). Electron donor had the most significant effect on Gly ($p < 0.0001$; Fig. 2.9A), which was enriched on sulfide and depleted on thiosulfate. Increasing light decreased Asx content ($p = 0.0003$; Fig. 2.9D) and enriched for Lys ($p = 0.0015$; Fig. 2.9F). Increased culture duration enriched for Pro ($p = 0.0008$; Fig. 2.9C) and decreased Arg ($p = 0.002$; Fig. 2.9B) and Gly ($p = 0.007$; Fig. 2.9-A).

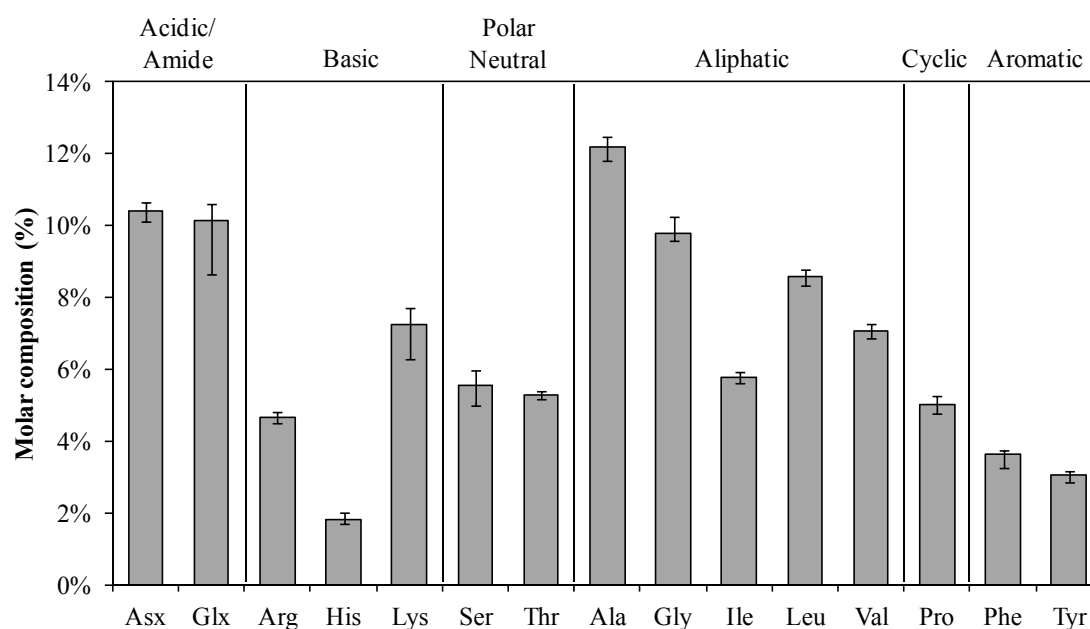


Figure 2.8 Average amino acid composition of unextracted, whole (WH) *C. tepidum* biomass. Columns represent the mean molar amino acid composition observed for WH samples from $N = 29$ independent cultures of *C. tepidum* (Table 2.1); error bars represent the full range of values observed.

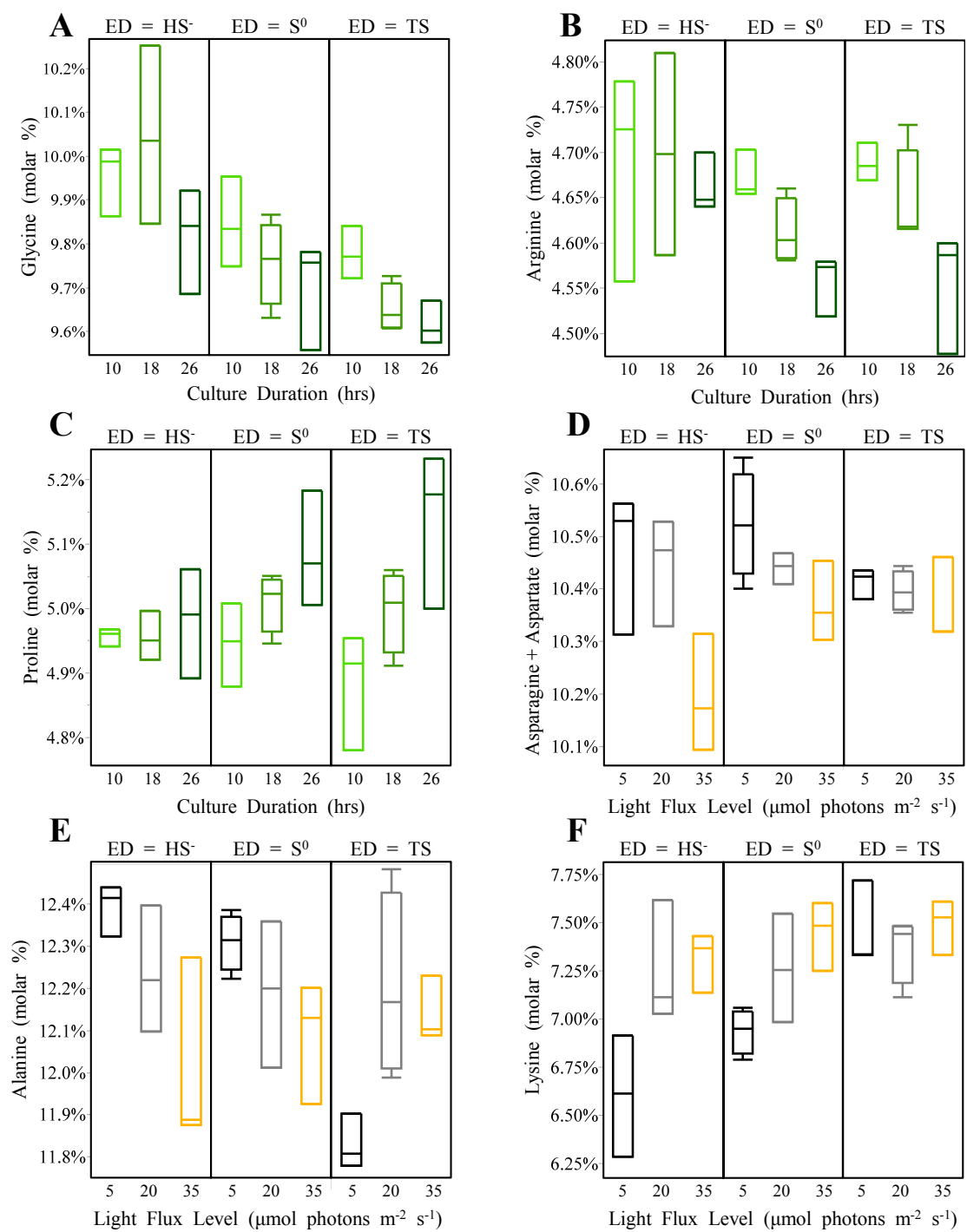


Figure 2.9 The composition of certain amino acids varied in response to electron donor identity, light, and culture duration. Standard box-and-whisker plots depict trends in measured amino acid compositions for cultures at the specified conditions. (A) Gly negatively correlated with culture duration and is enriched by sulfide; (B) Arg negatively correlated with culture duration (S^0 and thiosulfate only) (C) Pro positively correlated with culture duration (S^0 and thiosulfate only); (D) Asn + Asp negatively correlated with light flux level (HS^- and S^0 only) (E) Ala negatively correlated with light (sulfide and S^0 only); (F) Lys positively correlated with light (sulfide and S^0 only). HS^- = sulfide; TS = thiosulfate.

2.4.5 Light flux affects biomass amino acid composition according to amino acid biosynthetic cost

A closer inspection revealed that light induced more subtle changes to nearly all amino acids: high light flux enriched for amino acids with high biosynthetic ATP requirements, while low light flux enriched for amino acids with low biosynthetic ATP costs (Fig. 2.10A; values for photosynthetic bacteria from (Smith & Chapman 2010)). When the cost of amino acid synthesis for *C. tepidum* biomass ($\sim P_{avg}$) was calculated, using the amino acid composition data and the energetic costs of synthesizing each amino acid in terms of ATP required per amino acid (Smith & Chapman 2010), $\sim P_{avg}$ was positively correlated with light flux (Fig. 2.10B; $p = 0.002$ for light as a single factor; $p = 0.0008$ when including culture duration as a non-linear effect). The mean change in $\sim P_{avg}$ between the low and high light conditions was 0.14 ± 0.04 ATP (amino acid) $^{-1}$. Different amino acids did not contribute equally to the change in $\sim P_{avg}$ – for example Lys was the largest contributor while Pro and Thr slightly opposed the overall trend (Table 2.4). However, excluding individual amino acids from the $\sim P_{avg}$ calculation did not eliminate the relationship between $\sim P_{avg}$ and light flux (Table 2.5), consistent with a globally coordinated alteration of biomass composition.

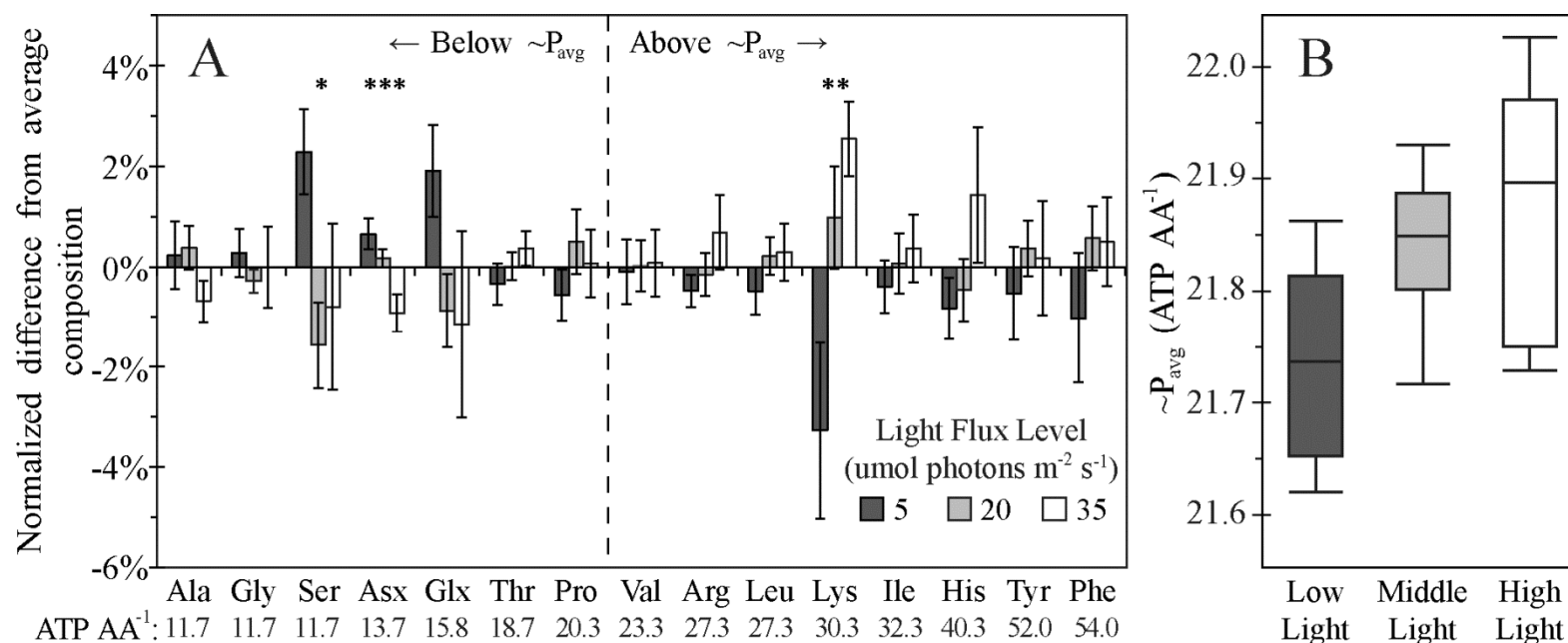


Figure 2.10 Light level affects variation in amino acid abundance according to biosynthetic cost. (A) Mean values of the normalized difference from the average composition are plotted as a function of light; statistical significance: * $p < 0.05$; ** $p < 0.01$; *** $p < 0.001$. Amino acids are arranged in order of increasing biosynthetic cost (ATP required per amino acid molecule) using values for phototrophic bacteria (45). The average amino acid biosynthetic cost for *C. tepidum* biomass (21.8 ATP (amino acid)⁻¹) is indicated by the vertical dashed line. Error bars represent the standard error of the mean within each light level. (B) Box-and-whisker plot representation of the distribution of the measured $\sim P_{avg}$ values for low, middle and high light.

Table 2.4 Changed abundance of amino acids in *C. tepidum* biomass did not contribute equally to the observed changes in $\sim P_{\text{avg}}$.

Amino Acid	Relative contribution to changes in $\sim P_{\text{avg}}$
Lys	26%
Glx	13%
Phe	13%
Ser	12%
Asx	9.4%
Ala	7.9%
His	5.4%
Tyr	4.7%
Ile	3.3%
Leu	2.6%
Arg	2.1%
Gly	2.0%
Val	1.3%
Pro	-0.32%
Thr	-0.80%

Table 2.5 Effect of excluding individual amino acids from the calculation of $\sim P_{\text{avg}}$ on the light-effect parameter B_1 in the relationship between $\sim P_{\text{avg}}$ and light.

Excluded amino acid(s)	Overall model ^a significance by F-test	B_1 parameter value ^a	B_1 parameter significance
None	0.0013	0.073	0.0008
Lys	0.0053	0.058	0.0048
Glx	0.0021	0.069	0.0010
Phe	0.0030	0.065	0.0011
Ser	0.0025	0.068	0.0022
Asx	0.0033	0.074	0.0023
Ala	0.0012	0.076	0.0008
His	0.0021	0.071	0.0014
Tyr	0.0009	0.071	0.0004
Lys, Glx	0.0082	0.054	0.0054
Lys, Glx, Phe	0.0147	0.043	0.0058

^a Modeled relationship between $\sim P_{\text{avg}}$ and light:

$$P_{\text{avg}} = B_0 + B_1 \times (\text{light}) + B_2 \times (\text{culture duration})^2$$

As *C. tepidum* is known to increase its BChl *c* content and chlorosome volume fraction in response to decreased light flux (Morgan-Kiss et al. 2009; Borrego et al. 1999), we considered the possibility that the observed bias in amino acid composition at low light could be the result of increased abundance of chlorosome-associated proteins. The BChl *c*:protein ratio increased with decreasing light for sulfide and S⁰-grown cultures as expected (Fig. 2.11A), although this trend did not occur for thiosulfate-grown cultures (see section 3.4.7 for further discussion). We found that BChl *c*:protein strongly correlated with the overall amino acid composition ($p = 0.0003$ by MANOVA), and cultures with similar BChl *c*:protein clustered together in a principal components analysis plot (Fig. 2.11B). However, BChl *c*:protein did not correlate with $\sim P_{\text{avg}}$ ($p = 0.8$; Fig. 2.11C), suggesting that the bias in composition towards amino acids with lower biosynthetic costs is not merely the result of increased chlorosome and chlorosome protein abundance.

There was no correlation between $\sim P_{\text{avg}}$ and growth rate ($p = 0.8$; data not shown). All cultures achieved exponential growth with maximal rates observed from 0-10 hours. Growth rates for low-light cultures were slower for all electron donors ($\mu = 0.09\text{-}0.11 \text{ hr}^{-1}$) than middle- ($0.19\text{-}0.22 \text{ hr}^{-1}$) and high-light cultures ($0.23\text{-}0.25 \text{ hr}^{-1}$). Growth rates slowed after 10 hours for cultures grown at middle (by 37-62%) and high light (by 65-76%), but cultures continued to grow through 26 hours.

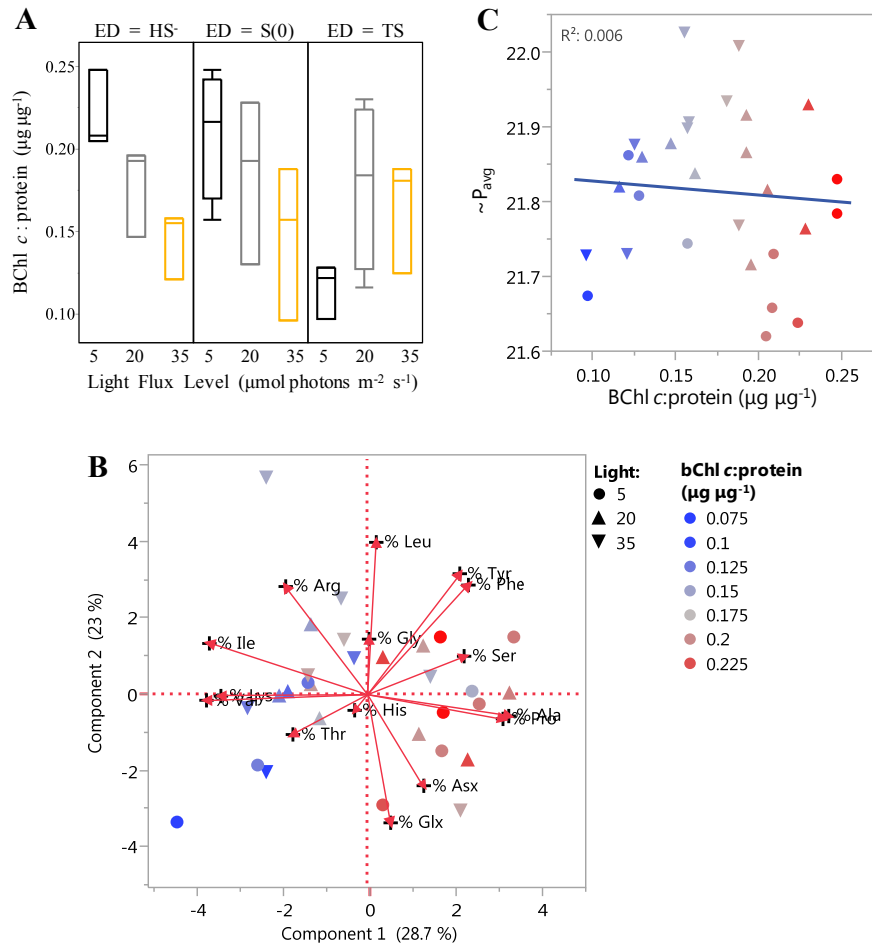


Figure 2.11 Overall amino acid composition varied with BChl *c* content, but BChl *c* content did not correlate with $\sim P_{\text{avg}}$. (A) Box-and-whisker plot showing the distribution of BChl *c*:protein ratio observed for cultures as a function of light for each electron donor. The BChl *c*:protein ratio negatively correlated with light flux level for sulfide and S⁰ grown cells, but not for thiosulfate grown cells. (B) Principal component analysis diagram depicting the variation of amino acid composition across the multivariate space; each point represents a culture, and the points are colored according to the measured ratio of BChl *c*:protein. Cultures with similar BChl *c*:protein are observed to cluster together on the plot, demonstrating the relationship between BChl *c*:protein and the overall amino acid composition. (C) Although BChl *c*:protein correlated with overall amino acid composition (MANOVA, $p = 0.0003$), BChl *c*:protein did not correlate with $\sim P_{\text{avg}}$ ($p = 0.8$; $R^2 = 0.006$).

2.5 Discussion

2.5.1 Prior extraction of biomass samples improves accuracy of indirect protein assays

Bradford and BCA protein assays are simple, rapid, and inexpensive, yet exhibit protein-to-protein variability, measure protein indirectly relative to a chosen protein standard, and are subject to interference from a range of compounds including photosynthetic pigments (Sapan et al. 1999). As *C. tepidum* pigment content changes in response to electron donor (Chan, Weber, et al. 2008), light (Borrego et al. 1999; Morgan-Kiss et al. 2009), and culture duration, we used cultures grown across the energy landscape to examine this interference using amino acid analysis (AAA) as a ‘gold standard’ for protein quantitation (Smith 1997).

This work established that BCA-EX measurements provided good overall accuracy in predicting *C. tepidum* protein without correction. This method should provide a convenient and more generally applicable method of protein determination for photosynthetic biomass samples. Slightly improved accuracy was obtained from BrR-EX and BrS-EX measurements with an empirical correction function (Table 2.3; Fig. 2.2). However, we expect that the correction factor will vary between organisms based on different pigment content, and therefore the correction would need to be determined for each organism independently. This study provides a roadmap for how to carry out such a correction if desired.

2.5.2 Extractable pools inferred from protein analyses

Pigments are typically removed by methanol extraction, and we found that this treatment introduced changes in biomass amino acid composition by preferential extraction of alanine, proline, and glutamate/glutamine. This result was interpreted to

be the loss of free intracellular amino acid pools in *C. tepidum*, as these amino acids are observed as free pools in other microorganisms (Brown & Stanley 1972; Clark et al. 1972). Prior studies on *C. tepidum* indicate that glutamine synthase/glutamine aminotransferase (GS/GOGAT) is the main route for ammonium assimilation in *C. tepidum* (Wahlund & Madigan 1993), which would be expected to contribute to free pools of glutamate and glutamine. Alanine dehydrogenase (ADH) has been suggested as an alternative ammonium assimilation pathway in *Chlorobium chlorochromatii* (Cerqueda-García et al. 2014), which is consistent with our observation of an extractable alanine pool. This hypothesis is further supported by *C. tepidum* transcriptome sequencing data (Eddie & Hanson 2013) which showed that genes for GS/GOGAT (*CT1411*, *CT0401-0402*) and ADH (*CT0650*, *CT0706*) were expressed at similar levels. The significance of free proline in *C. tepidum* is not clear, but free proline pools have been associated with osmotic stress (Brown & Stanley 1972; Ellar 1978; Neidhardt et al. 1990), where converting glutamate to proline enables an increase in intracellular solute concentration without requiring additional positively-charged solutes to balance charge (Ellar 1978).

The over-estimation of protein by BCA-WH measurements, but not BCA-EX, for a subset of the energy landscape treatments provides evidence for the transient accumulation of an intracellular, methanol-extractable compound that increases the reduction of Cu(II) to Cu(I) in the BCA assay. The increase in BCA-WH protein signal was predominantly observed in cells grown on sulfide or S⁰, particularly at short culture durations or low light (Fig. 2.4), and was not present in cultures grown with thiosulfate as the electron donor or where the electron donor was largely exhausted. The increase in BCA-WH could be due to intracellular pools of sulfide or

polysulfide, which have been detected in *C. tepidum* (unpublished data). Intracellular pools of polysulfides but not sulfide have also been observed in the purple sulfur bacterium *Allochromatium vinosum* (Franz et al. 2009). While intracellular pools of thiosulfate and sulfite have been previously quantified in *C. tepidum* (Rodriguez et al. 2011; Hiras 2012), these compounds are not soluble in methanol and would be unlikely to be extracted.

2.5.3 *C. tepidum* cell size changes suggest the formation of storage compounds

Positive relationships of growth rate and cell size for heterotrophic bacteria such as *Escherichia coli* and *Salmonella typhimurium* are textbook material (Neidhardt et al. 1990), but whether this property translates to less well studied systems like *C. tepidum* is not clear. Growth rate and cell size correlate across different species of cyanobacteria and heterotrophic bacteria, but data on changes within a given species are lacking (Kirchman 2016). Cell size was observed to correlate with growth rate for *Chromatium minus*, a purple sulfur phototrophic bacterium, where large variations in cell volume among cells of a constant growth rate were attributed to intracellular storage of sulfur and glycogen (Montesinos 1987). The *Chlorobiaceae* synthesize glycogen in the light as a carbon storage compound and ferment the stored glycogen in the dark to provide maintenance energy (Sirevåg & Ormerod 1977; Sirevåg 1975; Badalamenti et al. 2014; Overmann 2006; Habicht et al. 2011).

After accounting for growth rate differences, *C. tepidum* cells grown on sulfide were larger than on S^0 or thiosulfate, a difference that appears to be due to the accumulation of glycogen in sulfide-grown cells (Fig. 2.6B). While degradation of glycogen was previously described upon the transition from sulfide oxidation to S^0

oxidation for Chromatiaceae species (van Gemerden & Beftink 1978; Schmidt & Kamen 1970), this work directly compares glycogen production during oxidation of different electron donors in the *Chlorobiaceae*. Enhanced glycogen storage on sulfide suggests that *C. tepidum* may use glycogen synthesis in part to cope with and/or store excess reducing power available during sulfide oxidation. This hypothesis is consistent with the induction of a high velocity, low affinity sulfide:quinone oxidoreductase (CT1087) whose physiological role seems to be primarily sulfide tolerance (Chan et al. 2009; Eddie & Hanson 2013; Shuman & Hanson 2016).

The parallel effect of culture parameters on cell length and volume, but not on cell diameter, suggests that *C. tepidum* modulates cell size by altering length rather than diameter. Because *C. tepidum* chlorosomes are arranged at the perimeter of cells, chlorosome concentration per unit cell volume will be maximized by a smaller diameter. Thus, maintaining cell diameter may be advantageous for maximizing the light harvesting potential of the cells.

2.5.4 Amino acid composition changes induced by energy landscape parameters suggest biosynthetic streamlining at low energy can be observed with bulk measurements

At the outset, we did not expect to observe significant changes in amino acid composition across the energy landscape because we felt that protein expression changes would be too subtle to be detected in bulk biomass measurements. However, the data clearly indicate that *C. tepidum* biomass composition detectably shifts across the energy landscape. Furthermore, these shifts appear to be sensible in the context of the energy landscape when interpreted based on the energetics of amino acid biosynthesis. The $\sim P_{\text{avg}}$ decreased in response to decreased light flux, amounting to a difference of 0.14 ± 0.04 ATP (amino acid)⁻¹ from the high to the low light conditions

(Fig. 2.10B), which translates to a savings in amino acid synthesis costs of 0.64% from 21.87 ATP (amino acid)⁻¹ at high light. As noted above, tryptophan, the most energetically expensive amino acid (76.3 ATP (amino acid)⁻¹ (Smith & Chapman 2010)), is not measurable by the amino acid analysis method employed. Trp shares chorismate as a biosynthetic intermediate with Phe and Tyr, which both contribute positively to the $\sim P_{\text{avg}}$ change in response to light. Thus we expect that Trp would also positively contribute to an observed change in $\sim P_{\text{avg}}$.

This bias by *C. tepidum* towards using less energetically expensive amino acids at reduced light flux could potentially be an evolved response for coping with ATP limitation, as Chlorobiaceae are adapted to lower light flux than other phototrophs (Imhoff 2006; Biebl & Pfennig 1978). Interestingly, the first and third lowest-cost proteins in the *C. tepidum* proteome on a per amino acid basis (calculated using from the approach of Smith and Chapman (Smith & Chapman 2010)) are associated with light harvesting (chlorosome proteins CsmD and CsmF), and the fourth lowest-cost protein is associated with ATP generation (the ATP synthase subunit c).

Efficiency in the primary sequence of proteins has been observed previously: highly expressed bacterial genes (as assessed by major codon usage) tend to code for proteins that use less energetically expensive amino acids (Akashi & Gojobori 2002; Heizer et al. 2006; Raiford et al. 2012), and extracellular proteins tend to be composed of less energetically expensive amino acids than intracellular and membrane proteins (Smith & Chapman 2010). Furthermore, a survey of yeast transcriptomic data found that resource limitations (e.g. salt stress, reduced exogenous amino acid availability, etc.) induced gene expression changes that varied inversely with the length of the

coded proteins (Vilaprinyo et al. 2010). However, whereas these previous studies were based on inferences from bioinformatic analyses and ‘omic datasets, this work reports an experimentally measured shift in an organism’s bulk amino acid composition in response to growth conditions. That the bias toward amino acids with lower biosynthetic cost appears independent of BChl *c* content (Fig. 2.11C) suggests that this effect is the result of global changes in *C. tepidum* protein expression, and possibly evolved efficiency in the primary sequence of proteins important at low light, rather than a mere consequence of increased chlorosome expression.

While a 0.64% cost savings in the energy requirements of amino acid synthesis on first glance appears quite small, long term evolutionary success can be built on such incremental advances. Estimating that amino acid biosynthesis accounts for 57% of the cellular energy budget for a reverse tricarboxylic acid cycle autotroph (Mangiapietra & Scott 2016), this change in $\sim P_{\text{avg}}$ would translate to a 0.37% increase in growth rate, enabling a 10^{-6} initial proportion of the population to achieve greater than 99% of the population within 7,300 doublings. This timeframe is roughly 20 years, assuming a doubling time of 8 hours, which is consistent with the measured growth rate of *C. tepidum* at the low light conditions of this study. While this timeframe is long compared to typical laboratory growth experiments, twenty years is short compared to evolutionary timescales; for example, there is evidence that populations of green sulfur bacteria have consistently occurred in the Mediterranean Sea for over 200,000 years (Coolen & Overmann 2007), and potentially longer than 2 million years (Passier et al. 1999), and that purple sulfur bacteria have inhabited Mahoney Lake for over 9,000 years (Coolen & Overmann 1998). Furthermore, the energy savings and selection coefficient for this advantage ($2.5 \times 10^{-3} \text{ gen}^{-1}$; calculated by Dykhuizen

1990) are similar to the advantage for switching from low-frequency to high-frequency codons in highly expressed proteins (Brandis & Hughes 2016; Akashi & Gojobori 2002).

Given that the biases in the cost of amino acid synthesis were detectable by bulk analysis of biomass rather than by fine-grained ‘-omics’-type analyses emphasizes the role that energy flux may play in the evolved adaptations of organisms and provides experimental evidence for evolved efficiencies in microbial proteomes. Thus, future systems-based studies that explore the response of *C. tepidum* and other environmental microbes to changing energy flux have the potential to provide deeper insight into the environmental pressures that have shaped proteins critical for life in low energy flux environments.

2.6 Concluding remarks

The factorial approach employed in this work, coupled with efforts to reduce culturing variability and establish robust biomass quantitation, enabled a systematic analysis of the effects of electron donor, light flux level, and culture duration, as well as their interacting effects, on the physiology of *C. tepidum*. Through the range of treatments produced by this approach, protein-based biomass quantitation methods were calibrated and previously unidentified traits of *C. tepidum* were revealed. These include changes in glycogen storage as a function of electron donor and overall biomass amino acid composition in response to growth conditions. Our observation of a bias in the amino acid composition toward less energetically expensive amino acids under low light conditions provides a ‘real-time’ experimental observation of whole-biomass amino acid compositional shifts in response to energy limitation. Thus measures of biomass amino acid composition have the potential to provide a simple,

useful means to assess and diagnose energy stress or adaptations in applications such as bioreactor process monitoring. The experimental design approach employed here enabled simultaneous examination of multiple factors that revealed subtle and interacting-factor effects, which would have remained hidden in studies with single-factor designs. The generalized approach of carefully designed ‘landscape’ type studies can be extended to many other systems to enable the identification of previously undetected interactions in problems impacted by multiple interacting factors.

2.7 Acknowledgments

The authors would like to thank Cassandra Marnocha and Clara Chan for assistance with microscopy techniques and use of equipment. The authors are grateful to Jacob Hilzinger for sharing information on *C. tepidum*’s internal metabolite pools and to Kathleen Scott (University of South Florida) for help estimating amino acid synthesis cost in the context of the cellular energy budget. Amino acid analysis was performed by the Molecular Structure Facility at the University of California at Davis.

REFERENCES

- Akashi, H. & Gojobori, T., 2002. Metabolic efficiency and amino acid composition in the proteomes of *Escherichia coli* and *Bacillus subtilis*. *Proceedings of the National Academy of Sciences of the United States of America*, 99(6), pp.3695–3700.
- Azai, C., Harada, J. & Oh-oka, H., 2013. Gene expression system in green sulfur bacteria by conjugative plasmid transfer. *PLoS ONE*, 8(11), e82345. doi:10.1371/journal.pone.0082345.
- Badalamenti, J.P., Torres, C.I. & Krajmalnik-Brown, R., 2014. Coupling dark metabolism to electricity generation using photosynthetic cocultures. *Biotechnology and Bioengineering*, 111(2), pp.223–231.
- Biebl, H. & Pfennig, N., 1978. Growth yields of green sulfur bacteria in mixed cultures with sulfur and sulfate reducing bacteria. *Archives of Microbiology*, 117(1), pp.9–16.
- Borrego, C.M. et al., 1999. Light intensity effects on pigment composition and organisation in the green sulfur bacterium *Chlorobium tepidum*. *Photosynthesis Research*, 59, pp.159–166.
- Brandis, G. & Hughes, D., 2016. The selective advantage of synonymous codon usage bias in *Salmonella*. *PLoS Genetics*, 12(3), e1005926. doi:10.1371/journal.pgen.1005926.
- Brown, C.M. & Stanley, S.O., 1972. Environment-mediated changes in the cellular content of the “pool” constituents and their associated changes in cell physiology. *Journal of Applied Chemistry and Biotechnology*, 22(3), pp.363–389.
- Cerqueda-García, D. et al., 2014. Metabolic analysis of *Chlorobium chlorochromatii* CaD3 reveals clues of the symbiosis in “*Chlorochromatium aggregatum*.” *The ISME Journal*, 8(5), pp.991–998.
- Chan, L.-K., Weber, T.S., et al., 2008. A genomic region required for phototrophic thiosulfate oxidation in the green sulfur bacterium *Chlorobium tepidum* (syn. *Chlorobaculum tepidum*). *Microbiology*, 154(3), pp.818–829.

- Chan, L.-K., Morgan-Kiss, R.M. & Hanson, T.E., 2009. Functional analysis of three sulfide:quinone oxidoreductase homologs in *Chlorobaculum tepidum*. *Journal of Bacteriology*, 191(3), pp.1026–1034.
- Chan, L.-K., Morgan-Kiss, R.M. & Hanson, T.E., 2008. Genetic and proteomic studies of sulfur oxidation in *Chlorobium tepidum* (syn. *Chlorobaculum tepidum*). In R. Hell et al., eds. *Sulfur Metabolism in Phototrophic Organisms*. Advances in Photosynthesis and Respiration. Dordrecht, The Netherlands: Springer Science & Business Media, pp. 357–373.
- Clark, V.L., Peterson, D.E. & Bernlohr, R.W., 1972. Changes in free amino acid production and intracellular amino acid pools of *Bacillus licheniformis* as a function of culture age and growth media. *Journal of Bacteriology*, 112(2), pp.715–725.
- Coolen, M.J.L. & Overmann, J., 2007. 217 000-year-old DNA sequences of green sulfur bacteria in Mediterranean sapropels and their implications for the reconstruction of the paleoenvironment. *Environmental Microbiology*, 9(1), pp.238–249.
- Coolen, M.J.L. & Overmann, J., 1998. Analysis of subfossil molecular remains of purple sulfur bacteria in a lake sediment. *Applied and Environmental Microbiology*, 64(11), pp.4513–4521.
- Dahl, C. & Prange, A., 2006. Bacterial sulfur globules: occurrence, structure and metabolism. In J. M. Shivley, ed. *Inclusions in Prokaryotes*. Microbiology Monographs. Berlin: Springer-Verlag, pp. 21–51.
- Dykhuizen, D.E., 1990. Experimental studies of natural selection in bacteria. *Annual Review of Ecology and Systematics*, 21(1), pp.373–398.
- Eddie, B.J. & Hanson, T.E., 2013. *Chlorobaculum tepidum* TLS displays a complex transcriptional response to sulfide addition. *Journal of Bacteriology*, 195(2), pp.399–408.
- Eisen, J.A. et al., 2002. The complete genome sequence of *Chlorobium tepidum* TLS, a photosynthetic, anaerobic, green-sulfur bacterium. *Proceedings of the National Academy of Sciences of the United States of America*, 99(14), pp.9509–9514.
- Ellar, D.J., 1978. Some strategies of osmoregulation and ion transport in microorganisms. In K. Schmidt-Nielsen, L. Bolis, & S. H. P. Maddrell, eds. *Comparative Physiology: Water, Ions, and Fluid Mechanics*. New York: Cambridge University Press, pp. 125–150.

- Ernst, O. & Zor, T., 2010. Linearization of the Bradford Protein Assay. *Journal of Visualized Experiments*, 38, e1918. doi:10.3791/1918.
- Fortuny, M. et al., 2010. Oxidation of biologically produced elemental sulfur under neutrophilic conditions. *Journal of Chemical Technology & Biotechnology*, 85(3), pp.378–386.
- Franz, B. et al., 2009. Unexpected extracellular and intracellular sulfur species during growth of *Allochromatium vinosum* with reduced sulfur compounds. *Microbiology*, 155(2009), pp.2766–2774.
- Frigaard, N.-U. & Bryant, D.A., 2001. Chromosomal gene inactivation in the green sulfur bacterium *Chlorobium tepidum* by natural transformation. *Applied and Environmental Microbiology*, 67(6), pp.2538–2544.
- Frigaard, N.-U., Voigt, G.D. & Bryant, D.A., 2002. *Chlorobium tepidum* mutant lacking bacteriochlorophyll *c* made by inactivation of the *bchK* gene, encoding bacteriochlorophyll *c* synthase. *Journal of Bacteriology*, 184(12), pp.3368–3376.
- van Gernerden, H. & Beefink, H.H., 1978. Specific rates of substrate oxidation and product formation in autotrophically growing *Chromatium vinosum* cultures. *Archives of Microbiology*, 119(2), pp.135–143.
- Habicht, K.S. et al., 2011. Comparative proteomics and activity of a green sulfur bacterium through the water column of Lake Cadagno, Switzerland. *Environmental Microbiology*, 13(1), pp.203–215.
- Hanson, R.S. & Phillips, J.A., 1981. Chemical Composition. In P. Gerhardt et al., eds. *Manual of Methods for General Bacteriology*. Washington, DC: American Society for Microbiology, pp. 328–364.
- Hanson, T.E. et al., 2016. *Chlorobaculum tepidum* growth on biogenic S(0) as the sole photosynthetic electron donor. *Environmental Microbiology*, 18(9): pp.2856–2867.
- Hanson, T.E. & Tabita, F.R., 2001. A ribulose-1,5-biophosphate carboxylase/oxygenase (RubisCO)-like protein from *Chlorobium tepidum* that is involved with sulfur metabolism and the response to oxidative stress. *Proceedings of the National Academy of Sciences of the United States of America*, 98(8), pp.4397–4402.

- Heizer, E.M. et al., 2006. Amino acid cost and codon-usage biases in 6 prokaryotic genomes: A whole-genome analysis. *Molecular Biology and Evolution*, 23(9), pp.1670–1680.
- Hiras, J., 2012. *Characterization of a novel redox active thiol from Chlorobaculum tepidum*. Doctoral Dissertation, University of Delaware. United States of America.
- Holkenbrink, C. et al., 2011. Sulfur globule oxidation in green sulfur bacteria is dependent on the dissimilatory sulfite reductase system. *Microbiology*, 157, pp.1229–1239.
- Imhoff, J.F., 2006. The *Chromatiaceae*. In M. Dworkin et al., eds. *The Prokaryotes - Volume 6: Proteobacteria: Gamma Subclass*. Singapore: Springer Science+Business Media, L.L.C., pp. 846–873.
- Janssen, A.J.H., Ruitenberg, R. & Buisman, C.J.N., 2001. Industrial applications of new sulphur biotechnology. *Water Science and Technology*, 44(8), pp.85–90.
- Johnson, D.B., 2014. Biomining - biotechnologies for extracting and recovering metals from ores and waste materials. *Current Opinion in Biotechnology*, 30, pp.24–31.
- Kirchman, D.L., 2016. Growth Rates of Microbes in the Oceans. *Annual Review of Marine Science*, 8(1), pp.285–309.
- Kleinjan, W.E., de Keizer, A. & Janssen, A.J.H., 2003. Biologically produced sulfur. In R. Steudel, ed. *Elemental Sulfur and Sulfur-Rich Compounds I*. Topics in Current Chemistry. New York, NY: Springer-Verlag, pp. 167–188.
- Lavik, G. et al., 2009. Detoxification of sulphidic African shelf waters by blooming chemolithotrophs. *Nature*, 457(7229), pp.581–584.
- Lens, P.N.L. & Kuenen, J.G., 2001. The biological sulfur cycle: novel opportunities for environmental biotechnology. *Water science and technology*, 44(8), pp.57–66.
- Levy, A.T., Lee, K.H. & Hanson, T.E., 2016. *Chlorobaculum tepidum* modulates amino acid composition in response to energy availability, as revealed by a systematic exploration of the energy landscape of phototrophic sulfur oxidation. *Applied and Environmental Microbiology*, 82(21), pp.6431–6439.

- Leyva, A. et al., 2008. Rapid and sensitive anthrone-sulfuric acid assay in microplate format to quantify carbohydrate in biopharmaceutical products: Method development and validation. *Biologicals*, 36(2), pp.134–141.
- Macalady, J.L. et al., 2013. Energy, ecology and the distribution of microbial life. *Philosophical transactions of the Royal Society of London. Series B, Biological sciences*, 368, 20120383. doi:10.1098/rstb.2012.0383.
- Mangiapiia, M. & Scott, K., 2016. From CO₂ to cell: Energetic expense of creating biomass using the Calvin-Benson-Bassham and reductive citric acid cycles based on genome data. *FEMS Microbiology Letters*, 363(7), fnw054. doi:10.1093/femsle/fnw054.
- Mead, R., Gilmour, S.G. & Mead, A., 2012. *Statistical Principles for the Design of Experiments: Applications to Real Experiments.*, New York: Cambridge University Press.
- Montesinos, E., 1987. Change in Size of *Chromatium minus* cells in relation to growth rate, sulfur content, and photosynthetic activity: a comparison of pure cultures and field populations. *Applied and Environmental Microbiology*, 53(4), pp.864–871.
- Morgan-Kiss, R.M. et al., 2009. *Chlorobaculum tepidum* regulates chlorosome structure and function in response to temperature and electron donor availability. *Photosynthesis Research*, 99(1), pp.11–21.
- Mukhopadhyay, B., Johnson, E.F. & Ascano, M., 1999. Conditions for vigorous growth on sulfide and reactor-scale cultivation protocols for the thermophilic green sulfur bacterium *Chlorobium tepidum*. *Applied and Environmental Microbiology*, 65(1), pp.301–306.
- Neidhardt, F.C., Ingraham, J.L. & Schaechter, M., 1990. *Physiology of the Bacterial Cell.*, Sunderland, MA: Sinauer Associates, Inc.
- Ogunnaike, B.A., 2010. Design of Experiments. In *Random Phenomena: Fundamentals of Probability and Statistics for Engineers*. Boca Raton, FL: CRC Press, pp. 787–849.
- Overmann, J., 2006. The Family *Chlorobiaceae*. In M. Dworkin et al., eds. *The Prokaryotes Volume 7: Proteobacteria: Delta and Epsilon Subclasses. Deeply Rooting Bacteria*. Singapore: Springer Science+Business Media, L.L.C., pp. 359–378.

- Passier, H.F. et al., 1999. Sulphidic Mediterranean surface waters during Pliocene sapropel formation. *Nature*, 397(6715), pp.146–149.
- Raiford, D.W. et al., 2012. Metabolic and translational efficiency in microbial organisms. *Journal of Molecular Evolution*, 74(3–4), pp.206–216.
- Rawlings, D.E., 2005. Characteristics and adaptability of iron- and sulfur-oxidizing microorganisms used for the recovery of metals from minerals and their concentrates. *Microbial Cell Factories*, 4, 13. doi:10.1186/1475-2859-4-13.
- Rethmeier, J. et al., 1997. Detection of traces of oxidized and reduced sulfur compounds in small samples by combination of different high-performance liquid chromatography methods. *Journal of Chromatography A*, 760(2), pp.295–302.
- Rodriguez, J., Hiras, J. & Hanson, T.E., 2011. Sulfite oxidation in *Chlorobaculum tepidum*. *Frontiers in Microbiology*, 2(May), 112. doi: 10.3389/fmicb.2011.00112.
- Sánchez, O., Van Gernerden, H. & Mas, J., 1998. Utilization of reducing power in light-limited cultures of *Chromatium vinosum* DSM 185. *Archives of Microbiology*, 170(6), pp.411–417.
- Sapan, C. V., Lundblad, R.L. & Price, N.C., 1999. Colorimetric protein assay techniques. *Biotechnology and Applied Biochemistry*, 29, pp.99–108.
- Schmidt, G.L. & Kamen, M.D., 1970. Variable cellular composition of *Chromatium* in growing cultures. *Archiv für Mikrobiologie*, 73, pp.1–18.
- Shuman, K.E. & Hanson, T.E., 2016. A sulfide:quinone oxidoreductase from *Chlorobaculum tepidum* displays unusual kinetic properties. *FEMS Microbiology Letters*, 363(12), fnw100. doi:10.1093/femsle/fnw100.
- Siefert, E. & Pfennig, N., 1984. Convenient method to prepare neutral sulfide solution for cultivation of phototrophic sulfur bacteria. *Archives of Microbiology*, 139(1), pp.100–101.
- Sirevåg, R., 1975. Photoassimilation of acetate and metabolism of carbohydrate in *Chlorobium thiosulfatophilum*. *Archives of Microbiology*, 104(2), pp.105–111.
- Sirevåg, R. & Ormerod, J.G., 1977. Synthesis, Storage, and Degradation of Polyglucose in *Chlorobium thiosulfatophilum*. *Archives of Microbiology*, 111, pp.239–244.

- Smith, A.J., 1997. Postcolumn amino acid analysis. In B. J. Smith, ed. *Protein Sequencing Protocols*. Methods in Molecular Biology. Totowa, New Jersey: Humana Press, pp. 139–146.
- Smith, D.R. & Chapman, M.R., 2010. Economical evolution: Microbes reduce the synthetic cost of extracellular proteins. *mBio*, 1(3), e00131-10-10. doi: 10.1128/mBio.00131-10.
- Stanier, R.Y. & Smith, J.H.C., 1960. The chlorophylls of green bacteria. *Biochimica et Biophysica Acta*, 41, pp.478–484.
- Sturman, P.J. et al., 2008. Sulfur cycling in constructed wetlands. In J. Vymazal, ed. *Wastewater Treatment, Plant Dynamics, and Management in Constructed and Natural Wetlands*. Berlin, Heidelberg: Springer Science + Business Media B.V., pp. 329–344.
- Syed, M. et al., 2006. Removal of hydrogen sulfide from gas streams using biological processes - a review. *Canadian Biosystems Engineering*, 48, p.2.1-2.14.
- Turnbull, T.L., Adams, M.A. & Warren, C.R., 2007. Increased photosynthesis following partial defoliation of field-grown *Eucalyptus globulus* seedlings is not caused by increased leaf nitrogen. *Tree Physiology*, 27(10), pp.1481–1492.
- Vilaprinyo, E., Alves, R. & Sorribas, A., 2010. Minimization of biosynthetic costs in adaptive gene expression responses of yeast to environmental changes. *PLoS Computational Biology*, 6(2), e1000674. doi:10.1371/journal.pcbi.1000674.
- Wahlund, T.M. et al., 1991. A thermophilic green sulfur bacterium from New Zealand hot springs, *Chlorobium tepidum* sp. nov. *Archives of Microbiology*, 156, pp.81–90.
- Wahlund, T.M. & Madigan, M.T., 1995. Genetic transfer by conjugation in the thermophilic green sulfur bacterium *Chlorobium tepidum*. *Journal of Bacteriology*, 177(9), pp.2583–2588.
- Wahlund, T.M. & Madigan, M.T., 1993. Nitrogen fixation by the thermophilic green sulfur bacterium *Chlorobium tepidum*. *Journal of bacteriology*, 175(2), pp.474–478.
- Zor, T. & Selinger, Z., 1996. Linearization of the Bradford protein assay increases its sensitivity: theoretical and experimental studies. *Analytical Biochemistry*, 236(2), pp.302–308.

Zuroff, T.R., Xiques, S.B. & Curtis, W.R., 2013. Consortia-mediated bioprocessing of cellulose to ethanol with a symbiotic *Clostridium phytofermentans*/yeast co-culture. *Biotechnology for Biofuels*, 6(1), 59. doi:10.1186/1754-6834-6-59.

Chapter 3

ANALYSIS OF *CHLOROBACULUM TEPIDUM* SULFUR METABOLISM BY A FACTORIAL APPROACH

3.1 Preface

Several of the figures in this chapter are adapted from Marnocha, Levy, Powell, Hanson, and Chan (2016) with permission (see Appendix A.2). My contributions to that publication were data demonstrating the presence of polysulfides during S^0 production and S^0 degradation and data showing the dynamics of polysulfide compounds during production and degradation of S^0 by *Chlorobaculum tepidum*. These data were published as Fig. 4A, Fig. 4B, and Supplementary Figure S4 in Marnocha et al. (2016), and correspond to Fig. 3.6-A, Fig. 3.8-A, and Fig. 3.7 in this dissertation, respectively. The observation of soluble polysulfides during S^0 production and degradation, combined with the microscopy work and analyses performed by Cassandra Marnocha, led to the proposed model for S^0 generation and degradation that was published as Fig. 7 (Fig. 3.9 in this dissertation). All other data in this chapter were generated by myself, and have not been previously published.

3.1.1 Abstract

This chapter presents insights into *Chlorobaculum tepidum* S^0 metabolism that were enabled by analysis of sulfur metabolism across a factorial space of electron donors (sulfide, elemental sulfur (S^0), and thiosulfate) and light flux levels (5, 20, and 35 $\mu\text{mol photons m}^{-2} \text{s}^{-1}$) called the ‘Energy Landscape’ of phototrophic sulfur

oxidation. Analysis of growth yield on a per-electron basis across the energy landscape revealed that yield on S^0 as electron donor was less than on sulfide and greater than on thiosulfate. Interpreting this observation in the context of electron transport pathways in *C. tepidum* suggests that electrons from oxidation of S^0 to sulfite may not participate in membrane-bound electron transport in *C. tepidum*, in contrast to the pathways outlined in current models. An assessment of sulfur mass balance closure across the energy landscape identified ‘missing’ sulfur during early phases of S^0 production and S^0 degradation, motivating a search for additional intermediates of *C. tepidum* S^0 metabolism. Soluble extracellular polysulfides were observed to accumulate during S^0 production, and these compounds also provided a mechanism to explain microscopic observations of S^0 globules growing at a distance from cells. During S^0 degradation, a polysulfide species was detected but did not accumulate and was therefore unlikely to account for ‘missing’ sulfur; however, this compound could play a role in degradation of S^0 globules not attached to cells and growth of cells unattached to S^0 globules.

Beyond insights specifically into S^0 metabolism, this comprehensive study of the ‘energy landscape’ also suggested that *C. tepidum* alters the portion of cellular carbon derived from acetate versus CO_2 in response to light and electron donor. The prevalence of an increased recovery of sulfur in oxidation products than in the initially-provided electron donors in later phase cultures across the energy landscape suggested that *C. tepidum* cells had oxidized intracellular stores of sulfur compounds. Finally, a lack of thiosulfate oxidation by low light-grown *C. tepidum*, coupled with decreased BChl *c* content, suggested the inability of *C. tepidum* to utilize thiosulfate under these conditions. Trace oxygen contamination provides a possible explanation

for this observation, and raises interesting questions about the regulation of photosynthetic electron transport during oxygen stress. Together, the comprehensive approach to analyzing *C. tepidum* sulfur metabolism revealed new insights that would not have been observable by traditional, single factor experiments, and provided a high-level view of how *C. tepidum* adjusts to varying energy conditions and balances electron flows.

3.1.2 Importance

The factorial experimental design employed here provided a systematic approach to studying *C. tepidum* under a range of conditions, including different electron donors and light flux levels. By providing a global view of *C. tepidum* S⁰ metabolism, this approach enabled insight into mechanisms of S⁰ metabolism as well as into other aspects of *C. tepidum* metabolism without characterization of individual genes or gene products and without the use of flux-based analysis. Specifically, this work quantified a reduction in per-electron growth yield for S⁰ relative to sulfide that can only be explained by reduced opportunities for net energy conservation during S⁰ oxidation; this observation challenges current models for electron transport in *C. tepidum*. In addition, this work detected the presence of soluble, extracellular intermediates during S⁰ production and degradation. These observations complemented microscopic observations and enabled a new model for S⁰ production and degradation by *C. tepidum* where growth and degradation of S⁰ globules occurs at a distance from cells. While the factorial approach employed here will not replace focused studies of individual pathways or gene products, and cannot provide the level of detailed metabolic pathway information available from flux based analysis, this

approach is useful for identifying regions of the growth landscape that will yield the most productive areas for in-depth focused studies.

3.2 Introduction

In the context of using the stored reducing power in waste sulfur piles for microbially-catalyzed production of useful compounds, designing a platform organism for this process will require a range of considerations. Namely, a comprehensive understanding of the pathways of sulfur oxidation would be important for predicting potential intermediates, products, and by-products that could accumulate.

Furthermore, understanding how sulfur metabolism interacts with other metabolic modules (e.g. carbon metabolism, photosynthetic electron transfer) and understanding whether disruptions to sulfur metabolism will produce secondary effects in core metabolism or stress responses is important to the design of the platform organism.

Analyses of growth yields on sulfur electron donors and carbon sources is one approach to answering some of these questions, as observed changes in growth yields indicates the relative efficiency with which an organism converts electron and carbon substrates to biomass (or to a putative product). Reduced growth yields suggest physiological stress, whereas higher growth yields are characteristic of favorable growth conditions. To derive meaningful conclusions from yield studies, comprehensive measurements of biomass accumulation, substrate uptake, and product formation are required. These measurements can also facilitate “mass balance” analyses: the assessment of whether substrates (carbon, electrons, sulfur) can be stoichiometrically accounted for in products (biomass, oxidized products). The observation of growth regimes where mass balances are not closed can help identify

areas where the community's understanding of metabolic processes are incomplete, and can help direct further studies to closing these knowledge gaps.

As a first step towards answering some of these questions and as a demonstration of the utility of this approach, measurements (sulfide, S^0 , thiosulfate, sulfite, sulfate, acetate, protein, and storage carbohydrates) collected during the 'energy landscape' study described in Chapter 2 and Levy et al. (2016) were used to assess growth yields and closure of the sulfur mass balance. The factorial nature of the study design enabled observations of the interacting effect of electron donor type (sulfide, S^0 , or thiosulfate) and light flux level (5, 20, or 35 $\mu\text{mol m}^{-2} \text{s}^{-1}$) on growth yields and the ability to close a sulfur mass balance. This approach facilitated the observation that *C. tepidum* growth yield on a per-electron basis is greater for sulfide relative to S^0 and thiosulfate. This observation prompted an analysis of these measured yields in the context of known electron transport pathways, providing evidence that the electrons associated with the oxidation of S^0 to sulfite may not be linked with energy conservation mechanisms. Evaluation of the sulfur mass balance across the energy landscape revealed areas where sulfur recovery exceeded the baseline, suggesting the oxidation of intracellular sulfur pools. In addition, two regions of the energy landscape were identified where significant sulfur was not recovered. A closer investigation of these conditions led to the identification of soluble intermediates of sulfur metabolism that may play a role in S^0 globule growth and degradation at a distance from cells. Finally, this factorial approach led to the identification of an interesting growth regime where no oxidation of the electron donor was detected (thiosulfate), yet the cells grew and produced sulfate as an oxidized product. While

this effect requires further study, these observations could be indicative of a *C. tepidum* response to microaerobic conditions and trace oxygen contamination.

3.3 Materials and Methods

3.3.1 Bacterial strains and growth conditions

Chlorobaculum tepidum strain WT2321, a plating strain derivative of the original TLS1 isolate (Wahlund et al. 1991; Wahlund & Madigan 1995), was grown in 20 ml cultures with a 10 psig (177 kPa) headspace composed of 95%:5% N₂:CO₂ passed through a heated copper scrubber. Experimental cultures were inoculated to 4 µg protein ml⁻¹ from pre-cultures derived from cryogenic stocks, and were grown at 45-46 °C in a heated rotisserie culturing system (see Appendix B) except where indicated otherwise. Light was provided from 60 or 100 W Reveal® incandescent bulbs (GE Lighting) to the levels specified below, and the light flux was measured with a quantum photosynthetic active radiation sensor (LI-COR). To obtain attenuated light flux relative to the field provided, individual cultures were shaded using printed transparency films enabling multiple light levels within one rotisserie culturing run.

3.3.2 Culture media

Sulfur-free Pf-7 medium (Wahlund et al. 1991) was prepared by omitting sulfide and thiosulfate from Pf-7 prepared as previously described (Chan et al. 2008). Electron donors were added to individual tubes from concentrated, anoxic stock solutions. Sulfide stocks were pH-neutralized (Siefert & Pfennig 1984) and biogenic S⁰ was purified as previously described (Hanson et al. 2016). The electron donor concentrations in uninoculated media for the energy landscape studies were: sulfide: 3.4 ± 0.2 mM; S⁰: 9.3 ± 0.3 mM; thiosulfate: 10.2 ± 0.1 mM. Electron donor

concentrations for follow-up studies are as specified in the relevant sections below.

Acetate was provided at an initial concentration of 7.4 ± 0.3 mM to all cultures.

3.3.3 Quantification of sulfur compounds and acetate

Measurements of sulfide, sulfite, thiosulfate, and acetate were performed as described in Chan et al. (2008). Briefly, sulfide and sulfite in culture supernatants were derivatized with monobromobimane as described by Rethmeier et al. (1997) and were separated and quantified by reverse-phase high performance liquid chromatography (HPLC) using a Prevail™ C18 5 μ m column (Alltech Associates Inc.) and a gradient of 0.25% acetic acid, pH 4.0, and methanol. Derivatized compounds were detected by fluorescence (380 nm excitation, 450 nm emission); this method was also used for detection of polysulfides. Thiosulfate and acetate in culture supernatants were separated and quantified by HPLC using a Prevail™ Organic Acids 5 μ m column (Alltech Associates Inc.) with 25 mM potassium phosphate (pH 2.5) as mobile phase and UV detection at 210 nm. Elemental sulfur was extracted from cell pellets with 10:1 vol/vol chloroform:methanol; separation and quantitation was performed by reverse-phase HPLC with a Prevail™ C18 5 μ m column, 95%:5% v/v methanol:water as mobile phase, and UV detection at 260 nm. Sulfate was quantified by ion chromatography with suppressed conductivity detection (Metrohm) using an A Supp 5 100 x 4 mm column eluted with 3.2 mM Na_2CO_3 + 1.0 mM NaHCO_3 + 6.5 % v/v acetone in ultrapure water. Standard curves were prepared from sodium sulfide nonahydrate (ACS, Fisher), elemental sulfur powder (USP, Fisher), sodium thiosulfate pentahydrate (>99.5%, Sigma-Aldrich), sodium sulfate (>99%, Sigma-Aldrich), and sodium acetate (>99%, EM Science). The polysulfide standard was prepared by adding an anoxic sulfide solution to solid S_8 (2:1 molar ratio of S_8 /sulfide) in a sealed

tube under an atmosphere composed of 95%:5% N₂:CO₂ passed through a heated copper scrubber.

3.3.4 Protein and bacteriochlorophyll *c* determinations

Protein measurements were performed by Bradford method on methanol-extracted cell pellets as described in Levy et al. (2016) and section 2.3.5 of this dissertation; the values reported here are the corrected by the linear factor described in Levy et al. 2016 and section 2.4.1 of this dissertation. Bacteriochlorophyll *c* (BChl *c*) was determined by absorbance of methanolic extracts as described by Levy et al. (2016) and section 2.3.5 of this dissertation.

3.3.5 Cellular carbohydrate analysis

Carbohydrate content of acetone-extracted *C. tepidum* cell pellets were measured by the anthrone-sulfuric acid assay with glucose as standard as described by Levy et al. (2016) and section 2.3.8 of this dissertation.

3.3.6 Experimental design and statistical analysis

JMP® Pro (SAS institute) was used for experimental design, statistical analysis, and yield calculations. The ‘energy landscape’ experimental design, described in section 2.3.1 of this dissertation and in Levy et al. 2016, was a 3×3 factorial experiment that varied electron donor type (sulfide, S⁰, or thiosulfate), light flux level (5 (low), 20 (middle), or 35 (high) μmol photons m⁻² s⁻¹), and culture duration (10, 18, or 26 hours). The full design contained 48 independent culture units (Table 3.1) that were grown in groups of eight cultures across six culturing blocks (see Table 2.1).

Table 3.1 Number of biological replicates for each treatment combination in the energy landscape experimental design.

Electron donor	Light Flux Level ($\mu\text{mol photon m}^{-2} \text{ s}^{-1}$)	Culture duration (hrs)		
		10	18	26
Sulfide	35	2	1	2
	20	1	4	1
	5	2	1	2
S^0	35	2	1	2
	20	1	3	1
	5	2	2	2
Thiosulfate	35	2	1	2
	20	1	4	1
	5	2	1	2

This design enabled quantitative analysis of the effects of simultaneous changes in the energy landscape parameters and the effect of culturing block on *C. tepidum* growth by a third-order interaction model (Eq. 3.1).

$$Y = \beta_0 + \sum \beta_i x_i + \sum_{i < j} \beta_{ij} x_i x_j + \sum_{i < j < k} \beta_{ijk} x_i x_j x_k + \epsilon \quad 3.1$$

In Eq. 3.1, Y is the measured response, x_i are experimental factors, $\beta_{0,i,ij,ijk}$ are coefficients determined from multiple regression, and ϵ represents random error. β_0 is the mean value of the response; main effect terms (β_i) represent a factor's direct effect and cross-interaction terms (β_{ij} and β_{ijk}) represent the synergistic impact of two and three factors respectively. Responses were fit to Eq. 3.1 by linear least squares regression. Analysis of variance was used to assess overall model significance by F test, which can assess multiple coefficients simultaneously, and to estimate parameter coefficient values, where the significance of individual parameters was determined by t test. Statistically insignificant parameters, defined as $P > 0.2$, were sequentially eliminated to improve model significance and parameter estimates, and to identify the

factors with the largest influence on growth yield. Only effects with F test probabilities of $p < 0.01$ were considered to have a significant effect on the measured response. Continuous factors were coded between -1 and 1 before model fitting. Culturing block was investigated as a main effect factor but was not found to produce a significant effect in any model.

3.3.7 Yield calculations

To evaluate the effect of energy landscape parameters on growth yield, we considered that growth yield is defined as the amount of biomass created per unit of substrate uptake (Eq. 3.2).

$$\text{Yield} = (\text{biomass generation}) (\text{substrate uptake})^{-1} \quad 3.2$$

By appropriately selecting the measured response Y and experimental factors x_i, x_j, x_k in Eq. 3.1 and then rearranging to the form of Eq. 3.2, Eq. 3.1 can be used to evaluate the effects of electron donor and light on growth yield. To do this, culture protein (as a proxy of biomass; Levy et al. 2016) was used as the measured response (Y), and uptake of the substrate of interest ($\Delta\text{substrate}$), electron donor type (ED), and light flux level were used as the experimental factors x_i, x_j, x_k , respectively. It should be noted that in this analysis, substrate uptake replaced culture duration as an experimental factor to facilitate yield analysis. This approach is justified as substrate uptake is monotonically related to culture duration within an electron donor and light flux level up until the point of substrate depletion. For this reason, six cultures which had exhausted electron donor or acetate substrates were excluded in the yield analysis: these were 26 hour cultures grown on S^0 or thiosulfate at middle or high light levels (Table 3.1).

Substituting the measured response and experimental factors relevant for yield analysis into Eq. 3.1 results in Eq. 3.3.

$$\text{Protein} = \beta_0 + \beta_1 \cdot (\Delta\text{substrate}) + \beta_2 \cdot (\text{ED}) + \beta_3 \cdot (\text{light}) + \beta_{12} \cdot (\Delta\text{substrate}) \cdot (\text{ED}) + \beta_{13} \cdot (\Delta\text{substrate}) \cdot (\text{light}) + \beta_{23} \cdot (\text{ED}) \cdot (\text{light}) + \beta_{123} \cdot (\Delta\text{substrate}) \cdot (\text{ED}) \cdot (\text{light}) + \epsilon \quad 3.3$$

Eq. 3.3 can be rearranged to the general form of the yield equation (Eq. 3.2) by first collecting terms that include $\Delta\text{substrate}$ together on one side of the equation and terms that do not on the other (Eq. 3.4).

$$\text{Protein} - [\beta_0 + \beta_2 \cdot (\text{ED}) + \beta_3 \cdot (\text{light}) + \beta_{23} \cdot (\text{ED}) \cdot (\text{light}) + \epsilon] = (\Delta\text{substrate}) \cdot [\beta_1 + \beta_{12} \cdot (\text{ED}) + \beta_{13} \cdot (\text{light}) + \beta_{123} \cdot (\text{ED}) \cdot (\text{light})] \quad 3.4$$

Then, dividing both sides through by $(\Delta\text{substrate})$ puts Eq. 3.3 in the yield format of Eq. 3.2 (Eq. 3.4).

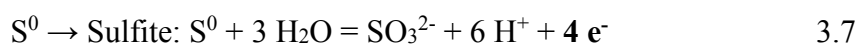
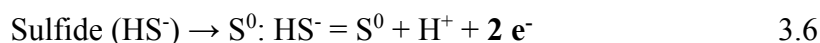
$$\text{Yield}_{\text{Substrate}} = \beta_1 + \beta_{12} \cdot (\text{ED}) + \beta_{13} \cdot (\text{light}) + \beta_{123} \cdot (\text{ED}) \cdot (\text{light}) \quad 3.5$$

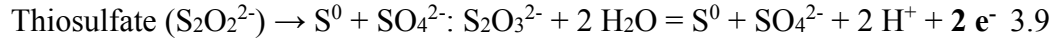
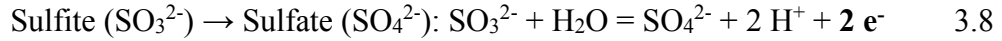
This procedure was used for evaluating the effect of electron donor and light flux on *C. tepidum* growth yields on various substrates as described below.

3.4 Results and Discussion

3.4.1 *C. tepidum* growth yield on an electron equivalent basis was highest with sulfide and lowest with thiosulfate as electron donor

To determine whether growth conditions affected the ability of *C. tepidum* to convert reducing equivalents obtained from sulfur electron donors into biomass, we assessed growth yields across the energy landscape on an electron equivalent (eeq) basis. The numbers of eeqs available from oxidation of sulfur compounds were obtained from balanced half reactions (Eq. 3.6-3.9).





Complete oxidation of thiosulfate to sulfate is achieved by the sum of equations 3.9, 3.7, and 3.8. Thus, 8 eeq are available from the oxidation of sulfide to sulfate, 6 eeq are available from the oxidation of S^0 to sulfate, and 8 eeq are available from the oxidation of thiosulfate to sulfate.

Measurements of the initial and final concentrations of the different sulfur compounds enables calculation of the amount of eeq oxidized, and there are two ways of doing the ‘accounting’ for these transactions. The first way is to determine the eeq oxidized from the disappearance of the electron donors (Eq. 3.10).

$$\Delta \text{eeq-ED} = (8 \text{ eeq (mmol HS}^-)^{-1}) \cdot \Delta[\text{HS}^-] + (6 \text{ eeq (mmol S}^0)^{-1}) \cdot \Delta[\text{S}^0] + (8 \text{ eeq (mmol S}_2\text{O}_3^{2-})^{-1}) \cdot \Delta[\text{S}_2\text{O}_3^{2-}] \quad 3.10$$

This method carries the implicit assumption that as soon as an electron donor is taken up, it is immediately oxidized. However, as intracellular stores of sulfide, sulfite, and thiosulfate have been detected (Hiras 2012; Rodriguez et al. 2011; Hilzinger & Hanson unpublished data) and inferred (Levy et al. 2016), it follows that uptake does not necessarily imply oxidation.

An alternative method of calculating the eeq oxidized is based on the appearance of oxidized product (OxP; Eq. 3.11).

$$\Delta \text{eeq-OxP} = (2 \text{ eeq (mmol S}^0)^{-1}) \cdot \Delta[\text{S}^0] + (8 \text{ eeq (mmol S}_2\text{O}_3^{2-})^{-1}) \cdot \Delta[\text{S}_2\text{O}_3^{2-}] + (8 \text{ eeq (mmol SO}_4^{2-})^{-1}) \cdot \Delta[\text{SO}_4^{2-}] \quad 3.11$$

As this method only considers an eeq as oxidized once the oxidized product appears, the appearance of OxP was selected as the more accurate method of determining the amount of eeq oxidized, although this method cannot account for intracellular storage of partially oxidized sulfur compounds.

Using $\Delta_{\text{eeq-OxP}}$ as the substrate uptake parameter in the assessment of *C. tepidum* yield across the energy landscape (Eq. 3.3-3.5) revealed that ED, but not light, interacted with $\Delta_{\text{eeq-OxP}}$. Eliminating the insignificant factors from Eq. 3.5 produced Eq. 3.12, which describes the effect of electron donor on biomass yield on an eeq basis.

$$\text{Yield}_{\text{eeq-OxP}} = \beta_1 + \beta_{12} \cdot (\text{ED}) \quad 3.12$$

Table 3.2 provides the significance of the effects and estimates of each of the parameters of Eq. 3.12.

Table 3.2 Significance of energy landscape parameter effects on *C. tepidum* growth yield based on eeq oxidized ($\text{Yield}_{\text{eeq-OxP}}$) and parameter estimates used in Eq. 3.12 to calculate the yield values displayed in Fig. 3.1-B.

Parameter	Factor	Overall <i>F</i> test effect significance	Estimate ^a	Std Error ^a
β_1	Baseline yield	<0.0001	4.82	0.08
β_{12}	ED:[HS] ^b	0.0004	0.45	0.12
	ED:[S ⁰]		-0.04	0.11
	ED:[TS] ^b		-0.41	0.11

^a Estimate and standard error are in units of mg protein (mmol eeq)⁻¹

^b HS = sulfide; TS = thiosulfate

This analysis revealed that yield was a function of electron donor identity, but not light flux, where sulfide as electron donor provided the highest yield and thiosulfate provided the lowest. This effect is visually depicted in Fig. 3.1-A, which shows *C. tepidum* culture protein concentration plotted versus $\Delta_{\text{eeq-OxP}}$ with different slopes (i.e. yields) for each electron donor, and Fig. 3.1-B, which depicts the calculated yields.

These data suggest that electrons from sulfide provide more cell production power than electrons from S^0 or thiosulfate. Furthermore, we previously observed that *C. tepidum* cells grown on sulfide accumulated increased storage carbohydrates, likely in the form of glycogen, relative to growth on S^0 or thiosulfate (Levy et al. 2016). To account for this glycogen production in the yield calculations, total biomass (using protein as a proxy) and total carbohydrate were normalized to the eeq required to synthesize these compounds. The value for eeq invested in total biomass ($0.40 \text{ eeq (mg protein)}^{-1}$) was based on averaged literature values for *Allochromatium vinosum* and *Thiocapsa roseopersicina* (Van Gemerden & Beftink 1978; De Wit 1989; Visscher 1992; Sánchez et al. 1998); the value for eeq invested in glycogen ($0.14 \text{ eeq (mg glycogen)}^{-1}$) was calculated from the half-reaction for oxidation of glycogen ($C_{24}H_{42}O_{21}$) to CO_2 . Repeating the yield analysis described above using these adjusted biomass values further increased in the calculated biomass yield value for sulfide relative to S^0 and thiosulfate (data not shown), emphasizing that *C. tepidum* exhibits higher growth yields on electrons from sulfide than other electron donors.

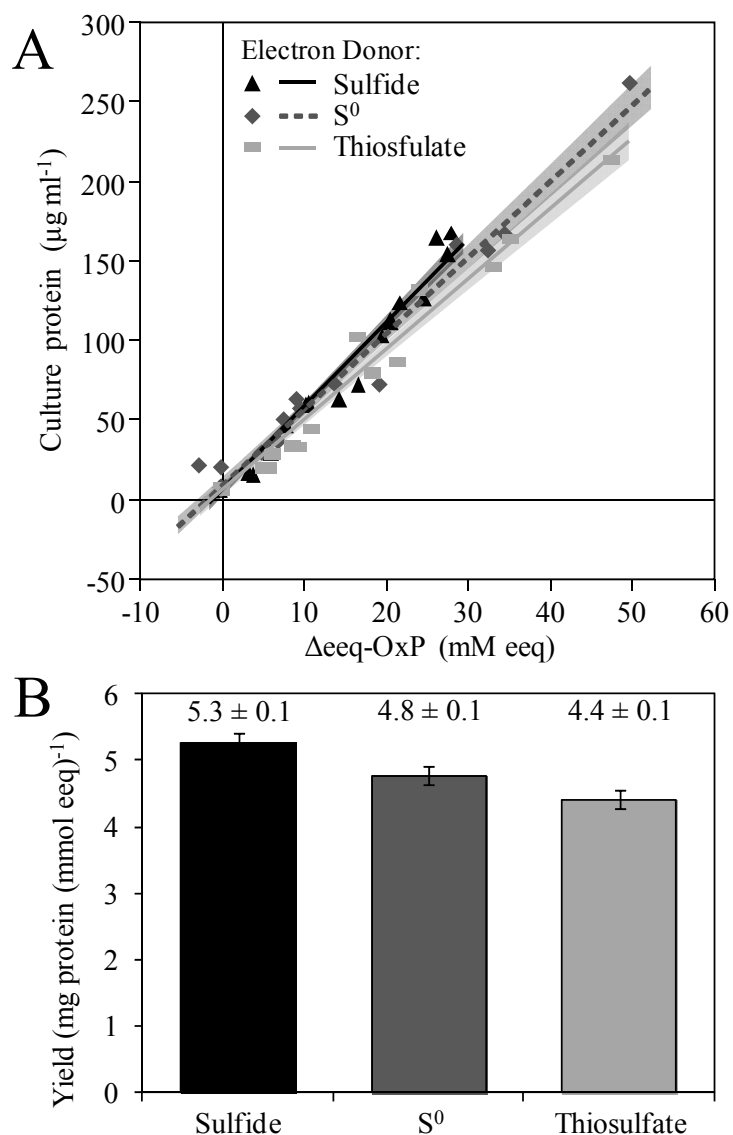


Figure 3.1 Effect of electron donor on *C. tepidum* growth yields based on electron equivalents oxidized. (A) Culture protein plotted as a function of electron equivalents oxidized ($\Delta\text{eeq-OxP}$), where the effect of different electron donors on yield appears as a change in the slope. (B) Calculated growth yields for *C. tepidum* using Eq. 3.12 and the parameters shown in Table 3.2. Sulfide as electron donor provides the highest growth yield on eeq oxidized, and thiosulfate provides the lowest. Error bars represent the standard error of the calculated values.

3.4.1.1 Comparison of measured *C. tepidum* growth yields to values reported in the literature

Growth yields of *C. tepidum* on various single electron donors have previously been reported (Table 3.3), and these values span a wide range. Interestingly, while the literature-reported yields on thiosulfate are comparable to those reported here, the growth yields on sulfide in the literature are lower than on S^0 or thiosulfate on a per electron basis and are 3- to 5-fold lower than those reported here. The literature-reported yields span a range of different culturing configurations and volumes, which could have resulted in incomplete oxidation of the initially provided electron donor if S^0 settled out and the cultures were not mixed, or if self-shading in a large volume culture led to light limitation. For most of the yield measurements cited (except for Azai et al. 2009), only the initial amount of electron donor provided, and not the final production of oxidized products, was reported and used in the yield calculation. Thus it is possible that not all sulfur electron donor compounds were oxidized by the time cultures were sampled, leading to artificially-reduced yield values. In addition, although the sample timing was not always reported, yield determinations in the studies summarized in Table 3.3 were often made on samples collected at the end of culture (e.g. Chan et al. 2008, Chan et al. 2009). This approach has the potential to allow cell death and lysis prior to biomass measurements if oxidizable electron donors have been long depleted by sampling, potentially leading to artificially-decreased protein measurements. Furthermore, while all yields reported in Table 3.3 were derived from cultures grown mixotrophically (on acetate as well as CO_2), it is probable that the yields reported for some of the cultures with higher initial concentrations of electron donor had exhausted acetate by sampling, leading to reduced growth yields.

Table 3.3 Previously reported yields for growth of *C. tepidum* on single electron donors and acetate and CO₂ as carbon source.

Electron donor	Initial electron donor concentration (mM)	Yield (mg protein (mmol eeq) ⁻¹)	Reference
Sulfide	continuous (< 0.1)	1.6	Mukhopadhyay et al. 1999
	2.5	2.0	Chan et al. 2008
	2	2.0	Chan et al. 2009
	2.5-3	1.3	Azai et al. 2009
	2-8	1.1	Chan et al. 2009
	4	1.6	Rodriguez et al. 2011
S ⁰	0-1.8	6.5	Hanson et al. 2016
Thiosulfate	12	3.9	Mukhopadhyay et al. 1999
	12.5	0.8	Chan et al. 2008
	9	3.0	Azai et al. 2009

By comparison, the yield values reported here were obtained under tightly controlled conditions across all three electron donors in terms of culture volume, mixing, light exposure, temperature, and basal medium composition. In addition, we assessed the amount of electron donor oxidized by the formation of oxidized products to ensure that the calculated yield was based on actual electron donor oxidized, increasing the accuracy of these determinations. Samples for yield determinations were collected at intervals before or within a maximum of 8 hours after the cultures entered stationary phase, thus minimizing the likelihood that cell death or lysis negatively influenced the culture protein measurements. Finally, as mentioned above, the yield values in this work were only derived from cultures prior to the depletion of acetate. Thus, the approach employed in assessing growth yields under tightly controlled conditions enabled a meaningful comparison of the relative growth yields on an eeq basis for sulfide, S⁰, and thiosulfate.

3.4.1.2 Differential growth yields on sulfide, S^0 , and thiosulfate provide evidence that electrons from oxidation of S^0 do not enter the membrane-bound electron transport chain

As our results suggest that there is a hierarchy in the biomass-producing capacity of electrons from sulfur electron donors, where electrons from sulfide produce the most biomass and those from thiosulfate produced the least, we attempted to quantitatively explain this observation in the context of electron transport pathways in *C. tepidum*. First, we developed a simplified conceptual model of the relationship between biomass yield, sulfur compound oxidation, and electron transport pathways in *C. tepidum* (Fig. 3.2-A). Biomass yield on an electron equivalent basis was divided into three components, which each relate to one of three categories of electron transport in *C. tepidum*:

1. Baseline Yield (Y_B ; green box in Fig. 3.2): The per-electron yield related to electron transport downstream of the photosynthetic reaction center, where photooxidation of the reaction centers produces reduced ferredoxin (Fd). Reduced ferredoxin is used for CO_2 fixation *via* the reverse tricarboxylic acid (rTCA) cycle and reduction of acetate to pyruvate, reduction of $NAD(P)^+$ to $NAD(P)H$, and production of ATP *via* Complex I (Feng et al. 2010; Seo & Sakurai 2002; Frigaard et al. 2003). This component of biomass yield (on an electron equivalent basis) was considered to be constant and therefore independent of the electron donor from which the electrons were originally derived.
2. Membrane-Bound Electron Transport-associated Yield (Y_{MB} ; red box in Fig. 3.2): Oxidation of certain sulfur compounds (see below) leads to membrane-bound (MB) electron transport upstream of the reaction center, resulting in the generation of proton motive force *via* the cytochrome *b/c*₁ complex (Oh-Oka & Blankenship 2013). This proton motive force is used for ATP synthesis, and provides a “boost” to biomass yield it reduces the amount of ATP that must be produced at the expense of the pool of reduced electron carriers *via* Complex I. This component of biomass yield was considered to be proportional to the fraction of electrons from each electron donor that is associated MB electron transport.

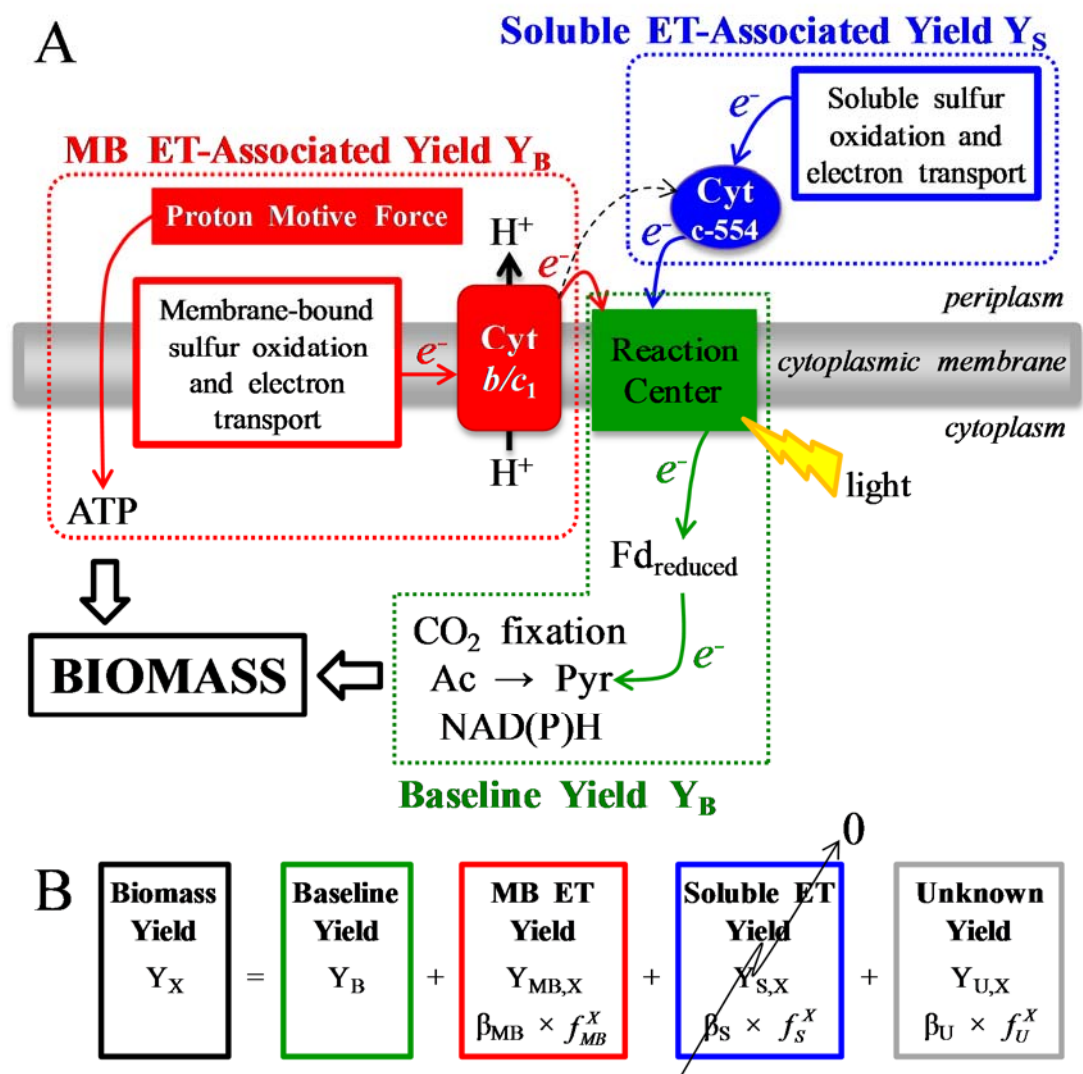


Figure 3.2 Model for relationship of *C. tepidum* growth yield to electron transport pathways. (A) Simplified diagram of electron transport pathways in *C. tepidum* and their relationship to Baseline, Membrane-Bound electron transport, and Soluble electron transport components. (B) Translation of electron transport pathways to model yield equations 3.13 and 3.14. Fractions of electrons associated with membrane-bound, soluble, and unknown electron transfer are presented in Table 3.4; the calculated breakdown of observed biomass yield in to the different components are presented in Table 3.5. MB = membrane-bound; ET = electron transport; Ac = acetate; Pyr = pyruvate; Fd = ferredoxin; Cyt = cytochrome.

3. Soluble Electron Transport-associated Yield (Y_S ; blue box in Fig. 3.2): Oxidation of other sulfur compounds (see below) leads to the reduction of soluble electron carriers, which donate electrons directly to the Reaction Center without electron transfer through the cytochrome b/c_1 complex. As these pathways do not directly produce proton motive force, electrons transferred through soluble pathways are not expected to produce any additional increase to biomass beyond the Baseline contribution, and Y_S is expected to be 0.

Next, each of the electron transfers associated with sulfur compound oxidation in *C. tepidum* were categorized by whether they were expected to result in membrane-bound or soluble electron transport upstream of the reaction center, based on the current understanding of electron transport in *C. tepidum*. This assessment is summarized in Table 3.4, and a detailed description of the current state of knowledge on electron transport in *C. tepidum* is provided below in section 3.4.1.3. The calculated fractions of electrons for each electron donor X that are involved in membrane bound (f_{MB}^X) or soluble (f_S^X) electron transport upstream of the reaction center are presented in Table 3.4. It became clear from the literature that the fate of the four electrons transferred in the oxidation of S^0 to sulfite was not well defined. Therefore these electrons were assigned an ‘Unknown’ fate, constitute fraction f_U^X for each electron donor X.

Table 3.4 Summary of the electron fate from oxidation of sulfide, S^0 , and thiosulfate based on known electron transport pathways in *C. tepidum*

	Number of electrons associated with Membrane Bound, Soluble, or Unknown Routes of electron transport				Fraction of e^-		
	Membrane Bound ET		Soluble ET	Unknown	MB	S	U
ED ^a	$HS^- \rightarrow S^0$	$SO_3^{2-} \rightarrow SO_4^{2-}$	$S_2O_3^{2-} \rightarrow S^0 + SO_4^{2-}$	$S^0 \rightarrow SO_4^{2-}$	f_X^{MB}	f_X^S	f_X^U
HS^-	2	2		4	0.50		0.5
S^0		2		4	0.33		0.67
$S_2O_3^{2-}$		2	2	4	0.25	0.25	0.50

^a HS^- = sulfide; $S_2O_3^{2-}$ = thiosulfate

We then used our conceptual model (Fig.3.2-A) to evaluate how the observed yields partitioned into the Baseline and MB electron transport-associated components and to determine whether the data could provide insight into the fate of the ‘Unknown’ electrons involved in S^0 oxidation to sulfite. Equation 3.13 below was used to represent biomass yield on electron donor X (Y_X) as the sum of the three components described above, and a fourth component ($Y_{U,X}$) to represent the contribution to yield from the ‘Unknown’ fate electrons (see also Fig. 3.2-B):

$$Y_X = Y_B + Y_{MB,X} + Y_{S,X} + Y_{U,X} \quad 3.13$$

In Eq. 3.13, Y_B represents the baseline yield that is constant for all electron donors; the values of $Y_{MB,X}$, $Y_{S,X}$, and $Y_{U,X}$ will be specific to electron donor X and each are proportional to the fraction of electrons associated with membrane-bound electron transport, soluble electron transport, and ‘Unknown’ electron transport, respectively.

Thus we can convert Eq. 3.13 to Eq. 3.14:

$$Y_X = Y_B + \beta_{MB} \times f_{MB}^X + \beta_S \times f_S^X + \beta_U \times f_U^X \quad 3.14$$

where β_{MB} , β_S , and β_U represent parameters relating yield to the fraction of electrons associated with each component. Because soluble electron transport should not produce any net positive contribution to biomass growth over the Baseline yield, we can assume that β_S is equal to zero. In this simplified model we also assumed that β_{MB} and β_U are constant across all electron donors (in essence assuming that all electrons that pass through the cyt *b/c*₁ complex have the same proton motive force efficacy and that S^0 oxidation to sulfite uses the same pathways regardless of original electron donor). Finally, we further justified our assumption that Y_B , β_{MB} , and β_U were constant over the experimental space investigated because light was not observed to affect yield and because only cultures prior to acetate depletion were used in the analysis.

Thus, using the known values for f_{MB}^X and f_U^X presented in Table 3.4 and the measured values of Y_X for sulfide, S^0 , and thiosulfate, we were able to solve for the unknown parameters Y_B , β_{MB} , and β_U . The calculated values of Y_B , β_{MB} , and β_U , along with the absolute and relative contributions of yield components Y_B , Y_{MB} , and Y_U are reported in Table 3.5. These results show that Y_B composes the largest portion of biomass yield for all three electron donors (62-74%), and that the component associated with membrane-bound electron transport is greatest for sulfide (32%) and smallest for thiosulfate (19%), as expected based on the relative fractions of electrons associated with membrane-bound electron transport. These results also suggest that the ‘Unknown’ component of the yield, while non-zero (5-8%), provides only a minor contribution to biomass yield. Furthermore, when we modeled the growth yields adjusted for storage carbohydrate production, the ‘Unknown’ portion of the yield shrank to only 2-3% (data not shown).

Table 3.5 Breakdown of the experimentally observed *C. tepidum* growth yields into the Baseline (Y_B), membrane-bound electron transport-associated (Y_{MB}), and ‘Unknown’ (Y_U) components (see Fig. 3.2, Eq. 3.13, and Eq. 3.14).

Parameter values:	$\beta_{MB} = 3.41^c$	$\beta_U = 0.55^d$	Sum of model components (= measured yield)
	Y_B^b	Y_{MB}^b	Y_U^b
HS^-^a	3.28 (62%)	1.71 (32%)	0.28 (5%)
S^0	3.28 (69%)	1.13 (24%)	0.37 (8%)
$S_2O_3^{2-}^a$	3.28 (74%)	0.85 (19%)	0.28 (6%)

^a HS^- = sulfide; $S_2O_3^{2-}$ = thiosulfate

^b Absolute contributions of each yield component are reported in units of mg protein (mmol e^-); relative contributions of each component are reported in parentheses

^c units = mg protein (mmol eq_{MB})⁻¹

^d units = mg protein (mmol eq_U)⁻¹

These results provide evidence that either the four electrons associated with S^0 oxidation to sulfite do not enter membrane-bound electron transport pathways, or that any proton motive force generated by these electron transfers is outweighed by other aspects of S^0 oxidation that have not yet been elucidated (e.g. energy-dependent transport of S^0 into the cell or reductive activation of S^0 prior to activation). Work towards clarifying the pathways of S^0 oxidation in the purple sulfur bacterium *Allochromatium vinosum* may provide some insight here, as described briefly in section 3.4.1.3.3 below. Further work to clarify the electron transport pathways during S^0 oxidation to sulfite in *C. tepidum*, as well as the pathways used for extracellular import of S^0 into the cell, will be interesting directions of future research.

In summary, the factorial design of the energy landscape of sulfur oxidation facilitated a comprehensive comparison of *C. tepidum* growth yields under varying growth conditions. This comparison resulted in the detection of measurable and significant differences in growth yields on different electron donors on a per-electron basis that provided insight into electron transport pathways in *C. tepidum*.

3.4.1.3 Current state of knowledge on electron transport from oxidation of sulfur compounds in *C. tepidum*

3.4.1.3.1 Electron fate for oxidation of sulfide to S^0

Electrons from the initial oxidation of sulfide are believed to enter the membrane bound electron transport chain at the level of the quinone pool *via* any of several sulfide:quinone oxidoreductases (SQR) encoded in the *C. tepidum* genome (CT0117, CT0876, CT1087; Chan et al. 2009; Shuman & Hanson 2016). While the fate of the immediate products of SQR (disulfide and/or polysulfides) is not yet fully elucidated, a polysulfide reductase-like complex 1 (PSRLC1) complex encoded by

CT0496-CT0494 is believed to play a role in oxidizing polysulfides to elemental sulfur (Eddie & Hanson 2013). Transcripts of the *PSRLC1* genes were increased after a sulfide spike, suggesting that their expression is increased in response to sulfide (Eddie & Hanson 2013). The PSRLC1 complex is expected to associate with the periplasmic side of the cytoplasmic membrane and transfer electrons to the quinone pool (Frigaard & Bryant 2008). While *C. tepidum* possesses the alternative sulfide-oxidizing enzyme flavocytochrome *c* sulfide dehydrogenase (FCC), which would not donate electrons to the quinone pool, SQR is expected to be more important than FCC in sulfide oxidation based on genetic and transcriptomic evidence (Chan et al. 2009; Eddie & Hanson 2013). Thus, the majority (if not all) of the two electrons transferred during oxidation of sulfide to S^0 is expected to be donated to the quinone pool upstream of the cytochrome *b/c1* complex and participate in membrane bound electron transport and proton motive force generation.

3.4.1.3.2 Electron fate for oxidation of S^0 to sulfite

In *C. tepidum*, S^0 is oxidized by the dissimilatory sulfite reductase (Dsr) system (Holkenbrink et al. 2011) as in the purple sulfur bacterium *Allochromatium vinosum*, although the fate of the four electron transfer is not fully resolved. Models for *C. tepidum* electron transport pathways predict that electrons from S^0 are donated to the quinone pool *via* the membrane bound DsrMKJOP (Holkenbrink et al. 2011; Eddie & Hanson 2013). However, recent studies on the Dsr system in *Allochromatium vinosum*, including biochemical characterization of the DsrMKJOP subunits and investigations of cytoplasmic sulfur trafficking, have suggested a different outcome - that electrons from the quinone pool may actually be donated to sulfur-carrying proteins in the cytoplasm by DsrMKJOP during cytoplasmic oxidation of S^0 (Grein et

al. 2010; Stockdreher et al. 2012; Stockdreher et al. 2014). An acceptor for the four electrons liberated from S^0 oxidation to sulfite has not been proposed. Thus, the fate of these electrons was categorized as unknown.

3.4.1.3.3 Electron fate for oxidation of sulfite to sulfate

Sulfite, the product of S^0 oxidation by the Dsr system, is oxidized *via* ApsBA, with a two-electron transfer to the quinone pool *via* QmoABC (Rodriguez et al. 2011), resulting in membrane-bound electron transport providing proton motive force. The final step in the oxidation to sulfate is catalyzed by an ATP sulfurylase (Sat), which is expected to produce a molecule of ATP (Rodriguez et al. 2011).

3.4.1.3.4 Electron fate for oxidation of thiosulfate to S^0 and sulfate

C. tepidum oxidizes thiosulfate using the soluble Sox system, producing one molecule of sulfate and one zero-valent sulfur atom per thiosulfate molecule. While the S^0 portion is believed to be subsequently oxidized by Dsr, ApsBA, QmoABC, and Sat as described above, the two electrons from the initial oxidation step are believed to reduce the photosynthetic reaction center by soluble electron transport pathways involving cytochrome c-554 and a second parallel, but yet undetermined, route (Sakurai et al. 2010).

3.4.2 Growth yield on acetate increased with increasing light flux but was reduced for growth on sulfide relative to growth on S^0 or thiosulfate

To determine whether *C. tepidum* growth yield on acetate was influenced by light and electron donor, the yield analysis approach described above was used by substituting acetate uptake (Δ acetate) as the substrate uptake parameter. This analysis revealed that light and a cross-interaction between electron donor and light had

significant effects on *C. tepidum* growth yield; electron donor had a weak effect on *C. tepidum* yield that was not statistically significant but that was retained in the model to improve the parameter estimates. The resulting description for the effect of electron donor (ED) and light on acetate yield is provided in Eq. 3.15.

$$\text{Yield}_{\text{Acetate}} = \beta_1 + \beta_{12} \cdot (\text{ED}) + \beta_{13} \cdot (\text{light}) + \beta_{123} \cdot (\text{ED}) \cdot (\text{light}) \quad 3.15$$

Table 3.6 provides the significance of the effects and estimates of each of the parameters of Eq. 3.15. The effect of energy landscape parameters on acetate yield is visually depicted in Fig. 3.3-A, which shows *C. tepidum* culture protein concentration plotted versus $\Delta\text{acetate}$ for each of the electron donor and light combinations, and in Fig. 3.3-B which depicts the yield values determined using Eq. 3.15.

Table 3.6 Significance of energy landscape effects on *C. tepidum* growth yield on acetate ($\text{Yield}_{\text{Acetate}}$) and parameter estimates used in Eq. 3.15 to calculate the yield values displayed in Fig. 3.3-B.

Parameter	Factor	Overall <i>F</i> test effect		
		significance	Estimate ^a	Std Error ^a
β_1	Baseline yield	<0.0001	24.2	0.6
β_{12}	ED:[HS] ^b	0.1321	-1.6	0.8
	ED:[S ⁰]		0.3	0.8
	ED:[TS] ^b		1.3	0.9
β_{13}	light	<0.0001	6.2	0.9
β_{123}	ED:[HS]·light	0.0040	-2.3	1.2
	ED:[S ⁰]·light		4.0	1.2
	ED:[TS]·light		-1.7	1.4

^a Estimate and standard error are in units of mg protein (mmol acetate)⁻¹

^b HS = sulfide; TS = thiosulfate

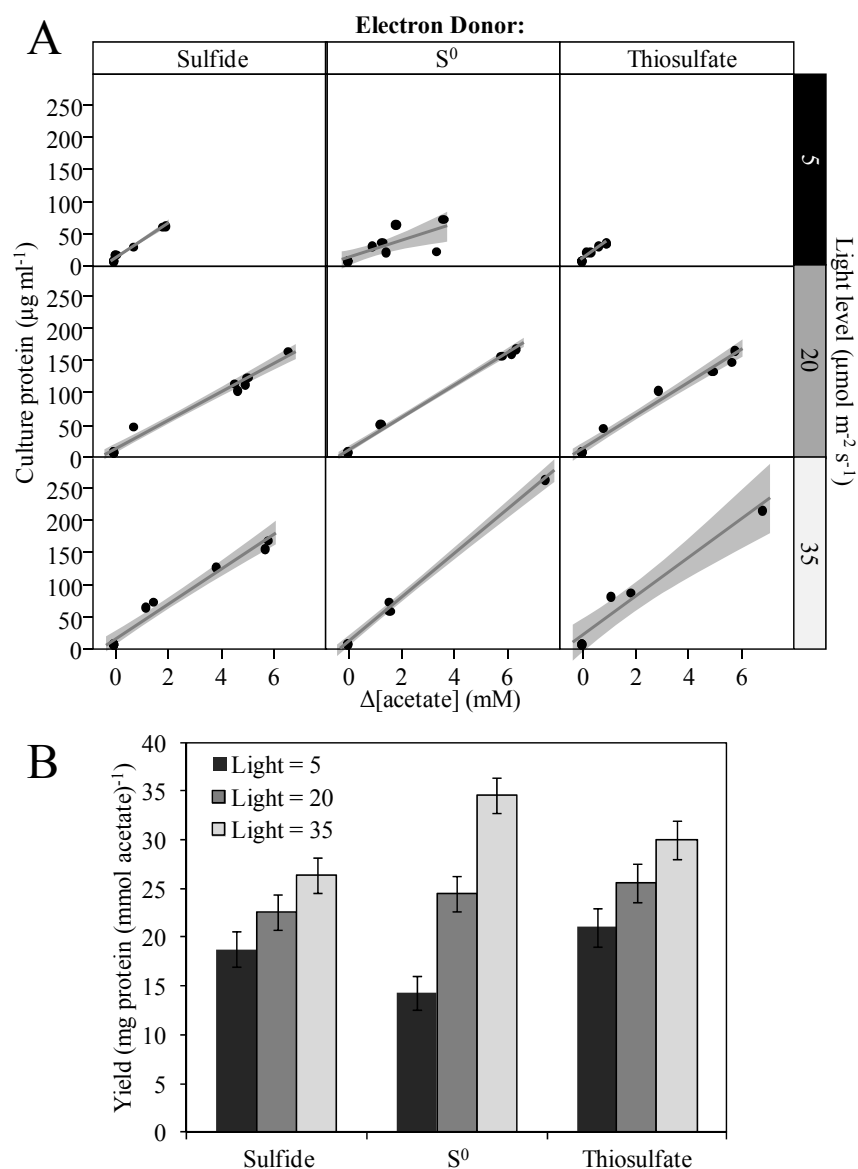


Figure 3.3 Effect of electron donor and light flux level on *C. tepidum* growth yields based on acetate uptake. (A) Culture protein plotted as a function of acetate uptake ($\Delta\text{acetate}$), where the effect of different electron donors and light flux levels on yield appears as a change in the slope. (B) Calculated growth yields for *C. tepidum* using Eq. 3.15 and the parameters shown in Table 3.6. Growth yield on acetate increases in response to increased light flux. Error bars represent the standard error of the estimated values.

Yield on acetate was found to increase with increasing light across all electron donors, suggesting that less biomass carbon is derived from acetate at higher light flux. This observation is sensible in the context of *C. tepidum* photosynthetic energy metabolism. First, increased light flux will increase the rate of electron transfer through the reaction center, increasing the rate of production of reduced ferredoxin (Fd). Ferredoxin reducing equivalents are required both for the fixation of two molecules of CO₂ by the reversed tricarboxylic acid cycle (rTCA), which produces acetate as its initial product, as well as for the reduction of acetate and CO₂ to pyruvate (Feng et al. 2010). Reduced Fd is also required for the production of NAD(P)H *via* ferredoxin-NAD(P)⁺ reductase (Seo & Sakurai 2002), where two reduced Fd are required for each NAD(P)H and two NAD(P)H equivalents are required for each turn of the rTCA cycle (Wahlund & Tabita 1997). Thus, whereas synthesis of pyruvate from acetate requires only one reduced Fd, synthesis of pyruvate from CO₂ requires a total of six reduced Fd. Thus, lower availability of reduced Fd at low light fluxes likely skews *C. tepidum* carbon flux to be more reliant on acetate as a carbon source relative to CO₂, which manifests as a reduced growth yield on acetate. The opposite effect would come into play at higher light flux, where increased availability of reduced Fd would enable a larger portion of the carbon precursors required for biomass synthesis to come from rTCA CO₂ fixation, increasing the apparent biomass yield on acetate; this effect is aligned with our observations.

In contrast to the yields on an electron equivalent basis, the overall average yield for sulfide growth on acetate was less than that for S⁰ or thiosulfate. This decreased yield implies that there is a higher degree of acetate uptake during growth on sulfide. As discussed above and as was noted in a previous publication (Levy et al.

2016), growth on sulfide led to increased production of storage carbohydrates relative to growth on S^0 or thiosulfate. Accounting for the increased glycogen produced by cells grown on sulfide brought the mean acetate-based yield for sulfide across all light levels closer to that for S^0 and thiosulfate (data not shown). This effect suggests that during growth on sulfide, acetate uptake increases to compensate for increased glycogen production without sacrificing total biomass growth.

These results imply regulation of *C. tepidum* central carbon metabolic flux in response to growth conditions, including changing light level and electron donor.

3.4.3 Discrepancies in the sulfur mass balance suggest intracellular storage of sulfur compounds by *C. tepidum*

Evaluating sulfur mass balance closure is important for assessing the validity of experimental conclusions. Furthermore, an incomplete sulfur mass balance, and the identification of either excess sulfur or missing sulfur, can elucidate gaps in the current understanding of sulfur oxidation pathways. Thus, measurements collected for the main intermediates of *C. tepidum* oxidative sulfur metabolism (sulfide, S^0 , thiosulfate, sulfite, and sulfate), were used to evaluate closure of the sulfur mass balance across the energy landscape.

Across most of the energy landscape, the sulfur mass balance tended to be closed within $\pm 10\%$ (Fig. 3.4-A). However, for later phase cultures grown on sulfide and S^0 at higher light levels, as well as for thiosulfate growth at low light, there was an overall tendency for the recovery of more sulfur in oxidized products than the sulfur initially provided (Fig. 3.4, 3.5). One explanation for this tendency is the compounding of slight inaccuracies in sulfur compound quantitation. However, some common trends in the appearance of the ‘extra’ sulfur suggest that this excess could

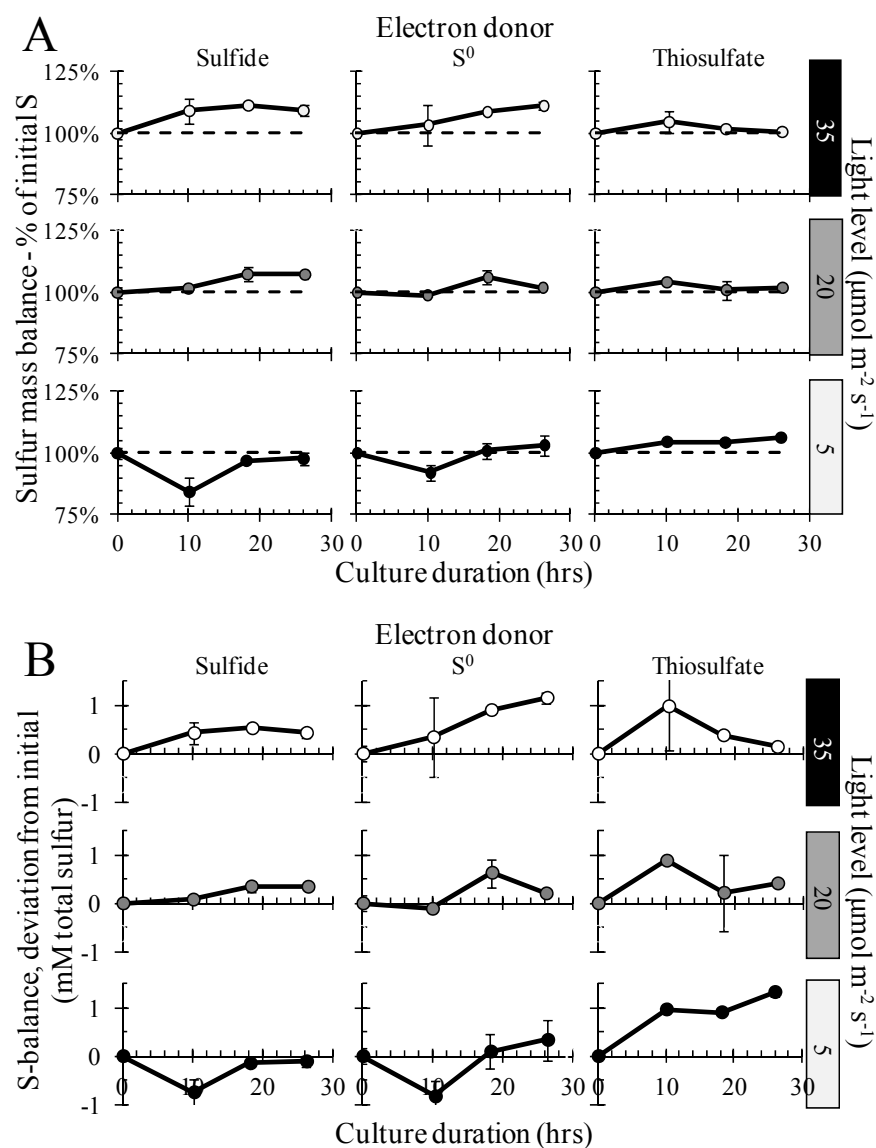


Figure 3.4 Sulfur mass balance closure across the energy landscape. (A) % deviation from initial sulfur; (B) absolute deviation from initial sulfur. Sulfur mass balance closure is shown versus culture duration for all electron donor and light flux level combinations. Points are the average of the sulfur mass balance value for all culture replicates at a given combination of electron donor, light flux level, and culture duration, except for treatments for which there was only a single replicate (see Table 3.1). Error bars represent the standard error of the mean for replicate cultures.

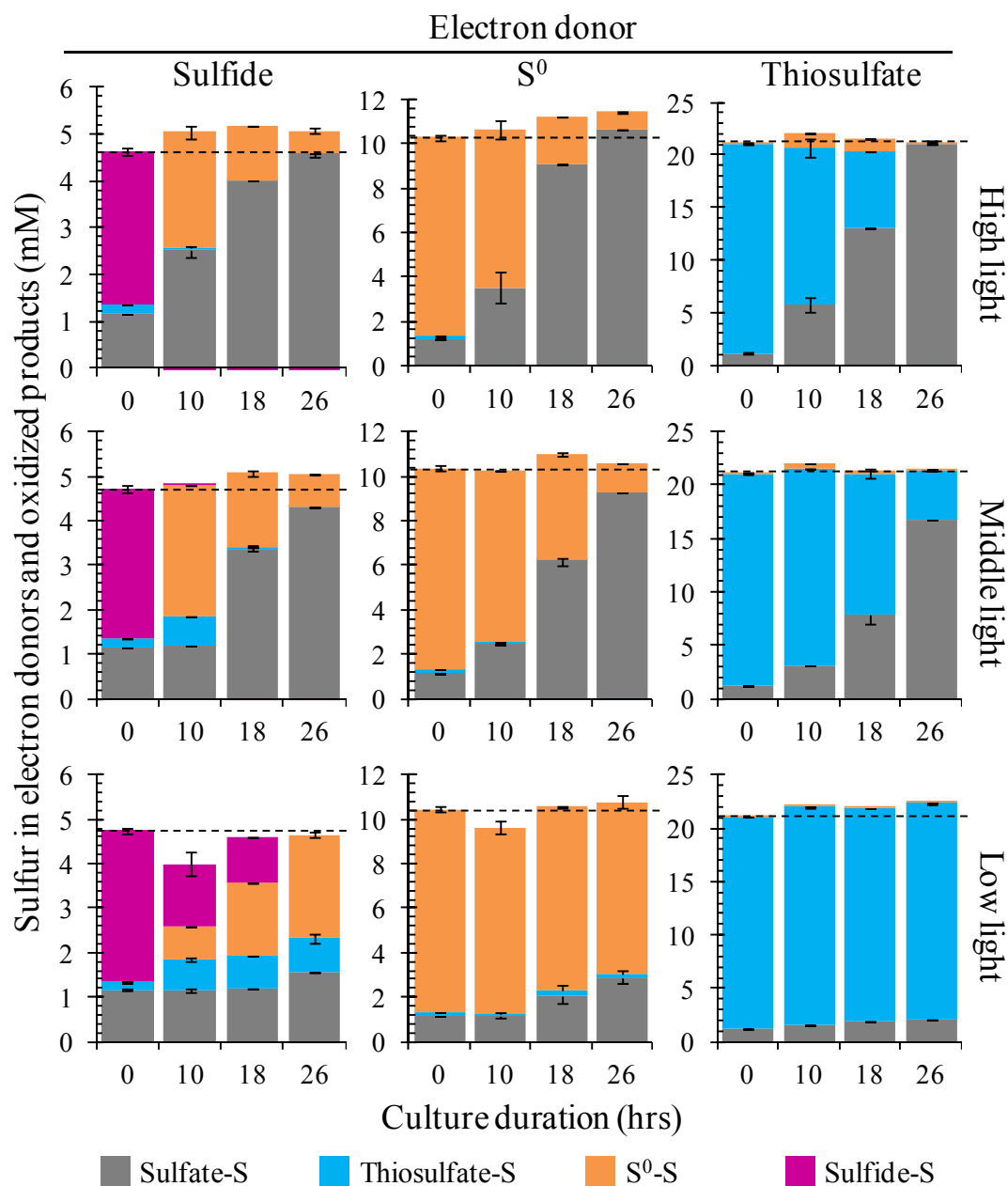


Figure 3.5 Breakdown of sulfur contained in the main intermediates of *C. tepidum* sulfur metabolism across the energy landscape. The dotted reference line indicates the starting total sulfur for each electron donor and allows evaluation of the absolute deviation in the sulfur mass balance. Bars represent the average amount of sulfur in each sulfur intermediate based on culture measurements, except for treatments for which there was only a single replicate (see Table 3.1). Error bars represent the standard error of the mean for replicate cultures.

instead indicate the oxidation of an internal pool of stored, reduced sulfur that was carried over into the experimental cultures from the inocula.

First, the maximum absolute deviation in the sulfur mass balance, +1.3 mM sulfur, was found for low light growth on thiosulfate, but a deviation of approximately +1 mM sulfur was common for the first culture timepoint of thiosulfate-oxidizing cultures across all light levels (Fig. 3.4-B), suggesting that this internal pool was oxidized first, and then later replenished by thiosulfate oxidation in the case of the middle and high light cultures. That no thiosulfate was oxidized in the low light culture (Fig. 3.5; discussed further in section 3.4.6 below), and that this deviation did not correct at later time points, provides some support for this hypothesis.

Second, the amount of ‘extra’ sulfur identified at the end of the high light S^0 cultures was around 1 mM (Fig. 3.4-B, Fig. 3.5), consistent with the amount that appeared in the thiosulfate grown cultures. This observation provides additional support that the amount of internal sulfur delivered to the experimental cultures was constant and derived from the inocula. Furthermore, this observation also suggests that the internal pool of sulfur may serve as an electron donor for phototrophic growth when extracellular electron donor becomes limiting, which would be expected at 26 hours of growth on S^0 at high light. While approximately 0.8 mM S^0 remained at this point, this S^0 could have constituted recalcitrant crystalline sulfur difficult for the cells to oxidize; microscopic images collected from these 26 hour cultures showed cells clustered on large S^0 aggregates (data not shown).

Finally, the appearance of ‘extra’ sulfur in the case of middle and high light sulfur cultures tended to appear after the cultures switched to oxidizing S^0 , although the amount of extra sulfur that appeared (0.35-0.5 mM) is less than what appeared for

growth on S^0 and thiosulfate. This tendency suggests that the pool of internal sulfur could be intermediates of S^0 oxidation, and that they were prevented from being oxidized during sulfide oxidation similar to how S^0 is not oxidized until after sulfide is depleted.

While these data cannot conclusively establish the presence or size of an internal reduced sulfur pool that is available for oxidation under certain growth conditions, these observations motivate future studies to characterize the identity of stored sulfur species and the size of their internal pools. Learning more about how sulfur is stored intracellularly, and the conditions under which the pools are depleted, may provide insight into *C. tepidum* regulation of sulfur oxidation pathways.

While most of the instances of sulfur mass balance discrepancies tended toward the recovery of greater than the starting amount of sulfur, low light growth on sulfide and S^0 revealed ‘missing’ sulfur at early time points (a maximum of $-16\% \pm 6\%$ for sulfide and $-8\% \pm 3\%$ for S^0 ; Fig. 3.4). That these discrepancies were in the opposite direction as was typical prompted deeper investigations of these growth regimes, described in the next two sections.

3.4.4 Polysulfides accumulate extracellularly during early phases of sulfide oxidation and S^0 globule formation

During low light growth on sulfide, depletion of sulfide outpaced the appearance of sulfur in oxidized products through 10 hours growth (Fig. 3.5), and the accumulation of extracellular polysulfides was observed (Fig. 3.6). No production of

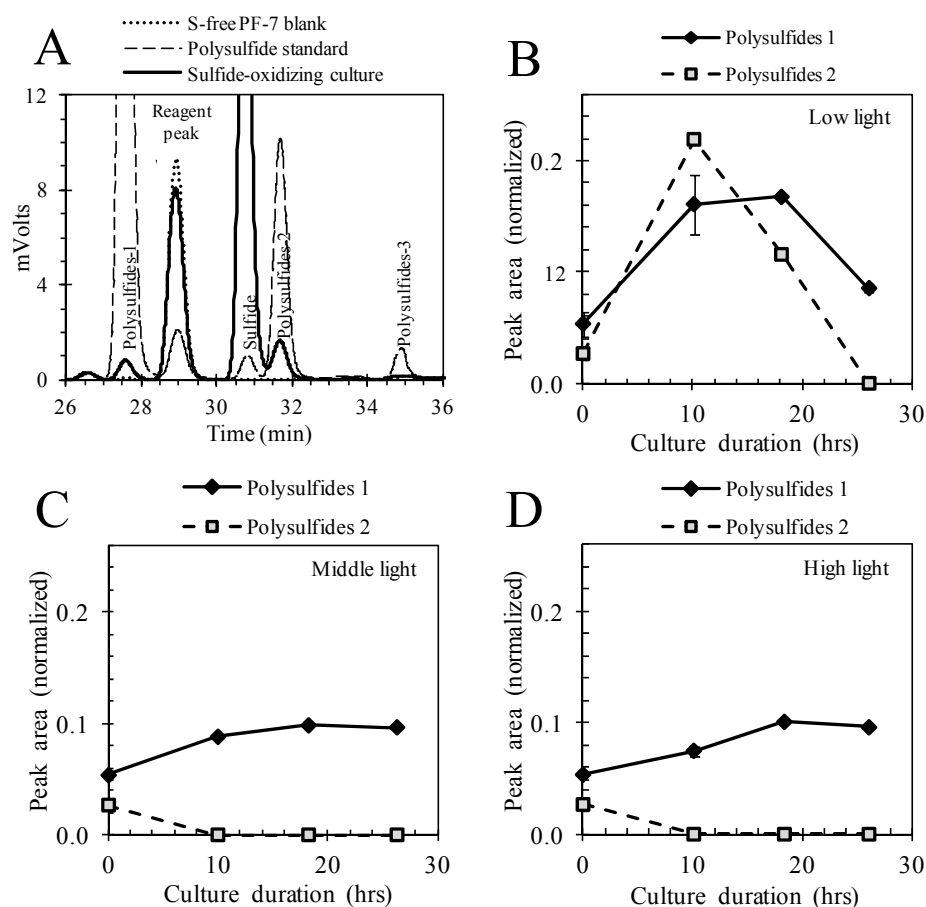


Figure 3.6 Accumulation of polysulfides during *C. tepidum* growth on sulfide. (A) Representative HPLC traces of culture supernatants from a sulfide-oxidizing, S^0 -producing *C. tepidum* culture show the presence of Polysulfide-1 and Polysulfide-2 peaks. Traces for a polysulfide standard and a sulfur-free Pf-7 medium blank are overlaid for comparison. (B) Sulfide oxidation, low light: the Polysulfide-1 and Polysulfide-2 peak areas were observed to change over time, attaining maxima around 10 hours culture. (C) Sulfide oxidation, middle light and (D) sulfide oxidation, high light: Polysulfide-1 and Polysulfide-2 peak areas did not demonstrate substantial increases, suggesting that polysulfides did not accumulate for the time points assessed in these cultures. Normalized peak area = area of the polysulfide peaks normalized to the summed areas of two reagent blank peaks to account for experiment-to-experiment variation in the method. A version of Panel A previously appeared as Fig. 4A in Marnocha et al. (2016).

sulfate was detected until 26 hours of culture when sulfide was depleted, consistent with previous studies of *C. tepidum* and other *Chlorobiaceae* oxidizing sulfide (van Gemerden 1986; Chan et al. 2008; Holkenbrink et al. 2011). An increase in thiosulfate was detected from 0 to 10 hours growth, and the presence of thiosulfate persisted at a remarkably constant level through all timepoints collected from low-light sulfide cultures. Thus, it is unlikely that error in either sulfate or thiosulfate measurements contributed to the ‘missing’ sulfur in the 10 hour timepoint.

Inspection of HPLC chromatographs of biamine-derivatized supernatants (Rethmeier et al. 1997) from these low-light sulfide-grown cultures revealed two soluble thiol-containing compounds that exhibited retention times identical to those of polysulfides in a standard. Fig. 3.6-A presents a representative chromatograph showing these peaks, labeled ‘Polysulfides 1’ and ‘Polysulfides 2’. The area of these peaks exhibited clear dynamics over the course of the low-light sulfide grown cultures (Fig. 3.6-B). Peak areas for Polysulfides-1 and Polysulfides-2 attained maxima around 10 hours cultures, corresponding to the timepoint where the largest discrepancy in the sulfur mass balance was recorded. After 10 hours the peak areas decreased, returning to baseline as sulfide was depleted.

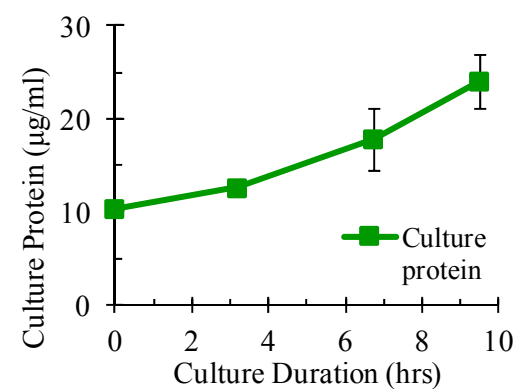
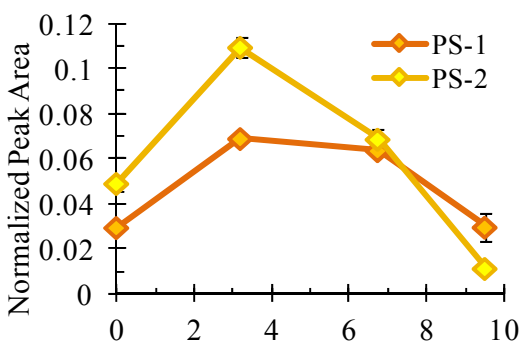
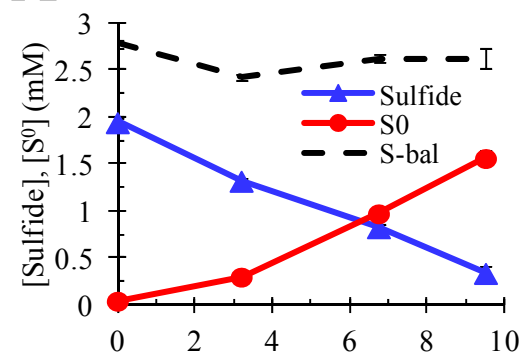
While the Rethmeier method cannot provide quantitative information on the amount of sulfur contained in these polysulfide pools, these data provide a qualitative view of changing polysulfide pool sizes during sulfide oxidation. That the maximum point of ‘missing’ sulfur (10 hours) corresponded to the point of the largest polysulfide peak areas suggests that the missing sulfur was at least partially contained in the accumulated extracellular polysulfides, and is not merely an artifact of errors in the measurement of sulfide or S^0 . Further evidence for this possibility is obtained from the

cultures grown on sulfide at middle and high light levels; at no points examined in these cultures was there 'missing' sulfur (Fig. 3.5) or an accumulation of extracellular polysulfides (Fig. 3.6-B, Fig. 3.6-C). However, because sulfide had been depleted in the middle and high light cultures by the time the first samples were collected, whether the accumulation of polysulfides was specific to the low light condition or had accumulated and subsequently been depleted in the higher light cultures could not be determined from these data.

To assess whether the accumulation of polysulfides during sulfide oxidation was specific to the low light conditions, a follow up study investigated the presence of polysulfides during the early phase of sulfide oxidation at $20 \mu\text{mol m}^{-2} \text{s}^{-1}$ light. The results of this study are presented in Fig. 3.7, Panel A, where extracellular polysulfides were also found to accumulate in the extracellular medium and an incomplete mass balance was observed when the polysulfide peak areas were at their maxima. The presence of polysulfides during sulfide oxidation at a range of light levels suggests that the accumulation of extracellular polysulfides during sulfide oxidation may be an inherent part of S^0 production and implicates the involvement of the PSRLC1 complex mentioned above. Whether the accumulating polysulfides are produced by PSRLC1 and accretion of polysulfides into S^0 is rate-limiting, or whether PSRLC1 oxidizes polysulfides and is itself rate-limiting, remains to be determined. Characterization of the role of PSRLC1 through deletion mutant studies is ongoing in the Hanson lab.

The implication of polysulfides as soluble agents enabling remote growth of S^0 globules is discussed in more detail below (section 3.4.6).

A Sulfide-oxidizing cultures (N = 2)



B S⁰-oxidizing cultures (N = 11)

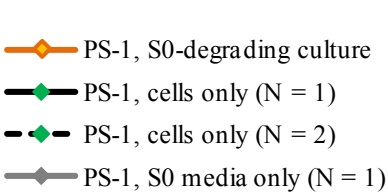
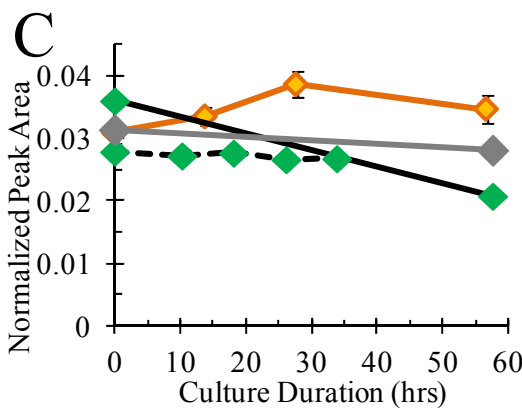
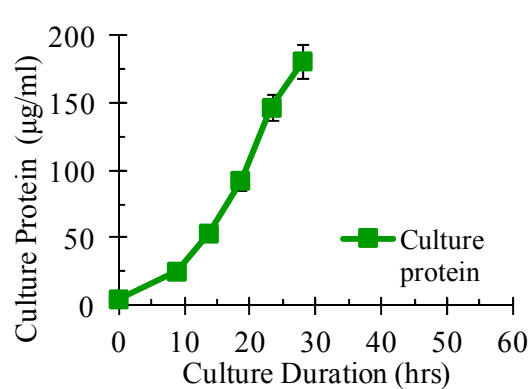
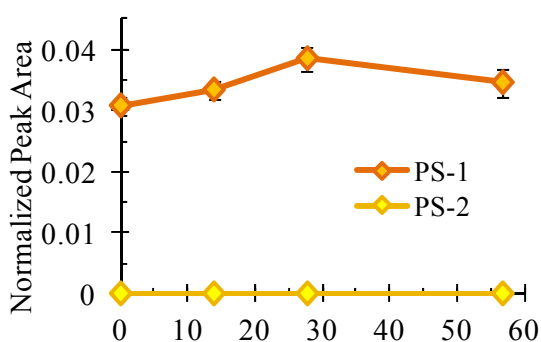
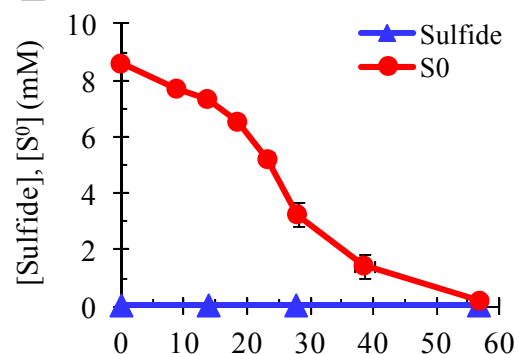


Figure 3.7 Timecourses showing electron donor oxidation, polysulfide presence, and *C. tepidum* growth for (A) sulfide oxidation/S⁰ production and (B) S⁰ degradation during growth at 20 $\mu\text{mol photon m}^{-2} \text{s}^{-1}$ light flux. (A) S⁰ production during oxidation of 1.9 ± 0.4 mM initial sulfide concentration (top graph) coincided with increases in HPLC peak areas of polysulfide species (PS) PS-1 and PS-2 (middle graph). Culture growth based on protein measurements is depicted in the bottom graph. These cultures were grown in a static water bath without mixing. (B) During S⁰ degradation (top graph), the area of peak PS-1 increased but no PS-2 was detected (middle graph). Culture growth based on protein measurements is shown in the bottom graph. Biogenic S⁰ was provided at an initial concentration of 8.6 ± 0.2 mM to all cultures. Cultures were either grown in the heated rotisserie culturing system described in the methods or were continuously stirred during growth in a heated water bath. (C) PS-1 timecourse for the S⁰-degrading cells from Panel B, overlaid with two controls: PS-1 timecourses for two instances of cells inoculated to the same initial density into media with no electron donor (sulfur-free media, N=2 and N=1) and the PS-1 timecourse for S⁰-containing media without cells (N=1). In these controls, PS-1 stayed constant or decreased, while PS-1 increased only for the S⁰-degrading cells. Throughout the cells-only experiments, sulfide was not detected, elemental sulfur remained below 0.01 mM, and culture protein concentrations remained in the range 4-11 $\mu\text{g/ml}$ (data not shown). Normalized peak area = area of the polysulfide peaks normalized to the summed areas of two reagent blank peaks to account for experiment-to-experiment variation. A version of this figure previously appeared as Supplementary Figure S4 in Marnocha et al. (2016).

3.4.5 During S⁰ oxidation at low light, production of sulfate lagged behind S⁰ oxidation

During low light growth on S⁰, no sulfate was produced for at least the first 10 hours of growth despite uptake of S⁰ (Fig. 3.5); only after 10 hours culture did sulfate production commence. No increases in extracellular sulfite or thiosulfate were detected. Unlike the sulfide-oxidizing scenario, polysulfides did not appear to accumulate in the extracellular medium. While a peak with a retention time similar to Polysulfides-1 was present throughout the duration of the low-light S⁰-oxidizing

culture, no Polysulfides-2 peak was detected (see Fig. 3.8-A for a representative chromatograph) and the size of the Polysulfides-1 was essentially constant (Fig. 3.8-B). Thus, it is unlikely that the presence of extracellular polysulfides can account for the ‘missing’ sulfur during the low-light oxidation of S^0 .

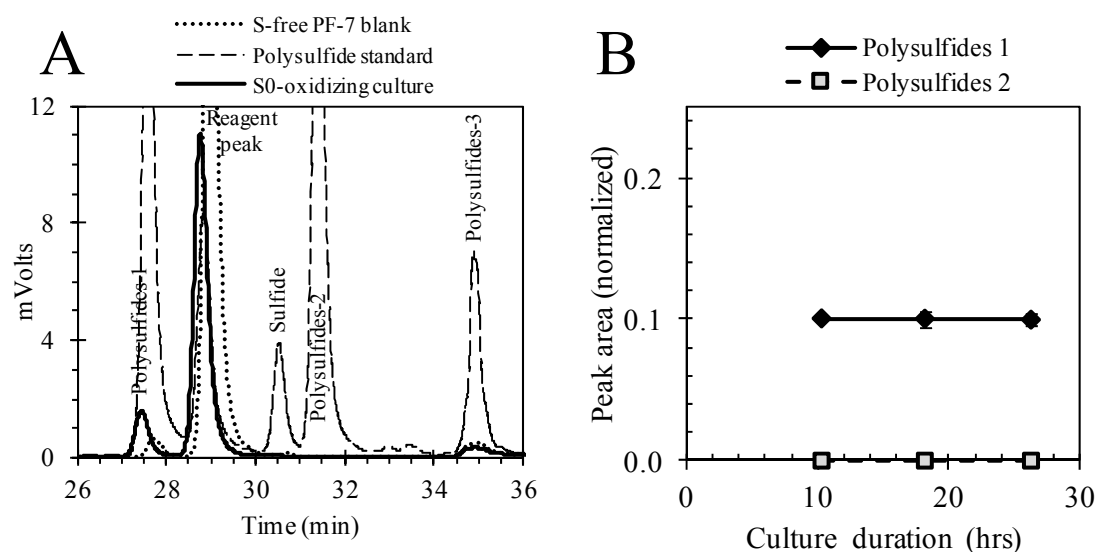


Figure 3.8 Polysulfides were present but did not accumulate during low light growth on S^0 . (A) Representative HPLC traces of culture supernatants from S^0 -degrading cultures showing the presence of only one peak with a retention time similar to Polysulfide-1. Traces for a polysulfide standard and a sulfur-free PF-7 medium blank are overlaid for comparison. (B) S^0 oxidation, low light: the Polysulfide-1 and Polysulfide-2 peak areas were constant with time. A version of Panel A previously appeared as Fig. 4B in Marnocha et al. (2016).

The open mass balance during S^0 oxidation at low light, but not during S^0 oxidation at middle or high light levels, suggests that some step in the oxidation of S^0 to sulfate is rate limited at low light (or very early in the oxidation of S^0), leading to

the accumulation of one or more unidentified intermediate sulfur species. As stated above, the lack of polysulfide accumulation during S^0 oxidation suggests that polysulfide pools are unlikely to be the unidentified intermediate(s). Instead, one possibility is that the intermediate(s) accumulated intracellularly. Another possibility is that the intermediate of S^0 degradation is an extracellular compound that is not detectable by the Rethmeier method (1997) used here, such as a polythionate. Identifying these intermediates as the aim of future studies may help elucidate the mechanisms of S^0 oxidation to sulfite, and employing light-limited growth to induce accumulation of intermediates could be a useful approach in identifying previously undetected intermediates of S^0 oxidation.

While polysulfides are not likely to account for the ‘missing’ sulfur in this growth regime, additional studies were conducted to explore the dynamics of the Polysulfides-1 peak at higher light levels. During S^0 oxidation at $20 \mu\text{mol m}^{-2} \text{s}^{-1}$ light, the Polysulfides-1 peak area appeared to grow over a 30 hour timecourse (Fig. 3.7 Panel B) when compared to the Polysulfide-1 peak areas of cells-only controls and S^0 media-only controls (Fig. 3.7 Panel C). These studies implicate the dissolved thiol species presenting as Polysulfide-1 as a potential candidate in enabling degradation of unattached S^0 globules and in facilitating growth of unattached cells during S^0 degradation; this possibility is discussed in more detail below (section 3.4.6).

3.4.6 Polysulfides as dissolved intermediates involved in S^0 globule production and dissolution at a distance

Recent time-lapse microscopic studies performed by our colleague Dr. Cassandra Marnocha on S^0 -producing and S^0 -degrading cultures of *C. tepidum* have

revealed a number of interesting features of S^0 dynamics that can possibly be explained by the presence of soluble polysulfide intermediates (Marnocha et al. 2016):

1. During sulfide oxidation, S^0 nucleation and growth can occur at a distance from cells.
2. All globules are nucleated within 30 minutes of illuminated incubation, after which point S^0 globules grow but no new globules are nucleated.
3. Growth of S^0 globules occurred whether or not they received transient cell contact during the growth phase, and S^0 globule growth rates were independent of cell contact.
4. During growth on S^0 as electron donor, only 20% of cells were attached to S^0 globules at a given time, but cells grew independently of attachment to S^0 .
5. S^0 globules appeared to degrade independently of contact from cells.
6. Partially degraded S^0 globules examined by scanning electron microscopy displayed a ‘pitted’ appearance, with small (less than the attached surface of cells) pits regularly distributed across the globule surface.

Observations 1, 2 and 3, in conjunction with the observation of transiently accumulating polysulfides during S^0 globule formation (Fig. 3.6, Fig. 3.7 Panel A) suggest that *C. tepidum* produces dissolved sulfur species (i.e. polysulfides) that contribute to S^0 globule nucleation and accretion during sulfide oxidation. A putative model for this process is presented in Fig. 3.9 (left panel), and involves the production of polysulfides during sulfide oxidation by *C. tepidum* that could first cyclize into S_8 rings and aggregate into small condensed sulfur particles; subsequently, polysulfides would continue to accrete onto the nucleated S^0 globules (Marnocha et al. 2016). By this model, S^0 globule nucleation is rapid and should not be rate limiting, and this prediction is aligned with the rapid globule nucleation observed by time-lapse microscopy (Observation 1 above).

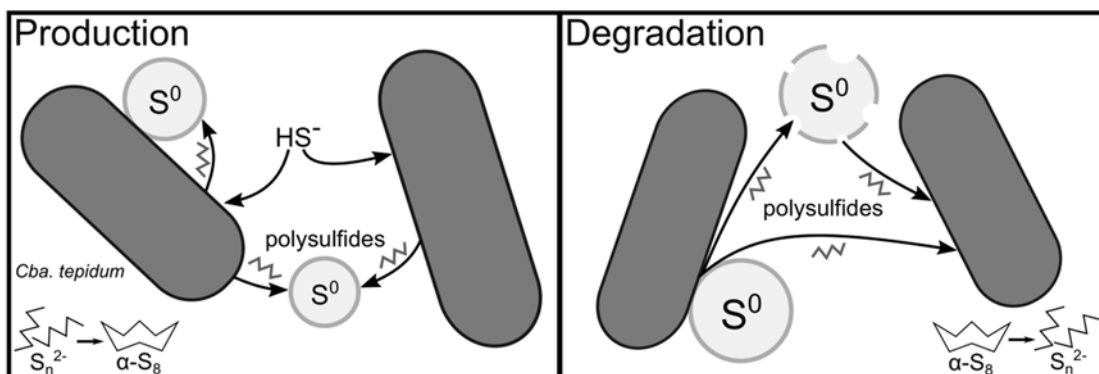


Figure 3.9 Model of S^0 globule production and degradation in *C. tepidum*. During globule production, cells oxidize sulfide (HS^-) to a pool of intermediate, soluble polysulfide. This pool can then accrete into globules. When sulfide is exhausted, globule degradation begins. Attached cells oxidize S^0 globules and produce polysulfide intermediates. These intermediates can then a) degrade globules at a distance from cells, and b) feed unattached cells. This figure was prepared by Cassandra Marnocha and a version previously appeared as Fig. 7 in Marnocha et al. (2016).

Observations 4, 5, and 6 regarding S^0 degradation suggest roles for dissolved intermediates in both degrading S^0 globules as well as in providing electron donor substrates to feed unattached cells. A putative model for this process is presented in Fig. 3.9 (right panel) and involves the initiation of globule degradation by attached cells that release soluble intermediates (possibly polysulfides, as shown in Fig. 3.7 Panel B and C); these polysulfides would both feed unattached cells and activate unattached S^0 globules for degradation by reductively opening S_8 rings and releasing more polysulfides (Marnocha et al. 2016).

Polysulfides have long been suggested to play a role in the production and degradation of S^0 globules (Trüper & Fischer 1982; van Gernerden 1984; Visscher & van Gernerden 1988; Brune 1995; Franz et al. 2009). Here, the combined observations of extracellular polysulfides in *C. tepidum* cultures and of S^0 growth and degradation

at a distance from cells provides evidence supporting a hypothesis of polysulfides as key intermediates of S^0 globule formation and degradation.

3.4.7 Lack of thiosulfate oxidation at low light raises interesting questions about regulation of photosynthetic electron transport under stress conditions

Thiosulfate uptake was not detected at low light (Fig. 3.5 lower right panel), although cells grew, sulfate was produced, and acetate was consumed (Fig. 3.10). The growth rates of the thiosulfate cultures at low light were similar to those for the sulfide and S^0 cultures for the first 20 hours of culture (Fig. 3.10-A), and while there was no sulfur-free control included in this experiment, the growth observed here was greater than that observed in the absence of an electron donor in other experiments (see Fig. 3.7-C). The rates of eeq oxidation and acetate uptake in the thiosulfate cultures were also similar to the low light sulfide cultures (Fig. 3.10-B and Fig. 3.10-C). It is worth noting that the unusual behavior of these cultures did not affect the conclusions drawn above; as yields were calculated based on formation of oxidized products the lack of thiosulfate oxidation had little effect. Furthermore, excluding all low-light thiosulfate cultures from the yield analysis described in section 3.4.1 did not change the hierarchy in biomass-producing power of electrons, and did not change the calculated yield values as a function of electron donor (data not shown).

Interestingly, the cells in the thiosulfate culture at low light demonstrated a much lower photosynthetic pigment content (BChl *c*:protein ratio) than the cells oxidizing sulfide and S^0 (Fig. 3.10-D). This decreased BChl *c*:protein ratio suggests that the cells in the thiosulfate culture down-regulated their photosynthetic apparatus, which occurs when the rate of light energy absorbed by the chlorosomes exceeds the rate of charge separation in the reaction center and photosynthetic electron transport

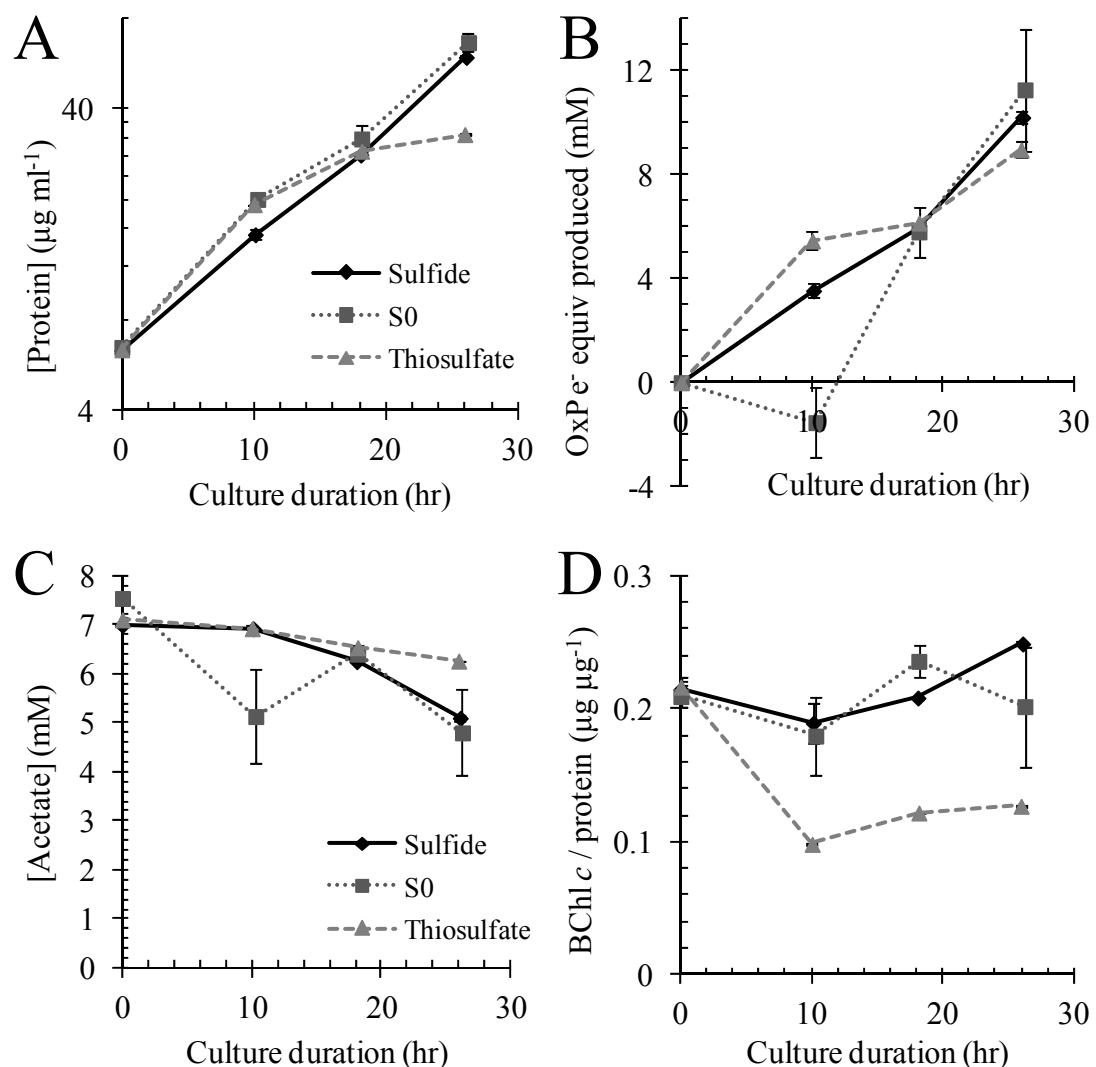


Figure 3.10 Profiles of growth and substrate consumption for energy landscape cultures grown at low light and provided sulfide, S^0 , or thiosulfate as sole electron donor. (A) culture growth, (B) oxidized product formation, (C) acetate consumption, and (D) BChl *c*:protein ratio. Points represent the average of replicate culture measurements, except for treatments for which there was only a single replicate (see Table 3.1). Error bars represent the standard error of the mean for replicate cultures. The legends shown in panels A and C apply to all panels.

(Morgan-Kiss et al. 2009). Imbalances of this sort can be caused by various stressors, including temperature and a lack of oxidizable electron donor for donating electrons to re-reduce the reaction center after photo-oxidation (Morgan-Kiss et al. 2009). Thus, the decreased BChl *c*:protein ratio is consistent with the lack of thiosulfate oxidation, and suggests that some condition was blocking the ability of *C. tepidum* to utilize thiosulfate as electron donor.

We attempted to repeat these results in a follow up study that compared growth on thiosulfate as a sole electron donor with that of cultures inoculated into sulfur-free medium at the low light condition. The results of this follow up experiment are overlaid with those from the energy landscape study in Fig. 3.11. Curiously, in the repeat experiment, thiosulfate was slowly oxidized (Fig. 3.11-C), although rates of growth (Fig. 3.11-A), sulfate production (Fig. 3.11-D) and acetate consumption (Fig. 3.11-E) were similar to the previous experiment. The cultures inoculated into sulfur-free medium (no electron donor) demonstrated similar initial rates of growth, sulfate production, and acetate uptake as the cultures provided thiosulfate, although these rates decreased markedly after 10 hours culture in the absence of thiosulfate. However, neither the thiosulfate or sulfur free cultures in the follow-up experiment demonstrated the depressed BChl *c*:protein ratios exhibited by the energy landscape cultures, suggesting that there was something very different about the physiology of the cells from that experiment.

One possible scenario that could explain some of these observations is the presence of trace oxygen in the medium of the energy landscape cultures, but not in the repeat experiment. Support for this possibility comes from anecdotal observations on the relative age of the media used in the two experiments: sulfur-free media

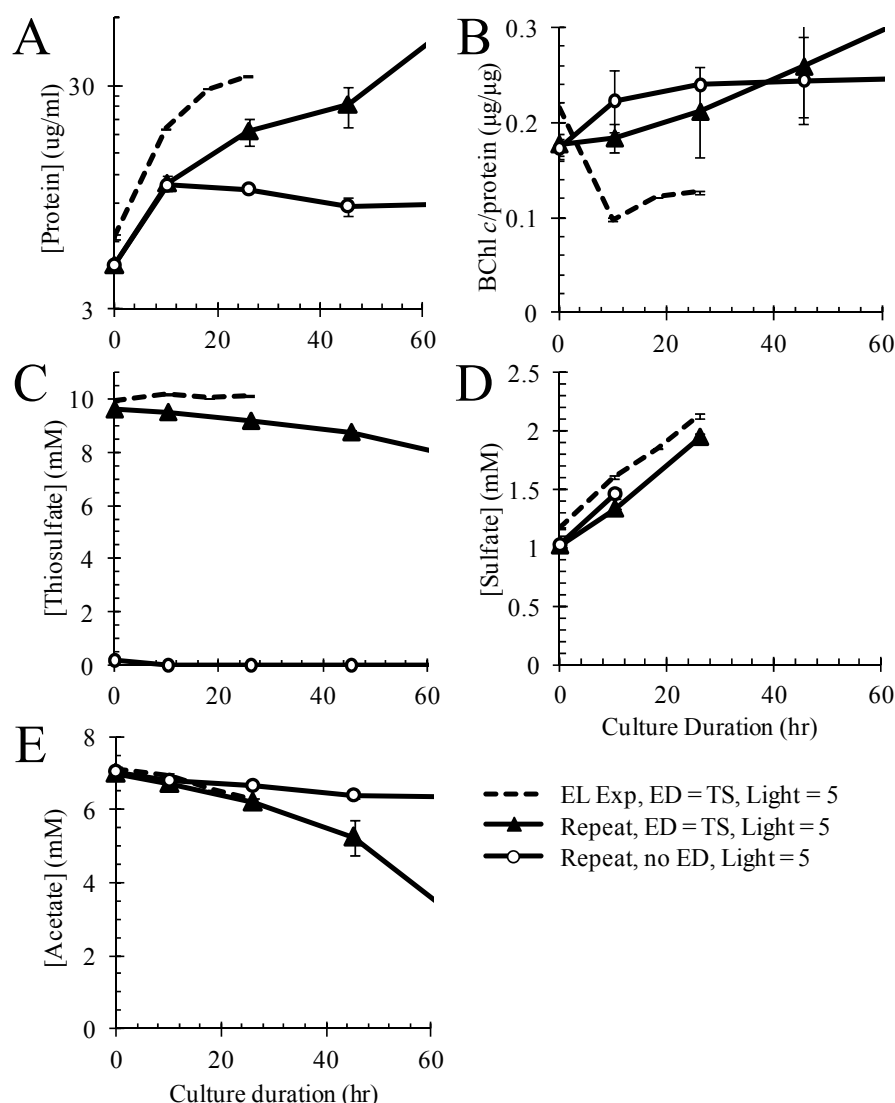


Figure 3.11 Profiles of growth and substrate consumption for cultures provided thiosulfate as sole electron donor at $5 \mu\text{mol photon m}^{-2} \text{s}^{-1}$, compared to cultures provided no electron donor. (A) protein, (B) BChl *c*:protein ratio, (C) thiosulfate, (D) sulfate, and (E) acetate. Points represent the average of replicate culture measurements, except for energy landscape treatments for which there was only a single replicate (see Table 3.1). Error bars represent the standard error of the mean for replicate cultures. Sulfate measurements for the sulfur-free control were not available past 10 hours culture due to an equipment issue. ED, electron donor; EL Exp, energy landscape experiment; TS, thiosulfate.

(subsequently amended with non-sulfide electron donors) used more recently after preparation have demonstrated increased failure rates in experiments, believed to be due to oxygen contamination during preparation that resolves in proportion with the length of storage in anaerobic conditions (see Appendix D). The media used for the energy landscape cultures was prepared 5-7 weeks before use, while the media used for the repeat experiment was prepared 10 weeks before use.

Conceptually, the effect of trace oxygen in the low light thiosulfate conditions would could have occurred as follows:

1. The presence of oxidizing conditions induced quenching of excited BChl *c* (Frigaard & Matsuura 1999), inhibiting photooxidation of the photosynthetic reaction center. Oxygen-dependent down-regulation of the light-harvesting apparatus led to reduced BChl *c* synthesis (through an unknown mechanism), manifesting in the reduced BChl *c* content observed.
2. An over-reduced population of reaction centers would block electron transfer from bound cytochrome *c_z*, which would prevent cytochrome *c_z* from accepting electrons from either the soluble cytochrome c-554 or from the cytochrome *b/c₁* complex. This scenario would keep both c-554 and the cytochrome *b/c₁* complex in a reduced state, limiting electron transfer to c-554 from the Sox system and preventing thiosulfate oxidation, and blocking electron transfer from the quinone pool to the cyt *b/c₁* complex and keeping the quinone pool in a reduced state.
3. The reduced quinone pool would still be able to supply electrons to cytochrome *bd* ubiquinol oxidase (CydA; CT1818) which is thought to have the capacity to reduce oxygen to water and which has been implicated in increasing *C. tepidum* survival through oxygen exposure in both the light and the dark (Li et al. 2009).
4. The production of sulfate could be explained by the oxidation of sulfite to sulfate, which would continue to supply electrons to the quinone pool *via* QmoABC for CydA-mediated O₂ reduction, and suggests that a component of the intracellular sulfur pool could be sulfite. Intracellular pools of sulfite have previously been detected in *C.*

tepidum (Rodriguez et al. 2011; Hiras 2012). Sulfate produced from sulfite oxidation coupled to oxygen reduction could also help explain the ‘extra’ sulfur observed at the 10 hour timepoint for all thiosulfate cultures (described above in section 3.4.3).

Presumably, down-regulation of *C. tepidum*’s photosynthetic apparatus under these conditions would limit photosynthetic electron transfer to ferredoxin. Decreased production of reduced ferredoxin would be expected to lead to decreased CO₂ fixation, acetate assimilation, and growth. Thus, it is curious that these *C. tepidum* cultures demonstrated rates of growth and acetate assimilation that were similar to the sulfide- and S⁰ oxidizing cultures at low light which did not display reduced BChl *c* content. It has been suggested that both the forward and reverse TCA cycles operate during acetate assimilation (Tang & Blankenship 2010); whether this scenario provides a mechanism for generation of reduced ferredoxin and *C. tepidum* growth and acetate assimilation under conditions of limited photosynthetic electron transfer is a possibility that has not been explored.

Another aspect the scenario of trace oxygen contamination would need to explain is why thiosulfate was able to be oxidized at higher light levels. One possibility is that O₂-induced BChl *c* quenching only partially blocks reaction center photooxidation. Thus, at higher light this ‘leaky’ blockage would allow some level of photosynthetic electron transfer and the production of ferredoxin and NADH reducing equivalents. The increased availability of these electron carriers could have enabled faster reduction of oxygen by Roo (rubredoxin oxygen oxidoreductase; CT2285), which has previously been shown to be important for *C. tepidum* survival in the light (Li et al. 2009). Roo obtains electrons from the electron carrier rubredoxin, and NADH reduces rubredoxin in *Clostridium acetobutylicum* by NADH-rubredoxin oxidoreductase (Guedon & Petitdemange 2001). While there is no annotated NADH-

rubredoxin oxidoreductase in the *C. tepidum* proteome, the protein product of *CT2078* is annotated as an NADH oxidase and is homologous to the NADH-rubredoxin oxidoreductase of *Clostridium acetobutylicum* (e-value of 10^{-15} by DELTA-BLAST). Thus, it is possible that at higher light, *C. tepidum* was simply able to reduce oxygen in a shorter timeframe, enabling normal thiosulfate oxidation to commence prior to the first timepoint at 10 hours culture. In fact, we have previously observed light-dependent removal of oxygen by *C. tepidum* cells (unpublished data; see Appendix D), although the exact mechanism for this observation has not yet been established.

In summary, the lack of thiosulfate oxidation under low light conditions is unlikely to be because *C. tepidum* is unable to derive electrons from this electron donor during light limitation; rather this effect was likely a symptom of a unique physiological state of *C. tepidum* potentially due to trace oxygen contamination in the media. These observations, including our inability to replicate them, raises interesting questions about the regulation of photosynthetic electron transport in *C. tepidum* during oxygen- and other stress conditions, as well as about *C. tepidum* mechanisms for coping with transient, trace oxygen in its environment.

3.5 Concluding Remarks

The factorial experimental design employed in this work enabled simultaneous investigation of the effects of different electron donors and varying light levels on *C. tepidum* sulfur metabolism. One example of the benefits of this sort of large, multi-factorial experimental approach is that it allows the identification of synergistic cross-interaction effects of multiple factors that could not be observed by single factor experiments. This approach also provides confidence that an observed effect is not

constrained to a singular condition; for example, we identified a difference in growth yields on eeq oxidized as a function of electron donor that held true across multiple light levels. The downside to a factorial experimental design is that they are labor-intensive at all levels of execution: in the planning, the experimental execution, and the data analysis. However, the amount of information able to be extracted from a single factorial design experiment surpasses the information available from many single factor experiments.

Employing this approach, we were able to detect a difference in *C. tepidum* growth yields as a function of the electron donor type, an effect which has not been previously reported. Furthermore, by modeling our observed growth yields in the context of known and unknown electron transport chain pathways, we obtained evidence that the four-electron transfer involved in the oxidation of S^0 to sulfite may not result in quinone pool reduction and energy conservation. We were also able to investigate the sulfur mass balance across the experimental space formed by different electron donors and light flux levels for cultures grown on tightly controlled conditions. Through this effort we identified regions of the energy landscape where the sulfur balance was not closed, suggesting the oxidation of intracellular stores of sulfur as well as providing evidence for soluble intermediates of S^0 production and degradation. These studies, in conjunction with time-lapse microscopy, have suggested a new model for S^0 production and degradation which involves polysulfides as putative soluble agents of S^0 globule production and dissolution at a distance (Marnocha et al. 2016).

These results have provided insight into uncharacterized steps of S^0 production and degradation, and also form a basis for new routes of investigation, including:

- Identification of the different polysulfide species involved in S^0 globule production and degradation, quantitation of the relative sizes of intracellular and extracellular polysulfide pools, and investigations into their dynamics during different phases of sulfur oxidation.
- Further elucidation of the role of polysulfides in S^0 growth after globule nucleation - are polysulfides alone sufficient for globule growth, or are other factors produced by cells also necessary?
- Investigation into the role of the Polysulfide-1 component during S^0 degradation - does the relatively constant peak area suggest a lack of involvement, or rather balanced production and consumption of this soluble component? Feeding isotopically labeled S^0 globules could to *C. tepidum* and tracing the flow of heavy sulfur isotopes could be a means of investigating the role of this component.

Developing a deeper understanding of the mechanisms of S^0 degradation, as well as S^0 production, will ultimately be important to incorporating all necessary systems into a designer microbe capable of converting the electrons stored in waste elemental sulfur for a useful purpose, and for devising ways of making waste elemental sulfur accessible for oxidation by this type of designer microbe.

REFERENCES

- Azai, C. et al., 2009. Sulfur oxidation in mutants of the photosynthetic green sulfur bacterium *Chlorobium tepidum* devoid of cytochrome c-554 and SoxB. *Photosynthesis Research*, 100(2), pp.57–65.
- Brune, D.C., 1995. Isolation and characterization of sulfur globule proteins from *Chromatium vinosum* and *Thiocapsa roseopersicina*. *Archives of Microbiology*, 163(6), pp.391–399.
- Chan, L.-K. et al., 2008. A genomic region required for phototrophic thiosulfate oxidation in the green sulfur bacterium *Chlorobium tepidum* (syn. *Chlorobaculum tepidum*). *Microbiology*, 154(3), pp.818–829.
- Chan, L.-K., Morgan-Kiss, R.M. & Hanson, T.E., 2009. Functional analysis of three sulfide:quinone oxidoreductase homologs in *Chlorobaculum tepidum*. *Journal of Bacteriology*, 191(3), pp.1026–1034.
- Eddie, B.J. & Hanson, T.E., 2013. *Chlorobaculum tepidum* TLS displays a complex transcriptional response to sulfide addition. *Journal of Bacteriology*, 195(2), pp.399–408.
- Feng, X. et al., 2010. Metabolic flux analysis of the mixotrophic metabolisms in the green sulfur bacterium *Chlorobaculum tepidum*. *The Journal of Biological Chemistry*, 285(50), pp.39544–39550.
- Franz, B. et al., 2009. Unexpected extracellular and intracellular sulfur species during growth of *Allochromatium vinosum* with reduced sulfur compounds. *Microbiology*, 155(2009), pp.2766–2774.
- Frigaard, N.-U. et al., 2003. *Chlorobium tepidum*: Insights into the structure, physiology, and metabolism of a green sulfur bacterium derived from the complete genome sequence. *Photosynthesis Research*, 78(2), pp.93–117.
- Frigaard, N.-U. & Bryant, D.A., 2008. Genomic insights into the sulfur metabolism of phototrophic green sulfur bacteria. In R. Hell et al., eds. *Sulfur Metabolism in Phototrophic Organisms*. Advances in Photosynthesis and Respiration. Dordrecht, The Netherlands: Springer, pp. 337–355.

- Frigaard, N.-U. & Matsuura, K., 1999. Oxygen uncouples light absorption by the chlorosome antenna and photosynthetic electron transfer in the green sulfur bacterium *Chlorobium tepidum*. *Biochimica et Biophysica Acta - Bioenergetics*, 1412(2), pp.108–117.
- van Gemerden, H., 1986. Production of elemental sulfur by green and purple sulfur bacteria. *Archives of Microbiology*, 146(1), pp.52–56.
- van Gemerden, H., 1984. The sulfide affinity of phototrophic bacteria in relation to the location of elemental sulfur. *Archives of Microbiology*, 139(4), pp.289–294.
- van Gemerden, H. & Beefink, H.H., 1978. Specific rates of substrate oxidation and product formation in autotrophically growing *Chromatium vinosum* cultures. *Archives of Microbiology*, 119(2), pp.135–143.
- Grein, F., Pereira, I.A.C. & Dahl, C., 2010. Biochemical characterization of individual components of the *Allochromatium vinosum* DsrMKJOP transmembrane complex aids understanding of complex function in vivo. *Journal of Bacteriology*, 192(24), pp.6369–6377.
- Guedon, E. & Petitdemange, H., 2001. Identification of the gene encoding NADH-rubredoxin oxidoreductase in *Clostridium acetobutylicum*. *Biochemical and Biophysical Research Communications*, 285(2), pp.496–502.
- Hanson, T.E. et al., 2016. *Chlorobaculum tepidum* growth on biogenic S(0) as the sole photosynthetic electron donor. *Environmental Microbiology*, 18(9), pp.2856–2867.
- Hiras, J., 2012. *Characterization of a novel redox active thiol from Chlorobaculum tepidum*. Doctoral Dissertation, University of Delaware, United States of America.
- Holkenbrink, C. et al., 2011. Sulfur globule oxidation in green sulfur bacteria is dependent on the dissimilatory sulfite reductase system. *Microbiology*, 157, pp.1229–1239.
- Levy, A.T., Lee, K.H. & Hanson, T.E., 2016. *Chlorobaculum tepidum* modulates amino acid composition in response to energy availability, as revealed by a systematic exploration of the energy landscape of phototrophic sulfur oxidation. *Applied and Environmental Microbiology*, 82(21), pp.6431–6439.
- Li, H. et al., 2009. Multiple antioxidant proteins protect *Chlorobaculum tepidum* against oxygen and reactive oxygen species. *Archives of Microbiology*, 191(11), pp.853–867.

- Marnocha, C.L. et al., 2016. Mechanisms of extracellular S⁰ globule production and degradation in *Chlorobaculum tepidum* via dynamic cell–globule interactions. *Microbiology*, 162(7), pp.1125–1134.
- Morgan-Kiss, R.M. et al., 2009. *Chlorobaculum tepidum* regulates chlorosome structure and function in response to temperature and electron donor availability. *Photosynthesis Research*, 99(1), pp.11–21.
- Mukhopadhyay, B., Johnson, E.F. & Ascano, M., 1999. Conditions for vigorous growth on sulfide and reactor-scale cultivation protocols for the thermophilic green sulfur bacterium *Chlorobium tepidum*. *Applied and Environmental Microbiology*, 65(1), pp.301–306.
- Oh-oka, H. & Blankenship, R.E., 2013. Green Bacteria: Secondary Electron Donor (Cytochromes). In W. J. Lennarz & M. D. Lane, eds. *Encyclopedia of Biological Chemistry*. Burlington, MA: Academic Press, pp. 510–512.
- Rethmeier, J. et al., 1997. Detection of traces of oxidized and reduced sulfur compounds in small samples by combination of different high-performance liquid chromatography methods. *Journal of Chromatography A*, 760(2), pp.295–302.
- Rodriguez, J., Hiras, J. & Hanson, T.E., 2011. Sulfite oxidation in *Chlorobaculum tepidum*. *Frontiers in Microbiology*, 2(May), 112. doi: 10.3389/fmicb.2011.00112.
- Sakurai, H. et al., 2010. Inorganic sulfur oxidizing system in green sulfur bacteria. *Photosynthesis Research*, 104(2), pp.163–176.
- Sánchez, O., Van Gemerden, H. & Mas, J., 1998. Utilization of reducing power in light-limited cultures of *Chromatium vinosum* DSM 185. *Archives of Microbiology*, 170(6), pp.411–417.
- Seo, D. & Sakurai, H., 2002. Purification and characterization of ferredoxin-NAD(P)(+) reductase from the green sulfur bacterium *Chlorobium tepidum*. *Biochimica et Biophysica Acta*, 1597(1), pp.123–132.
- Shuman, K.E. & Hanson, T.E., 2016. A sulfide:quinone oxidoreductase from *Chlorobaculum tepidum* displays unusual kinetic properties. *FEMS Microbiology Letters*, 363(12), fnw100. doi:10.1093/femsle/fnw100.
- Siefert, E. & Pfennig, N., 1984. Convenient method to prepare neutral sulfide solution for cultivation of phototrophic sulfur bacteria. *Archives of Microbiology*, 139(1), pp.100–101.

- Stockdreher, Y. et al., 2012. Cytoplasmic sulfurtransferases in the purple sulfur bacterium *Allochromatium vinosum*: Evidence for sulfur transfer from DsrEFH to DsrC. *PLoS ONE*, 7(7), e40785. doi: 10.1371/journal.pone.0040785.
- Stockdreher, Y. et al., 2014. New proteins involved in sulfur trafficking in the cytoplasm of *Allochromatium vinosum*. *Journal of Biological Chemistry*, 289(18), pp.12390–12403.
- Tang, K.-H. & Blankenship, R.E., 2010. Both forward and reverse TCA cycles operate in green sulfur bacteria. *Journal of Biological Chemistry*, 285(46), pp.35848–35854.
- Trüper, H.G. & Fischer, U., 1982. Anaerobic oxidation of sulfur compounds as electron donors for bacterial photosynthesis. *Philosophical Transactions of the Royal Society of London*, 298(1093), pp.529–542.
- Visscher, P.T., 1992. *Microbial sulfur cycling in laminated marine ecosystems*. Doctoral Dissertation, University of Groningen, The Netherlands.
- Visscher, P.T. & van Gemerden, H., 1988. Growth of *Chlorobium limicola* f. *thiosulfatophilum* on polysulfides. In *Green Photosynthetic Bacteria*. Boston, MA: Springer US, pp. 287–294.
- Wahlund, T.M. et al., 1991. A thermophilic green sulfur bacterium from New Zealand hot springs, *Chlorobium tepidum* sp. nov. *Archives of Microbiology*, 156, pp.81–90.
- Wahlund, T.M. & Madigan, M.T., 1995. Genetic transfer by conjugation in the thermophilic green sulfur bacterium *Chlorobium tepidum*. *Journal of Bacteriology*, 177(9), pp.2583–2588.
- Wahlund, T.M. & Tabita, F.R., 1997. The reductive tricarboxylic acid cycle of carbon dioxide assimilation: initial studies and purification of ATP-citrate lyase from the green sulfur bacterium *Chlorobium tepidum*. *Journal of Bacteriology*, 179(15), pp.4859–4867.
- De Wit, R., 1989. *Interactions between phototrophic bacteria in marine sediments*. Doctoral Dissertation, University of Groningen, The Netherlands.

Chapter 4

PROTEINS ASSOCIATED WITH *CHLOROBACULUM TEPIDUM* S⁰ PROVIDE INSIGHT INTO MECHANISMS OF S⁰ GENERATION

4.1 Preface

Portions of this chapter are adapted from Hanson, Bonsu, Tuerk, Marnocha, Powell, and Chan (2016) with permission (see Appendix A.3). My contributions to that publication were the comparison of S⁰-associated proteins to proteins from whole-cell *Chlorobaculum tepidum* lysates by one-dimensional denaturing gel electrophoresis, the identification of two uncharacterized proteins associated with *Chlorobaculum tepidum* S⁰, and bioinformatic analyses into these two proteins. These data were published in that work as Fig. 6A, Fig. 6B, Fig. 6C, and Supporting Information Table S1, and in correspond to Fig. 4.4, Fig. 4.5, Fig. 4.13, and Table 4.13 in this dissertation, respectively. Additionally, text that I wrote for this publication was updated and included in this dissertation in sections 4.4.2, 4.4.3, and 4.4.7. All other data in this chapter were generated by myself, and have not been previously published.

4.1.1 Abstract

The mechanisms by which *Chlorobaculum tepidum* and other green sulfur bacteria produce and degrade extracellular zero-valent sulfur globules (S⁰) are poorly understood. To better understand the role of the S⁰ surface in these processes, we used microscopic and proteomic techniques to explore S⁰ properties. During sulfide oxidation, *C. tepidum* cells exhibited a “blebbed” outer surface, where “blebs”

appeared to constitute S⁰ being extruded out of *C. tepidum* cells through the cell membrane. This observation, combined with staining of the S⁰ surface with a membrane-specific fluorescent dye, suggests that *C. tepidum* packages S⁰ into particles with a cell-membrane like coating. Comparing the protein profile of S⁰ with *C. tepidum* whole-cell lysate by one-dimensional denaturing polyacrylamide gel electrophoresis suggested that S⁰ is enriched in a subset of the *C. tepidum* proteome. Extraction of S⁰ proteins using shotgun proteomics-compatible methods enabled comprehensive profiling of the S⁰ “proteome.” The 101 proteins identified in association with S⁰ were enriched in outer membrane, periplasmic, and chlorosome proteins relative to the predicted *C. tepidum* proteome. Strikingly, the S⁰ proteome exhibited substantial overlap with the proteomes of outer membrane vesicles (OMV) of other gram-negative bacteria, where 64% of S⁰ proteins were homologs of OMV proteins. Of particular interest was the detection of DegP, Skp, and SurA homologs, proteins induced by the σ^E cell envelope stress response; these identifications suggest an S⁰ formation mechanism where insoluble S⁰ accumulating in the periplasm of *C. tepidum* is excreted *via* an outer membrane vesicle-like mechanism. Additionally, the identification of proteins involved in cell-envelope spanning transport complexes, cell division, cellular organization, energy-dependent ion transport, proton motive force generation, and ATP synthesis suggests the possibility that S⁰ originates from dedicated, locally-energized regions of the *C. tepidum* surface. Putative roles for uncharacterized proteins found in association with S⁰ are also discussed, including cell-S⁰ recognition, cell-S⁰ docking, and transport of sulfur intermediates of S⁰ metabolism. The specific proteins identified in association with S⁰ provide targets for characterizing their roles in S⁰ production and degradation by *C. tepidum*, and

knowledge gained from these studies will help identify the systems that microbes like *C. tepidum* use to access electrons in S^0 as the electron donor for metabolism. These efforts could enable the coupling of S^0 degradation and oxidation to the production of useful products in engineered bacteria, providing an alternative fate for the waste sulfur produced by petrochemical processing.

4.1.2 Importance

Crude oil and natural gas processing generates 1.8 million tons of waste sulfur annually in the United States, far in excess of demand. One unexplored route for use of this waste is to couple the elemental sulfur-degrading capacity of microbes to the synthesis of useful products. To better understand microbial mechanisms of degrading elemental sulfur, we analyzed the molecular signatures present on the surface of elemental sulfur globules (S^0) produced by the green sulfur bacterium *Chlorobaculum tepidum*. These efforts revealed a cell membrane-like coating on S^0 and produced the “proteome” of S^0 , which was found to contain proteins similar to the proteomes of outer membrane vesicles (OMVs). These observations provided initial evidence for a mechanism of S^0 formation analogous to that of OMVs, and identified protein candidates that could participate in cell- S^0 recognition or docking for S^0 degradation.

4.2 Introduction

The development of microbially-catalyzed processes for converting the energy and electrons stored in waste sulfur to useful compounds requires knowledge of the systems employed by microbes to use biogenic zero-valent sulfur as an electron donor. Insight into the mechanisms of cellular attachment to S^0 and the pathways for importing sulfur intermediates and delivering them to downstream oxidation systems

are key areas for exploration. Cultivating an improved understanding of how microbes generate zero-valent S^0 globules will provide insight into the properties which are imparted to S^0 by microbes, properties which could be very different from the form of sulfur from the waste sulfur produced by the petrochemical industry. Identifying differences between these forms of sulfur is important for determining which microbial S^0 degradation systems would be best suited for waste sulfur utilization and for assessing whether pre-treatment would be required before downstream utilization. To address these knowledge gaps, we focused on improving our understanding of the properties of S^0 produced by *Chlorobaculum tepidum* to provide insight into both S^0 production and degradation processes.

Certain aspects of dissimilatory sulfur oxidation in the *Chlorobiaceae* are well understood, and much of this sulfur oxidation machinery is shared with the well-studied purple sulfur bacterium *Allochromatium vinosum* (f. *Chromatium vinosum*) (Frigaard & Dahl 2009; Gregerson et al. 2011; Hanson et al. 2016). For example, sulfide is known to be oxidized to disulfide or polysulfides with electrons delivered to the quinone pool *via* sulfide:quinone oxidoreductase (SQR) (Chan et al. 2009; Gregerson et al. 2011; Shuman & Hanson 2016). The dissimilatory sulfite reductase system (DSR) is known to be essential for S^0 degradation (Holkenbrink et al. 2011), and is thought to oxidize cytoplasmic polysulfides or organic $R-S_n-H$ to sulfite (Gregerson et al. 2011). Finally, sulfite is oxidized to sulfate by either adenylylphosphosulfate reductase (APR), ATP sulfurylase (Sat), and a membrane bound oxidoreductase (QmoABC; Rodriguez et al. 2011) or through polysulfide reductase-like complex 3 (PSRL3; Gregerson et al. 2011). However, how the polysulfide product of SQR is packaged into extracellular S^0 globules, how sulfur

compounds from S^0 are imported back into the cell and cytoplasm prior to downstream oxidation, and how cells attach to S^0 during production and degradation are all poorly understood.

The surface of S^0 is believed to play a role in cell- S^0 attachment. Pure orthorhombic elemental sulfur is hydrophobic, but the hydrophilic properties of S^0 produced by diverse sulfur oxidizing microbes are well-documented (Janssen et al. 1994; Kleinjan et al. 2003), although the reason for this hydrophilic property has been debated and may be species-dependent (Kleinjan et al. 2003). While commercial elemental sulfur is able to be taken up and subsequently oxidized by *A. vinosum*, there have been no reports of successful growth of *C. tepidum* on this form of sulfur (Hanson et al. 2016). Attempts to grow *C. tepidum* on abiotic hydrophilic sulfur sols such as the Weimarn sol have also failed (Hanson et al. 2016). One explanation for these observations is that there is something unique about the surface of S^0 produced from sulfide oxidation by *C. tepidum* that enables its use by the bacterium.

Analyses of purified S^0 from *C. tepidum* have revealed that it contains carbon, nitrogen, and oxygen, and molecular signatures for proteins and other organics. Bulk elemental analysis detected 0.23-0.30% carbon and 0.28-0.36% oxygen for biogenic S^0 (compared to 0-0.13% carbon and no oxygen for commercial elemental sulfur), and analysis of the surface of S^0 globules by scanning electron microscopy electron dispersive X-ray spectroscopy (SEM-EDX) revealed a high and variable carbon content that exceeded the sulfur content (59% carbon vs. 41% sulfur) (Hanson et al. 2016). Although nitrogen was not detected by bulk analysis and was not detectable by the SEM-EDX method, molecular fragments with masses consistent with amino acid fragments were detected by time-of-flight secondary ion mass spectrometry (Hanson

et al. 2016). These results suggest the presence of a ‘coating’ on S^0 produced by *C. tepidum* that is composed of organic molecules. Interestingly, the presence of ‘remnants’, which are believed to be the shell of S^0 globules left behind after consumption, has been observed in sulfide-grown *C. tepidum* cultures where oxidation of sulfur substrates is allowed to progress to completion (C. Marnocha, unpublished data). Analyses of these remnants by nano-infrared spectroscopy have revealed bands characteristic of amide bonds, suggesting the presence of proteins, although the presence of other organics including lipids cannot currently be excluded. Transmission electron microscopy and electron energy loss spectroscopy of remnants also showed evidence of carbon and nitrogen (C. Marnocha, unpublished data). The sum of these observations suggests a model by which an organic ‘coating’ is deposited on S^0 globules by *C. tepidum*, and that this organic layer could be critical to enabling interactions between the globules and S^0 .

Previous studies that used a dialysis membrane to separate *C. tepidum* cells and S^0 have shown that cell- S^0 contact is required for S^0 globule oxidation and cell growth on S^0 as substrate (Hanson et al. 2016). However, only a portion of the cell population appears to be in contact with globules during either S^0 generation or degradation. Based on the portion of culture protein that remains in association with S^0 after separation of cells and S^0 from a S^0 -degrading culture by sucrose density centrifugation, Hanson et al. (2016) found that approximately 20% of cells were attached to S^0 . These results were confirmed by time-lapse microscopy, where less than 20% of cells were observed attached to S^0 at any one time (Marnocha et al. 2016). However, cells were found to grow and divide independently of whether or not they were attached to globules, and S^0 was degraded whether or not they were attached

to cells. Similar observations were made for S^0 generation, where S^0 globules grew both at a distance from cells as well as attached to cells, and where only transient contact between cells and certain S^0 globules was observed. These data suggested the involvement of soluble intermediates, which could (1) enable growth of previously-nucleated S^0 during sulfide oxidation, and (2) feed unattached cells during S^0 degradation. Polysulfide species were detected and proposed as candidates (Marnocha et al. 2016; see also Chapter 3 of this dissertation). However, these studies did not provide insight into what aspects of the *C. tepidum* cell and S^0 surface could modulate these interactions.

Based on the evidence for amino acids or proteins on the surface of S^0 , and the presence of protein envelopes surrounding the intracellular S^0 deposited by *A. vinosum*, *Beggiatoa alba*, and other organisms (Nicholson & Schmidt 1971; Strohl et al. 1981; Brune et al. 1995), we decided to use proteomic techniques, coupled with additional microscopy work, to investigate the proteins that tend to preferentially associate with S^0 . However, methods for the extraction of proteins from extracellular S^0 produced by the *Chlorobi* have not been well documented in the literature. While the sulfur globule proteins (SGPs) that associate with intracellular sulfur globules of *A. vinosum* and *Thiocapsa roseopersicina* have been identified (Brune 1995), no homologs for these proteins are encoded by the *C. tepidum* genome. These SGP proteins were first observed as prominent protein bands by sodium dodecyl sulfate polyacrylamide gel electrophoresis (SDS-PAGE), and were identified by N-terminal sequencing after extraction into 50% acetonitrile, 1% trifluoroacetic acid, and 10 mM dithiothreitol. The SGP proteins are unusually enriched in glycine and aromatic amino

acids (Brune 1995), which likely facilitated their extraction into 50% organic solvent extraction buffer.

In this work, observations of S⁰ globules protruding from the *C. tepidum* cell surface prompted the identification of proteins associating with S⁰. Initial proteomic investigations employed SDS-PAGE to extract and separate S⁰ proteins, and proteins from gel bands were identified by matrix-assisted laser desorption time of flight mass spectrometry (MALDI-TOF MS/MS). We subsequently developed protein extraction protocols compatible with shotgun proteomic characterization of S⁰ by liquid chromatography MALDI-TOF MS/MS, enabling a more comprehensive examination of the S⁰ ‘proteome’. *C. tepidum* S⁰ globules appeared to contain an enriched subset of the bulk cellular proteome, where the presence of proteins related to unfolded protein and envelope stress implied that S⁰ globule formation may be a stress response in *C. tepidum*. Other proteins identified in association with S⁰ included spatially-regulated proteins involved in cell shape and division, and proteins that mediate connections between the outer membrane, inner membrane and peptidoglycan. These observations suggest that S⁰ globules may be excreted from dedicated sites on the surface of *C. tepidum* cells. Finally, the *C. tepidum* S⁰ proteome exhibited a substantial overlap (63%) with the proteins found in association with the outer membrane vesicles of gram-negative bacteria, potentially implicating a vesiculation mechanism in S⁰ formation.

4.3 Materials and Methods

4.3.1 Strains and growth conditions

All experiments were conducted with *C. tepidum* wildtype (WT) strain WT2321, a plating strain derivative of the original TLS1 isolate (Wahlund et al. 1991) or a mutant strain of *C. tepidum* (strain C3) deficient in utilizing S^0 for growth (Hanson et al. 2016); strain C3 was produced from WT2321 by *in vitro* transposition mutagenesis (Chan et al. 2008). *C. tepidum* was grown in Pf-7 medium prepared as previously described (Chan et al. 2008) with a 177 kPa anaerobic headspace composed of 95% N_2 and 5% CO_2 passed through a heated copper scrubber. Cultures were inoculated to an initial density of $4 \mu\text{g protein ml}^{-1}$. In instances where cultures were grown with sulfide or S^0 as the sole electron donor, thiosulfate and sulfide were omitted from Pf-7 to make sulfur-free Pf-7 (SF Pf-7), and concentrated stocks of sulfide (Siefert & Pfennig 1984) or S^0 (see below) were used to amend SF Pf-7 to the desired concentrations. Standard growth conditions for WT2321 were 45-46 °C and a light field of $20 \mu\text{mol photons m}^{-2} \text{s}^{-1}$ measured with a light meter equipped with a quantum PAR sensor (LI-COR).

4.3.2 Light microscopy

Culture and S^0 samples collected for microscopy were preserved with formalin, and were stored in the dark at 4 °C. Phase contrast, differential interference contrast (DIC), and fluorescent microscopy were performed using an AxioImager Z1 light microscope (Zeiss), an AxioCam Mrm camera, and Axiovision software at 1000x total magnification. For lipophilic dye staining, S^0 slurry, Vectashield (Vector Laboratories), and FM® 1-43FX (Molecular Probes™) were mixed on a slide in a ratio of 8:1:1 by volume; epifluorescent microscopy was performed using an X-Cite®

120Q light source and 120-watt lamp (Excelitas Technologies Corporation) and Filter Set 38 HE (Zeiss).

4.3.3 Cryo-scanning electron microscopy and energy-dispersive x-ray spectroscopy

Samples were prepared for scanning electron microscopy (SEM) by gently filtering samples onto 0.2 μm pore size 25 mm black polycarbonate membrane filters (General Electric) and washing three times with deionized water. Samples were mounted onto specimen holders with Tissue Freezing Medium (Electron Microscopy Sciences). Samples were plunged into liquid nitrogen and a vacuum was pulled to transfer samples to a Gatan Alto 2500 cryo chamber at a temperature of $-125\text{ }^{\circ}\text{C}$. Samples were then sublimated for 10 minutes at $-90\text{ }^{\circ}\text{C}$ followed by cooling to $-125\text{ }^{\circ}\text{C}$. A thin layer of gold palladium was sputtered onto the samples, and they were then transferred into a Hitachi S-4700 Field-Emission Scanning Electron Microscope for imaging by SEM at the voltages indicated below. Elemental analysis was performed by energy-dispersive x-ray spectroscopy (EDX) using an Oxford Inca X-act detector.

4.3.4 Generation of S^0 by repeated sulfide feeding and S^0 purification

A list of the S^0 batches generated and purified by these methods is provided in Table 4.1. Cultures (0.5-1.0 L) of either WT2321 or strain C3 were grown on Pf-7 medium in narrow-mouth screw-cap bottles with an open phenolic cap and butyl rubber septa (Fisher Scientific) with the periodic addition of sulfide to a concentration of 2-4 mM from an anoxic, sterile, neutral sulfide solution (Siefert & Pfennig 1984). To qualitatively assay for the presence of sulfide, equal volumes of culture supernatant were mixed with 10 mM CuCl_2 , where the formation of a distinct grey precipitate indicated the presence of sulfide greater than 0.2 mM. Sulfide was added to cultures

when it was no longer detectable by this assay. Cultures were fed sulfide until sulfide uptake ceased, and S⁰ was harvested as described below after 7-10 days of culture.

Table 4.1 List of S⁰ batches used in Chapter 4 studies and details of their preparation.

S ⁰ batch ID	Strain	Sulfide feeding method	Secondary purification?	Purified S ⁰ storage prior to characterization studies
C3-A	C3	repeated	No ¹	Anaerobic chamber, room temperature
C3-B	C3	repeated	Yes	Anaerobic chamber at room temperature then -80 °C
WT-A	WT	repeated	No	Anaerobic chamber at room temperature then -80 °C
WT-B	WT	single	No	-80 °C
WT-C	WT	single	No	-80 °C

S⁰ was purified from cultures by sucrose density centrifugation (Donà 2011). All transfers were carried out in an anaerobic chamber (Coy Laboratory Products) using sterile, SF Pf-7 directly or as the solute for any solutions. For the primary purification, S⁰-containing cultures were transferred into sterile 250 ml centrifuge bottles with o-ring sealing caps (Nalgene, Thermo Fisher Scientific). Cells and S⁰ were collected by centrifugation at 1,000 × g (JA-14 rotor, Beckman-Coulter) for 10 min at 10 °C, except for batch C3-D where the initial collection was performed at 2,000 × g for 15 mins. The cell-containing supernatant was removed and cells plus S⁰ were suspended in a minimal volume. The resulting suspension was layered over 100 ml of sterile 2.5 M sucrose solution (density ~1.32 g ml⁻¹) in sterile 250 ml centrifuge bottles with o-ring sealing caps. The S⁰ was pelleted through the sucrose by centrifugation at 4,000 × g (JA-14 rotor) for 20 min at 4 °C. The supernatant was

removed and the collected S^0 from the pellet was centrifuged through 2.5 M sucrose two more times. For batches C3-C and C3-D, the speed and duration of centrifugation were increased (up to $5,000 \times g$ and 45 mins, respectively) to better pellet S^0 . Collected S^0 was washed to remove sucrose by suspending in S-free Pf-7 and centrifuging at $17,500 \times g$ (JA-14 rotor) for 5 min at $10^\circ C$; this step was repeated twice. S^0 collected from the initial purification was suspended in SF Pf-7 in a 15 ml conical tube, and stored at room temperature in an anaerobic chamber. S^0 generated by WT cells was used directly for subsequent studies without additional purification, as cell contamination was found to be negligible by phase contrast microscopy.

S^0 generated by the C3 mutant retained some cell contamination after the first purification stage, due to cells adhered to the S^0 that carried through purification. Therefore, C3 S^0 was allowed to rest at room temperature in an anaerobic chamber for 5-13 days to allow firmly attached cells to detach. During the rest period, the supernatant was periodically aspirated and replaced to remove detached cells. Subsequently, a secondary purification was performed (except batch C3-A). The S^0 was resuspended by vortexing, and deposited on top of 20 ml of 2.5 M sucrose in 50 ml centrifuge tubes with o-ring sealing caps (Nalgene, Thermo Fisher Scientific). The S^0 was pelleted through the sucrose by centrifugation ($6,000 \times g$, 50 min, $4^\circ C$) in a swinging bucket rotor (JS-13.1 rotor, Beckman-Coulter), which reduced disruption of the S^0 pellet during handling. The supernatant was removed, and the collected S^0 from the pellet was centrifuged through 2.5 M sucrose two more times. To remove sucrose, the S^0 was washed by suspending in SF Pf-7 and centrifuging at $17,500 \times g$ (JA-14 rotor) for 5 min at $10^\circ C$; this step was repeated twice. Finally, the S^0 was suspended in ~ 10 ml SF Pf-7. Samples for total protein content and sulfur content were collected

and stored at -20 °C until analysis. Purified S⁰ was stored in the anaerobic chamber at room temperature until proteomic analysis, unless otherwise specified (see Table 4.1).

4.3.5 Generation of S⁰ by single sulfide feeding and S⁰ purification

A list of the S⁰ batches generated and purified by these methods is provided in Table 4.1. Cultures (0.5-0.6 L) of strain WT2321 were grown on sulfide-only Pf-7 (4-5 mM sulfide) in narrow-mouth screw-cap bottles with an open phenolic cap and butyl rubber septa at 30 $\mu\text{mol photon m}^{-2} \text{ s}^{-1}$ for 1-1.5 days until sulfide was no longer detectable by the precipitation of Cu²⁺ ions, as described above. Cultures were transferred into sterile 250 ml centrifuge bottles with o-ring sealing caps (Nalgene, Thermo Fisher Scientific). Cells and S⁰ were collected by centrifugation at 1,000 $\times g$ (JA-14 rotor) for 10 min at 10 °C. The cell-containing supernatant was removed and cells plus S⁰ were suspended in a minimal volume. The resulting suspension was layered over 25 ml of sterile 2.5 M sucrose solution (density $\sim 1.32 \text{ g ml}^{-1}$) in sterile 50 ml centrifuge tubes with o-ring sealing caps (Nalgene, Thermo Fisher Scientific). The S⁰ was pelleted through the sucrose by centrifugation at 6,000 $\times g$ (JS-13.1 rotor) for 50 min at 4 °C. The supernatant was removed, and the resuspended pellet was centrifuged through 2.5 M sucrose two more times. Collected S⁰ was washed to remove sucrose by suspending in S-free Pf-7 and centrifuging at 17,500 $\times g$ (JS-13.1 rotor) for 5 min at 10 °C; this step was repeated twice. S⁰ was suspended in SF Pf-7 and immediately distributed into aliquots for characterization studies; aliquots were stored at -80 °C until use.

4.3.6 Protein measurements of *C. tepidum* cells and purified S⁰

Protein assay methods previously calibrated for *C. tepidum* cell samples (Levy et al. 2016) were used to estimate the protein content of purified S⁰ and cell pellet control samples. Briefly, pigments were first removed from *C. tepidum* cells collected by centrifugation ($16,873 \times g$, 5 mins) by methanol extraction (-20 °C, 10 mins). Depigmented cells or purified S⁰ was treated with 0.25 M NaOH (10 mins), neutralized with an equal volume of 0.25 M HCl, centrifuged gently to pellet S⁰ ($14 \times g$, 1 min), and diluted with 0.25 M NaCl prior to protein quantitation. Protein measurements by Bradford assay were performed using Protein Assay Dye Reagent Concentrate (BioRad Laboratories) according to manufacturer instructions. Protein measurements by BCA assay were performed with the Pierce® BCA kit (Thermo Scientific) at 37 °C incubation; the ratio of sample to working reagent was increased to 1:2 vol/vol. Bovine serum albumin (> 98%, EM Science OmniPur®) was used as a protein standard.

4.3.7 Extraction of S⁰-associated proteins for examination by one-dimensional sodium dodecyl sulfate polyacrylamide gel electrophoresis (SDS-PAGE)

To remove proteins from S⁰ for examination SDS-PAGE, a range of treatments involving different formulations of SDS-PAGE sample buffers were used. “L” sample buffers are formulated for Laemmli Tris-HCl gel chemistry, and at a 1X concentration contain 31.25 mM Tris-HCl (pH 6.8), 1% w/v SDS, 12.5% v/v glycerol, and 0.005% w/v bromophenol blue. “T” sample buffers are formulated for Tris-Tricine gel chemistry and at a 1X concentration contain 100 mM Tris-HCl (pH 6.8), 1% w/v SDS, 20% v/v glycerol, and 0.02% w/v Coomassie Brilliant Blue G-250. Laemmli and Tris-Tricine sample buffers containing a reducing agent (either 1% v/v beta-mercaptoethanol or 35 mM dithiothreitol) are designated LR and TR, respectively,

while sample buffers without reducing agents are L(-) and T(-) respectively. Sample buffers at 1X concentration were used to extract proteins from solid samples (i.e. S⁰ and *C. tepidum* cell pellets). In the case of proteins in solutions, protein solution was mixed with concentrated sample buffers to achieve a final 1X sample buffer concentration. The exact sequences of the treatments are specified in the relevant sections below. Proteins were extracted from *C. tepidum* cell control samples by resuspending cells collected by centrifugation ($16,873 \times g$, 5 mins) in the specified sample buffer. Prior to gel loading, all protein extracts were heated at 95°C in the presence of reducing agent (unless stated otherwise) and were centrifuged at $16,000 \times g$ for 2 mins to remove insoluble material, including S⁰. Protein molecular weight markers were loaded according to manufacturer instructions as controls in at least one lane of every gel.

4.3.8 One-dimensional SDS-PAGE

Solubilized proteins were loaded onto one-dimensional protein gels with gel chemistries targeted for protein molecular weight ranges of interest. Laemmli Tris-HCl SDS-PAGE gels were used for investigations of larger molecular weight proteins, while Tris-Tricine SDS-PAGE gels were used for investigations of peptides and smaller proteins. All gels were run at 100 V constant voltage until the dye front migrated close to the end of the gel using running buffer formulated for the gel chemistry. Laemmli running buffer for Tris-HCl gels contained 25 mM tris base, 192 mM glycine, and 0.1% SDS (pH = 8.3). Tris-Tricine running buffer contained 100 mM Tris base, 100 mM tricine, 0.1% SDS (pH = 8.3).

To minimize the loss of small peptides, Tris-Tricine gels were fixed (40% methanol and 10% acetic acid, 30 mins) after electrophoresis; SDS-PAGE gels were

washed in water (5 mins). Gels were stained either with Coomassie (Bio-Safe Coomassie Stain, BioRad) or Sypro® Ruby Protein Gel Stain (Life Technologies) according to manufacturer instructions. Gels stained with Coomassie were imaged by an AlphaImager® HP (Alpha Innotech, San Leandro, CA); gels stained with Sypro-Ruby were imaged by a FLA-3000 fluorescent imager (Fujifilm Corp.) or a Typhoon FLA-7000 (General Electric).

4.3.9 Protein identification from gels

Gel plugs were excised from protein bands of interest, and proteins were identified by mass spectrometry following trypsin digestion as previously described (Hayduk, et al. 2004; Levy et al. 2014). Briefly, gel plugs were subjected to digestion with trypsin (Promega Corporation). The resulting peptides were desalted and concentrated with C18 ZipTips (EMD Millipore) spotted onto stainless steel target plates with α -cyano-4-hydroxycinnamic acid (Sigma-Aldrich) as matrix. Analysis was performed by MALDI-TOF/TOF mass spectrometry on an AB Sciex 4800 MALDI-TOF/TOF Analyzer. Mass spectrometry (MS) and tandem MS spectra were submitted for Mascot v2.2 (Matrix Science Ltd.) database searches through GPS Explorer software v3.6 (AB Sciex). Spectra were searched against an NCBI database of the *C. tepidum* proteome (downloaded October 29, 2014) with a 50 ppm mass tolerance and oxidation of methionine and carbamidomethylation of cysteines as variable modifications. Identifications with 95% confidence or greater were accepted.

4.3.10 Extraction of proteins from S⁰ for shotgun proteomics

A variety of approaches to the extraction of proteins from S⁰ for shotgun proteomics were investigated. In general, purified WT S⁰ generated by single sulfide

feeding was resuspended in various extraction buffers, as described in the relevant sections below, and the samples were sonicated on ice (2 min increments, 10 mins total) to facilitate protein removal. S⁰ samples were centrifuged (16,000 × g, 30 mins) to pellet S⁰, and the supernatant with extracted proteins was removed. If sample clean-up for downstream compatibility with shotgun proteomics was required, one of two methods was used: precipitation and resuspension or detergent removal. For precipitation and resuspension, NaCl was added to the protein extract to a concentration of 100 mM, and the proteins were precipitated with 4 volumes cold methanol (-20 °C, > 1 hr). Precipitated proteins were pelleted by centrifugation (10,000 × g, 10 mins, 4 °C), and then resuspended in a shotgun-compatible buffer (0.5 M triethylammonium bicarbonate with 0.1% SDS or 0.2% CHAPS). For detergent removal, DetergentOUT™ GBS spin columns were used according to manufacturer instructions. For the shotgun proteomic study, proteins were extracted from S⁰ as described above using 100 mM TEAB with 2% CHAPS, detergent was removed by DetergentOUT™ GBS spin columns, and the proteins were concentrated by a SpeedVac™ vacuum concentrator (Thermo Fisher Scientific Inc.) at 37 °C prior to sample pretreatment and protein digestion for shotgun proteomics.

4.3.11 Sample pre-treatment and digestion for shotgun proteomics

Samples were resuspended in a shotgun compatible buffer (0.5 M triethylammonium bicarbonate (TEAB), 0.1% SDS) and reduced by the addition of tris-(2-carboxyethyl)phosphine (TCEP) to a concentration of 4.3 mM (60 °C, 1 hr). Free cysteines were blocked (8.3 mM methyl methane-thiosulfonate, 10 mins, room temperature). Proteins were digested overnight (37 °C) with trypsin (Promega) at a ratio of 1 µg trypsin to 10 µg protein, and the reaction was quenched with the addition

of formic acid to 1.5% v/v. Peptides were cleaned up prior to LC-MS/MS using Bond Elut OMIX C18 tips (Agilent) according to manufacturer instructions, and concentrated to dryness using a SpeedVacTM vacuum concentrator (Thermo Fisher Scientific Inc.) at 37 °C. Dried peptides were stored at -80 °C.

4.3.12 LC and MALDI-TOF/TOF MS

Peptides were separated by low pH reverse phase high performance liquid chromatography on a Tempo LC-MALDI spotter (Eksigent). Peptides were resolubilized in Mobile Phase A (2% acetonitrile, 0.1% trifluoroacetic acid (TFA), loaded onto a 1.2 µl CapRod 18E capillary column (Merck KGaA), and washed with 10 column volumes of 98% Mobile Phase A/2% Mobile Phase B (98% acetonitrile, 0.1% trifluoroacetic acid). Peptides were eluted by a 40 column volume (80 min) gradient to 55% acetonitrile and 0.1% TFA. Eluate was spotted in 10 second increments onto stainless steel target plates with α -cyano-4-hydroxycinnamic acid (Sigma-Aldrich) as matrix.

Peptides were identified by MALDI-TOF/TOF mass spectrometry in positive ion reflector mode on an AB Sciex 5800 MALDI-TOF/TOF Analyzer. MS data were collected over a mass range of 800-4000 m/z and were processed with internal calibration. A maximum of 15 precursors, with signal-to-noise ratios of at least 20, were selected per spot for MS/MS. Fragmentation was induced with 1 kV collision energy. MS/MS spectra were processed with default calibration and submitted for Mascot v2.4 database searchers through Protein Pilot software v4.5 (ABSciex). Spectra were searched against an NCBI database of the *C. tepidum* proteome (downloaded October 29, 2014). Peptide identifications with 95% confidence or

greater and protein identifications containing at least one significant unique peptide were accepted.

4.3.13 Protein sequence analysis

Subcellular locations of *C. tepidum* proteins were predicted using PSORTb v3.0.2 (Yu et al. 2010; <http://www.psort.org/psortb/>), except for the following proteins which were manually reassigned based on specific knowledge and the following justifications. Chlorosome proteins were reassigned from Unknown or Cytoplasmic to Chlorosome (CsmA, CsmB, CsmC, CsmD, CsmE, CsmJ, CsmX, CsmI, CsmH, FmoA). Sox system proteins were reassigned from Unknown to Periplasmic (SoxX, SoxY, SoxZ, SoxB, CT1020, SoxB). Sulfur quinone reductases CT1087 and CT0117 were reassigned from unknown to cytoplasmic membrane. Polysulfide reductase subunits CT0495, CT0496, CT2241 were reassigned from unknown to periplasmic. Proteins DsrF, DsrH, and ApsB were reassigned from unknown to cytoplasmic. Proteins identified as outer membrane proteins by the program BOMP (see below) that contained a Sec-system secretion signal (see below) were reassigned from unknown to outer membrane: CT0068, CT1073, CT1542, CT175, CT1801, CT2270. Finally, several additional proteins were reassigned or corrected based on their annotations: AtpE (unknown → cytoplasmic membrane), SecE (unknown → cytoplasmic membrane), AtpC-2 (unknown → cytoplasmic), OmpH (unknown → periplasmic), RpiJ (periplasmic → cytoplasmic).

Signal peptide regions and cleavage sites were predicted with SignalP 4.1 (Petersen, et al. 2011; <http://www.cbs.dtu.dk/services/SignalP/>), Phobius (Käll et al. 2004; <http://phobius.binf.ku.dk/>), and Pred-Tat (Bagos et al. 2010; <http://www.compgen.org/tools/PRED-TAT/>). To identify predicted lipoproteins and β -barrel outer

membrane (OM) proteins in the *C. tepidum* proteome, the programs LIPO (<http://services.cbu.uib.no/tools/lipo>; Berven et al. 2006) and BOMP (<http://services.cbu.uib.no/tools/bomp>; Berven et al. 2004) were used.

Proteins likely to be homologs of query proteins, based on sequence similarity, were identified with protein BLAST searches using default search parameters unless indicated otherwise below (https://blast.ncbi.nlm.nih.gov/Blast.cgi?PROGRAM=blastp&PAGE_TYPE=BlastSearch&LINK_LOC=blasthome). For smaller proteins, Delta-BLAST searches were used to identify homologs. High scoring segment pairs (HSPs) with E-values smaller than 0.005 were considered homologous. Conserved domains were identified using NCBI's Conserved Domain Search (<https://www.ncbi.nlm.nih.gov/Structure/cdd/wrpsb.cgi>). Disordered domains were identified with DISOPRED 3 (<http://bioinf.cs.ucl.ac.uk/psipred/>; Ward et al. 2004).

Protein sequence alignments were performed in MEGA6 using the CLUSTALW algorithm with scoring by the BLOSUM62 matrix. Alignment scores were determined by calculating the percentage of residues in a region of the query protein which are identities (exact amino acid matches with the subject protein) or positives (amino acids mismatched to the target protein but that are frequent evolutionary substitutions according to BLOSUM62 scoring). Gaps less than 10 residues in length in the middle of aligned regions were accounted for in a penalized alignment score but were not shown in alignment diagrams.

4.4 Results and Discussion

4.4.1 S⁰ globules are formed at the cell periphery and likely contain lipids

During early phases of growth in sulfide-only medium, light microscopic imaging of *C. tepidum* revealed a “blebbed” outer surface (Fig. 4.1). The blebs were observed in cells inoculated into sulfide-only medium (2.1 mM), occasionally exhibited a phase-bright appearance characteristic of sulfur globules, and persisted through the initial phase of sulfide oxidation at 20 $\mu\text{mol photons m}^{-2} \text{s}^{-1}$ (Fig. 4.1-A). As sulfide approached depletion, the appearance of the blebs diminished. This phenomenon also occurred during sulfide oxidation at lower light flux (5 $\mu\text{mol photons m}^{-2} \text{s}^{-1}$), where the phase-bright appearance of the blebs was enhanced and some cells in the population appeared ‘encrusted’ (Fig. 4.1-B). Under low light conditions, these blebs persisted through 18 hours of growth, but diminished by the time sulfide was depleted, at which point extracellular sulfur globules were observed (Fig. 4.1-B). Blebs of this nature were not observed during growth on thiosulfate or during oxidation of S⁰ for any light flux levels (5, 20, 35 $\mu\text{mol photons m}^{-2} \text{s}^{-1}$) or culture durations (10, 18, 26 hours) studied (data not shown). Furthermore, these blebs were observed in both formalin-fixed and unfixed cells, confirming that the blebs were not an artifact of fixation (data not shown).

These results suggested the possibility that these blebs may contain zero-valent sulfur being excreted packaged into S⁰ globules. Interestingly, blebbed cells were not observed by time-lapse microscopy (Hanson et al. 2016; Marnocha et al. 2016). Instead, S⁰ globules were observed both attached to, and at a distance from, cells during sulfide oxidation. Whether this discrepancy is because the time-lapse studies were conducted at lower initial concentrations of sulfide, because the configuration of

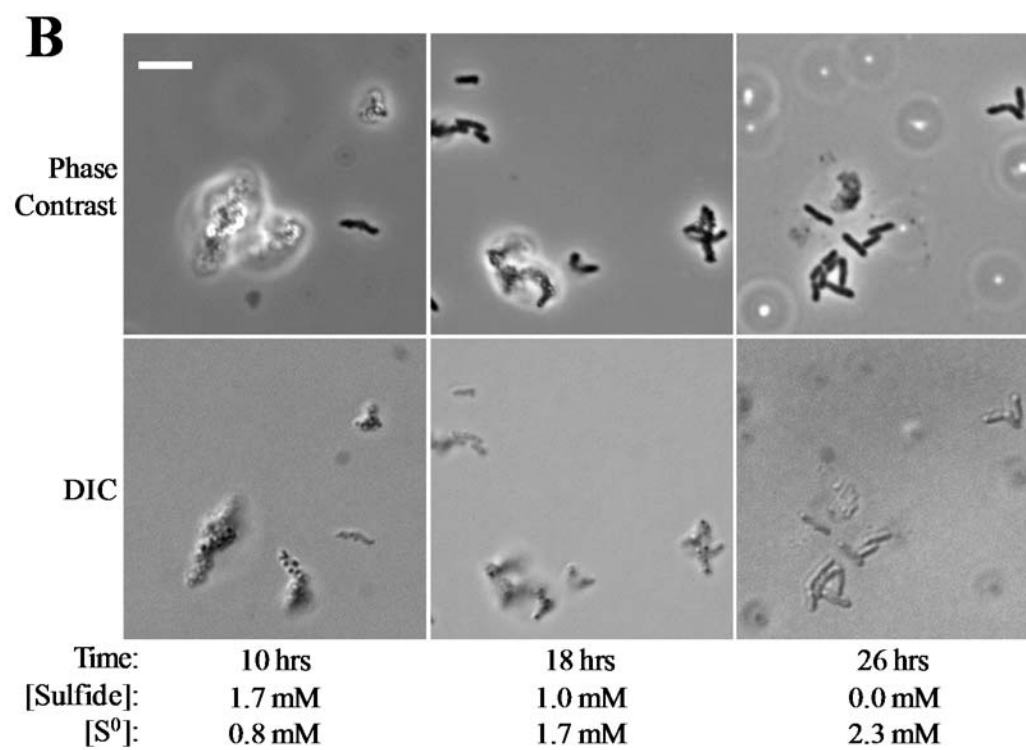
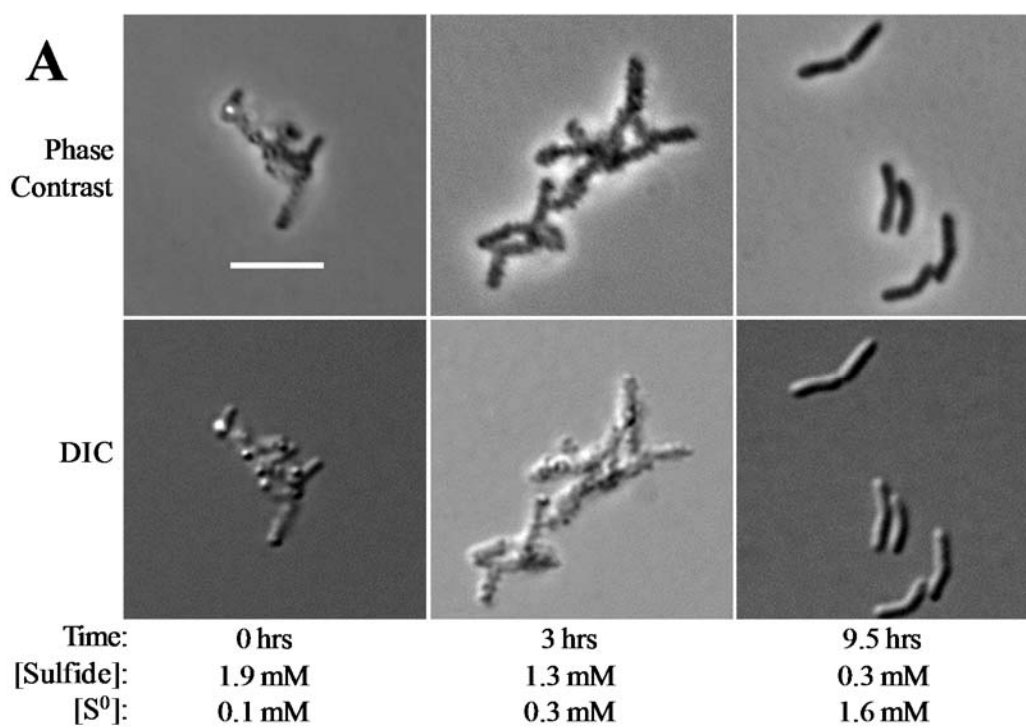


Figure 4.1 During the early phase of sulfide oxidation at (A) 20 $\mu\text{mol photons m}^{-2} \text{s}^{-1}$ and (B) 5 $\mu\text{mol photons m}^{-2} \text{s}^{-1}$, *C. tepidum* cells exhibit a ‘blebbed’, phase-bright outer surface that diminishes as sulfide is exhausted. Images show formalin-fixed cells (0.37% v/v) from sulfide-oxidizing, S^0 -producing cultures at various timepoints up to sulfide depletion. Prior to initiation of culture the cells were incubated in the dark at 37 °C for 1 hour. Initial sulfide concentrations were 2.1 mM and 3.3 mM, respectively. Scale bars indicate 5 μm and apply to all frames within each panel. The length of culture and concentrations of sulfide and S^0 at the time the samples were collected and fixed are indicated.

the growth chamber required for time-lapse microscopy created conditions that do not support formation of the blebs, or because scale of encrustation was not visible at the resolution limit (0.45 μm) of the lens used for imaging is not known at this time.

To more closely examine the appearance of these putative S^0 blebs, washed, formalin-fixed cells from the low-light sulfide oxidizing culture shown in Fig. 4.1-B were imaged by scanning electron microscopy (SEM). Using this technique, the blebs apparent on the *C. tepidum* cell surface exhibited a smooth appearance closer to that of non-attached S^0 globules than *C. tepidum* cells (Fig. 4.2-A). Energy-dispersive X-ray spectroscopy (EDX) was performed during SEM (Fig. 4.2-B) to probe the elemental composition of the blebs and globules. Six globules from the low-light sulfide oxidizing culture, both attached and unattached, exhibited similar elemental compositions (Table 4.2) with surprisingly low sulfur content (0.6-1.5%), along with carbon (89-90%) and oxygen (8.3-9.9%); nitrogen was not able to be detected by the method. By comparison, bipyramidal sulfur produced by a culture grown at 20 $\mu\text{mol m}^{-2} \text{s}^{-1}$ (Fig. 4.2-C, site 8) had no detectable carbon, 35 % oxygen, and 65% sulfur, while a larger globule of S^0 from the same culture had a low sulfur content (4.6%) similar to the globules from the low-light culture. The high carbon and oxygen signals

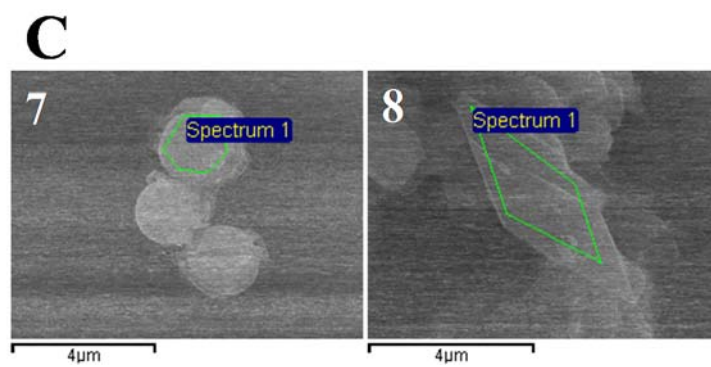
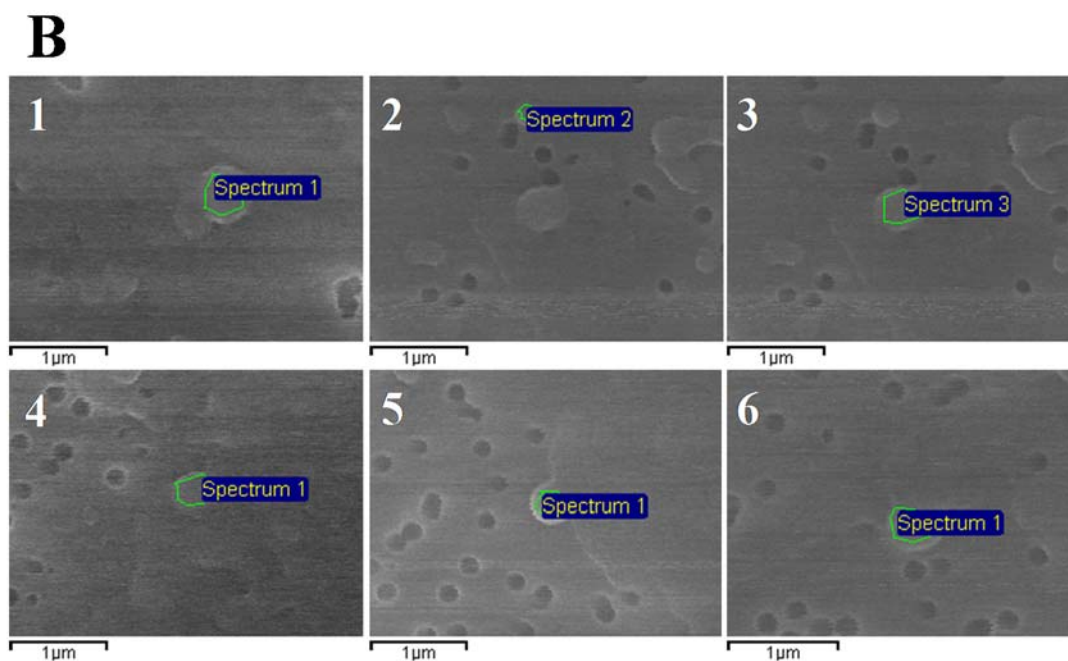
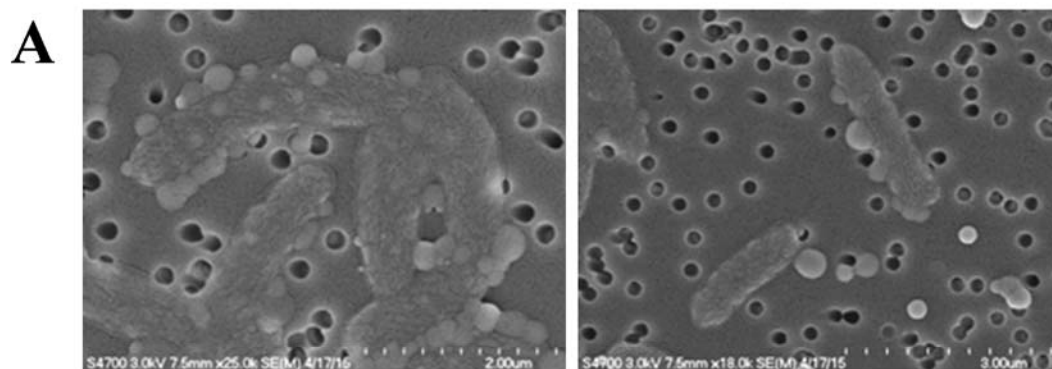


Figure 4.2 Scanning electron microscopic images and results of elemental composition by SEM-EDX of S^0 produced by *C. tepidum*. (A) Scanning electron microscopy images of formalin-fixed (0.37% v/v) *C. tepidum* cells and S^0 collected from the low-light ($5 \mu\text{mol photons m}^{-2} \text{s}^{-1}$) sulfide-oxidizing, S^0 producing culture shown in Fig. 4.1-B at 10 hrs culture. (B) Images of sites whose elemental composition was quantified by SEM-EDX. All sites in panel B were from the same *C. tepidum* sample as in panel A. Numbers correspond to site IDs in Table 4.2. (C) Images of sites whose elemental composition was quantified by SEM-EDX. The sites in panel C were from a S^0 -producing culture shortly after sulfide depletion ($20 \mu\text{mol photons m}^{-2} \text{s}^{-1}$ light). Numbers correspond to site IDs in Table 4.2.

Table 4.2 Elemental composition of *C. tepidum* S^0 as measured by SEM-EDX.

Culture growth conditions	Site ID ^a	Description	Carbon (%)	Oxygen (%)	Sulfur (%)
S^0 , low-light sulfide-oxidizing culture	1	globule, attached	89.84	8.62	1.54
	2	globule, unattached	89.57	9.86	0.56
	3	globule, attached	89.64	9.58	0.78
	4	globule, attached	89.57	9.07	1.35
	5	globule, attached	89.15	9.45	1.40
	6	globule, attached	90.21	8.34	1.44
S^0 , middle light culture just after sulfide depletion	7	large globule, unattached	84.89	10.39	4.56
	8	bipyramidal sulfur crystal	0.00	35.10	64.90

^a Site IDs correspond to the numbered identifications in Figure 4.2

of globules could be contamination from the membrane upon which the samples were fixed for the analysis or an artifact of formalin fixation. However, the large difference in composition between the globules and the sulfur crystal suggests that compounds other than sulfur may compose an S^0 coating.

That S⁰ globules appear to bleb outward from the surface of *C. tepidum* cells prior to release, along with the high carbon content of S⁰ globules, suggested the possibility that the coating on S⁰ could be derived from the *C. tepidum* cell envelope, possibly having similar properties to the outer membrane (OM) of *C. tepidum* itself. To investigate this possibility, a cationic styryl dye (FM® 1-43FX) that fluoresces upon insertion into the outer leaflet of membranes and that is expected to selectively associate with negatively charged phospholipids (Barák & Muchová 2013) was used to stain wildtype S⁰. A red fluorescent analog of this green fluorescent dye, FM® 4-64, has been previously used in the visualization and quantification of OMVs (Frias et al. 2010; McBroom et al. 2006. FM®-stained S⁰ exhibited weak fluorescence, where the dye was observed to be incorporated into a ‘shell’ at the outer surface of S⁰ globules (Fig 4.3); some biogenic sulfur crystals were also stained. FM® 1-43FX did not stain either abiotic sulfur sols, or abiotic sulfur sols incubated in spent medium. These results imply the presence of lipids on the surface of S⁰ globules able to interact with the dye, and suggested that S⁰ surface may comprise components of the *C. tepidum* cell envelope.

As a S⁰ coating derived from the cell envelope of *C. tepidum* should also possess cell envelope proteins, we subsequently used proteomic techniques to characterize the protein profile of purified S⁰.

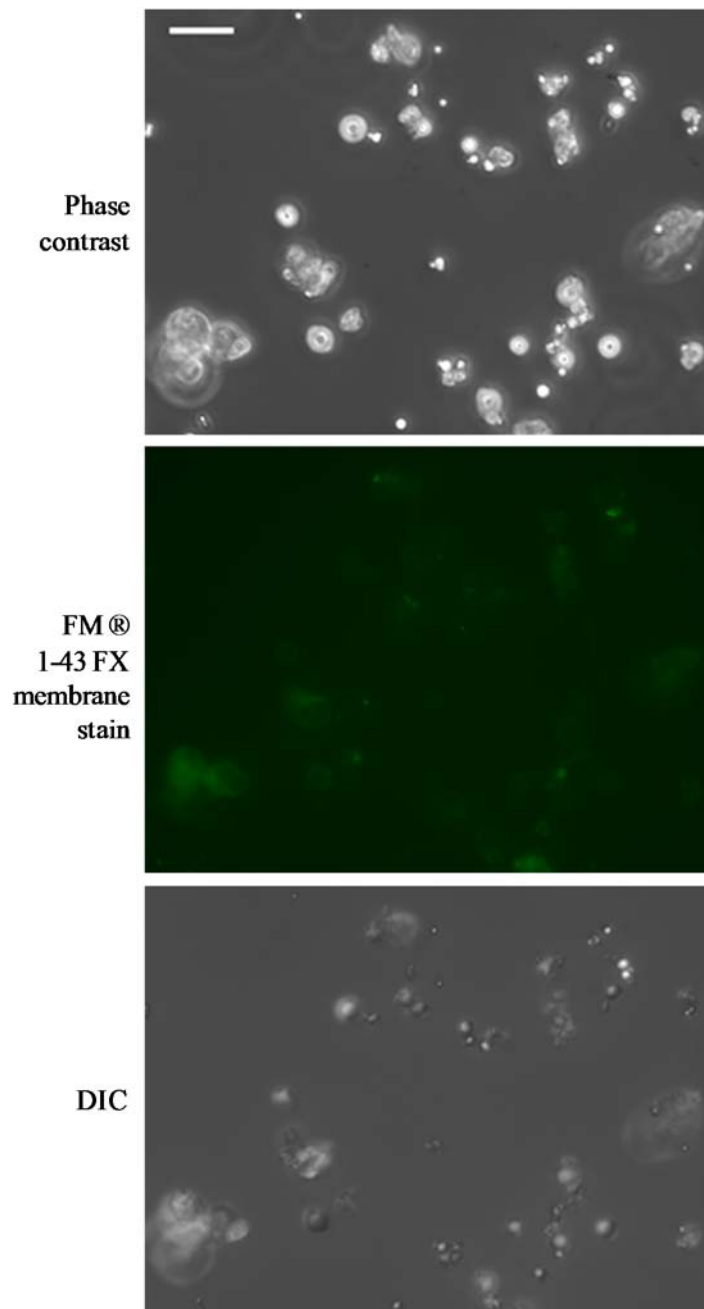


Figure 4.3 Images of unfixed S^0 produced by wildtype *C. tepidum* stained with FM® 1-43FX membrane stain, with phase contrast and DIC images for comparison. Scale bar is 10 μm and applies to all images. These data are courtesy of Dr. Cassandra Marnocha.

4.4.2 Proteins from purified S⁰ appear to constitute an enriched subset of the *C. tepidum* proteome

As an initial investigation of the proteins associated with S⁰, one-dimensional SDS-PAGE was used to compare the protein profile of S⁰ with that of cells. For this study, purified S⁰ produced by a mutant strain of *C. tepidum* deficient in S⁰ utilization (strain C3; Hanson et al. 2016) was used due to the ease with which this S⁰ could be produced. A one-dimensional gel comparing the protein profile of S⁰ batch C3-A with *C. tepidum* cells is presented in Fig. 4.4. Bands appearing in S⁰, along with the corresponding bands in *C. tepidum* lanes, were selected for protein identification by MALDI-TOF MS/MS (labeled a-h in Fig. 4.4).

Eight proteins were identified in association with S⁰ (Table 4.3), where one protein was unique to S⁰, the uncharacterized protein CT1320.1 (“d” in Fig. 4.4). In general, however, the proteins identified in S⁰ bands were identical to proteins identified in *C. tepidum* bands. These proteins included two chlorosome-associated proteins (FmoA and CsmC), three proteins predicted to be OM proteins (CT1353, an OmpA family protein homologous to peptidoglycan associated lipoprotein (Pal), and the uncharacterized proteins CT1804 and CT2144), a cytoplasmic membrane protein (cytochrome b₆f complex iron-sulfur subunit PetC), and a predicted cytoplasmic protein (heat shock protein Hsp20 family CT0644).

Most of the proteins identified in this study (Table 4.3) are likely to be highly abundant: the transcripts for all the identified proteins were found to be highly expressed in a prior transcriptomic study (Eddie & Hanson, 2013; see Table 4.3). That the bands appearing in S⁰ lanes matched some of the most intense *C. tepidum* bands, and that the proteins identified in S⁰ bands were generally the same as proteins identified in *C. tepidum* bands, suggests that proteins identified here in association

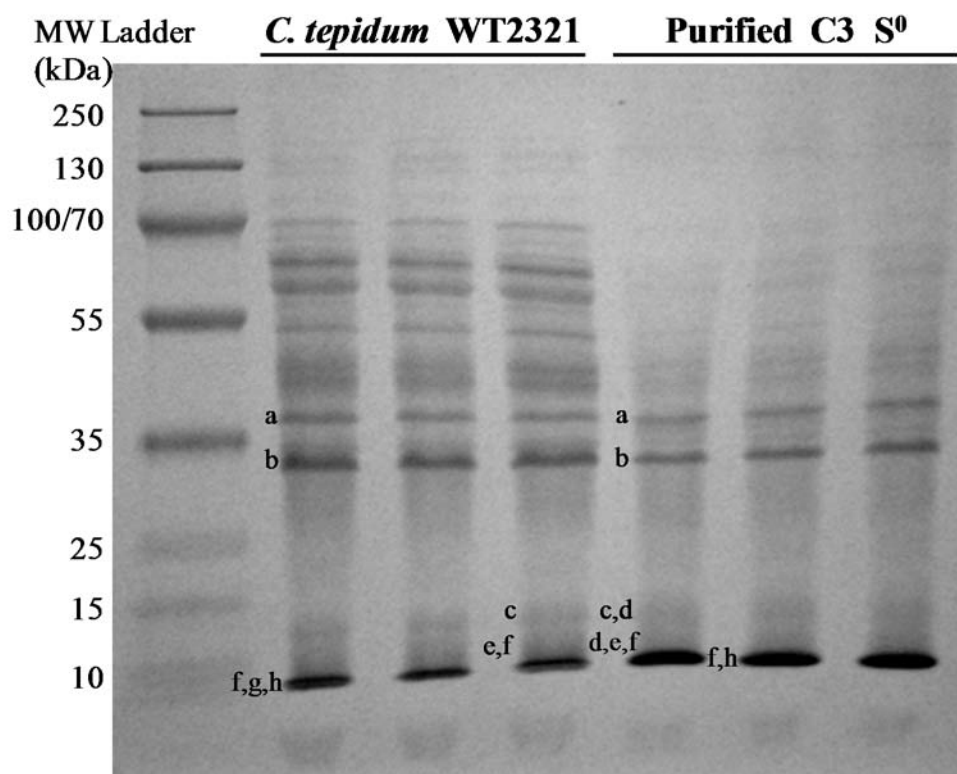


Figure 4.4 Protein profiles of purified S^0 and *C. tepidum* cells compared by one-dimensional SDS-PAGE. *C. tepidum* lanes contain proteins from independent biological replicates of strain WT2321 grown on S^0 as sole electron donor for 24.5 hr; S^0 lanes contain technical replicates of proteins extracted from S^0 batch C3-A. *C. tepidum* cell pellets and S^0 were each boiled in L(-) sample buffer (5 mins, 95 °C) to lyse cells and extract associated proteins; β -mercaptoethanol was added to the extracts at 1% v/v after heating. Protein extracts were loaded to target 10 μ g protein per lane of a 15% acrylamide Laemmli Tris-HCl gel. Protein bands were visualized by staining with Coomassie. Bands which were excised for protein identification are indicated by a lettered ID to the left of the band, where letter IDs correspond to protein identifications listed in Table 4.3. PageRuler™ Pre-stained Protein Ladder, 10-180 kDa (Fermentas) was used as the molecular weight ladder. A version of this figure originally appeared as Figure 6A in Hanson et al. 2016.

Table 4.3 List of the proteins identified in Laemmli Tris-HCl SDS-PAGE gel comparing protein profiles of S⁰ and *C. tepidum* (Fig. 4.4).

Band ID ^a	Obs. Size (kDa)	Locus Tag	Accession ^b	Gene Name	Description	Pred. Loc. ^c	Expected Size (kDa)	Identified in:	Rank of transcript abundance ^d
a	~38	CT1499	NP_662384	<i>fmoA</i>	Bacteriochlorophyll A protein	Csm#	40.3	cells, S ⁰	13
b	~32	CT1804	NP_662683		Uncharacterized protein	OM	42.8	cells, S ⁰	10
c	13	CT1353	NP_662240		OmpA family protein	OM	24.3	cells, S ⁰	20
d	13, 10	CT1320.1	AAY51681		Uncharacterized protein	U	22.0	S ⁰	277
e ^e	10	CT2144	NP_663018		Putative outer surface protein (LomR)	OM	20.0	cells, S ⁰	3
	10	CT0302	NP_661206	<i>petC</i>	Cytochrome b6-f complex iron-sulfur subunit	CM	18.9	cells, S ⁰	118
f	10, <10	CT0644	NP_661541		Heat shock protein, HSP 20 family	C	15.0	cells, S ⁰	5
g ^e	<10	CT0864	NP_661758	<i>aspB</i>	Adenylylsulfate reductase subunit beta	C#	16.1	cells	23
	<10	CT2175	NP_663049	<i>rpsH</i>	30S ribosomal protein S8	C	15.0	cells	74
h	<10	CT1943	NP_662820	<i>csmC</i>	Chlorosome envelope protein C	Csm#	14.3	cells, S ⁰	40

^a Band IDs correspond to numbering in Fig. 4.4.

^b Accessions are from RefSeq (NP_XXXXXX) or GenBank (AAYXXXXX)

^c Location prediction by pSORTb, except for manual annotations as described in the Methods (indicated by #). Csm: chlorosome; C: cytoplasmic; CM: cytoplasmic membrane; OM: outer membrane; P: periplasmic; U: unknown

^d During growth on thiosulfate (Eddie & Hanson 2013); rank is out of 2111 genes with transcript abundances higher than *nifH*, which was not expected to be expressed under the ammonia-replete conditions of the study.

^e 'e' and 'g' each refer to two protein identifications.

with S⁰ are also abundant proteins. Thus one possible conclusion of this study is that the proteins observed in association with S⁰ are merely contaminating, highly abundant proteins from residual *C. tepidum* cells.

However, several observations suggested an alternate conclusion: that S⁰ contains an enriched subset of the *C. tepidum* proteome. First, as a protein identification method, SDS-PAGE has low sensitivity and resolution, and so it is not surprising that the proteins identified from both *C. tepidum* and S⁰ would be highly abundant. Second, the proteins identified in association with S⁰ were enriched in predicted OM proteins (3 of 8 proteins; 38%) relative to the overall *C. tepidum* proteome, which contains only 1.6% OM proteins (Fig. 4.11-B). Because cytoplasmic proteins make up the majority of the *C. tepidum* proteome (46.9%), if the S⁰ proteins constituted cellular contamination we would have expected a higher proportion of cytoplasmic proteins among the proteins identified in association with S⁰. Another possibility to explain the prevalence of OM proteins is that attached fragments of *C. tepidum* membranes constitute the contamination rather than whole cells. Yet this possibility also motivated further study, as identification of *C. tepidum* membrane proteins that facilitate attachment to S⁰ could help elucidate mechanisms of cell-S⁰ attachment and S⁰ degradation. These results motivated further studies, where developing methods to distinguish proteins that strongly associate with S⁰ from those with non-specific interactions was considered to be a top priority.

Second, low molecular weight protein bands which migrated with the dye front appeared more intense in the S⁰ lanes than the *C. tepidum* lanes (Fig. 4.4). Interestingly, only two proteins were identified from these S⁰ bands (the HSP20 homolog CT0644 and CsmC), whereas four proteins were identified in the corresponding, but less

intense, *C. tepidum* bands. This observation suggested that either S^0 is enriched in CT0644 and CsmC relative to cells, or that additional proteins are present in these bands which were not identified in this limited study. The gel formulation used here (Tris-HCl, 15% acrylamide) provided optimal separation for proteins in the range of ~15-50 kDa, but did not resolve small molecular weight proteins. The desire to further explore low molecular weight proteins motivated the use of a different gel chemistry to separate and resolve small molecular weight proteins in a subsequent study (see section 4.4.3).

Finally, the uncharacterized protein CT1320.1, found only in association with S^0 , was identified as a protein potentially involved in S^0 production or degradation (see section 4.4.7 for additional discussion). CT1320.1 was detected with >99% confidence in two adjacent S^0 bands at approximately 10 and 13 kDa (Fig. 4.4, “d”). Bands corresponding to 10 and 13 kDa were also present in protein extracts from cells of *C. tepidum* grown on S^0 , but CT1320.1 was not identified in these bands: 2 of the 4 characteristic ions for CT1320.1 were detected, but at 4- to 20-fold lower signal to noise ratios than in the S^0 extract. This observation suggests that CT1320.1 is enriched in S^0 relative to *C. tepidum*. That the transcript levels of CT1320.1 in the prior transcriptomic study (Eddie & Hanson 2013) were 6- to 50-fold lower than those for the other proteins identified in this study (except PetC) suggests that this protein is less likely a contaminating protein.

In summary, this preliminary study suggested that S^0 may contain an enriched subset of the *C. tepidum* proteome, but that better methods for removing loosely-associated proteins were required to better identify important S^0 -associated proteins, and that approaches focusing on low-molecular weight proteins should be pursued.

4.4.3 Differentiation of proteins weakly and strongly associated with S⁰

Larger differences between the protein profiles of S⁰ and *C. tepidum* were observed through efforts to differentiate proteins weakly and strongly associated with S⁰. Proteins were extracted from S⁰ through a series of sequential treatments designed to disrupt increasingly strong associations with S⁰ (Table 4.4) and were compared with *C. tepidum* proteins on a tris-tricine gel to provide better separation of low molecular weight proteins (Fig. 4.5). While few protein bands observed in this study were selected for identification (Table 4.5), the use of differential extractions revealed information about the associations of different proteins with S⁰.

First, washes with sulfur-free Pf-7 medium (U treatment; Table 4.4) were effective in removing a number of proteins which were generally not present in the extracts of proteins from subsequent treatments. The removal of protein by washing with an aqueous solution (sulfur-free Pf-7) suggests that proteins removed by U treatment were non-specifically associated with S⁰. The batch of S⁰ used in this and the prior study described above, C3-A, was purified by only one series of sucrose-density centrifugations, and several anecdotal observations suggested the possibility that residual cell contaminating could have persisted. First, time-lapse microscopy of C3 mutant cultures showed cells collecting and aggregating on S⁰ towards the end of a culture (data not shown). One interpretation is that C3 mutant cells, unable to oxidize S⁰, tend to aggregate on and tightly attach to S⁰. In addition, observations of purified C3 S⁰ suspensions stored at room temperature revealed the appearance of a greenish tint to the liquid phase over the course of days to weeks, suggesting cells attached to the S⁰ detached over time (data not shown). Thus, to increase removal of residual cells, a 'rest' period for S⁰ and a second series of sucrose density centrifugations were added to the S⁰ purification procedure for subsequent batches (see Methods).

Table 4.4 Sequential treatments of S^0 to distinguish proteins that weakly and strongly associate with S^0 .

Treatment name	Nature of protein- S^0 interaction to be disrupted:	Treatment procedure prior to heating (95 °C, 5 mins), centrifugation (16,000 × g, 2 mins), and gel loading (unless described otherwise): ^a
U	<u>U</u> nassociated proteins	To remove unassociated proteins: 1. S^0 was washed three times by vortexing in sulfur-free Pf-7 medium, centrifuging (1,200 × g, 0.5 mins), and removing supernatant. 2. Pooled supernatants containing U proteins were concentrated with centrifugal filtration device (Amicon Ultra-0.5 3k NMWL, EMD Millipore). 3. U protein fraction was mixed 1:1 vol/vol with 2X concentrated LR sample buffer.
WH	<u>W</u> eak <u>H</u> ydrophobic	To remove proteins associated by WH interactions: 1. U-treated S^0 was incubated with L(-) sample buffer (5 mins, room temperature) and centrifuged (16,000 × g, 2 mins), and supernatant containing WH proteins was removed. 2. β -mercaptoethanol was added to WH supernatant at 1% v/v.
WD	<u>W</u> eak <u>D</u> isulfide bonds	To remove proteins associated by WD interactions: 1. WH-treated S^0 was incubated with LR buffer (5 mins, room temperature) and centrifuged (16,000 × g, 2 mins), and supernatant containing WD proteins was removed.
SHD	<u>S</u> trong <u>H</u> ydrophobic and <u>D</u> isulfide bonds	To remove proteins associated by SHD interactions: 1. WD-treated S^0 was heated in LR sample buffer (95 °C, 5 mins) and centrifuged (16,000 × g, 2 mins), and supernatant containing SHD proteins was removed for gel loading without further treatment.
AAP	<u>A</u> ll <u>A</u> ssociated <u>P</u> roteins	To remove all associated proteins: 1. U-treated S^0 was heated in LR sample buffer (95 °C, 5 mins) and then centrifuged (16,000 × g, 2 mins), and supernatant containing AA proteins was removed for gel loading without further treatment.

^a See section 4.3.7 for description of LR and L(-) sample buffers.

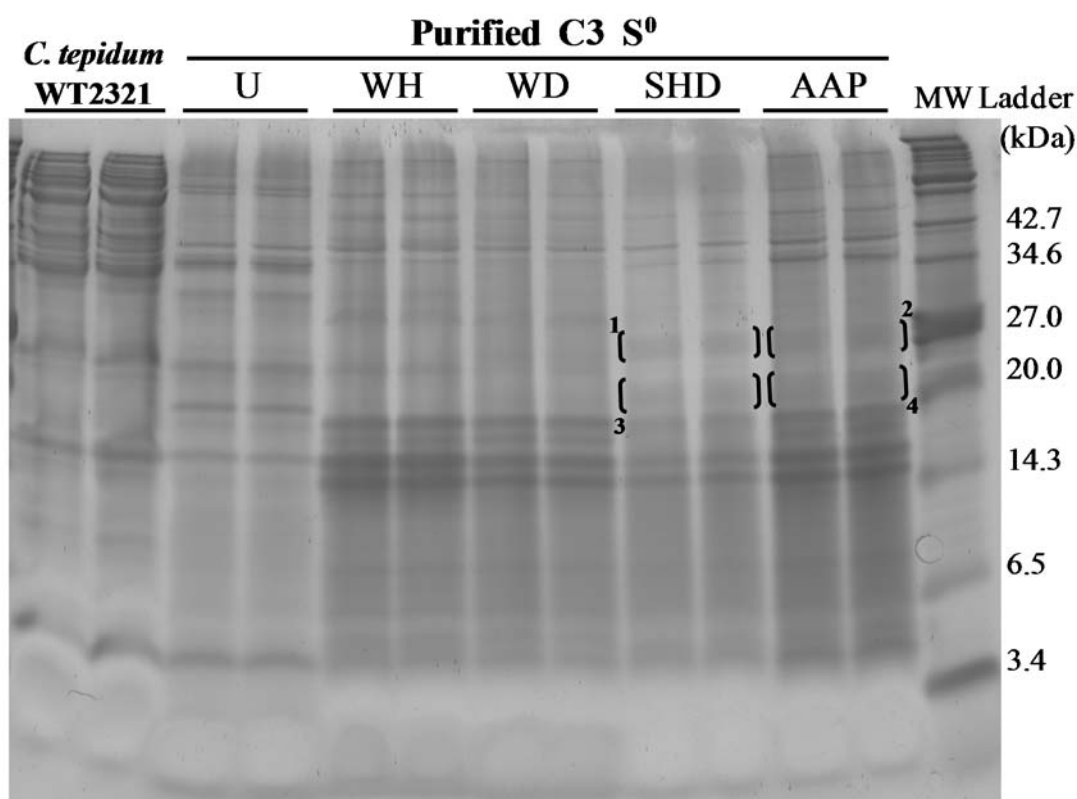


Figure 4.5 Protein profiles of differential extractions of S⁰ and *C. tepidum* compared by one-dimensional gel electrophoresis. S⁰ lanes contain technical replicates of proteins extracted from S⁰ batch C3-A according to the treatments listed in Table 4.4. *C. tepidum* lanes contain proteins extracted from strain WT2321 grown on Pf-7 for 3 days. Each lane of the 16.5% acrylamide Tris-Tricine gel was loaded to target 6.5 µg protein, and protein bands were visualized by staining with SYPRO® Ruby Protein Gel Stain. Bands which were excised for protein identification are bracketed and numbered, where numbers correspond to those listed in Table 4.5. Unstained Protein Ladder, Broad Range (2-212 kDa) (New England BioLabs) was used as the molecular weight ladder. A version of this figure originally appeared as Figure 6B in Hanson et al. 2016.

Table 4.5 List of proteins identified in bands from the Tris-Tricine SDS-PAGE gel shown in Figure 4.5 that are unique to SHD and AAP S⁰ extracts.

Band ID ^a	Obs. Size (kDa)	Locus Tag	Accession ^b	Gene Name	Description	Pred. Loc. ^c	Expected Size (kDa)	Identified in:	Rank of transcript abundance ^d
1	26	CT0644	NP_661541		Heat shock protein, HSP 20 family	C	15.0	SHD	5
1,2	26	CT0895	NP_661788		phosphate ABC transporter substrate-binding protein	IM	28.4	SHD, AAP	164
1,3	26, 21	CT1019	NP_661911	<i>soxA</i>	sulfur oxidation protein SoxA	P#	32.1	SHD	22
2	26	CT0089	NP_660995	<i>clpB-2</i>	ATP-dependent Clp protease, ATP binding subunit	C	49.6	AAP	53
2	26	CT1305	NP_661206		Putative uncharacterized protein	OM	54.8	AAP	161
3,4	21	CT0302	NP_661206	<i>petC</i>	Cytochrome b6-f complex iron-sulfur subunit	CM	18.9	SHD, AAP	118
3	21	CT0960	NP_661853	<i>purC</i>	phosphoribosylaminoimidazole -succinocarboxamide synthase	C	26.5	SHD	256
4	21	CT1577	NP_662460	<i>frr</i>	ribosome recycling factor	C	21.2	AAP	177

^a Band IDs correspond to numbering in Fig. 4.5.

^b RefSeq (NP_XXXXXX) or GenBank (AAYXXXXX) Accession

^c Location prediction by pSORTb, except for manual annotations as described in the Methods (indicated by #). Csm: chlorosome; C: cytoplasmic; CM: cytoplasmic membrane; OM: outer membrane; P: periplasmic; U: unknown

^d During growth on thiosulfate (Eddie & Hanson 2013), out of 2111 genes with transcript abundances higher than *nifH*, which was not expected to be expressed under the ammonia-replete conditions of the study.

Next, the incubation of S^0 with the denaturing detergent SDS at room temperature (treatment WH), removed a distinct subset of proteins from S^0 not removed by incubation with SF Pf-7, suggesting that these proteins were associated with S^0 by either ionic or hydrophobic interactions. It appeared that the addition of reducing agent to the room-temperature SDS incubation (treatment WD) did little to extract new proteins from S^0 based on the large degree of overlap between the bands in WH and WD lanes. This observation suggests that that weak disulfide bonds do not substantially contribute to protein- S^0 interactions. The degree of overlap between proteins extracted by WH and WD treatments also suggested that the single WH treatment was insufficient to disrupt all proteins associated through weak hydrophobic interactions. In fact, most of the WH protein bands persisted through WD treatment and were also visible in the SHD extracts, motivating the use of repeated WH treatments in subsequent studies to more completely remove WH proteins prior to SHD treatment.

As proteins strongly associated with S^0 were of particular interest, the protein profiles from SHD extracts, obtained by heating S^0 in the presence of SDS and β -mercaptoethanol, were searched for unique bands. Two broad bands, at approximate sizes of 21 and 26 kDa (see Fig. 4.5), were observed only in SHD and AAP extracts (containing all proteins associated with S^0) and did not have obvious counterparts in *C. tepidum* cell lanes. These bands were selected for protein identification. Among the proteins identified (Table 4.5), two were the same as proteins identified in the previous study, HSP20 protein CT0644 and PetC (Table 4.3). CT0644 was only identified in SHD extracts, although at a higher molecular weight than expected (26 kDa vs. 15 kDa), while PetC was identified in both SHD and AAP extracts. That these proteins

were identified in SHD extracts suggests that these proteins may be strongly associated with S^0 and not just proteins associated with S^0 due to cell contamination, although this does not necessarily suggest a functional role for these proteins in an S^0 coating.

The uncharacterized protein CT1305 was also identified in the ~26 kDa broad band in the AAP extracts with > 99% confidence. CT1305 is predicted to be an OM protein and is homologous to the uncharacterized protein CT1320.1 described above. While CT1305 was not detected in the corresponding band in the SHD extracts, fragments of CT1305 (4 of 5 diagnostic characteristic ions of CT1305) were detected, suggesting that it may have been present but at a lower abundance in the SHD band. CT1305 is discussed in more detail below in section 4.4.7.

4.4.4 The protein profile of S^0 from wild type *C. tepidum* WT2321 exhibits subtle differences from that of S^0 from mutant strain C3

The impaired ability of the C3 mutant to oxidize S^0 and the possibility that this phenotype could lead to differences in the protein profiles of C3 S^0 versus wildtype S^0 motivated a comparison of the protein profiles of wild type S^0 (batch WT-A) and C3 S^0 (batch C3-B). Interestingly, after the first purification procedure, WT S^0 exhibited much lower cell contamination relative to C3 S^0 (Fig. 4.6). While both S^0 batches were subjected to a second purification procedure, much of the WT S^0 was lost during this operation. Based the apparently minimal cell contamination of WT S^0 after just the single purification procedure, S^0 after just one purification was selected for comparison the C3 S^0 subjected to two purification operations.

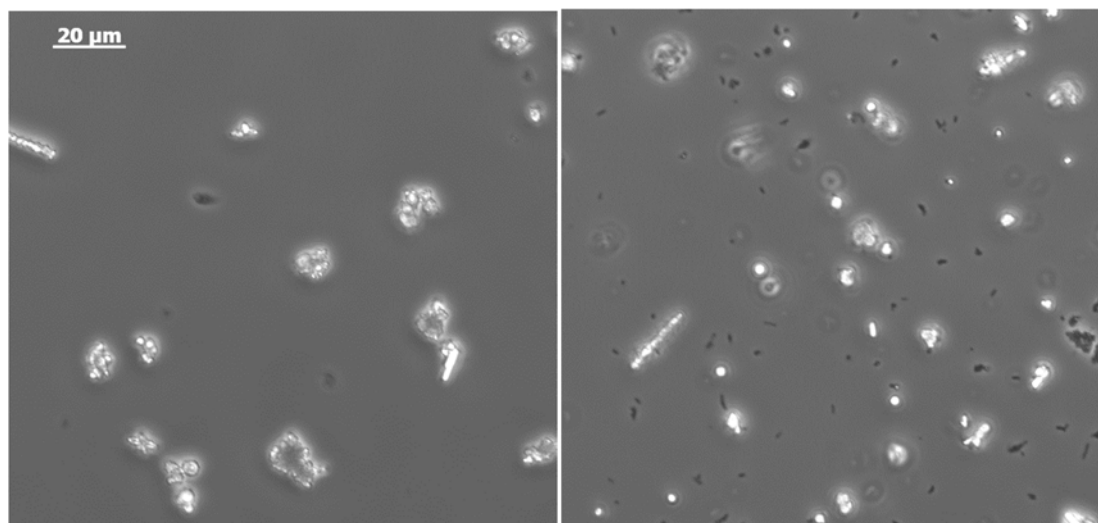


Figure 4.6 Purified S^0 from wildtype cultures exhibited much lower cell contamination after the first purification procedure (left panel) relative to S^0 from mutant strain C3 (right panel). Phase contrast microscopic images, 400x total magnification, of formalin-fixed (3.7% v/v) S^0

Proteins were extracted from S^0 batches WT-A and C3-B using a similar sequential extraction approach as the previous study (Table 4.6), with the addition of a 2M NaCl salt wash (treatment E) to remove proteins associated primarily by electrostatic interactions. Protein extracts were compared by one-dimensional SDS-PAGE on a Laemmli Tris-HCl gel with a 4-20% acrylamide gradient, providing optimal separation over a wide range of protein sizes. The results of this study are shown in Fig. 4.7 and Table 4.7.

Table 4.6 Sequential treatments of S^0 to distinguish proteins weakly and strongly associated with S^0 .

Treatment name	Nature of protein- S^0 interaction to be disrupted:	Treatment procedure prior to heating (95 °C, 5 mins), centrifugation (16,000 × g, 2 mins), and gel loading (unless described otherwise): ^a
U	<u>U</u> nassociated proteins	To remove unassociated proteins: <ol style="list-style-type: none"> 1. S^0 was washed twice by vortexing in sulfur-free Pf-7 medium, centrifuging (16,000 × g, 2 mins), and removing supernatant. 2. Pooled supernatants containing U proteins were concentrated with centrifugal filtration device (Amicon Ultra-0.5 3k NMWL, EMD Millipore). 3. U protein fraction was mixed 1:1 vol/vol with 2X concentrated LR sample buffer.
E	<u>E</u> lectrostatic	To remove proteins associated by E interactions: <ol style="list-style-type: none"> 1. S^0 was washed twice by vortexing in 2M NaCl in sulfur-free Pf-7, centrifuging (16,000 × g, 2 mins), and removing supernatant. 2. Pooled supernatants containing E proteins were concentrated with centrifugal filtration device (Amicon Ultra-0.5 3k NMWL, EMD Millipore). 3. E protein fraction was mixed 1:1 vol/vol with 2X concentrated LR sample buffer.
WH	<u>W</u> eak <u>H</u> ydrophobic	To remove proteins associated by WH interactions: <ol style="list-style-type: none"> 1. U- or E-treated S^0 was incubated with L(-) sample buffer (5 mins, room temperature) and centrifuged (16,000 × g, 2 mins), and supernatant containing WH proteins was removed. 2. DTT was added to WH supernatant to 35 mM.
SHD	<u>S</u> trong <u>H</u> ydrophobic and <u>D</u> isulfide bonds	To remove proteins associated by SHD interactions: <ol style="list-style-type: none"> 1. WH-treated S^0 was heated in LR sample buffer (95 °C, 5 mins) and centrifuged (16,000 × g, 2 mins), and supernatant containing SHD proteins was removed for gel loading without further treatment.

^a See section 4.3.7 for description of LR and L(-) sample buffers.

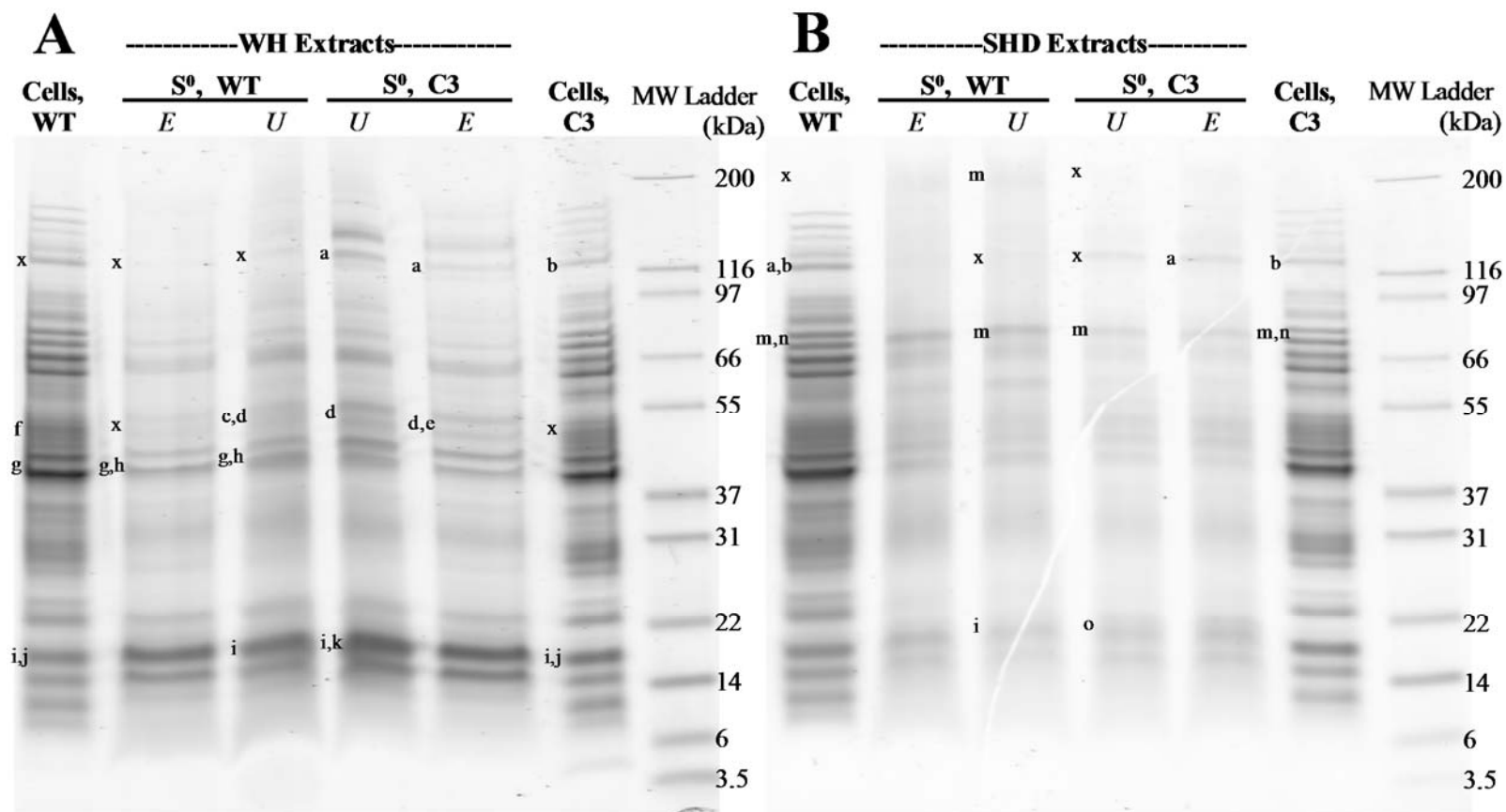


Figure 4.7 Protein profiles of (A) WH and (B) SHD extracts from wildtype S^0 and C3 S^0 and *C. tepidum* cells compared by one-dimensional gel electrophoresis (4-20% acrylamide Tris-HCl gel). S^0 proteins were extracted from batches C3-E and WT-A according to the treatments listed in Table 4.6, where italicized designations indicate whether U or E was the initial treatment. Cell proteins were extracted from *C. tepidum* strain WT2321 grown on Pf-7 for 20 hours or strain *C. tepidum* strain C3 grown on Pf-7 for 30 hours. Gel lanes with cells were loaded to target 3.0 μ g protein, while lanes with S^0 were loaded to target 4.0 μ g protein. Gels were stained with SYPRO® Ruby Protein Gel Stain. Bands which were excised for protein identification are indicated by a lettered ID to the left of the band, where letter IDs correspond to protein identifications listed in Table 4.7. Mark12™ Unstained Standard, 2.5-200 kDa (Thermo Fisher Scientific) was used as the molecular weight ladder.

Table 4.7 List of protein identifications from bands with differences between S⁰ produced by wildtype *C. tepidum* and S⁰ produced by *C. tepidum* mutant strain C3, and additional proteins unique to S⁰.

Band ID ^a	Obs. Size (kDa)	Locus Tag	Accession ^b	Gene Name	Description	Pred. Loc. ^c	Expected Size (kDa)	Identified in:
a	120	CT1239	NP_662127	<i>secA</i>	preprotein translocase subunit SecA	C	117.9	cells (WT) WH (C3) SHD (C3)
b	120	CT1628	NP_662511	<i>nifJ</i>	pyruvate flavodoxin/ferredoxin oxidoreductase	C	130.1	cells (C3)
c	50	CT2049	NP_662924		LipD protein, putative (type_I_sec_TolC)	OM	50.1	WH (WT)
d	50	CT1447	NP_662333		serine protease (degP_htrA_DO)	P	53.5	WH (WT, C3)
e	50	CT1305	NP_662193		uncharacterized protein	OM	54.8	WH (C3)
f	50	CT0722	NP_661617	<i>metK</i>	S-adenosylmethionine synthetase	C	41.1	cells (WT)
g	42	CT1804	NP_662683		uncharacterized protein	OM	42.8	cells (WT) WH (WT)
h	42	CT0893	NP_661786		uncharacterized protein (Porin_5)	OM	42.4	WH (WT)
i	17, 20	CT1970	NP_662846		HSP20 family protein	U	16.0	cells (WT, C3) WH (WT, C3) SHD (WT)
j	17	CT0864	NP_661758	<i>aspB</i>	adenylylsulfate reductase subunit beta	C#	16.1	cells (WT, C3)
k	17	CT0291	NP_661195		uncharacterized protein	U	18.6	WH (C3)

^a Band IDs correspond to numbering in Fig. 4.7.

^b RefSeq (NP_XXXXXX) or GenBank (AAYXXXXX) Accession

^c Location prediction by pSORTb, except for manual annotations as described in the Methods (indicated by #).

Csm: chlorosome; C: cytoplasmic; CM: cytoplasmic membrane; OM: outer membrane; P: periplasmic; U: unknown

Table 4.7 continued.

Band ID ^a	Obs. size (kDa)	Locus Tag	Accession ^b	Gene Name	Description	Pred. Loc. ^c	Expected Size (kDa)	Identified in:
m	200, 75	CT0643	NP_661540	<i>dnaK</i>	molecular chaperone DnaK	C	68.3	cells (WT, C3) SHD (WT, C3)
n	75	CT0351	NP_661255	<i>icd</i>	isocitrate dehydrogenase	C	80.8	cells (WT, C3)
o	20	CT1320.1	AA_Y51681		uncharacterized protein	U	22.0	SHD (C3)
x	--	-----	-----		no proteins identified			

^a Band IDs correspond to numbering in Fig. 4.7.

^b RefSeq (NP_XXXXXX) or GenBank (AA_YXXXXX) Accession

^c Location prediction by pSORTb, except for manual annotations as described in the Methods (indicated by #).
Csm: chlorosome; C: cytoplasmic; CM: cytoplasmic membrane; OM: outer membrane; P: periplasmic; U: unknown

No protein bands were visible in U or E extracts from either WT or C3 S⁰, even when the sensitivity of the fluorescent imager was increased to its maximum (data not shown). A lack of visible protein bands suggests that the secondary purification protocol may have reduced most of the non-specific protein contamination. Adding 2M NaCl to the initial wash of S⁰ appeared to have little effect on the extraction of protein by subsequent treatments.

However, while the protein profiles of WT and C3 S⁰ were similar within both WH and SHD extracts, a number of small differences between WT and C3 S⁰ were observed (Table 4.7). Several proteins were identified in C3 S⁰ but not WT S⁰. Both WH and SHD extracts of C3 S⁰ contained high-molecular weight bands not present in WT S⁰; one of these bands was identified as the preprotein translocase subunit SecA (a). The uncharacterized protein CT0291 (k) was identified in a WH extract of C3 S⁰ but not in the corresponding WT S⁰ band. CT1320.1 (o) was identified in a SHD extract from C3 S⁰, but not in WT S⁰ or the corresponding bands from cells.

Other proteins were identified in WT S⁰ but not C3 S⁰. The OM protein LipD (CT1353) (c) was identified in a WH extract of WT S⁰, but not C3 or cell bands; whether this protein was identified in corresponding bands in SHD extracts was not investigated. DnaK (m) appeared enriched in SHD extracts from WT S⁰ relative to extracts from C3 S⁰. Interestingly, DnaK appeared both close to its expected molecular weight, as well as at a molecular weight much higher than expected.

Finally, two additional proteins were identified in bands from S⁰ but not in corresponding bands from cells: the periplasmic serine protease CT1447 (d) was identified in WH extracts from both WT S⁰ and C3 S⁰, and the uncharacterized OM

protein CT0893 was identified in WH extracts from WT S⁰ (its presence was not investigated in extracts from C3 S⁰).

A total of 72 proteins in association with S⁰ (either from WT or strain C3) were identified across 7 gel-based studies (Appendix E). One of the limitations of gel-based proteomic studies is that comprehensively identifying all proteins observed in a gel is labor-intensive. Furthermore, that multiple proteins can be present in what appear as single bands hinders the ability for lower-abundance proteins to be detected if a highly-abundant protein dominates the mass spectra. Therefore, we decided to pursue a shotgun proteomic approach to more comprehensively profile the proteins in association with S⁰. Based on the possibility that S⁰ from C3 may not be representative of WT S⁰ as mentioned above, we next focused on shotgun proteomic profiling of WT S⁰.

4.4.5 Development of methods for shotgun proteomic profiling of S⁰ from *C. tepidum*

The extraction of proteins from S⁰ for gel electrophoresis-based studies relied upon the presence of detergent (SDS) and reducing agents (β -mercaptoethanol or DTT). However, these components, while critical for disrupting protein-S⁰ interactions and solubilizing proteins, are incompatible with shotgun proteomic studies for several reasons. First, because shotgun proteomic techniques rely upon the digestion of proteins into peptides, the presence of detergents during the digestion phase inhibit the activity of the proteases used to cleave peptide bonds. Furthermore, the presence of detergents can interfere with reverse-phase liquid chromatography separation steps by binding to the hydrophobic C₁₈ column. Fragmentation of detergents during mass spectrometry can also produce peaks which dominate the spectra, concealing peaks

from peptides. The presence of the free thiols present in reducing agents can interact with certain cysteine blocking reagents, such as the reversible methyl methane-thiosulfonate used in the iTRAQ quantitative proteomic protocol. Therefore, a protein extraction protocol that is compatible with shotgun proteomic methods must either ensure that concentrations of these compounds are maintained below acceptable levels through every step of the extraction phase, or must use a clean-up method to remove compounds prior to protein digestion. There are trade-offs between these two approaches: minimizing the concentration of detergents and reducing agents is likely to reduce the efficiency of protein extraction, but the use of a clean-up step can lead to protein losses. Thus, we sought to identify an extraction protocol for proteins that achieved an acceptable level of overall protein extraction with minimal losses.

Three different approaches using two different detergents (six different treatments) were screened for protein extraction efficacy on S⁰ batch WT-B (Table 4.8). The first approach (Treatments 1A and 1B) involved the use of extraction buffers that were directly compatible with the digestion step of shotgun proteomics; the buffers contained a low concentration of detergent and no reducing agent, thus a clean-up step prior to digestion would not be required. The second approach (Treatments 2A and 2B) used a strong extraction buffer that contained detergent in excess of the critical micelle concentration as well as a reducing agent, requiring protein precipitation and resuspension prior to digestion to ensure downstream compatibility. The third approach (Treatment 3A and 3B) used a detergent-rich extraction buffer without a reducing agent that could be cleaned-up for digestion by spin column detergent removal, eliminating the need for a precipitation step.

Table 4.8 Formulations of buffers used in screening of shotgun-compatible extraction approaches for protein extraction from *C. tepidum* S⁰.

Extraction buffer compatibility with digestion	Reducing agent in extraction buffer	Clean up approach	Detergent in extraction buffer	Treatment abbrev.
Compatible	None	None required	0.1% SDS	1A
			0.2% CHAPS	1B
Incompatible	40 mM DTT	Precip. & resuspension ^a	2% SDS	2A
			2% CHAPS	2B
Incompatible	None	DetergentOUT™	2% SDS	3A
			2% CHAPS	3C
In addition to the components listed above, all buffers contained 0.5 M triethylammonium bicarbonate (TEAB).				
^a Resuspension buffers were equivalent to the compatible extraction buffers.				

Two different detergents were used in this investigation, SDS and (3-((3-cholamidopropyl) dimethylammonio)-1-propanesulfonate) (CHAPS). SDS, an anionic detergent, was selected because it is extremely effective at solubilizing proteins. However, as this detergent is a strong denaturant, even a small amount can inhibit protease activity: Min et al. (2015) found a 50% reduction in trypsin and chymotrypsin activity in the presence of 0.01% SDS. This level is 5-fold lower than the maximum SDS concentration (0.05%) at the digestion step recommended for use in the commonly-used iTRAQ protocol (Applied Biosystems). Thus we also investigated the use the zwitterionic, non-denaturing detergent CHAPS. This detergent did not adversely affect trypsin digestion in a prior study, although it still produced interfering peaks in mass spectrometry (Zhang & Li 2004).

Proteins were extracted by sonicating S⁰ on ice in each of the extraction buffer treatments listed in Table 4.8. The various S⁰ extracts were compared with the protein profile of S⁰ extracted directly into LR sample buffer by one-dimensional SDS-PAGE (Fig. 4.8). Lanes were loaded with proteins from equivalent amounts of S⁰ to enable

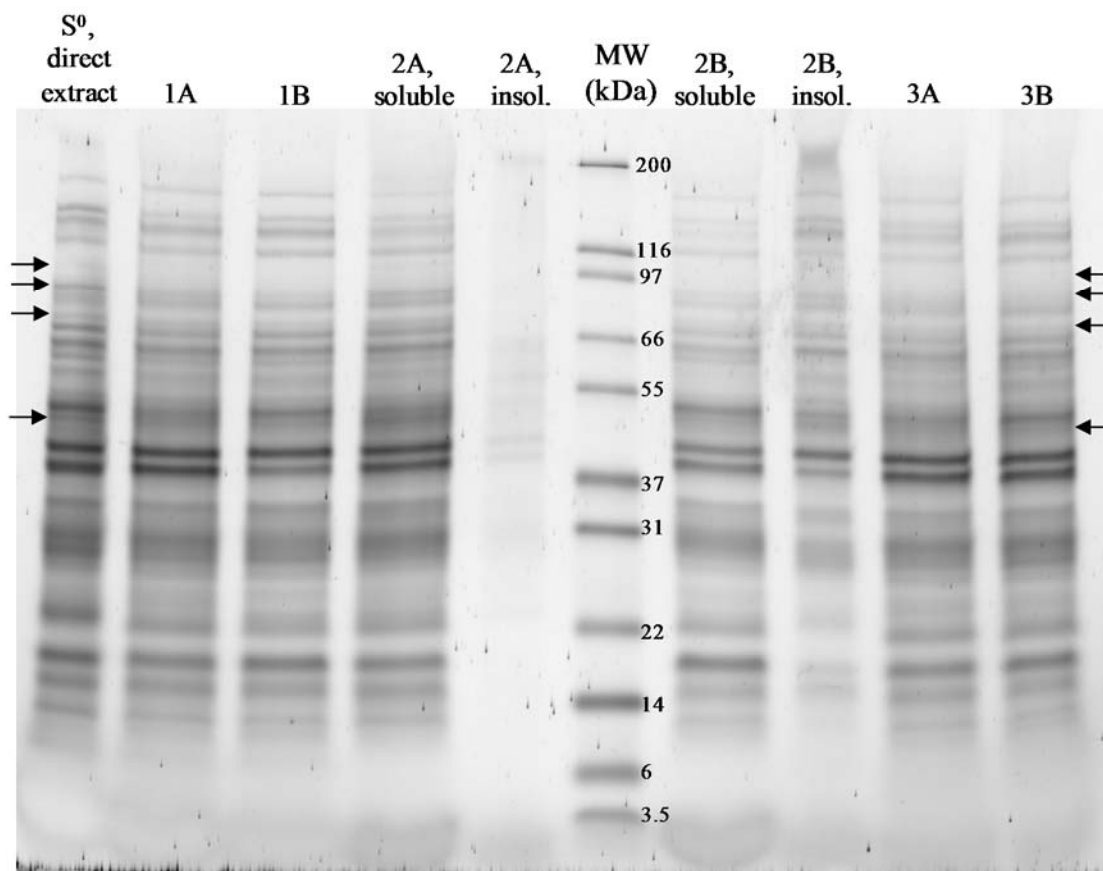


Figure 4.8 Protein profiles of wildtype S^0 extracts obtained from shotgun-compatible protocols compared to S^0 proteins directly extracted into L(+) sample buffer by one-dimensional gel electrophoresis. S^0 proteins were extracted from batch WT-B according to the treatments listed in Table 4.8; soluble and insoluble designations for treatment 2A and 2B refer to the portions of the precipitated pellets that did and did not go back into solution upon resuspension, respectively. Gel lanes were loaded to target proteins extracted from equal masses of S^0 to enable comparison of protein extraction efficiency. The 4-20% acrylamide Tris-HCl gel was stained with SYPRO® Ruby Protein Gel Stain. Arrows indicate the largest differences in protein band appearance between the extracts obtained by protocol 3B and the S^0 direct extraction control. Mark12™ Unstained Standard, 2.5-200 kDa (Thermo Fisher Scientific) was used as the molecular weight ladder.

qualitative comparison of extraction efficiency based on staining intensity. As the precipitated pellets from treatments 2A and 2B did not fully resolubilize, the insoluble pellet portions were also mixed with sample buffer and included as lanes of the gel to assess the degree of protein loss. In a second one-dimensional gel, the proteins remaining in association with S^0 after each of the extraction treatments were also extracted directly into SR sample buffer and compared with an untreated S^0 control (Fig. 4.9).

As observed in Fig. 4.8, the extraction efficiencies of the shotgun-compatible methods were comparable to direct extraction of S^0 proteins into LR sample buffer, although slight differences between the different treatments could be observed for some protein bands (indicated by arrows). Extracts obtained from CHAPS-based extraction buffers generally appeared similar to extracts from their SDS-based counterparts, except for treatment 2B, where less protein was able to be resolubilized from the precipitated protein pellet relative to 2A. SDS only provided a clear benefit over CHAPS in the directly shotgun-compatible approach, where more proteins were left in association with S^0 for treatment 1B than treatment 1A (Fig. 4.9). While the inclusion of DTT in the extraction buffer (treatments 2A and 2B) left less protein behind in association with S^0 (Fig 4.9), this benefit was largely negated by the inability to completely resolubilize the precipitated pellets (Fig. 4.8), particularly for the CHAPS-based protocol (treatment 2B). As the elimination of SDS in the extraction protocol would provide a substantial benefit during protein digestion by reducing inhibition of the protease, and the use of SDS did not appear to provide overwhelming benefits during protein extraction for treatments 1A vs. 1B and 3A vs. 3B, CHAPS-based extraction protocols were selected for further development. What was less clear

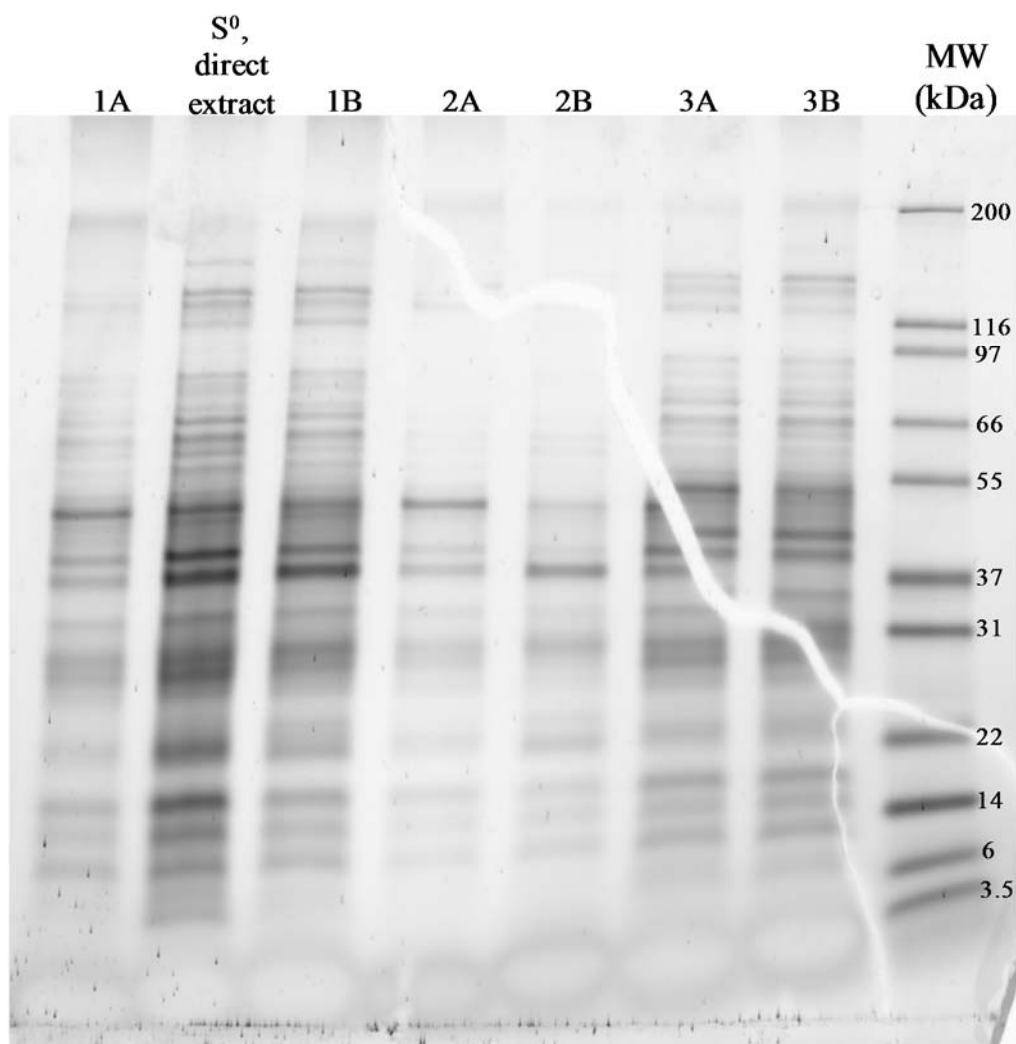


Figure 4.9 One-dimensional gel electrophoresis profiles of the proteins remaining in association with S^0 after extraction by shotgun-compatible protocols, compared to proteins from S^0 when directly extracted into L(+) sample buffer. S^0 proteins were extracted from batch WT-B according to the treatments listed in Table 4.8. Gel lanes were loaded to target proteins extracted from equal masses of S^0 to enable comparison of protein extraction efficiency. 4-20% acrylamide Tris-HCl gel was stained with SYPRO® Ruby Protein Gel Stain. Mark12™ Unstained Standard, 2.5-200 kDa (Thermo Fisher Scientific) was used as the molecular weight ladder.

in this study was whether the use of higher CHAPS concentration during extraction (and subsequent detergent removal; treatment 3B) provided a benefit over the minimal CHAPS buffer (treatment 1B).

In a follow up study, CHAPS-based protocols were quantitatively compared. This study repeated treatments 1B and 3B from the previous study, except in a reduced concentration of the TEAB buffer base (25 mM versus 0.5 M to facilitate to facilitate quantitative comparison of the treatments by protein assay). In addition, an additional treatment, the extraction of S^0 in the absence of detergent, was included to evaluate whether detergent was essential for protein extraction from S^0 . The protein content of each extract was estimated by BCA assay (Fig 4.10-A), and extracts and the residual S^0 -associated proteins from each of the treatments were compared to S^0 proteins extracted directly into LR sample buffer by one-dimensional gel electrophoresis (Fig. 4.10-B).

The best protein recovery was obtained with 2% CHAPS and DetergentOUT™ clean-up, which produced the most concentrated protein extract (Fig. 4.10-A) and the highest staining intensity (Fig 4.10-B). Very little protein was extracted from S^0 using the detergent-free extraction buffer, confirming the requirement for detergents to disrupt S^0 -protein interactions. Based on the results of these studies, a 2% CHAPS extraction buffer and DetergentOUT™-facilitated clean-up were selected as the protein extraction method for shotgun proteomic profiling of S^0 proteins.

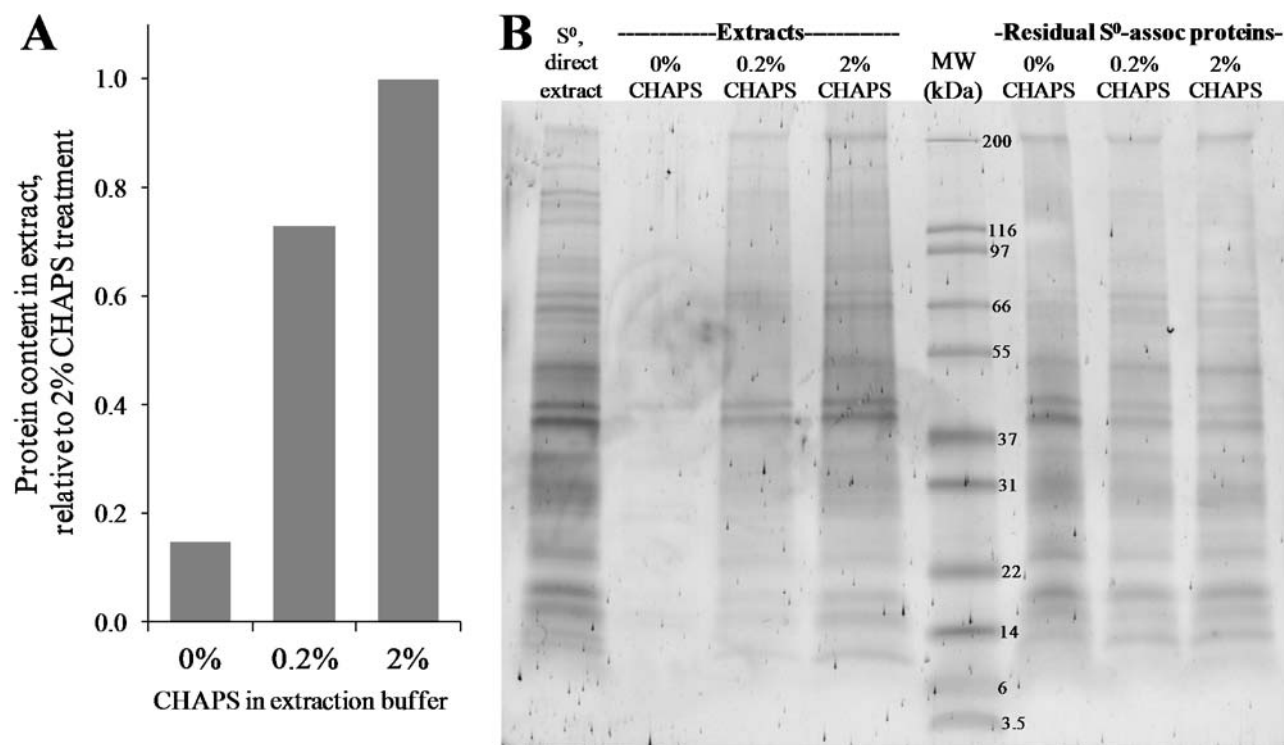


Figure 4.10 Extraction of S^0 with 2% CHAPS and DetergentOUT™ clean-up was found to extract the largest total amount of protein by BCA assay (A) and demonstrated the most protein bands by one-dimensional SDS-PAGE. Gel lands were loaded to target proteins extracted from equal amounts of S^0 . The 4-20% acrylamide Tris-HCl gel was stained with SYPRO® Ruby Protein Gel Stain. Mark12™ Unstained Standard, 2.5-200 kDa (Thermo Fisher Scientific) was used as the molecular weight ladder.

4.4.6 Shotgun proteomic exploration of WT S⁰ identified proteins consistent with the protein profiles of outer membrane vesicles from gram negative bacteria

From 17 µg of protein extracted from S⁰ batch WT-C, 99 proteins were identified by shotgun proteomics. These included 11 of the 13 proteins previously identified in association with WT S⁰ *via* gel-based studies, for a total of 101 proteins identified in association with WT S⁰ (Table 4.9); matched peptides and protein coverage are provided in Appendix F. Relative to the *C. tepidum* proteome, the identified S⁰ proteins were enriched in predicted OM proteins (by 5-fold) and chlorosome proteins (by 8-fold) (Fig 4.11), although cytoplasmic proteins still composed the majority of protein identifications. The most common functional annotations to which S⁰ proteins were assigned, based on Cluster of Orthologous Gene (COG) categories (Table 4.10), were translation (J; 20%) and post-translational modification, protein turnover, and chaperone functions (O; 13%), and a total of nearly 23% of S⁰ proteins were assigned to poorly characterized COG categories (R, S, or no COGs assigned).

Interestingly, the S⁰ protein profile was similar to the protein profiles of outer membrane vesicles (OMV) from other gram-negative bacteria. BLASTP searches identified 64 (63%) of the S⁰ proteins as homologs of proteins identified in a selection of OMV proteomic studies reported in the literature (Table 4.11). A list specifying the homologous OMV proteins for each *C. tepidum* S⁰ protein is provided in Appendix G. Of the 37 S⁰ proteins that were not homologous to OMV proteins, 22 were poorly functionally annotated (Table 4.10) and 15 had no homologs within any proteomes of the eight bacterial species from the OMV studies. Thus a significant number of the S⁰ proteins dissimilar to OMV proteins (e.g. chlorosome proteins and some

uncharacterized proteins) are likely to be specialized to the niche lifestyle of *C. tepidum*. Interestingly, none of the six proteins classified into COG category P (inorganic ion transport and metabolism) were homologs of OMV proteins. This attribute is in stark contrast to the other functionally-defined COG categories, where, in most cases, greater than 75% of S⁰ proteins in each of those categories were homologous with one or more OMV proteins (Table 4.10).

The sections below describe new insight into the biogenesis of S⁰ by *C. tepidum* derived from the S⁰ protein identifications. Similarities between the protein profiles of S⁰ and OMVs provided evidence that S⁰ globules may form *via* a membrane-vesicle-like mechanism. In addition, some of the more striking differences in the protein profile between S⁰ and OMVs have identified interesting targets for characterization that could provide novel insight into S⁰ globule production and oxidation in *C. tepidum*.

Table 4.9 List of proteins identified by shotgun proteomic analysis of S⁰ from wild type *C. tepidum*. Conserved domains for poorly-characterized proteins are provided in parentheses in the description. Proteins also identified in gel-based studies or in OMV proteomic studies from the literature are indicated. WT = wildtype.

Protein Information					Detected in:				
Locus Tag	Accession ^a	Gene Name	Description	Pred. Loc. ^b	COG Cat. ^c	WT S ⁰ , shotgun gel	WT S ⁰ , gel	C3 S ⁰ , gel	Cells, OMVs ^d
CT0018	NP_660924	<i>atpH</i>	ATP synthase F0F1 subunit delta	C	C	X			8
CT0020	NP_660926	<i>atpE</i>	ATP synthase F0 subunit C	CM#	C	X			7
CT0027	NP_660933		uncharacterized protein CT0027	U	--	X			
CT0031	NP_660937	<i>ftsA</i>	cell division protein FtsA	C	D	X			7,8
CT0068	NP_660974		hemagglutinin-related protein (LomR)	OM#	M		X		3,5
CT0089	NP_660995	<i>clpB-2</i>	ATP-dependent Clp protease, ATP-binding subunit ClpB	C	O	X		X	X 1,7,8
CT0131	NP_661037		uncharacterized protein CT0131 (SDR_a8, yfcH)	C	R	X			
CT0150	NP_661056	<i>nusG</i>	transcription antitermination protein NusG	C	K	X			1,7
CT0153	NP_661059	<i>rplJ</i>	50S ribosomal protein L10	C#	J	X			2,7,8,10
CT0154	NP_661060	<i>rplL</i>	50S ribosomal protein L7/L12	U	J	X			2
CT0155	NP_661061	<i>rpoB</i>	DNA-directed RNA polymerase subunit beta	C	K	X			X 1,2,7,8,9
CT0156	NP_661062	<i>rpoC</i>	DNA-directed RNA polymerase subunit beta'	C	K	X			1,2,7,8,9
CT0159	NP_661065	<i>efp</i>	elongation factor P	C	J	X			7

Table 4.9 continued.

Protein Information					Detected in:				
Locus	Gene			Pred.	COG	WT S ⁰	WT S ⁰	C3 S ⁰	Cells,
Tag	Accession ^a	Name	Description	Loc. ^b	Cat. ^c	shotgun gel	gel	gel	OMVs ^d
CT0160	NP_661066	<i>hupB</i>	DNA-binding protein HU-beta	C	L	X	X	X	7,8,9,10
CT0173	NP_661079	<i>serB</i>	phosphoserine phosphatase	C	E	X			9
CT0249	NP_661153		glutathione S-transferase	C	E	X			
CT0254	NP_661158	<i>ompH</i>	outer membrane protein OmpH	U	M	X			2,3,11
CT0264	NP_661168	<i>rho</i>	transcription termination factor Rho	C	K	X			8
CT0288	NP_661192	<i>rpsA</i>	30S ribosomal protein S1	C	J	X			2,7,8
CT0302	NP_661206	<i>petC</i> ⁵	cytochrome b6-f complex, iron-sulfur subunit	CM	C	X	X	X	1
CT0303	NP_661207	<i>petB</i>	cytochrome b-c complex, cytochrome b subunit	CM	C	X			1,7,8
CT0312	NP_661216		DnaK suppressor protein	C	T	X			
CT0350	NP_661254	<i>fabI</i>	enoyl-(acyl-carrier-protein) reductase	CM	I	X		X	1,10
CT0529	NP_661429	<i>groES</i>	co-chaperonin GroES	C	O	X			X 7
CT0530	NP_661430	<i>groEL</i>	chaperonin GroEL	C	O	X	X	X	X 1,2,3,6,7,8,9,10,11
CT0531	NP_661431		sensor histidine kinase/response regulator	CM	T	X			8,9
CT0547	NP_661447	<i>mreB-1</i>	rod shape-determining protein MreB	C	D	X			1,3,8
CT0563	NP_661463	<i>tyrS</i>	tyrosyl-tRNA synthetase	C	J	X			
CT0607	NP_661507		uncharacterized protein CT0607 (YqeY)	C	S	X			

Table 4.9 continued.

Protein Information				Detected in:						
Locus	Gene			Pred.	COG	WT S ⁰ ,	WT S ⁰ ,	C3 S ⁰ ,	Cells,	
Tag	Accession ^a	Name	Description	Loc. ^b	Cat. ^c	shotgun	gel	gel	gel	OMVs ^d
CT0638	NP_661535		peptidoglycan-associated lipoprotein (PRK10802, Pal_lipo)	OM	M	X				1,2,7,8,9,11
CT0642	NP_661539		uncharacterized protein CT0642 (C_GCAXxG_C_C)	C	--	X			X	
CT0643	NP_661540	<i>dnaK</i>	molecular chaperone DnaK	C	O	X	X	X	X	3,6,7,8
CT0644	NP_661541		HSP20 family protein	C	O	X	X	X	X	
CT0829	NP_661723	<i>htpG</i>	heat shock protein 90	C	O	X		X	X	7,8
CT0841	NP_661735	<i>trx-2</i>	thioredoxin	C	CO	X		X	X	
CT0893	NP_661786		uncharacterized protein (Porin_5)	OM	--	X	X			9
CT0903	NP_661796		transcriptional regulator (PhoU)	C	P	X				
CT0941	NP_661834	<i>btuR</i>	cob(I)alamin adenosyltransferase	C	H	X				
CT0960	NP_661853	<i>purC</i>	phosphoribosylaminoimidazole-succinocarboxamide synthase	C	F	X		X		7,8
CT0980	NP_661873		ArsA ATPase	C	P	X				
CT1007	NP_661900		uncharacterized protein CT1007 (DsrE/DsrF - like family)	CM	--	X				
CT1054	NP_661945	<i>prc</i>	carboxyl-terminal protease	CM	M	X		X		2,5,6,7,8,9
CT1133	NP_662024		uncharacterized protein (CRISPR-associated protein)	U	--		X	X		
CT1170	NP_662061		uncharacterized protein CT1170 (SRPBCC)	C	I	X				7
CT1225	NP_662115		N-acetylmuramoyl-L-alanine amidase	U	V	X				7,8,9

Table 4.9 continued.

Protein Information					Detected in:				
Locus Tag	Accession ^a	Gene Name	Description	Pred. Loc. ^b	COG Cat. ^c	WT S ⁰ , WT S ⁰ , C3 S ⁰ , Cells, shotgun gel	WT S ⁰ , WT S ⁰ , C3 S ⁰ , Cells, gel	WT S ⁰ , WT S ⁰ , C3 S ⁰ , Cells, gel	OMVs ^d
CT1239	NP_662127	<i>secA</i>	preprotein translocase subunit SecA	C	U	X		X	1,7,8,9
CT1297	NP_662185	<i>bchI</i>	magnesium-chelatase subunit I	C	R	X			
CT1309	NP_662197		uncharacterized protein CT1309 (Metal_resist)	U	--	X			
CT1353	NP_662240		OmpA family protein (type_VI_ompA, OmpA_C-like)	OM	M	X		X	2,7,8,9, 10,11
CT1361	NP_662248	<i>prsA</i>	ribose-phosphate pyrophosphokinase	C	EF	X			1,2,7,8
CT1362	NP_662249	<i>ctc</i>	50S ribosomal protein L25 general stress protein	C	J	X			7,8
CT1447	NP_662333		serine protease (degP_htrA_DO)	P	O	X	X	X	1,2,8,9, 11
CT1485	NP_662370	<i>grpE</i>	heat shock protein GrpE	C	O	X			7
CT1499	NP_662384	<i>fmoA</i>	bacteriochlorophyll A protein	Csm	--	X		X	
CT1577	NP_662460	<i>frf</i>	ribosome recycling factor	C	J	X		X	7
CT1591	NP_662474	<i>ribBA</i>	3,4-dihydroxy-2-butanone 4-phosphate synthase	C	H	X			1
CT1649	NP_662532	<i>pnp</i>	polynucleotide phosphorylase/polyadenylase	C	J	X		X	1,3,7,8, 10
CT1742	NP_662622	<i>feoB-1</i>	ferrous iron transport protein B	CM	P	X			
CT1743	NP_662623	<i>feoA-1</i>	ferrous iron transport protein A	U	P	X		X	
CT1744	NP_662624		uncharacterized protein CT1744 (FeoA)	U	P	X			

Table 4.9 continued.

Protein Information				Detected in:					
Locus Tag	Accession ^a	Gene Name	Description	Pred. Loc. ^b	COG Cat. ^c	WT S ⁰ , shotgun gel	WT S ⁰ , gel	C3 S ⁰ , gel	Cells, OMVs ^d
CT1745	NP_662625		uncharacterized protein CT1745 (Phenol_MetA_deg)	U	--	X		X	
CT1780	NP_662659	<i>tsf</i>	elongation factor Ts	C	J	X		X	1,7,10
CT1781	NP_662660	<i>rpsB</i>	30S ribosomal protein S2	C	J	X			1,2,7,8,10
CT1782	NP_662661	<i>rpsI</i>	30S ribosomal protein S9	C	J	X		X	2,7,8,10,11
CT1785	NP_662664		ATP-binding Mrp/Nbp35 family protein (ParA, minD_arch)	CM	D	X			1,3,8
CT1804	NP_662683		uncharacterized protein CT1804	OM	--	X	X	X	X
CT1833	NP_662712	<i>gatC</i>	aspartyl/glutamyl-tRNA amidotransferase subunit C	C	J	X			1
CT1867	NP_662744		uncharacterized protein CT1867 (SIMPL)	P	S	X			
CT1921	NP_662798		cysteine synthase/cystathionine beta-synthase	C	E	X			6,7
CT1939	NP_662816		ArsA ATPase	C	P	X			
CT1942	NP_662819	<i>csmA</i>	chlorosome envelope protein A	Csm	--	X		X	X
CT1943	NP_662820	<i>csmC</i>	chlorosome envelope protein C	Csm	--	X	X	X	X
CT1947	NP_662824	<i>ssb-I</i>	single-strand binding protein	C	L	X			4,7
CT1955	NP_662832		magnesium-chelatase, bacteriochlorophyll c-specific subunit	C	H	X		X	X
CT1970	NP_662846		HSP20 family protein	U	O	X	X	X	X

Table 4.9 continued.

Protein Information					Detected in:				
Locus Tag	Accession ^a	Gene Name	Description	Pred. Loc. ^b	COG Cat. ^c	WT S ⁰ , shotgun gel	WT S ⁰ , C3 S ⁰ , gel	Cells, gel	OMVs ^d
CT1986	NP_662862		uncharacterized protein CT1986 (WD40)	U	R	X			
CT2001	NP_662877	<i>bcp-2</i>	bacterioferritin comigratory protein, thiol peroxidase	C	O	X			6,7
CT2026	NP_662901		c-type cytochrome	U	--	X			
CT2033	NP_662908	<i>atpA</i>	ATP synthase F0F1 subunit alpha	C	C	X		X	1,3,6,7,8
CT2047	NP_662922		AcrB/AcrD/AcrF family protein	CM	V	X			8
CT2049	NP_662924		LipD protein, putative (type_I_sec_TolC)	OM	MU	X	X		2,9,11
CT2054	NP_662929	<i>csmB</i>	chlorosome envelope protein B	Csm	--	X		X	
CT2067	NP_662942		pentapeptide repeat-containing protein	E	S	X			
CT2097	NP_662971		uncharacterized protein CT2097 (CxxC_CxxC_SSSS)	U	S	X			
CT2101	NP_662975		uncharacterized protein CT2101 (DUF190)	C	S	X		X	
CT2129	NP_663003	<i>rplT</i>	50S ribosomal protein L20	C	J	X			2,7,8,10
CT2144	NP_663018		outer surface protein, putative (LomR)	OM	M	X	X	X	3,10
CT2147	NP_663021		uncharacterized protein CT2147	C	--	X			
CT2151	NP_663025	<i>bchB</i>	light-independent protochlorophyllide reductase subunit B	C	C	X			
CT2160	NP_663034	<i>gidB</i>	16S rRNA methyltransferase GidB	C	J	X			

Table 4.9 continued.

Protein Information				Detected in:					
Locus	Gene		Pred.	COG	WT S ⁰	WT S ⁰	C3 S ⁰	Cells,	
Tag	Accession ^a	Name	Description	Loc. ^b	Cat. ^c	shotgun gel	gel	gel	OMVs ^d
CT2161	NP_663035	<i>rplQ</i>	50S ribosomal protein L17	C	J	X		X	2,7,8,10
CT2162	NP_663036	<i>rpoA</i>	DNA-directed RNA polymerase subunit alpha	C	K	X			1,7,8,10
CT2177	NP_663051	<i>rplE</i>	50S ribosomal protein L5	C	J	X			1,2,7,8,10,11
CT2182	NP_663056	<i>rplP</i>	50S ribosomal protein L16	C	J	X			2,7,10
CT2186	NP_663060	<i>rplB</i>	50S ribosomal protein L2	C	J	X			1,2,7,8,10,11
CT2191	NP_663065	<i>tuf</i>	elongation factor Tu	C	J	X		X	1,2,5,7,8,9,11
CT2215	NP_663089	<i>gatB</i>	aspartyl/glutamyl-tRNA amidotransferase subunit B	C	J	X			1,6
CT2216	NP_663090		uncharacterized protein CT2216	CM	S	X		X	
CT2234	NP_663108	<i>atpD-2</i>	ATP synthase F0F1 subunit beta	C	C	X		X	1,3,6,7,8
CT2264	NP_663137	<i>surA</i>	peptidyl-prolyl cis-trans isomerase SurA	P	O	X			2,7,8,11
CT2281	NP_663152	<i>clpB-1</i>	ATP-dependent Clp protease, ATP-binding subunit ClpB	C	O	X		X	1,7,8

^a RefSeq (NP_XXXXXX) or GenBank (AAYXXXXX) Accession

^b Location prediction by pSORTb, except for manual annotations as described in the Methods (indicated by #). Csm: chlorosome; C: cytoplasmic; CM: cytoplasmic membrane; OM: outer membrane; P: periplasmic; U: unknown.

^c Abbreviations for COG functional categories is provided in Table 4.10

^d Numbers correspond to study IDs are listed in Table 4.11

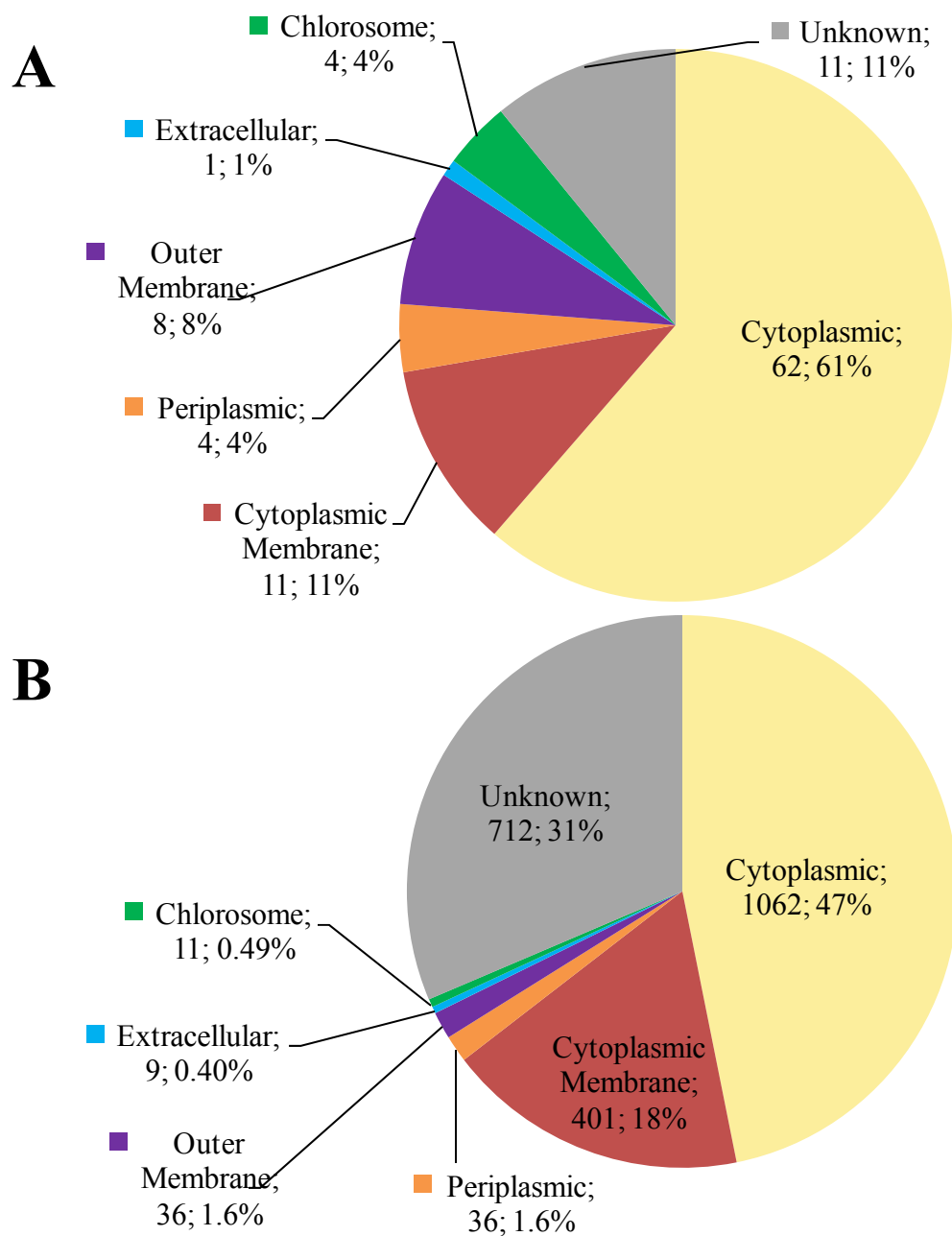


Figure 4.11 Breakdown of predicted subcellular location for proteins identified from wildtype *S⁰* (A) versus the whole *C. tepidum* proteome (B). For each subcellular location, the data label indicates number of proteins and percentage of the total associated with that location (#; %).

Table 4.10 Functional classification of proteins associated with S⁰ based on COG categories, and portion of proteins within COG categories with homologs previously identified in proteomic studies of outer membrane vesicles.

COG Category		All S ⁰ proteins count ^a % of total ^a		S ⁰ proteins with OMV protein homologs count ^a % in COG category ^a	
C	Energy production and conversion	8	7.9%	6	75%
D	Cell cycle control, cell division, chromosome partitioning	3	3.0%	3	100%
E	Amino acid metabolism and transport	4	4.0%	3	75%
F	Nucleotide metabolism and transport	2	2.0%	2	100%
H	Coenzyme metabolism and transport	3	3.0%	1	33%
I	Lipid metabolism and transport	2	2.0%	2	100%
J	Translation, ribosomal structure and biogenesis	20	19.8%	18	90%
K	Transcription	5	5.0%	5	100%
L	Replication, recombination and repair	2	2.0%	2	100%
M	Cell wall/membrane/envelope biogenesis	7	6.9%	7	100%
O	Post-translational modification, protein turnover, chaperones	13	12.9%	11	85%
P	Inorganic ion transport and metabolism	6	5.9%	0	0%
R	General Functional Prediction only	3	3.0%	0	0%
S	Function Unknown	6	5.9%	0	0%
T	Signal Transduction mechanisms	2	2.0%	1	50%
U	Intracellular trafficking, secretion, and vesicular transport	2	2.0%	2	100%
V	Defense Mechanisms	2	2.0%	2	100%
	No COG assigned	14	13.9%	1	7%

^a Count and % sum to greater than 101 and 100%, respectively, as a small number of proteins were assigned to more than one COG category.

Table 4.11 List of outer membrane vesicle proteomic studies included in the compilation of OMV proteins against which the *C. tepidum* S⁰ protein identifications were compared.

Study ID	Bacterial species and strain	Reference
1	<i>Campylobacter jejuni</i> NCTC11168	Jang et al. 2014
2	<i>Escherichia coli</i> DH5a	Lee et al. 2007
3	<i>Legionella pneumophila</i> Philadelphia-1 strain JR32	Galka et al. 2008
4	<i>Myxococcus xanthus</i> DK1622	Whitworth et al. 2015
5	<i>Neisseria meningitidis</i> serogroup B strain NMB (NMB-ACE1)	Post et al. 2005
6	<i>Neisseria meningitidis</i> unencapsulated mutants of strains MC58 (ST-74) and 2120 (ST-11)	Lappann et al. 2013
7	<i>Pseudomonas aeruginosa</i> PAO1	Ballok et al. 2014
8	<i>Pseudomonas aeruginosa</i> UCBPP-PA14 or <i>Pseudomonas aeruginosa</i> clinical isolate	Choi et al. 2011
9	<i>Pseudomonas aeruginosa</i> PAO1	Couto et al. 2015
10	<i>Salmonella enterica</i> serovar Typhimurium 14028S (ATCC 14028)	Bai et al. 2014
11	<i>Vibrio cholerae</i> El Tor biotype strain C6706	Altindis et al. 2014

4.4.6.1 Commonalities between S⁰ globule proteome and OMVs include cell envelope spanning transport complexes and cell division machinery

One theme among the S⁰ proteins previously identified as OMV proteins is that a number of them have been implicated in cell envelope stability and cell division, based on studies of deletion mutants in other bacteria (Table 4.12). Four of these S⁰ proteins are members of membrane-spanning protein complexes (Table 4.12): CT0638 and CT1353 are homologs of the outer membrane peptidoglycan-associated lipoprotein (Pal) member of the Tol-Pal system, and CT2049 and CT2047 are homologs of two protein members (TolC, AcrB) of the AcrAB-TolC multidrug efflux pumps. The Tol-Pal complex, which is involved in the uptake of certain bacteriocins

Table 4.12 Proteins identified in association with S⁰ as well as in previous proteomic studies of OMVs that suggest involvement of outer membrane-inner membrane connectivity and cell envelope stress response in S⁰ biogenesis.

System/ Function	Protein/ Domain family	Description	Role in cell envelope stability	Examples of deletion mutant phenotypes	<i>C. tepidum</i> S ⁰ - associated homologs		
					Locus tag	COG Cat	Pred Loc
Tol-Pal	Pal	Peptidoglycan associated lipoprotein	Cell-envelope spanning complex; links OM and IM during cell division (Gerding et al. 2007)	<i>E. coli</i> : hypervesiculation (Bernadac et al. 1998; McBroom et al. 2006); <i>S.</i> <i>typhimurium</i> : increased vesiculation at division septa and increased sensitivity to deoxycholate (Deatherage et al. 2009)	CT0638 CT1353	M	OM
RND Pump	TolC	Outer membrane efflux protein	Cell-envelope spanning complex	<i>E. coli</i> : Increased sensitivity to detergents and dyes (Morona & Reeves 1982);	CT2049	MU	OM
	AcrB/D/ F	Multidrug efflux pump, inner membrane subunit	Cell-envelope spanning complex	<i>E. coli</i> : Increased susceptibility to small inhibitor molecules (Ma et al. 1995)	CT2047	V	IM
Cell cycle control and division	MreB	bacterial actin	Cell shape; Localizes with septal ring during cell division	<i>H. influenza</i> : hypervesiculation (Roier et al. 2016); <i>E. coli</i> : accumulation of intracellular vesicles (Bendezú & de Boer 2008)	CT0547	D	C
	FtsA	actin-family ATPase	Localizes with septal ring during cell division	<i>B. subtilis</i> : filamentous growth (Beall & Lutkenhaus, 1992)	CT0031	D	C

Table 4.12 continued.

System/ Function	Protein/ Domain family	Description	Role in cell envelope stability	Examples of deletion mutant phenotypes	<i>C. tepidum</i> S ⁰ - associated homologs		
					Gene loci	COG Cat	Pred Loc
Cell cycle control and division (cont'd)	ParA/ MinD family	plasmid partitioning ATPase	Critical for proper cell division	<i>P. aeruginosa</i> : production of anucleate cells, inhibited swarming motility (Lasocki et al. 2007)	CT1785	D	IM
	DnaK	70 kDa heat shock protein	Undetermined	<i>E. coli</i> : Impaired cell division (Bukau & Walker 1989)	CT0644	O	C
	GroEL	60 kDa chaperonin	Localizes to SR during cell division (Ogino, 2004)	<i>E. coli</i> : Filamentous growth (Fujiwara & Taguchi 2007)	CT0530	O	C
PTMs and trafficking of cell envelope proteins	SurA	peptidyl-prolyl cis-trans isomerase	Proper trafficking of unfolded OM proteins	<i>E. coli</i> : Increased vesiculation (McBroom Brooks 2006), decreased outer membrane density (Sklar et al. 2007)	CT2264	O	P
	DegP	chaperone- protease	Proper trafficking of unfolded OM proteins	<i>Multiple species</i> : Increased vesiculation (McBroom et al. 2006; Tashiro et al. 2009) <i>V. cholerae</i> : altered protein content of OMVs (Altindis et al. 2014)	CT1447	O	P
	Skp (OmpH)	chaperone	Proper trafficking of unfolded OM proteins	<i>N. meningitidis</i> : Reduced levels of outer membrane porins PorA and PorB (Volokhina et al. 2011)	CT0254	M	P#

and phage DNA (Walburger et al. 2002) and plays a role in maintaining cell envelope stability (Lazzaroni et al. 1999; Lloubès et al. 2001), connects the OM to the IM *via* transient interactions between the outer membrane protein Pal and an inner membrane protein member TolA (Gerding et al. 2007). Pal is also known to form direct, non-covalent linkages between the OM and PG (Gerding et al. 2007). Interestingly Tol-Pal has also been implicated in facilitating cell division as all five proteins of the complex have been found to accumulate at sites of cell constriction in *E. coli*, and are critical for proper invagination of cell envelope layers during cell division (Gerding et al. 2007). AcrAB-TolC multidrug efflux pumps are tripartite systems responsible for transporting a range of compounds out of the cell (Koronakis et al. 2004; Du et al. 2014). These pumps consist of three protein members: the outer membrane channel protein TolC, the inner membrane transporter protein AcrB, and a periplasmic protein AcrB which fuses together the integral membrane proteins, connecting the OM to the IM (Du et al. 2014). Besides their common cell envelope spanning characteristics, both Tol-Pal and AcrAB-TolC are energy-consuming complexes driven by the proton motive force (Cascales et al. 2001; Lloubès et al. 2001; Seeger et al. 2006).

Despite these similarities, however, Tol-Pal appears to play a larger role in membrane stability than AcrAB-TolC. Deletion mutants of Pal and the other Tol-Pal complex proteins were characterized by overall increased production of OMVs in *E. coli* (Bernadac et al. 1998; McBroom et al. 2006) and increased production of larger OMVs and OMVs at cell division septa in *Salmonella typhimurium* (Deatherage et al. 2009), along with increased susceptibility to the chaotrope deoxycholate (Deatherage et al. 2009). By contrast, the phenotypes of AcrAB-TolC deletion mutants were characterized by increased susceptibility to detergents, dyes, and small inhibitor

molecules (Morona & Reeves 1982; Ma et al. 1995) without increased vesiculation (Bernadac et al. 1998), suggesting that the primary role of these complexes is efflux of inhibitory compounds rather than maintaining OM-IM connectivity.

It has been hypothesized that the hypervesiculation phenotypes of Tol-Pal deletion mutants are due to reduced connectivity between the OM, IM, and peptidoglycan (PG). Along with Tol-Pal and Pal linkages with PG, in *E. coli* and other gram-negative bacteria, additional covalent and non-covalent linkages between the OM and PG are formed by the murein lipoprotein Lpp and the outer membrane porin OmpA, respectively (Schwechheimer & Kuehn 2015; Schwechheimer et al. 2013; Gerding et al. 2007). However, that increased expression of Pal in an *E. coli lpp* deletion mutant was found to compensate for the missing Lpp-PG linkages suggests that Pal-PG complexes are more important for maintaining cell envelope stability (Cascales et al. 2002). Interestingly, *C. tepidum* does not possess homologs of either OmpA or Lpp, suggesting that other proteins in *C. tepidum* must be responsible for maintaining OM-PG links, including its two Pal homologs. Of the two *C. tepidum* homologs of Pal, it is likely that CT0678 is the bona-fide Pal member of the Tol-Pal system, based on its gene's proximity within the genome to the genes for the other Tol-Pal system proteins (CT0633-CT0637). Thus, CT1353 could be a candidate protein for providing additional linkages between the OM and PG, and investigations into the role of this protein would be interesting.

The presence of proteins from two different cell-envelope spanning complexes in S^0 is intriguing in the context of potential S^0 excretion mechanisms and in the context of the large number of cytoplasmic and inner membrane proteins detected in association with S^0 , as it suggests the possibility that S^0 globules bud out from specific

regions of the *C. tepidum* cell surface with increased IM-OM connectivity. Deatherage et al. (2009) found differences between the OMVs that budded from constricted septa during cell division and from the cell body, and concluded that the larger OMVs that budded from constricted septa were modulated by localized OM-PG-IM connections from the Tol-Pal complex, whereas the smaller cell-body derived OMVs were modulated by linkages between the OMP-PG *via* OmpA and Lpp (Deatherage et al. 2009). Thus the presence of Pal, TolC, and AcrB homologs in *C. tepidum* S⁰ suggests the possibility that S⁰ may preferentially bud from regions with increased OM-IM connectivity and/or from cell division septa, a possibility which is discussed next.

In contrast to these results, it should be noted here that one of the prevailing mechanisms thought responsible for OMV biogenesis is that local decreases in outer membrane-peptidoglycan (PG) connectivity provides sites that allow the outer membrane to bulge outward and pinch off (Bonnington & Kuehn, 2014; Schwechheimer & Kuehn, 2015), carrying periplasmic material away in the lumen of the OMV. This theory is obviously in direct opposition to what the S⁰ protein identifications described above suggest. However, this theory fails to explain the frequent presence of cytoplasmic and inner membrane proteins in OMV protein profiles. Furthermore, all of these proteins described above have also been detected in association with OMVs, and it is becoming more recognized that multiple mechanisms may contribute to OMV biogenesis and that OMV populations may actually be heterogeneous both in terms of size, properties, and protein cargo (Bonnington & Kuehn 2014; Deatherage et al. 2009). Thus, one possibility is that the S⁰ generation process may be analogous to one route for OMV biogenesis, but distinct from the more well-established pathways.

Another theme among S^0 associated proteins homologous to OMV proteins is the identification of multiple proteins involved in cell shape regulation and cell division (Table 4.12). Both the *C. tepidum* homologs of MreB (CT0547) and FtsA (CT0031) were detected in S^0 , which are ATPases of the actin superfold family. MreB, known as the rod-shape determining protein for bacterial species such as *E. coli*, *Bacillus subtilis*, and *Caulobacter crescentus*) (Shaevitz & Gitai 2010), forms helices of membrane-associated filaments (Strahl, 2014). These filaments have been shown to create membrane regions of increased fluidity (Strahl et al. 2014), to direct the insertion of new cell wall material, and to regulate the subcellular organization of bacterial proteins including large protein complexes and organelles (Strahl et al. 2014). Deletion of MreB is often lethal, and viable MreB deletion mutants in *E. coli* have demonstrated accumulation of intracellular vesicles (Bendezú et al. 2008), emphasizing the role of this protein in maintaining cell wall structure.

One of the protein complexes that MreB helps to spatially organize is the septal ring (or Z-ring) during cell division, where MreB interacts directly with the tubulin protein FtsZ (Fenton & Gerdes 2013). While FtsZ was not detected in S^0 , other proteins that are recruited to the septal ring during later stages of cell division (Lutkenhaus et al. 2012; Ogino et al. 2004) were detected in S^0 : FtsA as described above and GroEL (CT0530), which are both required for proper cell division (Beall & Lutkenhaus 1992; Fujiwara & Taguchi 2007). Another protein likely involved in cell division that was detected in S^0 was CT1785, of the ParA/MinD family. ParA is responsible for plasmid partitioning during cell division, and is homologous to MinD which is involved in preventing septal ring formation at the cell poles (Lutkenhaus et al. 2012). Interestingly, FtsA and MinD have been observed to exhibit a helical pattern

on the surface of *B. subtilis*, which appears to be due to preferential binding to helical lipid domains enriched in phosphatidylglycerol (Barák and Muchová 2013). It has been proposed that these phosphatidylglycerol helical regions may serve as attachment loci for the Sec secretory complex, and SecA is another protein we found in association with S⁰ and has also been found in OMVs (Table 4.9).

Two additional proteins identified in association with S⁰ that could be involved with cell division and potentially also localize to similar sites as MreB, FtsA, and/or ParA/MinD are the chaperone DnaK and the uncharacterized protein CT2216. DnaK is also a member of the same actin super-family as MreB and FtsA, although DnaK is not known to polymerize into filaments (Shaevitz & Gitai, 2010). DnaK deletion mutants exhibit impaired cell division (Bukau & Walker 1989), although the mechanism of its involvement in the cell cycle is currently unknown. However, DnaK has been observed to interact with liposomes by inserting directly into the lipid bilayer and forming dimers (Lopez et al. 2016), providing a potential mechanism to explain our observation that DnaK is detected as a strongly-associated S⁰ protein and was detected at a much higher molecular weight than expected by one-dimensional SDS-PAGE (Fig. 4.7). CT2216 contains the Ysc84 version of the SYLF lipid-binding domain, which has been shown to bind liposomes as well as bind and bundle actin filaments. Thus CT2216 could potentially be another protein member that localizes to a similar site as the proteins mentioned above.

The different roles of these proteins in conferring cell envelope stability and or function during cell division provide evidence that S⁰ may originate from specific sites along the *C. tepidum* surface with increased connectivity between the outer and inner membranes and sites which may associate with bacterial lipid domains.

Interestingly, the cell poles were observed to be a frequent attachment site for S⁰ during both S⁰ production (Marnocha et al. 2016), although the microscopy work reported above showed the distribution of S⁰ ‘blebs’ across the entire cell surface (Fig. 4.1, 4.2). Obviously, more work is required to determine whether the proteins described above are directly involved with the formation of S⁰ or help to localize yet-to-be determined S⁰ production machinery, and whether the spatial location of S⁰ globule formation is affected by growth conditions including light levels and sulfide concentration. However, these results provide interesting protein targets for functional characterization in the context of S⁰ metabolism, and suggest new directions of research.

4.4.6.2 S⁰ globule proteins not typically found in OMVs are involved in energy-dependent ion transport

As mentioned above, the COG category relating to inorganic ion transport and metabolism was an outlier among the functionally categorized COG categories, as none of the S⁰ proteins in this category had OMV protein homologs. Of the six S⁰ proteins in the inorganic ion transport and metabolism, two are annotated as ArsA anion-transporting ATPases (CT0980, CT1939). ArsA proteins are the catalytic subunits of inner-membrane ATP-driven efflux pumps, which typically are composed of ArsA and a second membrane subunit ArsB, and are responsible for excreting oxyanions of arsenic and antimony. Interestingly, while *C. tepidum* possesses a total of six ArsA homologs, no ArsB homologs are observed in the proteome, suggesting that these ArsA homologs could function of the catalytic portions of another transport complex. Furthermore, ArsA are expected to reside on the cytoplasmic side of the inner membrane, and while PSORTb assigned cytoplasmic predictions to both

CT0980 and CT1939 and neither has predicted transmembrane helices, they both have a predicted Sec secretion signal peptide. Thus the predicted subcellular location of these two efflux pumps is uncertain.

Interestingly, ArsA homolog CT1939 is predicted to be part of an operon with CT1940 (Eddie & Hanson 2013), an uncharacterized, predicted cytoplasmic protein with homologs only within the *Chlorobiaceae*. Immediately upstream of this locus are the genes for the chlorosome proteins CsmA and CsmC, which were also identified in the S⁰ proteome (along with CsmB and BChl a binding protein FmoA), and for another ArsA homolog CT1945. The similarity of the genetic organization of *CT1945-csmCA-CT1940-CT1939* to that around the *csmA* gene of *Chloroflexus aurantiacus* was previously recognized by Frigaard et al. (2003), and they suggested the possibility that these gene products of *CT1945*, *CT1940*, and *CT1939* may have roles in chlorosome biogenesis. The identification of the ArsA homolog in association with S⁰ along with CsmA, CsmC, CsmB, and FmoA is intriguing, and suggests the possibility that S⁰ biogenesis is an ATP dependent process that co-localizes with chlorosomes in *C. tepidum*.

The gene for the ArsA homolog CT0980 was not predicted to be part of an operon (Eddie & Hanson 2013), but is located immediately downstream of *CT0979*, which is predicted to encode a membrane-bound lytic murein transglycolase, an enzyme which cleaves bonds in peptidoglycan and is involved in bacterial cell wall degradation. Interestingly, the transcript expression levels and trends for these two genes were very similar in another transcriptomic study (Eddie & Hanson, unpublished data), suggesting the possibility that they may actually be co-transcribed. Whether there is any potential functional link between the ArsA homolog CT0980 and

a CT0979 in modulating cell envelope connectivity during S^0 is entirely speculative. However, these two proteins, along with CT1939 and CT1940, constitute interesting targets for future characterization in the context of S^0 globule formation.

Three other S^0 proteins classified in COG category inorganic ion transport and metabolism (CT1742, CT1743, and CT1744), and a fourth S^0 protein without any assigned COGs (CT1745) are protein products of a cluster of Fe^{2+} acquisition, transport, and storage genes that demonstrated a large (7-fold to 22-fold) increase in transcript expression in response to sulfide (Eddie and Hanson, 2013). CT1745, the product of the first gene in the cluster, is an uncharacterized, predicted beta-barrel outer membrane protein containing the conserved domain Phenol_MetA_deg whose role is unknown. Proteins CT1744 and CT1743 both contain domains for FeoA, a small, potentially metal-binding protein that may interact with the cytoplasmic domain of FeoB (CT1742) (Lau et al. 2013), the product of the fourth gene of the cluster. FeoB is predicted to reside in the cytoplasmic membrane and constitute the pore for iron transport (Lau et al. 2013; Weaver et al. 2013); an N-terminal P-loop motif suggests that FeoABC-mediated iron transport is GTP-dependent. The remaining proteins from this gene cluster (the transcriptional regulator FeoC/CT1741, ferritin/CT1740, an uncharacterized protein CT1739, the flavodoxin FldA/CT1738, and the iron-dependent repressor CT1737) were not detected in S^0 . Recently, the FeoA, FeoB, and FeoC proteins of *V. cholerae* were observed to form a complex *in vivo*, but only FeoA and FeoB were required for complex formation (Stevenson et al. 2016).

As the increase in Fe^{2+} iron transport-related genes upon sulfide addition was unexplained, Eddie and Hanson (2013) explored several potential causes for this

transcript response, and concluded that the transient increase in the expression of *CTI739-CTI745* was likely a non-specific redox change-mediated induction rather than reduced bioavailability of iron or increased cellular demand for iron. However, our identification of the protein products from the first four genes of this cluster in association with S^0 provides a new, alternative explanation for the observed increase in transcript abundance: that these proteins are actually incorporated into budding S^0 globules.

Interestingly, a number of different proteins involved in Fe^{3+} transport (e.g. the Fe^{3+} dicitrate transport protein FecA, the iron-regulated outer membrane protein receptor FetA, and the periplasmic member Fe^{3+} ABC transporter Fbp/ FetB), but not Fe^{2+} transport, were found in association with OMVs of *P. aeruginosa*, *E. coli*, *N. meningitidis*, and *V. cholerae* in the literature studies surveyed (Post et al. 2005; Lappann et al. 2013; Couto et al. 2015; Choi et al. 2011; Lee et al. 2007; Altindis et al. 2014). The presence of iron acquisition proteins in OMVs has also been previously recognized (Schwechheimer & Kuehn 2015). One of the proposed functions of OMVs is nutrient acquisition and delivery to bacterial cells, and iron acquisition *via* OMVs has been described (Kulp & Kuehn 2010; Schwechheimer & Kuehn, 2015). These iron acquisition proteins are outer membrane and periplasmic proteins, and inner-membrane iron transport proteins were not found in association with OMVs. As ferric iron is highly insoluble, dedicated outer membrane receptors and transport pathways for ferric complexes are required for its transport (Lau et al. 2016). Fe^{3+} limitation was also found to induce increased OMV production in *Haemophilus influenza*, *V. cholerae*, and *E. coli* in a recent study that described a novel mechanism of OMV biogenesis (Roier et al. 2016). While the exact relationship was unclear, it appeared

that Fe^{3+} limitation led to the down regulation of the VacJ/Yrb ABC lipid transport system *via* the ferric uptake regulator. The researchers found that VacJ/Yrb was responsible for maintaining the lipid asymmetry of the OM, and that disruptions in or decreased expression of VacJ/Yrb ABC transporter allowed phospholipid accumulation in the outer leaflet of the outer membrane, leading to asymmetric expansion, outward bulging of the outer membrane, and subsequent OMV production.

Insoluble Fe^{3+} is expected to be the dominant form of iron in aerobic environments, whereas the more soluble Fe^{2+} is expected to dominate in the anaerobic environment (Lau et al. 2016) of *C. tepidum*. As Fe^{2+} is thought to diffuse freely through outer membrane porins into the periplasm, outer membrane transporters for Fe^{3+} are not required. The observation of Fe^{2+} transport proteins in the S^0 globule proteome could represent a dual function of S^0 as both a means of sulfur storage, as well as an Fe^{2+} -scavenging function, accumulating Fe^{2+} for uptake during subsequent S^0 oxidization. That the iron transport proteins observed both in *C. tepidum* S^0 are inner membrane associated, with the exception of CT1745 which has an unknown subcellular location, again raises the question of how these proteins are incorporated into these extracellular vesicles, and how this GTP-dependent transport system would be able to function outside of the cell.

4.4.6.3 S^0 biogenesis: originating from locally-energized sites of OM-IM connectivity?

The sections above detailed our observation of a number of proteins identified in association of S^0 that are inner membrane or cytoplasmic, are responsible for connectivity between OM-PG and OM-IM, and which require energy in the form of ATP/GTP (MreB, FtsA, ParA/MinD, ArsA, FeoAB) or proton motive force (Tol-Pal

OM-PG-IM connectivity; AcrAB-TolC) for function. These proteins would not be expected to be functional as components of extracellular particles such as S^0 or OMV because of the lack of a mechanism for providing ATP/GTP or proton motive force, yet they have all been identified as frequent components of OMVs. Interestingly, protein subunits of two cytoplasmic membrane energy-generating complexes were also detected in S^0 : those of ATP synthase (the cytoplasmic AtpA, AtpD, and AtpH, and the inner membrane AtpE) as well as the proton motive force (PMF) generating cytochrome b6-f complex (PetC and PetB).

In addition to the possibility that S^0 is generated from regions of *C. tepidum* with increased OM-IM connectivity, the presence of these ATP- and PMF-generating complexes in S^0 suggests that these regions may also be locally energized, which would provide ATP and PMF for proper function of these protein components. Thus, the availability of energy would be likely to modulate OM-IM connectivity, and could also be available for packaging zero-valent sulfur into the S^0 particles if this process is energy-dependent. Interestingly, proper localization of MreB, FtsA, MinD and several other proteins was found to be dependent upon the transmembrane potential component of the proton motive force in another study (Strahl & Hamoen 2010). Further studies to probe the roles of these various protein components and the role of cellular energy states including ATP availability and trans-membrane potential in producing (and potentially degrading) S^0 will provide novel insight into these processes.

One final aspect of the S^0 proteome worth mentioning in the context of IM-OM connectivity is the identification of a large number of cytoplasmic proteins involved with translation, transcription, and DNA replication and repair (COG categories J, K,

and L): 27 (26%) of the S⁰ fell into these categories (Table 4.9). One possible explanation for the presence of these proteins in S⁰ is that they passively deposited on S⁰ as the result of cell lysis; however, as the S⁰ used in this work was collected from a culture shortly after the exhaustion of sulfide, when S⁰ was still highly abundant, it is unlikely that significant cell death had released proteins into the extracellular medium. Furthermore, nearly all of these proteins (25) were previously identified in at least one of the OMV proteomic studies surveyed (Table 4.9), and the prevalence of these types of cytoplasmic proteins as components of OMV proteomes have long been recognized (Lee et al. 2008; Kulp & Kuehn 2010; Bonnington & Kuehn 2014; Schwechheimer & Kuehn 2015). While some have contended that cytoplasmic proteins in OMVs could potentially result from cellular contamination due to cell lysis or improper OMV purification techniques and have urged caution in interpreting the results of proteomic OMV studies (Kulp & Kuehn 2010), the prevalence of cytoplasmic proteins among even carefully prepared OMVs (Schwechheimer & Kuehn 2015) suggests that they could be valid components of OMVs. One possibility is that these proteins are sorted into OMVs when the translation of cell envelope proteins occurs simultaneously with their trafficking to and integration into the membrane (Lee et al. 2008). A mechanism where both OMV and S⁰ are synthesized from sites of the cell with increased OM-IM connectivity could provide a basis for this observation.

4.4.6.4 S⁰ proteins homologous to three periplasmic chaperones suggest the possibility that that S⁰ production may be related to the σ^E envelope stress response

Of the four periplasmic proteins identified in association with S⁰, three are homologs of periplasmic chaperones (Table 4.12) which have important roles in trafficking of unfolded outer membrane proteins (uOMPs) prior to insertion in the

outer membrane envelope (Sklar et al. 2007; Volokhina et al. 2011; Lyu & Zhao 2015): SurA (CT2264), Skp (OmpH; CT0254), and DegP (CT1447). SurA is believed to be the preferred path for uOMP trafficking based on both experimental evidence (Sklar et al. 2007) and a computational model (Costello et al. 2016), while Skp is predicted to play a role in quality control and in redirecting unfolded proteins back into the SurA pathway (Sklar et al. 2007). DegP functions as both a chaperone and a protease, and degrades misfolded proteins to prevent the accumulation of proteinaceous waste in the periplasm (Schwechheimer et al. 2013; Strauch et al. 1989).

These chaperones are all induced by the σ^E envelope stress response, which is activated in response to accumulation of uOMPs (Sklar et al. 2007). Cell envelope stress is also believed to induce OMV production, where increased vesiculation is associated with conditions expected to increase periplasmic accumulation of proteinaceous waste (Schwechheimer & Kuehn 2013; Schwechheimer & Kuehn 2015), and the release of outer membrane vesicles was demonstrated to correlate with the level of protein accumulation in the cell envelope (McBroom & Kuehn 2007). Increased vesiculation phenotypes were found to be characteristic of deletion mutants of both DegP (McBroom et al. 2006; Tashiro et al. 2009) and of SurA (McBroom Brooks 2006; Sklar et al. 2007). DegP was also found to affect the protein content of OMVs in *V. cholerae*, and has been previously recognized as a frequent component of OMV proteomes (Lee et al. 2008; Appendix G). Furthermore, the *C. tepidum* DegP homolog has been one of the most frequently detected proteins in association with S⁰ through the gel-based studies (Appendix E), and the *C. tepidum* Skp homolog was the protein with the 2nd highest number of matched peptides in the shotgun proteomic study of S⁰, suggesting that it is one of the more highly abundant proteins in S⁰.

In the context of S^0 production, the relationship between OMV production and accumulation of periplasmic material is particularly interesting, especially because this response appears to extend to material beyond misfolded proteins including PG fragments and lipopolysaccharide (Schwechheimer & Kuehn 2015). S^0 is produced as a byproduct of sulfide oxidation, where periplasmic sulfide is oxidized first to disulfide and/or polysulfides by one or more of the membrane-bound sulfide quinone oxidoreductases (CT0117, CT0876, and CT1087) (Chan et al. 2009; Shuman & Hanson 2016). From here the pathway from disulfide and polysulfides to S^0 is less clear, although current models implicate polysulfide reductase complexes (CT0494-0496; CT2240-2241) in oxidizing periplasmic sulfide and disulfide to longer polysulfide chains (Eddie & Hanson, 2013). While soluble polysulfides should be able to diffuse out of the periplasm if a suitable porin is expressed, a hallmark of the sulfur contained in S^0 globules is that it is insoluble. Thus, soluble polysulfides are likely converted to insoluble zero-valent sulfur prior to excretion into S^0 , and it is possible that accumulating S^0 in the periplasm prior to excretion could activate a cell envelope stress response, corroborating the presence of the SurA, DegP, and Skp homologs in S^0 , and stimulating the extrusion of S^0 out of the cell in membrane vesicle-like particles; Figure 4.12 provides a visual representation of the hypothesized S^0 generation process. Whether the periplasmic chaperone homologs SurA, DegP, and Skp have a more specific role in S^0 globule generation in *C. tepidum* would be an interesting arc of future research.

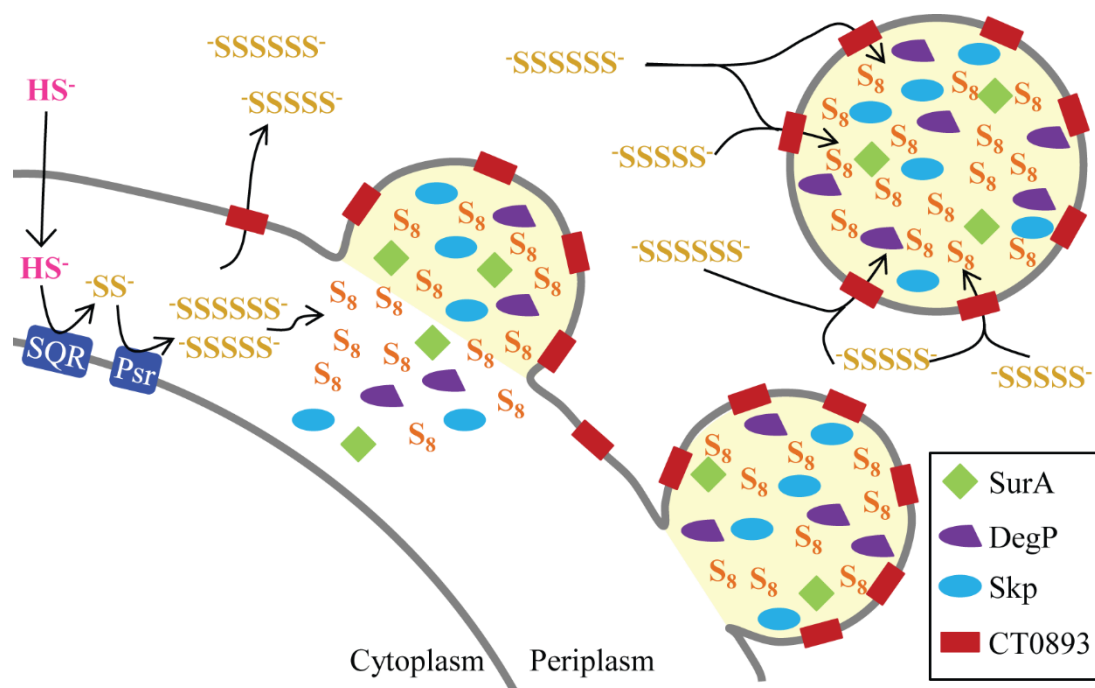


Figure 4.12 Schematic of proposed process for extracellular S^0 globule formation by membrane vesicle-like mechanism. Oxidation of sulfide (HS^-) to disulfide (SS^-) and polysulfides ($SSSSSS^-$, $SSSSS^-$) leads to formation of insoluble cyclo-octasulfur (S_8) which accumulates in the periplasm. This accumulation of insoluble periplasmic material induces the σ^E stress response, recruiting periplasmic proteins SurA, DegP, and Skp (OmpH), and leading to the extrusion of S_8 into S^0 globules *via* a membrane vesicle-like process. Periplasmic polysulfides can also diffuse out of the cell *via* porin transporters (possibly CT0893). These extracellular polysulfides can then accrete onto extracellular S^0 *via* CT0893, which may be shed on the surface of S^0 . Note: relative abundance of SurA, DegP, Skp, and CT0893 in S^0 and actual number of sulfur atoms per polysulfide are not known.

One final S^0 -associated protein worth mentioning here is the uncharacterized protein CT0893, a protein with no known functional classification predicted to be a beta-barrel outer membrane protein of the Porin_5 superfamily. This protein was previously identified as a major component of the secreted fraction of wildtype *C.*

tepidum, but accumulated in the periplasm of a mutant strain (Ω RLP; Hanson & Tabita 2003) with a pleiotropic phenotype characterized by increased accumulation of oxidative stress-related proteins and deficient in S^0 utilization (Hanson & Tabita 2001). The periplasmic accumulation of CT0893 in Ω RLP could indicate a defect in the SurA/DegP/Skp outer membrane protein trafficking system as part of the oxidative stress phenotype, which would implicate CT0893 as an outer membrane protein trafficked by this system. One potential role for the porin protein CT0893 is as a transporter of polysulfides. CT0893 present in a putative membrane coating of S^0 could then enable uptake of polysulfides by S^0 globules, enabling S^0 growth at a distance as observed by Marnocha et al. (2016). That CT0893 was identified as a major component of the secreted fraction of *C. tepidum* in Hanson & Tabita (2001) is also interesting. As CT0893 is a predicted beta-barrel porin, its structure is dependent on it being an integral outer membrane protein. Thus, if it is truly a secreted protein, it would likely be in an unfolded, nonfunctional state unless secreted as part of an outer membrane vesicle. The method Hanson & Tabita (2003) used for isolating the secreted fraction of *C. tepidum* involved collecting ($7,500 \times g$, 5 min) and concentrating (5 kDa molecular weight cut-off filter) the supernatant of a sulfide-oxidizing mid-exponential phase culture. If outer membrane vesicles were being produced by this culture, it is very likely that they would have been retained in the 'secreted' fraction. A model of S^0 biogenesis where CT0893 is an integral membrane protein component of extracellular membrane vesicles responsible for trafficking of insoluble S^0 from cells to previously nucleated S^0 globules is an intriguing possibility, and one that should be directly tested in future studies.

4.4.7 CT1305 and CT1320.1 are two proteins identified only in association with S⁰ produced by strain C3

Two of the poorly-functionally annotated proteins repeatedly identified in extracts of S⁰ from mutant strain C3 in gel-based studies (Appendix E) are of particular interest for further functional characterization. CT1320.1 and CT1305 are proteins of unknown function, with predicted unknown and outer membrane subcellular locations, respectively. They have only been identified in extracts of S⁰ from the C3 mutant strain of *C. tepidum* defective in S⁰ oxidation (see Table 4.3, Figure 4.4, Table 4.5, Fig. 4.5, Table 4.7, Fig. 4.7), but not in S⁰ from wildtype S⁰ or in *C. tepidum* cells even when proteins in corresponding bands were identified, suggesting that these proteins are enriched in S⁰ from C3.

The observed molecular weights for CT1320.1 and CT1305 on gels covered a wide range, and were often significantly smaller than the predicted masses of gene products, 22.1 kDa for CT1320.1 and 54.1 kDa for CT1305. CT1305 was observed in bands ranging in apparent size from 12-50 kDa, and CT1320.1 was observed in bands ranging from 10-20 kDa. CT1305 contains a second methionine at residue 45 that is likely the true translation initiation site based on homology with related Chlorobi proteins (Fig. 4.13) and transcript sequence coverage from previous RNA-seq work (Eddie & Hanson 2013; http://zippo.dbi.udel.edu/gb2/gbrowse/c_tepidum/). CT1320.1 and CT1305 both contain predicted non-cytoplasmic signal peptides (Fig. 4.13) that would produce mature, secreted CT1320.1 at 18.2 kDa and CT1305 at 47.2 kDa. Further processing of CT1320.1 and CT1305 to produce the observed masses is supported by the detection of peptides only after residue 98 for CT1320.1 and residue 112 for CT1305 in MS analysis (data not shown).

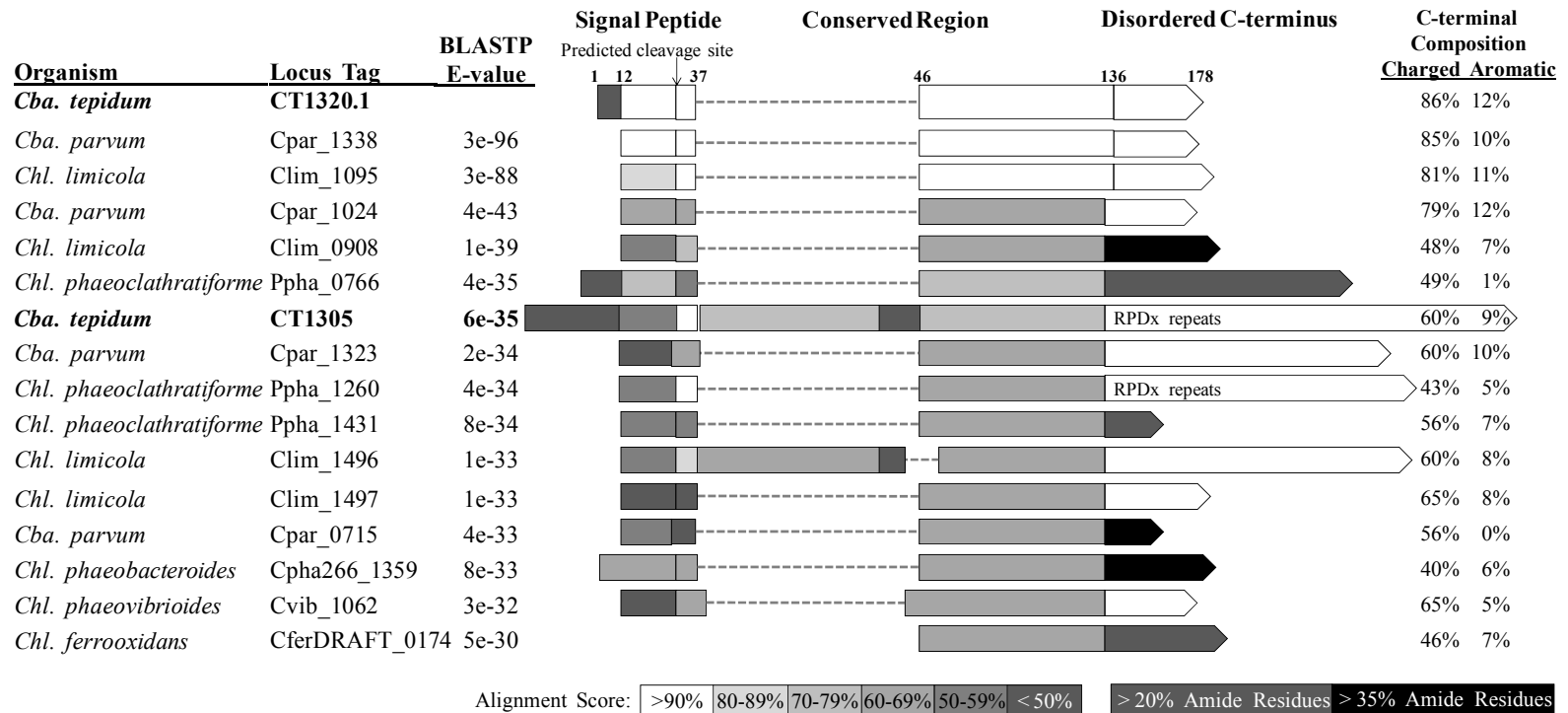


Figure 4.13 Annotated schematic of the alignment of CT1320.1 and CT1305 homologs in the *Chlorobiaceae*. Alignment quality and enrichment of amide side chain amino acids in the C-terminus are indicated by shading. CT1320.1 was the seed for the alignment. A version of this figure originally appeared as Figure 6C in Hanson et al. 2016.

These two proteins are representatives of a group that has an extremely limited distribution in prokaryotes, where CT1320.1 and CT1305 are homologs of each other and of proteins in other *Chlorobiaceae* (Fig. 4.13 and Table 4.13). The closest homologs in the UniProt knowledge base (BLASTP e-value < 1E-30) also contain predicted non-cytoplasmic signal sequences and 1 or 2 copies of a conserved region that is enriched in charged and aromatic amino acid residues. CT1305 carries two copies of this conserved region that share >90% amino acid sequence identity with each other, while CT1320.1 and most of the other close homologs carry a single copy. Only one other protein, Clim_1496 from *Chlorobium limicola*, also has two copies of this region, with >60% amino acid sequence identity to the region in CT1320.1. These proteins also have a low complexity C-terminal region that is predicted to be disordered and is highly enriched in charged residues that often contains RPDx repeats, proline rich regions, and/or amide residues. Most *Chlorobi* genomes contain between 1 and 4 genes encoding homologs of CT1320.1 and CT1305, of which one is a close homolog (e-value < E-30). Only the most basal member of the *Chlorobi*, *Chloroherpeton thalassium* strain ATCC 35110 / GB-78, has no predicted homologs to either CT1320.1 or CT1305.

When searches were performed with less stringent match criteria (BLASTP E-value < 1E-10), a total of 48 sequences similar to CT1305 and CT1320.1 are found in the UniProt knowledge base (T). In addition to those *Chlorobi* sequences described above, weaker homologs are found in *Chlorobium luteolum* strain DSM 273 (1 copy; e-value = 4E-28), *Prosthecochloris aestuarii* strain DSM 271 / SK 413 (1 copy; e-value = 5E-25), *Chlorobium phaeobacteroides* strain BS1 (1 copy; e-value = 2E-24), and *Chlorobium chlorochromatii* strain CaD3 (3 copies; e-values from 7E-22 to 8E-

19). Beyond the *Chlorobi*, homologs of CT1305 and CT1320.1 are only found in the class *Deltaproteobacteria* (*Geobacter* spp. and *Pelobacter* spp., 18 and 2 sequences, respectively) and *Alphaproteobacteria* (*Sphingobacteria*, 3 sequences). That the majority of these homologs are found in *Geobacter* spp. is intriguing as these organisms transfer electrons to extracellular electron acceptors, such as Fe(III) oxides, and must establish direct contact with these solid surfaces to reduce them (Nevin & Lovely, 2000; Reguera et al. 2005). *Pelobacter propionicus* strain DSM 2379 is the only non-*Geobacter* species within the *Deltaproteobacteria* with CT1305/CT1320.1 homologs.

Whether these proteins associate with C3 S⁰ as a direct result of the mutant phenotype (i.e. that they represent differences in S⁰ produced by the C3 mutant) or whether these proteins are cell envelope components important during S⁰ oxidation that associate with S⁰ because of the tight interaction between the C3 mutant and S⁰ after sulfide depletion, is not known at this time. However, that these uncharacterized proteins are homologs of proteins in other organisms that also utilize insoluble extracellular substrates in energy metabolism makes them even more interesting as subjects for future targets for characterization by gene deletion studies.

Table 4.13 Results of a BLASTP search using CT1320.1 as the query sequence against the UniProt knowledge base (www.uniprot.org). Only homologs with an e-value < 1E-10 were considered significant. A version of this table originally appeared as Supplemental Table 1 in Hanson et al. 2016.

E-value	%ID	Locus Tag	Organism
2.00E-138	100%	CT1320.1	<i>Chlorobium tepidum</i> strain ATCC 49652 / DSM 12025 / TLS
3.00E-96	81%	Cpar_1338	<i>Chlorobaculum parvum</i> strain NCIB 8327
3.00E-88	73%	Clim_1095	<i>Chlorobium limicola</i> strain DSM 245 / NBRC 103803
4.00E-43	47%	Cpar_1024	<i>Chlorobaculum parvum</i> strain NCIB 8327
1.00E-39	46%	Clim_0908	<i>Chlorobium limicola</i> strain DSM 245 / NBRC 103803
4.00E-35	43%	Ppha_0766	<i>Pelodictyon phaeoclathratiforme</i> strain DSM 5477 / BU-1
6.00E-35	48%	CT1305	<i>Chlorobium tepidum</i> strain ATCC 49652 / DSM 12025 / TLS
2.00E-34	41%	Cpar_1323	<i>Chlorobaculum parvum</i> strain NCIB 8327
4.00E-34	44%	Ppha_1260	<i>Pelodictyon phaeoclathratiforme</i> strain DSM 5477 / BU-1
8.00E-34	44%	Ppha_1431	<i>Pelodictyon phaeoclathratiforme</i> strain DSM 5477 / BU-1
1.00E-33	47%	Clim_1496	<i>Chlorobium limicola</i> strain DSM 245 / NBRC 103803
1.00E-33	41%	Clim_1497	<i>Chlorobium limicola</i> strain DSM 245 / NBRC 103803
4.00E-33	47%	Cpar_0715	<i>Chlorobaculum parvum</i> strain NCIB 8327
8.00E-33	40%	Cpha266_1359	<i>Chlorobium phaeobacteroides</i> strain DSM 266
3.00E-32	42%	Cvib_1062	<i>Prosthecochloris vibrioformis</i> strain DSM 265
5.00E-30	48%	CferDRAFT_0174	<i>Chlorobium ferrooxidans</i> DSM 13031
4.00E-28	39%	Plut_0782	<i>Pelodictyon luteolum</i> strain DSM 273
1.00E-26	37%	GM18_3380	<i>Geobacter sp.</i> strain M18
4.00E-25	37%	Ppha_0232	<i>Pelodictyon phaeoclathratiforme</i> strain DSM 5477 / BU-1
5.00E-25	33%	Paes_1442	<i>Prosthecochloris aestuarii</i> strain DSM 271 / SK 413

Table 4.13 continued.

E-value	%ID	Locus Tag	Organism
7.00E-25	37%	GM21_0953	<i>Geobacter sp.</i> strain M21
9.00E-25	46%	CferDRAFT_0912	<i>Chlorobium ferrooxidans</i> DSM 13031
2.00E-24	36%	Cpham1_1042	<i>Chlorobium phaeobacteroides</i> strain BS1
1.00E-23	34%	Gbem_3294	<i>Geobacter bemidjiensis</i> strain Bem / ATCC BAA-1014 / DSM 16622
7.00E-22	38%	Cag_1040	<i>Chlorobium chlorochromatii</i> strain CaD3
1.00E-21	31%	Cag_1035	<i>Chlorobium chlorochromatii</i> strain CaD3
2.00E-21	31%	Glov_3620	<i>Geobacter lovleyi</i> strain ATCC BAA-1151 / DSM 17278 / SZ
2.00E-20	31%	Geob_3281	<i>Geobacter daltonii</i> strain DSM 22248 / JCM 15807 / FRC-32
2.00E-19	30%	Gura_2496	<i>Geobacter uraniireducens</i> strain Rf4
8.00E-19	45%	Cag_1038	<i>Chlorobium chlorochromatii</i> strain CaD3
8.00E-19	39%	CferDRAFT_0301	<i>Chlorobium ferrooxidans</i> DSM 13031
2.00E-18	36%	Gura_0384	<i>Geobacter uraniireducens</i> strain Rf4
6.00E-18	34%	GSU1247	<i>Geobacter sulfurreducens</i> strain ATCC 51573 / DSM 12127 / PCA
6.00E-18	34%	KN400_1221	<i>Geobacter sulfurreducens</i> strain DL-1 / KN400
1.00E-17	38%	GeomeDRAFT_2756	<i>Geobacter metallireducens</i> RCH3
1.00E-17	38%	Gmet_0131	<i>Geobacter metallireducens</i> strain GS-15 / ATCC 53774 / DSM 7210
2.00E-17	36%	Gbem_1180	<i>Geobacter bemidjiensis</i> strain Bem / ATCC BAA-1014 / DSM 16622
1.00E-16	33%	GM21_3095	<i>Geobacter sp.</i> strain M21
2.00E-16	34%	Ppro_2263	<i>Pelobacter propionicus</i> strain DSM 2379
3.00E-16	32%	Ppro_1752	<i>Pelobacter propionicus</i> strain DSM 2379
1.00E-15	30%	GeomeDRAFT_1961	<i>Geobacter metallireducens</i> RCH3
1.00E-15	30%	Gmet_1763	<i>Geobacter metallireducens</i> strain GS-15 / ATCC 53774 / DSM 7210
2.00E-15	37%	GM18_3260	<i>Geobacter sp.</i> strain M18
2.00E-11	34%	Geob_1880	<i>Geobacter daltonii</i> strain DSM 22248 / JCM 15807 / FRC-32
4.00E-11	47%	BV97_04864	<i>Novosphingobium resinovorum</i>

Table 4.13 continued.

E-value	%ID	Locus Tag	Organism
4.00E-11	47%	BV98_04864	<i>Sphingobium herbicidovorans</i> NBRC 16415
4.00E-11	47%	LH128_23776	<i>Sphingomonas</i> sp. LH128
2.00E-10	40%	GM18_4328	<i>Geobacter</i> sp. strain M18

4.5 Concluding Remarks

The proteins responsible for oxidizing sulfide to disulfides/polysulfides (Chan et al. 2008; Eddie & Hanson, 2013; Shuman & Hanson 2016), and, subsequently, for oxidizing intracellular, soluble forms of zero-valent sulfur to sulfite and sulfate (Holkenbrink et al. 2011, Rodriguez et al. 2011) are reasonably well established for *C. tepidum* and other *Chlorobiaceae*. However the mechanism(s) by which polysulfides and insoluble sulfur are packaged into extracellular S⁰ globules, how S⁰ is degraded, and how sulfur compounds are imported back into the cell for oxidation have remained elusive.

The microscopic and proteomic work presented here suggest the possibility that *C. tepidum* packages S⁰ into membrane like-vesicles: S⁰ appears to ‘bleb’ out from the *C. tepidum* cell surface and S⁰ produced by *C. tepidum* is stained by a styryl dye specific to cell membranes; the proteins that associate with S⁰ appear to constitute a subset of the *C. tepidum* proteome and require the presence of detergents for their dissociation; the protein profile of S⁰ shares striking similarities with the protein profiles of outer membrane vesicles from gram-negative bacteria. The specific proteins which were identified in a shotgun proteomic study of S⁰ included spatially-regulated proteins and proteins involved in connectivity between the outer and inner membranes, suggesting that S⁰ may bud out from dedicated, locally-energized regions on the *C. tepidum* surface. These results motivate studies to probe the precise involvement of these different protein components in S⁰ formation, as well as the specific effects of ATP availability and membrane potential on S⁰ formation. Furthermore, the identification of periplasmic proteins involved in the cell envelope stress response could indicate a mechanism of S⁰ packaging into vesicle-like particles

as a response to the periplasmic accumulation of insoluble zero-valent sulfur intermediates, another mechanism that would be interesting to explore. Finally, a number of uncharacterized proteins found in association with S^0 provide targets for future deletion mutant studies to evaluate their role in the context of S^0 production and degradation.

Thus a conclusion from this work is that the mechanisms of S^0 production and degradation in *C. tepidum* may be more complex than previously anticipated. The possibility that S^0 is packaged into membrane vesicle-like particles in an ATP- and proton motive force-dependent manner means that the other proteins detected in association with S^0 could play specific roles facilitating the recognition of and docking to S^0 by *C. tepidum* during degradation. While candidates for this type of role were not discussed here in the interest of space and time, a number of proteins similar to outer surface antigens of pathogenic bacteria as well as components of signal transduction systems were identified, and probing the role of these proteins as the subjects of future studies will be critical. A requirement for specialized recognition sites to utilize S^0 would certainly complicate the use of waste elemental sulfur as an energy or electron source for the production of a useful compound *via* a microbially-catalyzed process. However, based on the range of morphologies of elemental sulfur that are observed as produced and degraded by wild type *C. tepidum* it is possible that there are simultaneous complementary pathways, and developing a more detailed understanding of these processes is required for the long-term success of biotechnology-based and synthetic biology approaches to solving sulfur-associated issues in industry.

REFERENCES

- Altindis, E., Fu, Y. & Mekalanos, J.J., 2014. Proteomic analysis of *Vibrio cholerae* outer membrane vesicles. *Proceedings of the National Academy of Sciences of the United States of America*, 111(15), pp.E1548-E1556. doi: 10.1073/pnas.1403683111.
- Bagos, P.G. et al., 2010. Combined prediction of Tat and Sec signal peptides with hidden Markov models. *Bioinformatics*, 26(22), pp.2811–2817.
- Bai, J. et al., 2014. Identification and characterization of outer membrane vesicle-associated proteins in *Salmonella enterica* Serovar Typhimurium. *Infection and Immunity*, 82(10), pp.4001–4010.
- Ballok, A. E. et al., 2014. Epoxide-Mediated Differential Packaging of Cif and Other Virulence Factors into Outer Membrane Vesicles. *Journal of Bacteriology*, 196(20), pp.3633–3642.
- Barák, I. & Muchová, K., 2013. The role of lipid domains in bacterial cell processes. *International Journal of Molecular Sciences*, 14(2), pp.4050–4065.
- Beall, B. & Lutkenhaus, J., 1992. Impaired cell division and sporulation of a *Bacillus subtilis* strain with the *ftsA* gene deleted. *Journal of Bacteriology*, 174(7), pp.2398–2403.
- Bendezú, F.O. & De Boer, P.A.J., 2008. Conditional lethality, division defects, membrane involution, and endocytosis in *mre* and *mrd* shape mutants of *Escherichia coli*. *Journal of Bacteriology*, 190(5), pp.1792–1811.
- Bernadac, A. et al., 1998. *Escherichia coli* *tol-pal* mutants form outer membrane vesicles. *Journal of Bacteriology*, 180(18), pp.4872–4878.
- Berven, F.S. et al., 2006. Analysing the outer membrane subproteome of *Methylococcus capsulatus* (Bath) using proteomics and novel biocomputing tools. *Archives of Microbiology*, 184(6), pp.362–377.
- Berven, F.S. et al., 2004. BOMP: A program to predict integral β -barrel outer membrane proteins encoded within genomes of Gram-negative bacteria. *Nucleic Acids Research*, 32(suppl_2.), pp.W394-399. doi:10.1093/nar/gkh351.

- Bonnington, K.E. & Kuehn, M.J., 2014. Protein selection and export via outer membrane vesicles. *Biochimica et Biophysica Acta - Molecular Cell Research*, 1843(8), pp.1612–1619.
- Brune, D.C., 1995. Isolation and characterization of sulfur globule proteins from *Chromatium vinosum* and *Thiocapsa roseopersicina*. *Archives of Microbiology*, 163(6), pp.391–399.
- Bukau, B. & Walker, G.C., 1989. Cellular defects caused by deletion of the *Escherichia coli dnaK* gene indicate roles for heat shock protein in normal metabolism. *Journal of Bacteriology*, 171(5), pp.2337–2346.
- Cascales, E., Lloubès, R. & Sturgis, J.N., 2001. The TolQ-TolR proteins energize TolA and share homologies with the flagellar motor proteins MotA-MotB. *Molecular Microbiology*, 42(3), pp.795–807.
- Chan, L.-K. et al., 2008. A genomic region required for phototrophic thiosulfate oxidation in the green sulfur bacterium *Chlorobium tepidum* (syn. *Chlorobaculum tepidum*). *Microbiology*, 154(3), pp.818–829.
- Chan, L.-K., Morgan-Kiss, R.M. & Hanson, T.E., 2009. Functional analysis of three sulfide:quinone oxidoreductase homologs in *Chlorobaculum tepidum*. *Journal of Bacteriology*, 191(3), pp.1026–1034.
- Choi, D.-S. et al., 2011. Proteomic analysis of outer membrane vesicles derived from *Pseudomonas aeruginosa*. *Proteomics*, 11(16), pp.3424–3429.
- Costello, S.M. et al., 2016. Dynamic periplasmic chaperone reservoir facilitates biogenesis of outer membrane proteins. *Proceedings of the National Academy of Sciences of the United States of America*, 113(33), pp.E4794–E4800. doi:10.1073/pnas.1601002113.
- Couto, N. et al., 2015. Proteome profiles of outer membrane vesicles and extracellular matrix of *Pseudomonas aeruginosa* biofilms. *Journal of Proteome Research*, 14(10), pp.4207–4222.
- Deatherage, B.L. et al., 2009. Biogenesis of bacterial membrane vesicles. *Molecular Microbiology*, 72(6), pp.1395–1407.
- Donà, C., 2011. *Mobilization of sulfur by green sulfur bacteria – Physiological and molecular studies on Chlorobaculum parvum DSM 263*. Doctoral Dissertation, University of Bremen, Germany.

- Du, D. et al., 2014. Structure of the AcrAB-TolC multidrug efflux pump. *Nature*, 509(7501), pp.512–515.
- Eddie, B.J. & Hanson, T.E., 2013. *Chlorobaculum tepidum* TLS displays a complex transcriptional response to sulfide addition. *Journal of Bacteriology*, 195(2), pp.399–408.
- Fenton, A.K. & Gerdes, K., 2013. Direct interaction of FtsZ and MreB is required for septum synthesis and cell division in *Escherichia coli*. *The EMBO Journal*, 32(13), pp.1953–1965.
- Frias, A. et al., 2010. Membrane vesicles: a common reature in the extracellular matter of cold-adapted antarctic bacteria. *Microbial Ecology*, 59(3), pp.476–486.
- Frigaard, N.-U. et al., 2003. *Chlorobium tepidum*: Insights into the structure, physiology, and metabolism of a green sulfur bacterium derived from the complete genome sequence. *Photosynthesis Research*, 78(2), pp.93–117.
- Frigaard, N.-U. & Dahl, C., 2009. Sulfur metabolism in phototrophic sulfur bacteria. In R. K. Poole, ed. *Advances in Microbial Physiology*. Burlington, MA: Academic Press, pp. 103–200.
- Fujiwara, K. & Taguchi, H., 2007. Filamentous morphology in GroE-depleted *Escherichia coli* induced by impaired folding of FtsE. *Journal of Bacteriology*, 189(16), pp.5860–5866.
- Galka, F. et al., 2008. Proteomic Characterization of the whole secretome of *Legionella pneumophila* and functional analysis of outer membrane vesicles. *Infection and Immunity*, 76(5), pp.1825–1836.
- Gerding, M.A. et al., 2007. The trans-envelope Tol-Pal complex is part of the cell division machinery and required for proper outer-membrane invagination during cell constriction in *E. coli*. *Molecular Microbiology*, 63(4), pp.1008–1025.
- Gregersen, L.H., Bryant, D.A. & Frigaard, N.-U., 2011. Mechanisms and evolution of oxidative sulfur metabolism in green sulfur bacteria. *Frontiers in Microbiology*, 2(May), 116. doi:10.3389/fmicb.2011.00116.
- Hanson, T.E. et al., 2016. *Chlorobaculum tepidum* growth on biogenic S(0) as the sole photosynthetic electron donor. *Environmental Microbiology*, 18(9), pp.2856–2867.

- Hanson, T.E. & Tabita, F.R., 2001. A ribulose-1,5-biophosphate carboxylase/oxygenase (RubisCO)-like protein from *Chlorobium tepidum* that is involved with sulfur metabolism and the response to oxidative stress. *Proceedings of the National Academy of Sciences of the United States of America*, 98(8), pp.4397–4402.
- Hanson, T.E. & Tabita, F.R., 2003. Insights into the stress response and sulfur metabolism revealed by proteome analysis of a *Chlorobium tepidum* mutant lacking the Rubisco-like protein. *Photosynthesis Research*, 78(3), pp.231–248.
- Hayduk, E.J., Choe, L.H. & Lee, K.H., 2004. A two-dimensional electrophoresis map of Chinese hamster ovary cell proteins based on fluorescence staining. *Electrophoresis*, 25(15), pp.2545–2556.
- Holkenbrink, C. et al., 2011. Sulfur globule oxidation in green sulfur bacteria is dependent on the dissimilatory sulfite reductase system. *Microbiology*, 157, pp.1229–1239.
- Jang, K.-S. et al., 2014. Comprehensive proteomic profiling of outer membrane vesicles from *Campylobacter jejuni*. *Journal of Proteomics*, 98, pp.90–98.
- Janssen, A.J.H., de Keizer, A. & Lettinga, G., 1994. Colloidal properties of a microbiologically produced sulphur suspension in comparison to a LaMer sulphur sol. *Colloids and Surfaces B: Biointerfaces*, 3, pp.111–117.
- Käll, L., Krogh, A. & Sonnhammer, E.L.L., 2004. A combined transmembrane topology and signal peptide prediction method. *Journal of Molecular Biology*, 338(5), pp.1027–1036.
- Kleinjan, W.E., de Keizer, A. & Janssen, A.J.H., 2003. Biologically produced sulfur. In R. Steudel, ed. *Elemental Sulfur and Sulfur-Rich Compounds I*. Topics in Current Chemistry. New York, NY: Springer-Verlag, pp. 167–188.
- Koronakis, V., Eswaran, J. & Hughes, C., 2004. Structure and function of TolC: the bacterial exit duct for proteins and drugs. *Annual Review of Biochemistry*, 73(1), pp.467–489.
- Kulp, A. & Kuehn, M.J., 2010. Biological functions and biogenesis of secreted bacterial outer membrane vesicles. *Annual Review of Microbiology*, 64, pp.163–184.
- Lappann, M. et al., 2013. Comparative proteome analysis of spontaneous outer membrane vesicles and purified outer membranes of *Neisseria meningitidis*. *Journal of Bacteriology*, 195(19), pp.4425–4435.

- Lasocki, K. et al., 2007. Deletion of the *parA* (*soj*) homologue in *Pseudomonas aeruginosa* causes ParB instability and affects growth rate, chromosome segregation, and motility. *Journal of Bacteriology*, 189(15), pp.5762–5772.
- Lau, C.K.Y. et al., 2013. Solution structure of *Escherichia coli* FeoA and its potential role in bacterial ferrous iron transport. *Journal of Bacteriology*, 195(1), pp.46–55.
- Lau, C.K.Y., Krewulak, K.D. & Vogel, H.J., 2016. Bacterial ferrous iron transport: The Feo system. *FEMS Microbiology Reviews*, 40(2), pp.273–298.
- Lazzaroni, J.-C. et al., 1999. The Tol proteins of *Escherichia coli* and their involvement in the uptake of biomolecules and outer membrane stability. *FEMS Microbiology Letters*, 177(2), pp.191–197.
- Lee, E.-Y. et al., 2007. Global proteomic profiling of native outer membrane vesicles derived from *Escherichia coli*. *Proteomics*, 7(17), pp.3143–3153.
- Lee, E.-Y. et al., 2008. Proteomics in gram-negative bacterial outer membrane vesicles. *Mass Spectrometry Reviews*, 27, pp.535–555.
- Levy, A.T., Lee, K.H. & Hanson, T.E., 2016. *Chlorobaculum tepidum* modulates amino acid composition in response to energy availability, as revealed by a systematic exploration of the energy landscape of phototrophic sulfur oxidation. *Applied and Environmental Microbiology*, 82(21), pp.6431–6439.
- Levy, N.E. et al., 2014. Identification and characterization of host cell protein product-associated impurities in monoclonal antibody bioprocessing. *Biotechnology and Bioengineering*, 111(5), pp.904–912.
- Lloubès, R. et al., 2001. The Tol-Pal proteins of the *Escherichia coli* cell envelope: An energized system required for outer membrane integrity? *Research in Microbiology*, 152(6), pp.523–529.
- Lopez, V. et al., 2016. Bacterial Hsp70 (DnaK) and mammalian Hsp70 interact differently with lipid membranes. *Cell Stress and Chaperones*, 21(4), pp.609–616.
- Lutkenhaus, J., Pichoff, S. & Du, S., 2012. Bacterial cytokinesis: From Z ring to divisome. *Cytoskeleton*, 69(10), pp.778–790.
- Lyu, Z.X. & Zhao, X.S., 2015. Periplasmic quality control in biogenesis of outer membrane proteins. *Biochemical Society Transactions*, 43(2), pp.133–138.

- Ma, D. et al., 1995. Genes *acrA* and *acrB* encode a stress-induced efflux system of *Escherichia coli*. *Molecular Microbiology*, 16(1), pp.45–55.
- Marnocha, C.L. et al., 2016. Mechanisms of extracellular S⁰ globule production and degradation in *Chlorobaculum tepidum* via dynamic cell–globule interactions. *Microbiology*, 162(7), pp.1125–1134.
- McBroom, A.J. et al., 2006. Outer membrane vesicle production by *Escherichia coli* is independent of membrane instability. *Journal of Bacteriology*, 188(15), pp.5385–5392.
- McBroom, A.J. & Kuehn, M.J., 2007. Release of outer membrane vesicles by Gram-negative bacteria is a novel envelope stress response. *Molecular Microbiology*, 63(2), pp.545–558.
- McBroom Brooks, A.J., 2006. *Bacterial nanoparticles: genetic, biochemical, and functional characterization of outer membrane vesicle production by gram-negative bacteria*. Doctoral Dissertation, Duke University, United States of America.
- Min, L., Choe, L.H. & Lee, K.H., 2015. Improved protease digestion conditions for membrane protein detection. *Electrophoresis*, 36(15), pp.1690–1698.
- Morona, R. & Reeves, P., 1982. The *tolC* locus of *Escherichia coli* affects the expression of three major outer membrane proteins. *Journal of Bacteriology*, 150(3), pp.1016–1023.
- Nevin, K.P. & Lovley, D.R., 2000. Lack of production of electron-shuttling compounds or solubilization of Fe(III) during reduction of insoluble Fe(III) oxide by *Geobacter metallireducens*. *Applied and Environmental Microbiology*, 66(5), pp.2248–2251.
- Nicolson, G.L. & Schmidt, G.L., 1971. Structure of the *Chromatium* sulfur particle and its protein membrane. *Journal of Bacteriology*, 105(3), pp.1142–1148.
- Ogino, H. et al., 2004. FtsZ-dependent localization of GroEL protein at possible division sites. *Genes to Cells*, 9(9), pp.765–771.
- Petersen, T.N. et al., 2011. SignalP 4.0: discriminating signal peptides from transmembrane regions. *Nature Methods*, 8(10), pp.785–786.
- Post, D.M.B. et al., 2005. Biochemical and functional characterization of membrane blebs purified from *Neisseria meningitidis* serogroup B. *Journal of Biological Chemistry*, 280(46), pp.38383–38394.

- Reguera, G. et al., 2005. Extracellular electron transfer *via* microbial nanowires. *Nature*, 435(7045), pp.1098–1101.
- Rodriguez, J., Hiras, J. & Hanson, T.E., 2011. Sulfite oxidation in *Chlorobaculum tepidum*. *Frontiers in Microbiology*, 2(May), 112. doi: 10.3389/fmicb.2011.00112.
- Roier, S. et al., 2016. A novel mechanism for the biogenesis of outer membrane vesicles in Gram-negative bacteria. *Nature Communications*, 7, 10515. doi:10.1038/ncomms10515.
- Schwechheimer, C. & Kuehn, M.J., 2015. Outer-membrane vesicles from Gram-negative bacteria: biogenesis and functions. *Nature Reviews Microbiology*, 13(10), pp.605–619.
- Schwechheimer, C., Sullivan, C.J. & Kuehn, M.J., 2013. Envelope control of outer membrane vesicle production in Gram-negative bacteria. *Biochemistry*, 52(18), pp.3031–3040.
- Seeger, M.A. et al., 2006. Structural asymmetry of AcrB trimer suggests a peristaltic pump mechanism. *Science*, 313(5791), pp.1295–1298.
- Shaevitz, J.W. & Gitai, Z., 2010. The structure and function of bacterial actin homologs. *Cold Spring Harbor Perspectives in Biology*, 2(9), a000364. doi:10.1038/ncomms10515.
- Shuman, K.E. & Hanson, T.E., 2016. A sulfide:quinone oxidoreductase from *Chlorobaculum tepidum* displays unusual kinetic properties. *FEMS Microbiology Letters*, 363(12), fnw100. doi:10.1093/femsle/fnw100.
- Siefert, E. & Pfennig, N., 1984. Convenient method to prepare neutral sulfide solution for cultivation of phototrophic sulfur bacteria. *Archives of Microbiology*, 139(1), pp.100–101.
- Sklar, J.G. et al., 2007. Defining the roles of the periplasmic chaperones SurA, Skp, and DegP in *Escherichia coli*. *Genes and Development*, 21(19), pp.2473–2484.
- Stevenson, B., Wyckoff, E.E. & Payne, S.M., 2016. *Vibrio cholerae* FeoA, FeoB, and FeoC interact to form a complex. *Journal of Bacteriology*, 198(7), pp.1160–1170.
- Strahl, H., Bürmann, F. & Hamoen, L.W., 2014. The actin homologue MreB organizes the bacterial cell membrane. *Nature Communications*, 5, 3442. doi:10.1038/ncomms4442.

- Strahl, H. & Hamoen, L.W., 2010. Membrane potential is important for bacterial cell division. *Proceedings of the National Academy of Sciences of the United States of America*, 107(27), pp.12281-12286.
- Strauch, K.L., Johnson, K. & Beckwith, J., 1989. Characterization of *degP*, a gene required for proteolysis in the cell envelope and essential for growth of *Escherichia coli* at high temperature. *Journal of Bacteriology*, 171(5), pp.2689–2696.
- Strohl, W.R., Geffers, I. & Larkin, J.M., 1981. Structure of the sulfur inclusion envelopes from four *Beggiatoas*. *Current Microbiology*, 6(2), pp.75–79.
- Tashiro, Y. et al., 2009. Outer membrane machinery and alginate synthesis regulators control membrane vesicle production in *Pseudomonas aeruginosa*. *Journal of Bacteriology*, 191(24), pp.7509–7519.
- Volokhina, E.B. et al., 2011. Role of the periplasmic chaperones Skp, SurA, and DegQ in outer membrane protein biogenesis in *Neisseria meningitidis*. *Journal of Bacteriology*, 193(7), pp.1612–1621.
- Wahlund, T.M. et al., 1991. A thermophilic green sulfur bacterium from New Zealand hot springs, *Chlorobium tepidum* sp. nov. *Archives of Microbiology*, 156, pp.81–90.
- Walburger, A., Lazdunski, C. & Corda, Y., 2002. The Tol/Pal system function requires an interaction between the C-terminal domain of TolA and the N-terminal domain of TolB. *Molecular Microbiology*, 44(3), pp.695–708.
- Ward, J.J. et al., 2004. Prediction and functional analysis of native disorder in proteins from the three kingdoms of life. *Journal of Molecular Biology*, 337(3), pp.635–645.
- Weaver, E.A. et al., 2013. FeoA and FeoC are essential components of the *Vibrio cholerae* ferrous iron uptake system, and FeoC interacts with FeoB. *Journal of Bacteriology*, 195(21), pp.4826–4835.
- Whitworth, D.E., Slade, S.E. & Mironas, A., 2015. Composition of distinct sub-proteomes in *Myxococcus xanthus*: metabolic cost and amino acid availability. *Amino Acids*, 47(12), pp.2521–2531.
- Yu, N.Y. et al., 2010. PSORTb 3.0: Improved protein subcellular localization prediction with refined localization subcategories and predictive capabilities for all prokaryotes. *Bioinformatics*, 26(13), pp.1608–1615.

Zhang, N. & Li, L., 2004. Effects of common surfactants on protein digestion and matrix-assisted laser desorption/ionization mass spectrometric analysis of the digested peptides using two-layer sample preparation. *Rapid Communications in Mass Spectrometry*, 18(8), pp.889–896.

Chapter 5

CONCLUSIONS AND RECOMMENDATIONS FOR FUTURE WORK

5.1 Conclusions

Towards enabling biotechnological approaches to using waste sulfur, this work aimed to gain improved understanding of S^0 production and degradation processes in *Chlorobaculum tepidum*. To attain reproducible growth across a range of S^0 -producing and S^0 -degrading conditions, a rotisserie culturing system was implemented. In addition to enabling reproducible growth, this system also facilitated study of *C. tepidum* across a 3×3 factorial space of different electron donors (sulfide, S^0 , thiosulfate), light flux levels (5, 20, and $35 \mu\text{mol m}^{-2} \text{s}^{-1}$), and culture duration (10, 18, 26 hours), termed the ‘energy landscape’ of sulfur oxidation. This experimental approach facilitated simultaneous examination of multiple factors and revealed subtle and interacting-factor effects, effects which would have remained undetected in traditional single-factor design experiments.

Specifically these studies revealed the unexpected observation that the bulk amino acid composition of *C. tepidum* is biased towards less energetically expensive amino acids under energy-limited, low light flux conditions. While not directly related to mechanisms of S^0 production and degradation, this finding suggests that proteins with increased expression under energy-limiting conditions may have biased compositions to minimize the energy burden of protein synthesis. While biased amino acid compositions for highly expressed proteins and secreted proteins has been previously deduced by bioinformatics approaches (Akashi & Gojobori 2002; Smith &

Chapman 2010), this result provided a ‘real-time’ experimental observation of a similar phenomenon. This finding has implications for improved design of engineered proteins, and provides a proof-of-concept demonstration of the utility of bulk biomass amino acid composition measurements for identifying energy stress or adaptations.

The factorial experimental approach also enabled analysis of *C. tepidum* growth yields across the energy landscape, where per-electron growth yields on S^0 were less than those for sulfide and greater than those for thiosulfate. Quantitatively analyzing these observed growth yields in the context of electron transport pathways in *C. tepidum* suggested that the four electron transfer involved in the oxidation of S^0 to sulfite may not provide net energy conservation *via* reduction of the quinone pool. Across much of the energy landscape (including late-phase cultures grown on sulfide and S^0 and early-phase cultures grown on thiosulfate), ‘excess’ sulfur was recovered in oxidized products relative to the sulfur present in the initially-provided electron donor, suggesting the preferential oxidation of intracellular stored sulfur compounds when thiosulfate was provided as electron donor or when exogenous electron donor became limiting. By contrast, a deficit in sulfur recovered in oxidized products under low-light, early phase oxidation of sulfide and S^0 suggested the presence of unaccounted-for intermediates. The identification of extracellular polysulfides during S^0 production and degradation, combined with observations of S^0 globules that grow and degrade independently of attachment to cells, implicated polysulfides as putative soluble agents of S^0 globule metabolism and led to a new model for S^0 formation and dissolution.

To obtain insight into the nature of the S^0 surface and its role in S^0 production and degradation, microscopic and proteomic studies were undertaken. Microscopy

showed S⁰ particles ‘blebbing’ out from the *C. tepidum* surface, and revealed that S⁰ stains with a membrane-specific dye. Proteomic studies identified a total of 101 proteins that associate with S⁰ and revealed that the S⁰ proteome shares characteristics with the proteomes of outer membrane vesicles. Together these observations suggested the possibility that *C. tepidum* packages S⁰ into membrane-like vesicles. In particular, the identification of periplasmic proteins involved in the σ^E envelope stress response in association with S⁰ suggested a model for S⁰ generation where accumulating insoluble elemental sulfur in the periplasm leads to its extrusion out of the cell in membrane- and protein-coated particles.

This work revealed that the mechanisms of S⁰ production and degradation by *C. tepidum* may not be as simple as originally anticipated, where some of the uncharacterized proteins associated with S⁰ could mediate cellular recognition of and/or attachment to S⁰. The possibility that S⁰ degradation may depend on specialized recognition sites would complicate the use of waste elemental sulfur as a substrate for microbes in a biotechnological process. Further work is required to improve our understanding of the specific roles of S⁰-associated proteins in S⁰ production and utilization, knowledge which will help facilitate biotechnology-based approaches to industrial sulfur management. The work presented here forms a basis for both comprehensive, systems-based analyses of *C. tepidum* as well as targeted studies to probe the functions of specific proteins. Additional exploration of the mechanisms of S⁰ production and degradation in *C. tepidum* could also be useful in illuminating more general mechanisms of outer membrane vesicle formation, and could also provide insight into mechanisms of microbial attachment to solid surfaces useful for functionalizing surfaces for biocompatibility.

5.2 Recommendations for Future Work

5.2.1 Investigate biased amino acid composition as a mechanism for energy conservation under light- and energy-limited conditions.

As described in Chapter 2, a small but significant shift in the composition of *C. tepidum* towards less energetically expensive amino acids was detected at limiting light flux ($5 \mu\text{mol m}^{-2} \text{s}^{-1}$), an effect that appeared to be the result of coordinated changes across all amino acids. We suggested that if proteins with increased expression under low light possessed compositions that were biased toward these less energetically expensive amino acids, this effect could have produced the detectable shift in the bulk *C. tepidum* biomass. Thus, the next logical step is to establish whether this hypothesis is supported by experimental evidence.

First, quantitative shotgun proteomics could be used to identify proteins with altered expression as a function of light flux. As an initial experiment, *C. tepidum* cultures should be grown under single-electron donor oxidizing-conditions at a range of light levels (e.g. $5\text{-}35 \mu\text{mol photons m}^{-2} \text{s}^{-1}$) to a protein concentration of $\sim 50 \mu\text{g/ml}$. This protein concentration will ensure that sufficient doublings occur to allow the cells to adjust their proteome composition to the new conditions (~ 3.5 doublings), but will mitigate artifacts associated with light attenuation as culture density increases. Use of thiosulfate as electron donor is recommended to ensure that a single mode of electron donor oxidation is maintained for all cultures. Relative protein abundance among the different conditions can be compared by a multiplexed quantitative shotgun proteomic approach, such as the iTRAQ protocol (Aggarwal et al. 2006; Valente et al. 2015). Once proteins with significant differences in protein abundance according to light flux are identified, multivariate analysis of variance should be employed to determine

whether differentially expressed proteins exhibit compositional biases in terms of amino acid energy costs.

By extension, it is also expected that conserved protein homologs should have biased amino acid compositions across bacterial species according to the energy flux to which different bacteria are evolutionarily adapted. For example, a logical hypothesis is that a bacterium adapted to an oligotrophic, low energy flux environment would tend to have versions of conserved proteins that encode less expensive amino acids than the homologous counterparts in a bacterium adapted to a high energy flux environment. To investigate this possibility, conserved protein homologs across diverse bacterial species should first be identified and bacterial species should be classified by the energy flux to which they are adapted. Care should be taken to compare proteins that are both highly abundant and also less abundant, as highly expressed proteins are already known to possess compositions biased toward less expensive amino acids (Akashi & Gojobori 2002). Next, the amino acid compositions should be determined, and multivariate statistical analyses used to determine whether the energy flux associated with different ecological niches is predictive of compositional biases.

5.2.2 Identify constituents of intracellular sulfur pools and their dynamics

C. tepidum was observed to possess an internal pool of reduced sulfur compounds that appears to be oxidized under electron-donor limiting conditions. In Chapter 2 (Fig. 2.4), the presence of an intracellular pool of reductant was implied for early-phase batch cultures oxidizing sulfide and S^0 , but not thiosulfate. Inversely, sulfur in excess of that originally provided to thiosulfate-grown cultures was recovered early in the culture phase (Fig. 3.4-B), while recovery of excess sulfur did not appear

in sulfide- and S^0 -grown cultures until late in the culture. These observations suggest that the internal reductant pools could have been reduced sulfur compounds that were rapidly oxidized in thiosulfate-grown cultures, leading to the initial ‘excess’ of sulfur observed, and that these pools were maintained in sulfide- and S^0 -grown cultures until depletion of electron donor. Identifying pool constituents and quantifying their dynamics will provide insight into (1) the strategies of *C. tepidum* for balancing rates of reaction center oxidation with photosynthetic electron transport and (2) pathways for sulfur oxidation based on observed accumulation and depletion of different intracellular intermediates. Towards this second aim, performing studies at limiting light flux will likely increase the accumulation of certain intermediates, providing insight into which steps of sulfur oxidation pathways are rate-limiting. The method of Rethmeier (1997) should be used as a first pass, which will provide good quantitation of sulfide, thiosulfate and sulfite in internal pools (Rodriguez et al. 2011; Hiras 2012). If polysulfides are found to be components of the pools, the methyl triflate method reported by Kamyshny et al. (2009) would be appropriate for quantifying polysulfides well as for polythionates, but would need to be adapted for intracellular measurements.

5.2.3 Protein expression differences between S^0 -attached and S^0 -unattached cells during S^0 production and degradation

During S^0 production and generation, cells are observed to grow independently of their attachment to S^0 , and only a small population of the cells appear attached to S^0 . One possibility suggested by these observations is that attached and unattached cells are performing different roles in S^0 production and degradation. To provide insight into whether unattached and attached cells are performing different metabolic

tasks, iTRAQ-based quantitative proteomics should be used to compare protein expression of attached and unattached cells under S^0 -producing (sulfide oxidizing) and S^0 -degrading conditions. Cultures growing on sulfide as sole electron donor should be harvested prior to sulfide depletion, and parallel cultures should be harvested within one doubling of the transition to S^0 degradation to minimize interfering effects due to light limitation induced by self-shading. From these cultures, fractions enriched in attached and unattached cells should be prepared using sucrose density centrifugation as previously reported (Hanson et al. 2016). An initial study should examine differential protein expression in whole-cell lysate. If the initial study demonstrates a substantial number of proteins differentially expressed between attached and unattached cells, a second proteomics experiment on protein fractions enriched for membrane proteins could be conducted to focus on identifying proteins that may mediate interactions with S^0 . In addition, shotgun proteomic profiling of proteins extracted from purified S^0 obtained from both the S^0 -production and S^0 -degradation stage could be included as part of this study qualitatively compare the protein profile of freshly produced and partially-degraded S^0 .

5.2.4 Probing the roles of S^0 -associated proteins in S^0 production, degradation, and cell- S^0 attachment by mutagenesis studies

A number of proteins identified in association with S^0 in Chapter 4 are worth further study by mutagenesis studies. For uncharacterized proteins with unknown functions, construction of deletion mutants is a logical start. Methods for deletion by homologous recombination (Burns & DiChristina 2009; Gibson et al. 2009; Azai et al. 2013) have been successfully used in the Hanson lab. High-priority genes for deletion mutagenesis studies are listed in Table 5.1.

Table 5.1 List of high-priority S⁰-associated proteins for characterization by mutagenesis studies.

Gene locus	Gene product	Deletion or fusion protein approach	Rationale
<i>CT0893</i>		deletion & fusion	uncharacterized outer membrane protein previously observed in secreted fraction of wildtype, periplasmic fraction in mutant deficient in S ⁰ oxidation (Hanson & Tabita 2003)
<i>CT1305</i>		deletion	uncharacterized outer membrane protein only observed in C3 S ⁰ ; highly conserved within <i>Chlorobi</i> , <i>Geobacter</i> (Hanson et al. 2016)
<i>CT1320.1</i>		deletion	uncharacterized outer membrane protein only observed in C3 S ⁰ ; highly conserved within <i>Chlorobi</i> , <i>Geobacter</i> (Hanson et al. 2016)
<i>CT1745</i>		deletion	initial protein in iron(II) transport operon with increased expression after sulfide spike (Eddie & Hanson 2013)
<i>CT1353</i>		deletion & fusion	outer membrane lipoprotein homolog of Pal
<i>CT2144</i>		deletion & fusion	uncharacterized protein with opacity protein domain
<i>CT0537</i>	MreB	fusion	putative role in localizing to site of S ⁰ production
<i>CT0530</i>	GroEL	fusion	putative role in localizing to site of S ⁰ production
<i>CT0643</i>	DnaK	fusion	putative role in S ⁰ coating
<i>CT0254</i>	OmpH	deletion & fusion	envelope stress response role in S ⁰ production
<i>CT1447</i>		deletion & fusion	DegP homolog; envelope stress response role in S ⁰ production
<i>CT2264</i>	SurA	fusion	envelope stress response role in S ⁰ production

A standard protocol for characterizing the phenotype of deletion mutants would be (1) construct mutant and verify genotype, (2) grow mutant each on sulfide, S⁰, and thiosulfate as sole electron donor with wildtype controls, (3) collect (at a minimum) protein, sulfide, S⁰, thiosulfate, and sulfate measurements and fix culture

samples for microscopy over at least three culture timepoints. These samples and measurements should be used to screen mutants for deficiencies in growth rate, growth yield, oxidation of sulfur compounds, discrepancies in sulfur mass balances, and differences in cell or S⁰ morphology or abundance relative to the wildtype. Based on the outcomes of these studies, interesting mutants can be pursued for further studies for better characterization of the phenotype.

Alternative approaches will be required to characterize the roles in S⁰ metabolism for proteins that are already associated with other critical cellular functions, such as MreB and GroEL, as deletion of these genes are likely to have wide-reaching effects on *C. tepidum* physiology outside of S⁰ metabolism. In these cases, an option is creating variants of native *C. tepidum* proteins that are fused with polypeptide tags to facilitate labeling with fluorophores (such as with SNAP-tag® technology; New England BioLab). This approach will enable visualization of protein localization during S⁰ production and degradation. Another benefit of SNAP-tag® technology is that many substrates are cell permeable, which would enable live-cell imaging. A list of protein candidates for study by this approach is listed in Table 5.1. The best approach would be to design a protein variant that will be knocked-in to the existing *C. tepidum* protein by homologous recombination, rather than expression from a plasmid, which could produce unintended effects. This approach could also be used for genes for which deletion mutagenesis is unsuccessful, such as in the case of essential genes.

An interesting extension of the live-cell imaging feature would be the labeling of tagged proteins growing on thiosulfate, and then observing the localization of the protein during S⁰ production after a sulfide spike. Transfer of a tagged membrane

protein variant would provide support for a vesicle-like mechanism for S^0 generation. Following the location of the tagged protein through depletion of sulfide could then provide insight into the fate of the S^0 coating through S^0 degradation. Logistically, this type of experiment could be performed by labeling a culture collecting the first visualization sample, spiking with sulfide, and then collecting periodic samples for visualization over defined lengths of time.

REFERENCES

- Aggarwal, K., Choe, L.H. & Lee, K.H., 2006. Shotgun proteomics using the iTRAQ isobaric tags. *Briefings in Functional Genomics and Proteomics*, 5(2), pp.112–120.
- Akashi, H. & Gojobori, T., 2002. Metabolic efficiency and amino acid composition in the proteomes of *Escherichia coli* and *Bacillus subtilis*. *Proceedings of the National Academy of Sciences of the United States of America*, 99(6), pp.3695–3700.
- Azai, C., Harada, J. & Oh-oka, H., 2013. Gene expression system in green sulfur bacteria by conjugative plasmid transfer. *PLoS ONE*, 8(11), e82345. doi:10.1371/journal.pone.0082345.
- Burns, J.L. & DiChristina, T.J., 2009. Anaerobic respiration of elemental sulfur and thiosulfate by *Shewanella oneidensis* MR-1 requires *psrA*, a homolog of the *phsA* gene of *Salmonella enterica* serovar typhimurium LT2. *Applied and Environmental Microbiology*, 75(16), pp.5209–5217.
- Eddie, B.J. & Hanson, T.E., 2013. *Chlorobaculum tepidum* TLS displays a complex transcriptional response to sulfide addition. *Journal of Bacteriology*, 195(2), pp.399–408.
- Gibson, D.G. et al., 2009. Enzymatic assembly of DNA molecules up to several hundred kilobases. *Nature Methods*, 6(5), pp.343–345.
- Hanson, T.E. et al., 2016. *Chlorobaculum tepidum* growth on biogenic S(0) as the sole photosynthetic electron donor. *Environmental Microbiology*, 18(9), pp.2856–2867.
- Hanson, T.E. & Tabita, F.R., 2003. Insights into the stress response and sulfur metabolism revealed by proteome analysis of a *Chlorobium tepidum* mutant lacking the Rubisco-like protein. *Photosynthesis Research*, 78(3), pp.231–248.
- Hiras, J., 2012. *Characterization of a novel redox active thiol from Chlorobaculum tepidum*. Doctoral Dissertation, University of Delaware, United States of America.

- Kamyshny, A., Borkenstein, C.G. & Ferdelman, T.G., 2009. Protocol for quantitative detection of elemental sulfur and polysulfide zero-valent sulfur distribution in natural aquatic samples. *Geostandards and Geoanalytical Research*, 33(3), pp.415–435.
- Rethmeier, J. et al., 1997. Detection of traces of oxidized and reduced sulfur compounds in small samples by combination of different high-performance liquid chromatography methods. *Journal of Chromatography A*, 760(2), pp.295–302.
- Rodriguez, J., Hiras, J. & Hanson, T.E., 2011. Sulfite oxidation in *Chlorobaculum tepidum*. *Frontiers in Microbiology*, 2(May), 112. doi: 10.3389/fmicb.2011.00112.
- Smith, D.R. & Chapman, M.R., 2010. Economical evolution: Microbes reduce the synthetic cost of extracellular proteins. *mBio*, 1(3), e00131-10-10. doi: 10.1128/mBio.00131-10.
- Valente, K.N., Lenhoff, A.M. & Lee, K.H., 2015. Expression of difficult-to-remove host cell protein impurities during extended Chinese hamster ovary cell culture and their impact on continuous bioprocessing. *Biotechnology and Bioengineering*, 112(6), pp.1232–1242.

Appendix A

REPRINT PERMISSIONS

Reprint permissions for Chapter 2

Publication: Levy, A.T., Lee, K.H., & Hanson, T.E., 2016. *Chlorobaculum tepidum* modulates amino acid composition in response to energy availability as revealed by a systematic exploration of the energy landscape of phototrophic sulfur oxidation. *Applied and Environmental Microbiology*, 82(21), p. 6431-6439.
doi:10.1128/AEM.02111-16.

Permission: Authors in ASM journals retain the right reuse the full article in his/her dissertation or thesis, according to the author rights at http://journals.asm.org/site/misc/ASM_Author_Statement.xhtml. See also Figure A.1.



RightsLink®

Home

Account
Info

Help



AMERICAN
SOCIETY FOR
MICROBIOLOGY

Title: Chlorobaculum tepidum
modulates amino acid
composition in response to
energy availability, as revealed by
a systematic exploration of the
energy landscape of phototrophic
sulfur oxidation

Logged in as:
Amalie Levy
Account #:
3001071156

LOGOUT

Author: Amalie T. Levy, Kelvin H. Lee,
Thomas E. Hanson et al.

Publication: Applied and Environmental
Microbiology

Publisher: American Society for Microbiology

Date: Aug 26, 2016

Copyright © 2016, American Society for Microbiology

Permissions Request

Authors in ASM journals retain the right to republish discrete portions of his/her article in any other publication (including print, CD-ROM, and other electronic formats) of which he or she is author or editor, provided that proper credit is given to the original ASM publication. ASM authors also retain the right to reuse the full article in his/her dissertation or thesis. For a full list of author rights, please see: http://journals.asm.org/site/misc/ASM_Author_Statement.xhtml

BACK

CLOSE WINDOW

Copyright © 2016 [Copyright Clearance Center, Inc.](#) All Rights Reserved. [Privacy statement.](#) [Terms and Conditions.](#)
Comments? We would like to hear from you. E-mail us at customercare@copyright.com

Figure A.1 Copyright information for Chapter 2

Reprint permissions for Chapter 3

Publication: Marnocha, C.L., Levy, A.T., Powell, D.H., Hanson, T.E., Chan, C.S., 2016. Mechanisms of extracellular S⁰ globule production and degradation in *Chlorobaculum tepidum* via dynamic cell-globule interactions. *Microbiology*, 162(7), p. 1125-1134. doi: 10.1099/mic.0.000294.

Permission: Copyright for this article, published by the Microbiology Society, belongs to the authors, which grants authors nonexclusive rights to reproduce the Article in whole or in part in any printed work of which they are the Author(s). See also Figure A.2-A through Figure A.2-C.

Licence to Publish: Standard version

PUBLICATION: (Choose from: Microbiology/Journal of Medical Microbiology/Journal of General Virology)

Microbiology

ARTICLE ID: MIC-D-15-00430

TITLE: Mechanisms of extracellular S(0) globule production and degradation in *Chlorobaculum tepidum* via dynamic cell-globule interactions

AUTHORS: Cassandra L. Marnocha; Deborah H. Powell; Amalie T. Levy; Thomas E. Hanson; Clara S. Chan

To allow your Article to be distributed as widely as possible in (the Publication), you grant the Microbiology Society (the Publisher) a licence in perpetuity to publish the above Article. The Article is deemed to include all material submitted for publication, including, but not limited to, abstract, text, figures, tables and supplementary material. The rights required to be granted by each different category of author(s) are as below. Please tick the first of these that applies and sign below.

- ☐ A. The Article is in the public domain. One or more of the authors are employees of the US Federal Government acting in the course of their employment, no copyright exists and the Contribution is in the public domain so no licence is required to be granted.
- ☐ B. Copyright belongs to the Employer(s). One or more of the authors are employees of the copyright holder (e.g. UK Crown, CSIRO, Canadian Government) acting in the course of their employment. A non exclusive Licence, as set out below is granted. All provisions of this document apply. The non exclusivity relates to the original submitted manuscript, video, films, images, photographs, diagrams and/or illustrative material only.
- ☒ C. Copyright belongs to the Author(s). One or more of the authors owns the copyright. An exclusive Licence, as set out below, is granted. All provisions of this document apply.

Please sign below as appropriate.

Signed for and on behalf of all the Author(s): Clara Chan

Print name: Clara Chan Date: 2/6/2016

If your Employer(s) (e.g. HMSO, CSIRO) claims copyright in this Article (option B above) then this form must also be signed by a person authorized to sign for and on behalf of your Employer(s), as confirmation that your Employer(s) accepts the terms and conditions of this licence

Signed for and on behalf of the Employer(s): _____

Print name: _____ Date: 2/6/2016

Figure A.2 Microbiology Society License to Publish, pg. 1

Indicate the exact text to be used for the article's copyright statement:

Declaration

1. The Author(s) warrants and represents that:
 - a) they are the sole Author(s) in the Article;
 - b) any Author who has signed this agreement for or on behalf of all other Authors has the full right, power and authority to enter into this agreement with the Publisher and that all Co-Authors have read and agreed the terms of this agreement;
 - c) the Article is not under consideration for publication elsewhere;
 - d) the material is original and has not been previously published elsewhere;
 - e) the material contains no violation of any existing duty of confidentiality, contract or intellectual property rights (including without limitation copyright, patent or trademark or other third-party right);
 - f) all of the institutions in which the work reported in the Article was carried out have authorized publication of the Article;
 - g) nothing in the article is obscene, defamatory, libellous or unlawful or in any way actionable;
 - h) all statements purporting to be facts contained in the Article are true and any formula or instruction contained in the Article will not, if followed accurately, cause any injury, illness or damage to the user;
 - i) if the Article includes excerpts from other copyright works, the Author(s) has obtained permission from the copyright holders of such material to enable the Author(s) to grant the rights contained herein and that such material has been appropriately acknowledged in the Article;
 - j) copies of all such permissions are attached to this licence and returned to the Publisher;
 - k) they will indemnify and keep indemnified the Publisher in respect of claims made against it by third parties for copyright infringement related to publication of the material, or any actions concerning the ownership of the material or rights to publish the material.
2. In consideration of the Publisher publishing the Article, the Author(s) hereby grants to the Publisher for the full term of copyright and extensions thereto an exclusive licence to:
 - a) publish, adapt, reproduce, distribute, display and store the Article for commercial purposes in all forms in all media whether now known or developed hereafter (including without limitation, print, digital and electronic) in all territories worldwide;
 - b) seek payment of fees from corporate bodies or individuals for the privilege of making copies of the Article from the conventional printed form or from articles stored electronically, e.g. by document delivery services or pay per view;
 - c) translate the Article into other languages, create electronic links to third-party material wherever it may be situated; create adaptations, abstracts, summaries or extracts, or other derivative works based on the Article and exercise all of the rights set out in 2(a) and 2(b) above in such translations, electronic links, abstracts, summaries and extracts, or other derivative works, and licence others to do any or all of the above;
 - d) re-licence article metadata without restriction (including but not limited to author name, title, abstract, citation, references and keywords).
3. Ownership of copyright remains with the Author(s) (or the Author(s)'s Employer if the Employer owns the copyright in the work) and provided that, when reproducing the Article or extracts from it, the provenance of the Publication is acknowledged in standard bibliographic citation form, the Author(s) retains the following nonexclusive rights:
 - a) to use the Article as long as it is not sold or given away in ways which would conflict directly with the Publisher's commercial interests;
 - b) to reproduce the Article in whole or in part in any printed work of which they are the Author(s);

Figure A.2 Microbiology Society License to Publish, pg. 2

c) to use the Article in whole or in part for the purposes of teaching at the academic organization at which they work, including use in course packs;

d) to post an electronic version (Word or PDF) of the manuscript of the Article as accepted after peer review on the Author(s)'s own website or institutional repository 12 months after the printed Publication is in the public domain, provided that they give a hyperlink from the Article to the Publication's website, together with the following text: 'The final version of record is available at <http://xxx.microbiologyresearch.org/>'. You need not seek permission from the Microbiology Society to apply these rights. Please note: You are NOT permitted to post the Version of Record* online.

4. The Author(s) hereby authorizes the Microbiology Society at their own expense to act to defend their copyright if it believes that a third party is infringing or is likely to infringe copyright in the Article, although there is no obligation on the Microbiology Society to act in this way. The Microbiology Society reserves the right to retain half of any damages awarded, after deducting their costs.

5. This agreement shall be governed by and construed in accordance with the laws of England and Wales. The parties irrevocably agree that the courts of England and Wales shall have exclusive

jurisdiction to settle any dispute or claim that arises out of connection with this Agreement.

Data protection: The Microbiology Society will store your name and contact details in electronic format to correspond with you about your Article.

Notes

1. Please contact the Editorial Office if you have any questions (journals@microbiologysociety.org).
2. Your Article will not be published until the completed Licence to Publish form has been received by the Microbiology Society.
3. *Version of Record - the final published version of the Article, after processes such as copy editing, proof corrections, layout and typesetting have been applied.
4. Please return this form by uploading to the submission system as a supplementary file (file type 'author form') with the manuscript, or email to journals@microbiologysociety.org

Figure A.2 Microbiology Society License to Publish, pg. 3

Reprint permissions for Chapter 4

Publication: Hanson, T.E., Bonsu, E., Tuerk, A. L., Marnocha, C.L., Powell, D.H., Chan, C.S., 2016. Chlorobaculum tepidum growth on biogenic S(0) as the sole photosynthetic electron donor. *Environmental Microbiology*, 18(9), p. 2856-2867. doi: 10.1111/1462-2920.12995.

Permission: This is a License Agreement between Amalie T Levy and John Wiley and Sons provided by Copyright Clearance Center.

Table A.1 License agreement for Chapter 4.

License number	3967231487104
License date	Oct 13, 2016
License content publisher	John Wiley and Sons
Licensed content publication	Environmental Microbiology
Licensed content title	Chlorobaculum tepidum growth on biogenic S(0) as the sole photosynthetic electron donor
Licensed copyright line	© 2015 Society for Applied Microbiology and John Wiley & Sons Ltd
Licensed content author	Thomas E. Hanson, Ernest Bonsu, Amalie L. Tuerk, Cassandra L. Marnocha, Deborah H. Powell, Clara S. Chan
Licensed content date	Aug 28, 2015
Licensed content pages	12
Licensed content volume	18
Licensed content issue	9
Start page	2856
End page	2867
Type of use	Dissertation/Thesis
Requestor type	Author of this Wiley article
Portion	Full article
Title of thesis/dissertation	INSIGHTS INTO ELEMENTAL SULFUR METABOLISM AND LOW-ENERGY ADAPTATIONS IN CHLOROBACULUM TEPIDUM FOR NOVEL TECHNOLOGIES IN WASTE SULFUR MANAGEMENT

Appendix B

COMPARISON OF ROTISSERIE OVEN AND STIRRED WATER BATH CULTURE

This Appendix is adapted from the Supplemental Text A from Levy, Lee and Hanson (2016) with permission, and describes efforts to improve reproducibility of *Chlorobaculum tepidum* growth by implementing a rotisserie culturing system.

B.1 Results

To provide consistent growth conditions (light exposure and mixing) for up to eight simultaneous cultures of *Chlorobaculum tepidum*, a rotisserie oven (RO) culturing system with axial rotation was implemented. Growth of *C. tepidum* in 20 ml cultures at 20 $\mu\text{mol photons m}^{-2} \text{ s}^{-1}$ light flux were compared for the RO system and a stirred water bath (WB) system, where either insoluble biogenic sulfur globules (S^0) or thiosulfate was provided as the sole electron donor. The growth rates determined during the exponential growth phase were indistinguishable between the two culturing systems for both electron donors (Table B.1); furthermore, the growth rates on S^0 and thiosulfate as sole electron donor were indistinguishable.

Table B.1 Measured growth rates for *C. tepidum* during exponential growth in each culturing system while oxidizing S^0 or thiosulfate.

Culturing Configuration	Electron Donor:	Measured growth rate (hr^{-1})	
		S^0	Thiosulfate
RO		0.14 ± 0.03	0.11 ± 0.02
WB		0.12 ± 0.01	0.12 ± 0.05

RO culture was also found to reduce culture-to-culture variability relative to stirred WB cultures. Relative to WB culture, RO culture reduced the coefficient of variation (CV) of protein concentration measurements across within-experiment replicates by 23% and 27% for S^0 - and thiosulfate-grown cultures, respectively. RO culture also substantially reduced variability in bacteriochlorophyll *c* concentration (CVs reduced by 31% for S^0 and 27% for thiosulfate). Variability in electron donor substrate concentrations were slightly reduced by RO culture (CV reduced by 8% for S^0 and 3% for thiosulfate).

B.2 Discussion

The growth rates determined for *C. tepidum* cultures grown on S^0 or thiosulfate as sole electron donor at a light flux of $20 \mu\text{mol photons m}^{-2} \text{s}^{-1}$ were indistinguishable between the RO and WB culturing systems (Table B.1), and correspond to doubling times of ~5 hr for growth on S^0 and ~5-6 hr for growth on thiosulfate. As discussed previously by Hanson et al. (2015), these growth rates are markedly slower than previous reports of maximum growth rates for *C. tepidum*, which approached a doubling time of 2 hours (Wahlund et al. 1991; Mukhopadhyay et al. 1999; Chan et al. 2008). However, these previous reports were all performed in the presence of sulfide, the preferred electron donor for *C. tepidum* (Chan et al. 2008), and the growth rates reported in Wahlund et al. (1991) and Mukhopadhyay et al. (1999) were conducted at higher light flux (~105 and $40 \mu\text{mol photons m}^{-2} \text{s}^{-1}$, respectively). Therefore, it is not surprising that the observed growth rates under the conditions employed in this work would be slower.

The RO culture system reported here could impact *C. tepidum* physiology relative to the WB cultures because it exposes cultures to periodically fluctuating light

flux as they rotate through the light path (ranging from 8 to 34 $\mu\text{mol photons m}^{-2} \text{ s}^{-1}$). By contrast, the WB cultures experience a constant, continuous light flux of 20 $\mu\text{mol photons m}^{-2} \text{ s}^{-1}$. A radial rotating culturing system for *C. tepidum* has been reported previously (Frigaard et al. 2002), and was used primarily for growth rate measurements. Unlike our axial rotating system, it is likely the radial system did not induce fluctuations in light flux throughout the path of rotation. The timescale of light flux variation in our RO culture system between the maximum and minimum levels is on the order of 1 s, and the time-weighted average light flux experienced by RO cultures was the same as cultures grown in the WB. Because the growth rates were indistinguishable between the two systems, this suggests that the effects of light cycling were negligible at least on overall growth rate of the organism. Furthermore, the maximum culture density attained by RO cultures was indistinguishable from WB cultures grown on the same electron donor (data not shown). While we cannot rule out that fluctuating light exposure for RO cultures produced more subtle changes in *C. tepidum* physiology, these data indicate that RO culture was an appropriate means to achieve consistent light exposure between experimental treatments and replicates, and to achieve the mixing necessary for growth on the solid substrate S^0 .

B.3 Methods

Bacterial strains, growth conditions, culture media, sulfur compound quantitation, and protein and BChl *c* quantitation were performed as described in sections 2.3.2-2.3.5, with the following exceptions. Initial electron donor concentrations were $9.2 \pm 0.0 \text{ mM}$ thiosulfate and $8.6 \pm 0.2 \text{ mM S}^0$. For stirred waterbath cultures, autoclaved 1.2 x 0.5 cm Teflon-coated stirbars were added to autoclaved media in culture tubes; tubes were stirred using a magnetic stir plate.

Reported growth rates were calculated as the average observed growth rate between 6 and 22 hours of culture based on culture protein concentration measurements by Bradford assay.

References

- Chan, L.-K. et al., 2008. A genomic region required for phototrophic thiosulfate oxidation in the green sulfur bacterium *Chlorobium tepidum* (syn. *Chlorobaculum tepidum*). *Microbiology*, 154(3), pp.818–829.
- Frigaard, N.-U., Voigt, G.D. & Bryant, D.A., 2002. *Chlorobium tepidum* mutant lacking bacteriochlorophyll *c* made by inactivation of the *bchK* gene, encoding bacteriochlorophyll *c* synthase. *Journal of Bacteriology*, 184(12), pp.3368–3376.
- Hanson, T.E. et al., 2016. *Chlorobaculum tepidum* growth on biogenic S(0) as the sole photosynthetic electron donor. *Environmental Microbiology*, 18(9), pp.2856–2867.
- Levy, A.T., Lee, K.H. & Hanson, T.E., 2016. *Chlorobaculum tepidum* modulates amino acid composition in response to energy availability, as revealed by a systematic exploration of the energy landscape of phototrophic sulfur oxidation. *Applied and Environmental Microbiology*, 82(21), pp.6431–6439.
- Mukhopadhyay, B., Johnson, E.F. & Ascano, M., 1999. Conditions for vigorous growth on sulfide and reactor-scale cultivation protocols for the thermophilic green sulfur bacterium *Chlorobium tepidum*. *Applied and Environmental Microbiology*, 65(1), pp.301–306.
- Wahlund, T., Woese, C. & Castenholz, R., 1991. A thermophilic green sulfur bacterium from New Zealand hot springs, *Chlorobium tepidum* sp. nov. *Archives of Microbiology*, 156, pp.81–90.

Appendix C

DETAILS OF CALCULATIONS FOR CHAPTER 2

This Appendix is adapted from the Supplemental Texts B and C from Levy, Lee and Hanson (2016) with permission, and describes calculations used in that publication and Chapter 2 of this dissertation.

C.1 Calculating prediction accuracy of protein assays

A quantitative assessment of prediction accuracy (see section 2.4.1) was obtained by calculating the residuals (R_i) between the indirect measurement (Bradford or BCA) and the amino acid analysis (AAA) measurement for a given sample i (Equation C.1).

$$R_i = \text{indirect}_i - \text{AAA}_i \quad \text{C.1}$$

An aggregate assessment of indirect protein assay accuracy over N samples was provided by calculating the root mean square of the residuals, i.e. the root mean square error (RMSE; Equation C.2) and by calculating the root mean square of residuals normalized to AAA measurements, the normalized root mean square error (nRMSE; Equation C.3).

$$\text{RMSE} = \sqrt{\frac{\sum_{i=1}^N (R_i)^2}{N-k}} \quad \text{C.2}$$

$$\text{nRMSE} = \sqrt{\frac{\sum_{i=1}^N \left(\frac{R_i}{\text{AAA}_i}\right)^2}{N-k}} \quad \text{C.3}$$

In Equations C.2 and C.3, k is the number of model parameters. For assessing accuracy of the raw protein measurements without correction, $k = 0$. When Equations C.3 and C.3 were used to calculate accuracy for protein measurements corrected by the linear, two-parameter correction functions (Equation 4.2; Table 4.3), $k = 2$.

C.2 Identifying amino acids depleted by methanol extraction

To see whether a particular amino acid AA was preferentially depleted by methanol extraction (section 2.4.2), we first determined the ratio ($\gamma_{AA,i}$) of AA's mass (m_{AA}) in each pair i of extracted (EX) and whole, unextracted (WH) samples (Equation C.4).

$$\gamma_{AA,i} = m_{AA,EX,i} / m_{AA,WH,i} \quad C.4$$

The ratio ($\gamma_{P,i}$) of the mass of total protein in the paired EX (P_{EX}) and WH (P_{WH}) samples was also calculated (Equation C.5).

$$\gamma_{P,i} = P_{EX,i} / P_{WH,i} \quad C.5$$

Two-tailed matched pairs analysis was used to compare $\gamma_{AA,i}$ and $\gamma_{P,i}$ for all $N = 16$ sample pairs by taking the difference for each pair ($\delta_{AA,i}$; Equation C.6).

$$\delta_{AA,i} = \gamma_{AA,i} - \gamma_{P,i} \quad C.6$$

Finally, the average difference in composition for amino acid AA (δ_{AA}) was determined across N sample pairs (Equation C.7), and δ_{AA} was compared to zero by t-test to determine whether amino acid AA was preferentially depleted ($\delta_{AA} < 0$) in methanol extracted samples.

$$\delta_{AA} = \sum_i^N \delta_{AA,i} / N \quad C.7$$

References

- Levy, A.T., Lee, K.H. & Hanson, T.E., 2016. *Chlorobaculum tepidum* modulates amino acid composition in response to energy availability, as revealed by a systematic exploration of the energy landscape of phototrophic sulfur oxidation. *Applied and Environmental Microbiology*, 82(21), pp.6431–6439.

Appendix D

***CHLOROBACULUM TEPIDUM* OXYGEN TOLERANCE STUDIES**

This Appendix describes the outcome of preliminary experiments investigating the oxygen tolerance of *Chlorobaculum tepidum*. These studies were motivated by the anecdotal observation of an inverse relationship between the “age” of sulfide-free Pf-7 medium prior to use and success rate of *C. tepidum* cultures. The detection of dissolved oxygen in sulfide-free Pf-7 that diminished with storage time implicated trace oxygen contamination as a root cause for failed culture growth in the absence of sulfide. Based on a dilution series of oxygen in thiosulfate-only media, the oxygen tolerance of *C. tepidum* was estimated to be at least 10 μM dissolved O_2 . Finally, *C. tepidum* cultures were observed to remove O_2 from solution, where the rate of O_2 removal was a function of light flux and exhibited light-saturation behavior.

D.1 Results and Discussion

D.1.1 Evidence for trace oxygen contamination as a root cause of culture failure

When *C. tepidum* was grown in the absence of sulfide, i.e. on thiosulfate or S^0 as sole electron donor, a high proportion of cultures “failed”, where either no or little growth was observed. The frequency of failed cultures was generally higher when the length of time between medium preparation and culture inoculation was 10 days or less, and culture success rate increased with increasing time between medium preparation and use (Fig. D.1-A). When growth of *C. tepidum* on freshly prepared sulfur-free Pf-7, amended with either 10 mM thiosulfate or 10 mM S^0 , was directly

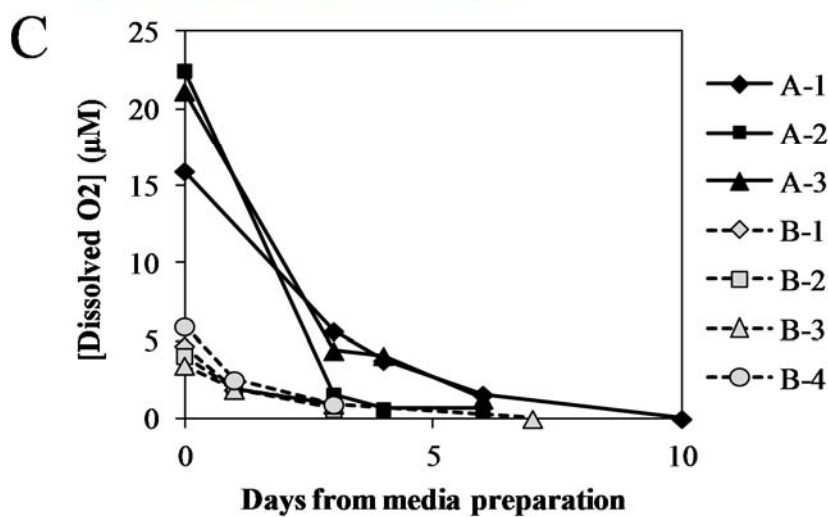
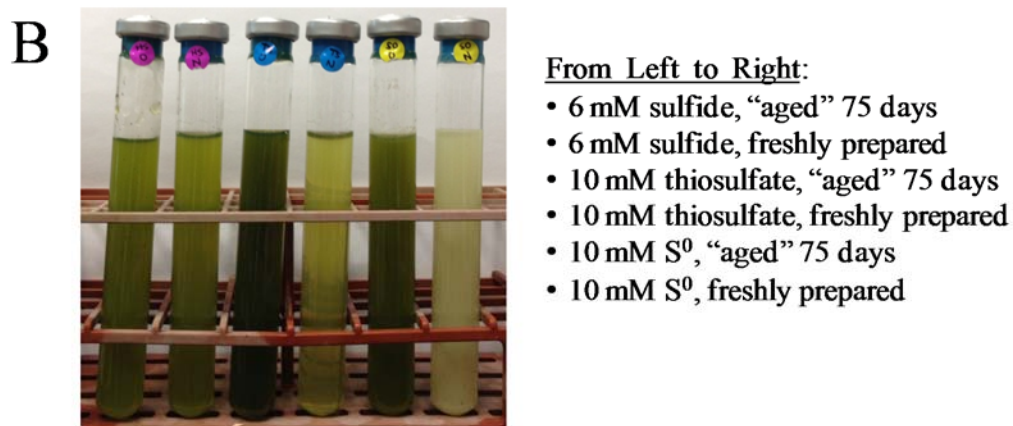
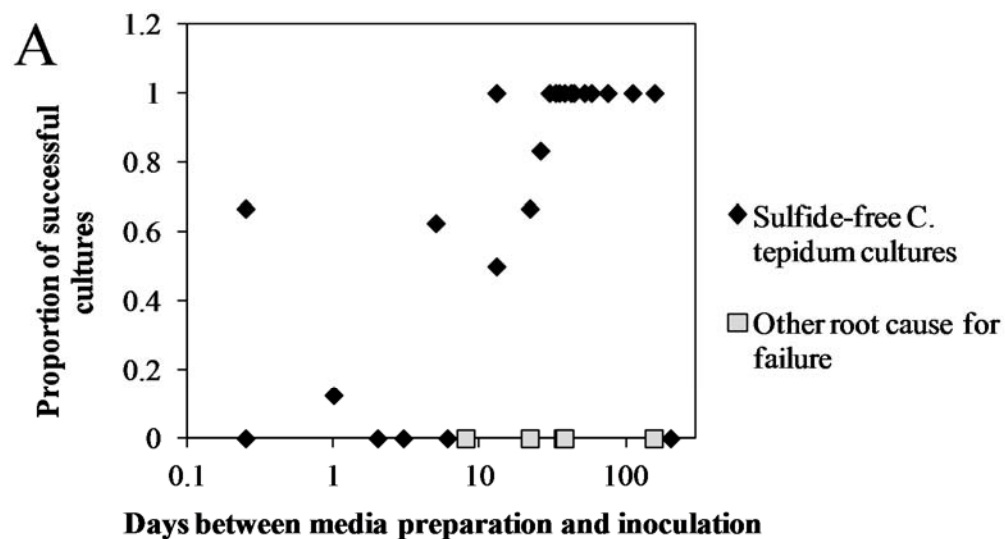


Figure D.1 Trace oxygen contamination in sulfide-free Pf-7 medium may contribute to failed *C. tepidum* cultures. (A) The proportion of failed (non-growing or stunted growth cultures) in experiments decreased when the time between medium preparation and use increased. Experiments where cultures failed for other root causes (e.g. poor source cultures; overheated culturing system) are indicated. (B) Image of *C. tepidum* cultures grown for 17.3 hours on either freshly prepared sulfur-free media amended with sulfide, thiosulfate, or S^0 as sole electron donor, or previously prepared media, where 75 days since the original preparation of the sulfur-free medium had elapsed. Growth of *C. tepidum* on the “aged” medium is superior for thiosulfate and S^0 as electron donor, but there is little difference when sulfide was electron donor. Initial concentrations of electron donors are indicated. (C) Oxygen initially present in two batches (A and B) of sulfur-free Pf-7 medium was found to rapidly decrease in the first 10 days of storage in anaerobic conditions. Each trace represents measurements from a different bottle of media.

compared to growth on “aged” thiosulfate-only and S^0 -only medium, the growth on the freshly prepared media was markedly inferior (Fig. D.2-B). However, this difference in growth between freshly prepared and aged medium was not observed when 6 mM sulfide was provided as electron donor (Fig. D.2-B). Incomplete removal of oxygen during preparation of sulfur-free medium could explain these observations: increased success of *C. tepidum* growth on “aged” medium could be rationalized by the diffusion of dissolved oxygen present in the liquid medium out into the headspace of the bottle or tube during storage under anaerobic conditions, where subsequent transfers of media from bottles into tubes in an anaerobic chamber and additional storage time would provide opportunities for oxygen removal. That “aging” of the medium did not affect *C. tepidum* when sulfide was electron donor could also be explained by the presence of oxygen in the medium, as adding sulfide would serve to directly reduce oxygen.

The concentration of oxygen in two batches of sulfur-free Pf-7 media, each consisting of three and four bottles, was monitored periodically after preparation (Fig. D.1-C). Freshly prepared media had dissolved oxygen concentrations ranging from 5-23 μM , and these levels exhibited time-dependent decay. Within 10 days, dissolved oxygen concentrations had decreased to less than the detection limit of the measurement device (0.01 ppm O_2 ; 0.3 μM O_2). As each oxygen sampling operation of these media required the headspace of the bottles to be exchanged, the sampling procedure may have served to accelerate the removal of dissolved oxygen relative to media stored in bottles without frequent sampling. However, it is interesting that the timeframe over which the media demonstrated rapid decreases in dissolved oxygen concentration corresponded to the timeframe of the largest increases in experimental culture success (Fig. D.1-A). These observations motivated studies to characterize the oxygen tolerance of *C. tepidum*.

D.1.2 *C. tepidum* can recover from dissolved oxygen concentrations of approximately 10 μM

To evaluate the oxygen tolerance of *C. tepidum*, a “dilution series” of oxygen in the headspace of culture tubes containing thiosulfate-only Pf-7 medium (10 mM thiosulfate) was prepared by controlled injection of ambient air. This effort targeted gas-phase oxygen concentrations that were expected to produce liquid-phase oxygen concentrations of 0.08, 0.19, 1.2, 11, and 103 μM O_2 after equilibration according to Henry’s Law and at the temperature of *C. tepidum* culture (46 °C). These expected concentrations were also based on an assumed concentration of 0.08 μM O_2 in the “aged” thiosulfate-only base medium.

Growth of *C. tepidum* in these O₂-treated media was compared to growth in full Pf-7 and sulfur-free Pf-7 as positive and negative controls, respectively. Over the first 15 hours of culture, growth rates of *C. tepidum* in the 0.08 and 0.12 μ M O₂ treatments were similar to the positive control (Fig. D.2-A). However, the growth rate of *C. tepidum* in media with higher O₂ were slower, where each order-of-magnitude increase in O₂ led to an approximately equal decrease in growth rate (Fig. D.2-A). Interestingly, growth yields were similar for all cultures over the first 15 hours of growth, except for the highest O₂ level which did not grow (Fig. D.2-B). By 38 hours growth, the 1.2 and 11 μ M O₂ cultures had largely recovered, demonstrating similar final culture protein concentrations as the lower O₂ treatments (data not shown). However, even at 38 hours growth, the 103 μ M O₂ cultures had not demonstrated net growth or thiosulfate consumption, indicating that this level of oxygen completely inhibited *C. tepidum* growth. Based on the O₂ concentrations that were targeted in these experiments, we anticipate that *C. tepidum* is able to recover from O₂ of at least 10 μ M. Unfortunately, a means to accurately measure the actual initial concentrations of dissolved O₂ in these cultures was not available.

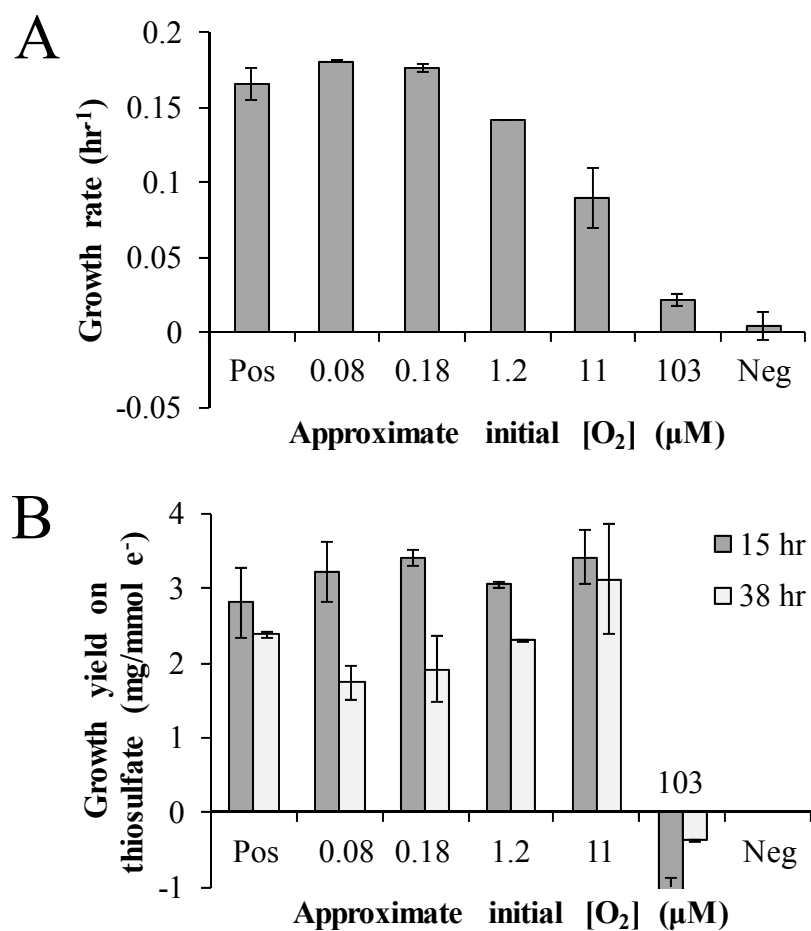


Figure D.2 Oxygen added to thiosulfate-only media induced lag in *C. tepidum* growth but did not affect overall growth yields except for highest O₂ treatment. (A) Growth rate over the first 15 hours of culture is plotted versus the initial targeted dissolved O₂ concentration. Oxygen at levels of 1.2 μM and higher led to reduced growth rates during the initial culture phase. (B) Growth yields on a thiosulfate-electron basis are plotted versus the initial targeted O₂ concentration; yields were calculated based on protein-based growth and thiosulfate consumption at 15 hours and 38 hours culture. In both plots, bars represent the average value for two independent experiments; error bars represent the standard error of the mean.

D.1.3 *C. tepidum* cells remove oxygen in light-dependent manner

While measuring the dissolved oxygen concentration in a *C. tepidum* culture grown on 10 mM thiosulfate-only Pf-7 medium, it was observed that measureable O₂ rapidly decreased after it was introduced to the culture by a spike of aerobic water. Oxygen that was introduced to sulfide-free, 10 mM thiosulfate-only medium did not decrease (Fig. D.3-A), nor did O₂ spiked into the cell-free spent medium from a thiosulfate-grown *C. tepidum* culture (data not shown), suggesting that the O₂ removal was dependent upon the presence of the cells. O₂ introduced to Pf-7 medium containing ~1 mM sulfide also decreased, but at a slower rate than in the *C. tepidum* culture (Fig. D.3-A).. This was likely due to the sulfide present in Pf-7 medium which can directly reduce oxygen. These observations suggested that the decrease in O₂ in the *C. tepidum* culture may be due to the activity of the cells.

To explore this phenomenon further, both Pf-7 medium and the *C. tepidum* culture previously grown on thiosulfate were exposed to light flux from 0 to 50 $\mu\text{mol photon m}^{-2} \text{s}^{-1}$ and the rate of O₂ removal was measured (see Fig. D.3-A). While the rate of O₂ removal by Pf-7 medium remained essentially constant as a function of light, the O₂ removal rate for *C. tepidum* cells was found to be dependent on light flux (Fig. D.3-B). Furthermore, O₂ removal rate exhibited saturated behavior above ~30 $\mu\text{mol photons m}^{-2} \text{s}^{-1}$, approximately the same level at which *C. tepidum* growth rate saturates in response to increased light exposure (Morgan-Kiss et al. 2009). This effect was repeated with a *C. tepidum* culture grown for 13 hours on Pf-7 medium, where the rate overall rate of O₂ reduction demonstrated a similar response to changing light flux (Fig. D.3-B). Oxygen removal by *C. tepidum* was non-zero in the absence of incident light flux; this baseline O₂ removal could be enabled by light provided from the

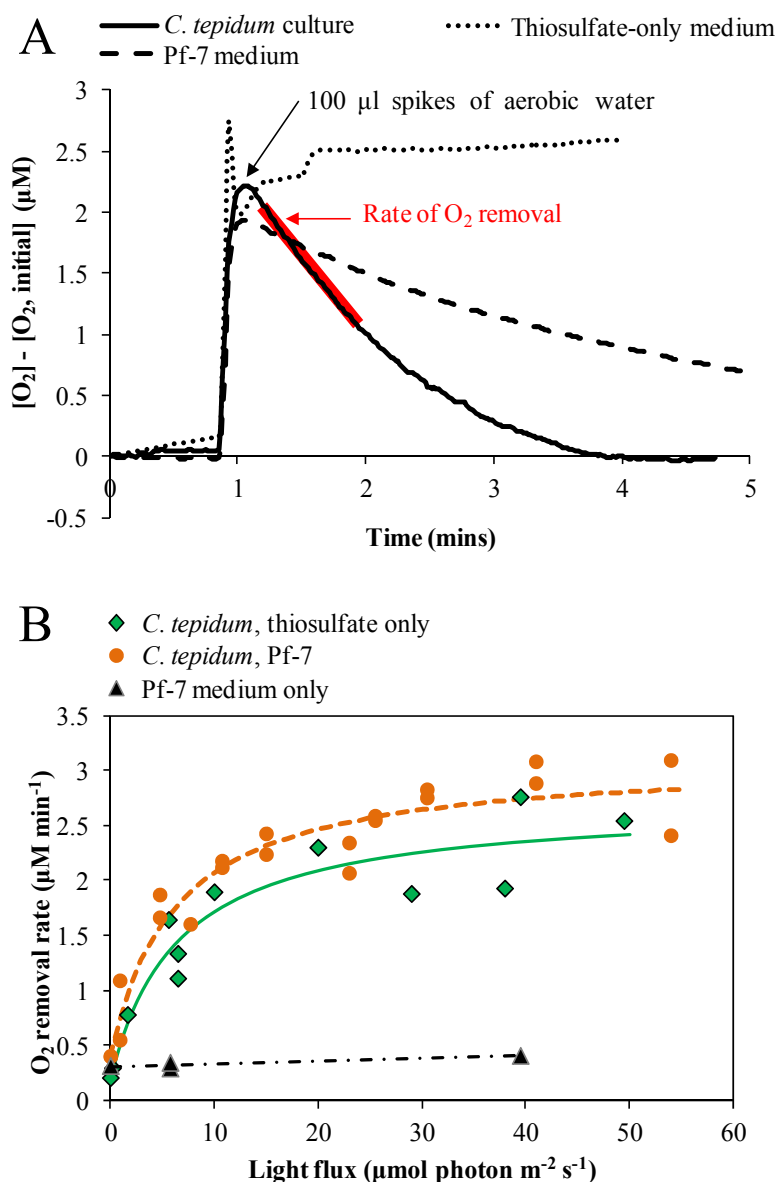


Figure D.3 *C. tepidum* removed O_2 from culture in a light-dependent manner. (A) Example traces of O_2 concentration as a function of time after O_2 introduction by an anaerobic water spike. Both *C. tepidum* culture and sulfide-containing Pf-7 media led to O_2 removal, while thiosulfate-only media did not demonstrate O_2 removal. (B) Rate of O_2 removal for two independent *C. tepidum* cultures are plotted as a function of incident light flux; the rate of O_2 removal for Pf-7 medium is overlaid for comparison and is not dependent on light flux.

flashing LED in the O₂ probe, or it could be due to baseline O₂ reduction by *C. tepidum* cells that is not dependent upon light (see discussion below). A direct comparison of the specific rate of O₂ removal for these two cultures is not available as culture protein measurements were not collected.

The *C. tepidum* genome contains genes for several proteins predicted to have the capability to reduce oxygen to water: *cydA* (CT1818), which encodes cytochrome *bd* ubiquinol oxidase subunit I, *nox* (CT2078), which encodes NADH oxidase, and *roo* (CT2285), which encodes rubredoxin oxygen oxidoreductase (Li et al. 2009). A previous study that investigated *C. tepidum* deletion mutants for *cydA*, *nox*, and *roo* found that deletion of *cydA* and *roo* affected *C. tepidum* survival through oxygen exposure in both the light and the dark, while deletion of *nox* had no effect on *C. tepidum* survival (Li et al. 2009). Deletion of *roo* had a stronger effect on *C. tepidum* survival in the light, while deletion of *cydA* had an approximately equal effect on *C. tepidum* survivability in the light and in the dark. Roo couples O₂ reduction to rubredoxin oxidation, where in other species such as *Clostridium acetobutylicum* electrons are originally derived from NADH (Guedon & Petitdemange 2001). As NADH reduction is coupled to ferredoxin oxidation *via* ferredoxin-NAD(P)⁺ reductase (Seo & Sakurai 2002), and reduced ferredoxin is produced *via* light-induced oxidation of the *C. tepidum* reaction centers, it is possible that Roo is the light-dependent mechanism responsible for O₂ removal in these studies. CydA, on the other hand, should obtain electrons for reduction of O₂ directly from the quinone pool, and therefore this process would not be expected to be light-dependent, consistent with the observations of Li et al. (2009). It is possible that the activity of CydA is at least

partially responsible for the baseline rate of O₂ removal observed by *C. tepidum* in the absence of light.

Studies to elucidate the mechanism of O₂ removal by *C. tepidum* is an interesting aim for future studies. Measuring the rates of O₂ removal for the *roo* and *cydA* deletion mutants would help determine the relative contributions to O₂ reduction by these enzymes. The use of inhibitors specific to the electron transport chain (e.g. cyanide) could also help in quantifying the relative contribution to O₂ reduction from Roo and CydAB, as the Roo pathway for O₂ reduction is insensitive to cyanide in *Desulfovibrio gigas* (Lemos et al. 2001). The source of electrons for O₂ reduction is also an interesting question. In *Clostridium acetobutylicum* rubredoxin is reduced using electrons from NADH by NADH-rubredoxin oxidoreductase (Guedon & Petitdemange 2001). While there is no annotated rubredoxin oxidoreductase in *C. tepidum*, Nox encoded by CT2078 is homologous to the *C. acetobutylicum* NADH-rubredoxin oxidoreductase, as described in section 3.4.7. However, that deletion of CT2078 did not affect *C. tepidum* survival in response to oxygen exposure (Li et al. 2009) suggests that there is an alternate route for electron transfer to rubredoxin in *C. tepidum*.

D.2 Methods

D.2.1 Bacterial strains, growth conditions, and culture media

Chlorobaculum tepidum strain WT2321, a plating strain derivative of the original TLS1 isolate (Wahlund et al. 1991; Wahlund & Madigan 1995), was grown in 20 ml cultures with a 10 psig (177 kPa) headspace composed of 95%:5% N₂:CO₂ passed through a heated copper scrubber. Experimental cultures were inoculated to 4

$\mu\text{g protein ml}^{-1}$ from pre-cultures derived from cryogenic stocks, and were grown at 45-46 °C in a heated rotisserie culturing system (see Appendix B). Light was provided from 60 W Reveal® incandescent bulbs (GE Lighting) to $20 \mu\text{mol m}^{-2} \text{s}^{-1}$ and was measured with a quantum photosynthetic active radiation sensor (LI-COR). Pf-7 medium was prepared as previously described (Wahlund et al. 1991) and sulfur-free Pf-7 medium was prepared by omitting sulfide and thiosulfate from Pf-7 as previously described (Chan et al. 2008). Electron donors were amended to sulfur-free Pf-7 from concentrated, anoxic stock solutions to the concentrations specified above.

D.2.2 Oxygen measurements

For measuring oxygen in Pf-7 media, samples of media were removed from media bottles and transferred to 50 ml conical tubes inside an anaerobic chamber (Coy). Liquid phase O_2 measurements were made using a SevenGo Duo pro™ meter and OptiOx™ optical dissolved oxygen probe (Mettler Toledo). At each use, the O_2 meter was calibrated using a one-point calibration with air-saturated water; the dissolved O_2 in a zero-oxygen standard was routinely checked to ensure a 0.00 ppm reading was obtained.

As the response time of this probe was extremely long and the limit of O_2 detection was relatively high (0.01 ppm or $0.3 \mu\text{M O}_2$), an oxygen probe with a faster response time and higher sensitivity was used for real-time measurements of O_2 removal by *C. tepidum* cultures. Dissolved oxygen measurements were made using a FireStingO2 optical oxygen meter and a Retractable Trace Range Oxygen Minisensor TROXR430 (Pyro Science GmbH) set to a measurement time of 60 ms and LED intensity of 30%. Measurements were made by inserting the probe needle into a stoppered 11.5 ml vial with a Teflon-coated magnetic stirbar, extending the probe tip,

and flushing the vial with anaerobic gas until the O₂ measurement leveled off; this measurement was used as the baseline. Samples (culture or media) were collected using a needle and syringe and were injected into the vial to displace the gas until no headspace remained. Once the vial was filled, stirring of the sample was begun, and the O₂ measurement was taken as the difference between the stabilized measured value for the sample and the pre-sample baseline. Removal of oxygen by *C. tepidum* cultures was monitored continuously after a 100 µl spike of aerobic water to the sample. Spike recovery was calculated from the O₂ measurements before the spike and the maximum O₂ observed after the spike; rates of O₂ removal were calculated from the slope of O₂ concentration versus time during the decrease from 90% to 50% of the peak height (see Fig. D.3-A).

D.2.3 Measurements of culture protein and thiosulfate

Protein measurements were performed by Bradford method on methanol-extracted cell pellets as described in Levy et al. (2016) and section 2.3.5 of this dissertation; the values reported here are uncorrected. Protein measurements were used for calculation of culture growth rates and growth yields. Thiosulfate measurements were performed as described in Chan et al. (2008). Briefly thiosulfate in culture supernatants was separated and quantified by HPLC using a Prevail™ Organic Acids 5 µm column (Alltech Associates Inc.) with 25 mM potassium phosphate (pH 2.5) as mobile phase and UV detection at 210 nm. Standard curves were prepared from sodium thiosulfate pentahydrate (>99.5%, Sigma-Aldrich).

References

- Chan, L.-K. et al., 2008. A genomic region required for phototrophic thiosulfate oxidation in the green sulfur bacterium *Chlorobium tepidum* (syn. *Chlorobaculum tepidum*). *Microbiology*, 154(3), pp.818–829.
- Guedon, E. & Petitdemange, H., 2001. Identification of the gene encoding NADH-rubredoxin oxidoreductase in *Clostridium acetobutylicum*. *Biochemical and Biophysical Research Communications*, 285(2), pp.496–502.
- Lemos, R.S. et al., 2001. The “strict” anaerobe *Desulfovibrio gigas* contains a membrane-bound oxygen-reducing respiratory chain. *FEBS Letters*, 496(1), pp.40–43.
- Levy, A.T., Lee, K.H. & Hanson, T.E., 2016. *Chlorobaculum tepidum* modulates amino acid composition in response to energy availability, as revealed by a systematic exploration of the energy landscape of phototrophic sulfur oxidation. *Applied and Environmental Microbiology*, 82(21), pp.6431–6439.
- Li, H. et al., 2009. Multiple antioxidant proteins protect *Chlorobaculum tepidum* against oxygen and reactive oxygen species. *Archives of Microbiology*, 191(11), pp.853–867.
- Morgan-Kiss, R.M. et al., 2009. *Chlorobaculum tepidum* regulates chlorosome structure and function in response to temperature and electron donor availability. *Photosynthesis Research*, 99(1), pp.11–21.
- Seo, D. & Sakurai, H., 2002. Purification and characterization of ferredoxin-NAD(P)(+) reductase from the green sulfur bacterium *Chlorobium tepidum*. *Biochimica et Biophysica Acta*, 1597(1), pp.123–132.
- Wahlund, T.M. et al., 1991. A thermophilic green sulfur bacterium from New Zealand hot springs, *Chlorobium tepidum* sp. nov. *Archives of Microbiology*, 156, pp.81–90.

Appendix E

LIST OF ALL PROTEIN IDENTIFICATIONS FROM GEL-BASED STUDIES OF S⁰

Table E.1 provides a compiled list of all proteins identified from gel-based studies of purified S⁰ from *C. tepidum*. For each protein, the number of times the protein was identified in extracts from cells (wildtype or mutant C3) or from purified S⁰ (from wildtype or mutant C3) is indicated. In addition, the number of times that each protein was identified in differential extracts of S⁰ is indicated. Numbers of identifications are not intended for quantitative comparisons of abundance between different categories, as the different categories were not sampled equally for protein identifications.

Notes for Table E.1:

^a RefSeq or GenBank accession number

^b Cluster of Orthologous Genes category; A = RNA processing and modification; B = chromatin structure and dynamics; C = Energy production and conversion; D = cell cycle control, cell division, chromosome partitioning; E = amino acid metabolism and transport; F = nucleotide metabolism and transport; G = carbohydrate metabolism and transport; H = coenzyme metabolism and transport; I = lipid metabolism and transport; J = translation, ribosomal structure, and biogenesis; K = transcription; L = replication, recombination, and repair; M = cell wall/membrane/envelope biogenesis; N = cell motility; O = post-translational modification, protein turnover, chaperones; P = inorganic ion transport and metabolism; Q = secondary metabolites biosynthesis, transport, and catabolism; R = general functional prediction only; S = function unknown; T = signal transduction mechanisms; U = intracellular trafficking, secretion, and vesicular transport; V = defense mechanisms.

^c Number of times protein was identified in extracts from whole *C. tepidum* cells. WT = wildtype cells; C3 = C3 mutant cells.

^d Number of times protein was identified in extracts from purified S⁰ from *C. tepidum*. WT = S⁰ from wildtype *C. tepidum*; C3 = S⁰ from C3 mutant *C. tepidum*.

^e Number of times protein was identified in differential extracts of S⁰; treatments are as described in Tables 4.4 and Table 4.6. U = unassociated proteins; WH = proteins associated with S⁰ by weak hydrophobic interactions; SHD = proteins associated with S⁰ by strong hydrophobic or disulfide interactions; AAP = all associated proteins.

Table E.1 List of all protein identifications from gel based studies of purified S⁰ from *C. tepidum*.

Locus Tag	Gene Name	Accession ^a	Description	COG Cat ^b	Times ID'd in cells: ^c		Times ID'd in S ⁰ : ^d		Times ID'd in S ⁰ treatments: ^e			
					WT	U3	WT	U3	U	WH	SHD	AAP
CT0058		NP_660964	histidine triad (hit) family protein	FGR	1	0	0	3	0	1	2	0
CT0068		NP_660974	hemagglutinin-related protein		0	0	1	0	0	1	0	0
CT0089	<i>clpB-2</i>	NP_660995	ATP-dependent Clp protease, ATP binding subunit ClpB		1	1	0	4	0	3	0	1
CT0160	<i>hupB</i>	NP_661066	Hu-beta, DNA binding protein	L	1	2	1	7	0	5	2	1
CT0163		NP_661069	alpha oxoglutarate ferredoxin oxidoreductase subunit C alpha	C	0	0	0	1	0	0	1	0
CT0240	<i>nusA</i>	NP_661144	transcription elongation factor NusA	K	0	0	0	1	0	0	1	0
CT0291		NP_661195	uncharacterized protein CT0291		0	0	0	5	0	2	1	2
CT0293	<i>apt</i>	NP_661197	adenine phosphoribosyltransferase	F	0	0	0	4	0	3	1	0
CT0295		NP_661199	DNA-binding protein HU-alpha	L	0	0	0	2	0	2	0	0
CT0302	<i>petC</i>	NP_661206	Cytochrome b6-f complex iron-sulfur subunit	C	3	2	1	12	0	5	4	4
CT0312		NP_661216	DnaK suppressor protein		0	0	0	2	0	0	2	0
CT0331	<i>pdxJ</i>	NP_661235	pyridoxine 5'-phosphate synthase	H	0	1	0	2	0	0	2	0
CT0350	<i>fabI</i>	NP_661254	enoyl-ACP reductase	I	0	0	0	1	0	0	1	0
CT0530	<i>groEL</i>	NP_661430	molecular chaperone GroEL	O	1	1	1	21	1	12	9	0
CT0643	<i>dnaK</i>	NP_661540	molecular chaperone DnaK	O	3	3	4	30	2	5	27	0
CT0644		NP_661541	Heat shock protein, HSP 20 family	O	4	2	1	18	0	7	8	4

Table E.1 continued.

Locus Tag	Gene Name	Accession ^a	Description	COG Cat ^b	Times ID'd in cells: ^c		Times ID'd in S ⁰ : ^d		Times ID'd in S ⁰ treatments: ^e			
					WT	U3	WT	U3	U	WH	SHD	AAP
CT0670		NP_661566	ABC transporter, periplasmic substrate-binding protein	P	0	0	0	2	0	0	2	0
CT0722	<i>metK</i>	NP_661617	S-adenosylmethionine synthetase	EH	1	0	0	1	0	0	1	0
CT0760		NP_661655	histidine triad (hit) family protein	FGR	0	0	0	2	0	0	2	0
CT0785	<i>trx-1</i>	NP_661680	thioredoxin	OC	0	0	0	1	0	0	1	0
CT0829	<i>htpG</i>	NP_661723	heat shock protein 90	O	2	1	0	9	0	2	7	0
CT0841	<i>trx-2</i>	NP_661735	thioredoxin	OC	4	2	0	2	0	1	1	0
CT0853	<i>dsrB-1</i>	NP_661747	sulfite reductase, dissimilatory type subunit beta	C	0	0	0	1	0	1	0	0
CT0857	<i>dsrH</i>	NP_661751	DsrH protein	P	0	2	0	4	0	0	4	0
CT0864	<i>aspB</i>	NP_661758	adenylylsulfate reductase subunit beta		6	3	0	2	0	1	1	0
CT0893		NP_661786	uncharacterized protein CT0893		0	0	2	0	0	2	0	0
CT0895		NP_661788	phosphate ABC transporter substrate-binding protein	P	1	1	0	4	0	1	2	1
CT0960	<i>purC</i>	NP_661853	phosphoribosylaminoimidazole-succinocarboxamide synthase	F	0	0	0	2	0	0	2	0
CT0985		NP_661878	P-II family protein	E	0	0	0	2	0	0	2	0
CT1017	<i>soxY</i>	NP_661909	sulfur oxidation protein SoxY		2	2	0	3	0	1	2	0
CT1018	<i>soxZ</i>	NP_661910	sulfur oxidation protein SoxZ		2	3	0	2	0	1	1	0
CT1019	<i>soxA</i>	NP_661911	sulfur oxidation protein SoxA		3	3	0	11	0	0	11	0
CT1021	<i>soxB</i>	NP_661913	sulfur oxidation protein SoxB		1	1	0	1	0	0	1	0
CT1023	<i>soxW</i>	NP_661915	thioredoxin family thiol:disulfide interchange protein		1	1	0	1	0	0	1	0

Table E.1 continued.

Locus Tag	Gene Name	Accession ^a	Description	COG Cat ^b	Times ID'd in cells: ^c		Times ID'd in S ⁰ : ^d		Times ID'd in S ⁰ treatments: ^e			
					WT	Δ3	WT	Δ3	Δ	WH	SHD	AAP
CT1053	<i>fbaA</i>	NP_661944	fructose-bisphosphate aldolase	G	0	0	0	1	0	0	1	0
CT1054	<i>prc</i>	NP_661945	carboxyl-terminal protease	M	0	0	0	5	0	4	1	0
CT1133		NP_662024	uncharacterized protein CT1133		0	0	1	2	0	1	1	1
CT1213		NP_662103	uncharacterized protein CT1213	R	0	0	0	2	0	2	0	0
CT1215		NP_662105	thioredoxin	O	2	2	0	2	0	0	2	0
CT1239	<i>secA</i>	NP_662127	preprotein translocase subunit SecA	U	1	0	0	4	0	2	2	0
CT1305		NP_662193	uncharacterized protein CT1305		0	0	0	16	0	15	0	1
CT1320.1		AAY51681	uncharacterized protein CT1320.1		0	0	0	3	0	0	0	3
CT1327		NP_662214	rubrerythrin		0	0	0	1	0	0	1	0
CT1353		NP_662240	OmpA family protein		4	3	0	3	0	2	0	1
CT1447		NP_662333	serine protease	O	1	1	1	15	0	13	3	0
CT1499	<i>fmoA</i>	NP_662384	bacteriochlorophyll A protein		1	0	0	10	1	4	4	1
CT1555	<i>accD</i>	NP_662438	acetyl-CoA carboxylase, carboxyl transferase subunit I beta		0	0	0	3	0	2	1	0
CT1577	<i>frr</i>	NP_662460	ribosome recycling factor	J	1	1	0	3	0	1	1	1
CT1634		NP_662517	uncharacterized protein CT1634		2	2	0	2	0	0	2	0
CT1649	<i>pnp</i>	NP_662532	polynucleotide phosphorylase	J	0	0	0	5	1	3	1	0
CT1743	<i>feoA-1</i>	NP_662623	ferrous iron transport protein A	P	0	0	0	1	0	0	1	0
CT1780	<i>tsf</i>	NP_662659	elongation factor Ts	J	0	0	0	1	0	0	1	0
CT1804		NP_662683	uncharacterized protein CT1804		5	2	2	2	0	3	0	1

Table E.1 continued.

Locus Tag	Gene Name	Accession ^a	Description	COG Cat ^b	Times ID'd in cells: ^c		Times ID'd in S ⁰ : ^d		Times ID'd in S ⁰ treatments: ^e			
					WT	U3	WT	U3	U	WH	SHD	AAP
CT1860		NP_662737	uncharacterized protein CT1860		0	0	0	1	0	1	0	0
CT1888		NP_662765	SpoU rRNA methylase	J	0	0	0	1	0	1	0	0
CT1897		NP_662774	uncharacterized protein CT1897		0	0	0	1	0	1	0	0
CT1898	<i>hemY</i>	NP_662775	protoporphyrinogen oxidase		0	0	0	1	0	1	0	0
CT1942	<i>csmA</i>	NP_662819	Bacteriochlorophyll c-binding protein		2	1	0	2	0	0	1	1
CT1943	<i>csmC</i>	NP_662820	chlorosome envelope protein C		2	2	1	13	0	9	3	2
CT1955		NP_662832	magnesium-chelatase, bacteriochlorophyll c-specific subunit	H	2	0	0	2	0	1	1	0
CT1970		NP_662846	HSP20 family protein	O	3	3	3	12	0	10	5	0
CT2032	<i>atpG</i>	NP_662907	ATP synthase F0F1 subunit gamma	C	0	0	0	2	0	0	2	0
CT2049		NP_662924	LipD protein, putative		0	0	1	0	0	1	0	0
CT2054	<i>csmB</i>	NP_662929	Chlorosome envelope protein B		0	1	0	5	0	1	2	2
CT2131		NP_663005	uncharacterized protein CT2131		0	0	0	1	0	0	1	0
CT2144		NP_663018	outer surface protein, putative		2	1	0	3	1	1	0	1
CT2175	<i>rpsH</i>	NP_663049	30S ribosomal protein S8	J	4	1	0	2	0	2	0	0
CT2190	<i>rpsJ</i>	NP_663064	30S ribosomal protein S10	J	1	1	0	3	0	2	1	0
CT2191	<i>tuf</i>	NP_663065	elongation factor Tu	J	0	0	0	9	0	2	7	0
CT2216		NP_663090	uncharacterized protein CT2216		0	0	0	2	0	1	1	0
CT2233		NP_663107	thiol:disulfide interchange protein, thioredoxin family protein		0	0	0	1	0	0	1	0

Table E.1 continued.

Locus Tag	Gene Name	Accession ^a	Description	COG Cat ^b	Times ID'd in cells: ^c		Times ID'd in S ⁰ : ^d		Times ID'd in S ⁰ treatments: ^e			
					WT	Δ3	WT	Δ3	Δ	WH	SHD	AAP
CT2250	<i>dsrC-2</i>	NP_663123	sulfite reductase, dissimilatory type subunit gamma	P	2	2	0	1	0	0	1	0
CT2281	<i>clpB-1</i>	NP_663152	ATP-dependent Clp protease, ATP binding subunit ClpB		0	0	0	7	0	0	7	0

Appendix F

SHOTGUN PROTEOMIC IDENTIFICATIONS FROM *C. tepidum* S⁰

Table F.1 lists protein identifications from wildtype S⁰ from *C. tepidum*, along with the number of unique peptides matched to each protein (> 95% confidence), and the protein coverage obtained from peptides matched at >95% confidence. Proteins are sorted in decreasing order by number of unique matched peptides.

Table F.1 Shotgun proteomic protein identifications from wildtype *C. tepidum* S⁰, organized by number of total matched peptides per protein. Conserved domains for poorly-characterized proteins are provided in parentheses in the description.

Locus ID	Gene name	Description	# unique matched peptides	Protein Coverage (%)
CT0829	<i>htpG</i>	heat shock protein 90	11	19.7
CT0254	<i>ompH</i>	outer membrane protein OmpH	10	44.3
CT1447		serine protease (degP, htrA_DO)	10	23.2
CT0089	<i>clpB-2</i>	ATP-dependent Clp protease, ATP-binding subunit ClpB	7	16.4
CT1499	<i>fmoA</i>	bacteriochlorophyll A protein	7	22.1
CT0547	<i>mreB-1</i>	rod shape-determining protein MreB	6	19.6
CT2162	<i>rpoA</i>	DNA-directed RNA polymerase subunit alpha	6	20.7
CT0154	<i>rplL</i>	50S ribosomal protein L7/L12	5	39.7
CT0155	<i>rpoB</i>	DNA-directed RNA polymerase subunit beta	5	4.6
CT0530	<i>groEL</i>	chaperonin GroEL	5	11.6
CT0643	<i>dnaK</i>	molecular chaperone DnaK	5	8.1
CT1804		uncharacterized protein CT1804	5	13.5

Table F.1 continued.

Locus ID	Gene name	Description	# unique matched peptides	Protein Coverage (%)
CT1054	<i>prc</i>	carboxyl-terminal protease	4	6.5
CT1297	<i>bchI</i>	magnesium-chelatase subunit I	4	10.7
CT2191	<i>tuf</i>	elongation factor Tu	4	12.2
CT2281	<i>clpB-1</i>	ATP-dependent Clp protease, ATP-binding subunit ClpB	4	11.1
CT1353		OmpA family protein n(type_VI_ompA, OmpA_C-like)	3	19.1
CT1361	<i>prsA</i>	ribose-phosphate pyrophosphokinase	3	13.0
CT1649	<i>pnp</i>	polynucleotide phosphorylase/polyadenylase	3	4.0
CT1745		uncharacterized protein CT1745 (Phenol_metA_deg)	3	13.5
CT1942	<i>csmA</i>	chlorosome envelope protein A	3	35.4
CT0131		uncharacterized protein CT0131 (SDR_a8, yfcH)	2	8.0
CT0160	<i>hupB</i>	DNA-binding protein HU-beta	2	35.2
CT0529	<i>groES</i>	co-chaperonin GroES	2	31.6
CT0841	<i>trx-2</i>	thioredoxin	2	21.1
CT0893		uncharacterized protein (Porin_5)	2	7.0
CT0903		transcriptional regulator (PhoU)	2	10.7
CT0980		ArsA ATPase	2	6.8
CT1309		uncharacterized protein CT1309 (Metal_resist)	2	9.9
CT1485	<i>grpE</i>	heat shock protein GrpE	2	9.8
CT1742	<i>feoB-1</i>	ferrous iron transport protein B	2	2.9
CT1743	<i>feoA-1</i>	ferrous iron transport protein A	2	17.3
CT1781	<i>rpsB</i>	30S ribosomal protein S2	2	7.6
CT1939		ArsA ATPase	2	6.3
CT1943	<i>csmC</i>	chlorosome envelope protein C	2	13.0
CT1955		magnesium-chelatase, bacteriochlorophyll c-specific subunit	2	2.0
CT2026		c-type cytochrome	2	13.5
CT2033	<i>atpA</i>	ATP synthase F0F1 subunit alpha	2	4.0
CT2144		outer surface protein, putative (LomR)	2	11.5
CT2186	<i>rplB</i>	50S ribosomal protein L2	2	7.5

Table F.1 continued.

Locus ID	Gene name	Description	# unique matched peptides	Protein Coverage (%)
CT2234	<i>atpD-2</i>	ATP synthase F0F1 subunit beta	2	5.2
CT2264	<i>surA</i>	peptidyl-prolyl cis-trans isomerase SurA	2	5.7
CT0018	<i>atpH</i>	ATP synthase F0F1 subunit delta	1	3.9
CT0020	<i>atpE</i>	ATP synthase F0 subunit C	1	12.3
CT0027		uncharacterized protein CT0027	1	14.5
CT0031	<i>ftsA</i>	cell division protein FtsA	1	1.8
CT0150	<i>nusG</i>	transcription antitermination protein NusG	1	4.2
CT0153	<i>rplJ</i>	50S ribosomal protein L10	1	6.4
CT0156	<i>rpoC</i>	DNA-directed RNA polymerase subunit beta'	1	0.8
CT0159	<i>efp</i>	elongation factor P	1	7.4
CT0173	<i>serB</i>	phosphoserine phosphatase	1	2.0
CT0249		glutathione S-transferase	1	4.3
CT0264	<i>rho</i>	transcription termination factor Rho	1	2.1
CT0288	<i>rpsA</i>	30S ribosomal protein S1	1	1.4
CT0302	<i>petC</i>	cytochrome b6-f complex, iron-sulfur subunit	1	10.5
CT0303	<i>petB</i>	cytochrome b-c complex, cytochrome b subunit	1	3.0
CT0312		DnaK suppressor protein	1	7.5
CT0350	<i>fabI</i>	enoyl-(acyl-carrier-protein) reductase	1	2.7
CT0531		sensor histidine kinase/response regulator	1	1.8
CT0563	<i>tyrS</i>	tyrosyl-tRNA synthetase	1	1.7
CT0607		uncharacterized protein CT0607 (YqeY)	1	13.2
CT0638		peptidoglycan-associated lipoprotein (PRK10802, Pal_lipo)	1	7.1
CT0642		uncharacterized protein CT0642 (C_GCAXxG_C_C)	1	6.0
CT0644		HSP20 family protein	1	5.3
CT0941	<i>btuR</i>	cob(I)alamin adenosyltransferase	1	7.5
CT0960	<i>purC</i>	phosphoribosylaminoimidazole-succinocarboxamide synthase	1	3.8
CT1007		uncharacterized protein CT1007 (DsrE/DsrF - like family)	1	4.4

Table F.1 continued.

Locus ID	Gene name	Description	# unique matched peptides	Protein Coverage (%)
CT1170		uncharacterized protein CT1170 (SRPBCC)	1	5.5
CT1225		N-acetylmuramoyl-L-alanine amidase	1	3.9
CT1239	<i>secA</i>	preprotein translocase subunit SecA	1	0.7
CT1362	<i>ctc</i>	50S ribosomal protein L25 general stress protein	1	5.0
CT1577	<i>frr</i>	ribosome recycling factor	1	7.0
CT1591	<i>ribBA</i>	3,4-dihydroxy-2-butanone 4-phosphate synthase	1	3.5
CT1744		uncharacterized protein CT1744 (FeoA)	1	10.8
CT1780	<i>tsf</i>	elongation factor Ts	1	5.6
CT1782	<i>rpsI</i>	30S ribosomal protein S9	1	7.8
CT1785		ATP-binding Mrp/Nbp35 family protein (ParA, minD_arch)	1	4.5
CT1833	<i>gatC</i>	aspartyl/glutamyl-tRNA amidotransferase subunit C	1	10.5
CT1867		uncharacterized protein CT1867 (SIMPL)	1	5.6
CT1921		cysteine synthase/cystathionine beta-synthase	1	2.0
CT1947	<i>ssb-1</i>	single-strand binding protein	1	4.3
CT1970		HSP20 family protein	1	9.9
CT1986		uncharacterized protein CT1986 (WD40)	1	2.4
CT2001	<i>bcp-2</i>	bacterioferritin comigratory protein, thiol peroxidase	1	7.4
CT2047		AcrB/AcrD/AcrF family protein	1	1.1
CT2049		LipD protein, putative (type_I_sec_TolC)	1	1.8
CT2054	<i>csmB</i>	chlorosome envelope protein B	1	14.7
CT2067		pentapeptide repeat-containing protein	1	2.7
CT2097		uncharacterized protein CT2097 (CxxC_CxxC_SSSS)	1	9.5
CT2101		uncharacterized protein CT2101 (DUF190)	1	7.3
CT2129	<i>rplT</i>	50S ribosomal protein L20	1	6.1
CT2147		uncharacterized protein CT2147	1	2.9
CT2151	<i>bchB</i>	light-independent protochlorophyllide reductase subunit B	1	3.0

Table F.1 continued.

Locus ID	Gene name	Description	# unique matched peptides	Protein Coverage (%)
CT2160	<i>gidB</i>	16S rRNA methyltransferase GidB	1	4.6
CT2161	<i>rplQ</i>	50S ribosomal protein L17	1	5.7
CT2177	<i>rplE</i>	50S ribosomal protein L5	1	4.4
CT2182	<i>rplP</i>	50S ribosomal protein L16	1	5.8
CT2215	<i>gatB</i>	aspartyl/glutamyl-tRNA amidotransferase subunit B	1	1.7
CT2216		uncharacterized protein CT2216	1	7.8

Appendix G

HOMOLOGS OF S⁰ PROTEINS FOUND IN PROTEOMIC STUDIES OF OUTER MEMBRANE VESICLES

Table G.1 provides a list of S⁰-detected proteins that were found to have homologs in the proteomes of gram-negative outer membrane vesicles (OMV); each OMV protein matched is listed. Table G.2 lists S⁰ proteins that were not found to have homologs in OMV proteomes, and whether there were no homologs for the S⁰ protein within any of the bacterial species from which the OMVs had been collected.

Notes for Tables G.1 and G.2:

^a Name of conserved domains in parentheses for uncharacterized proteins

^b Codes for literature references: 1, Altindis et al. 2014; 2, Bai et al. 2014; 3, Ballock et al. 2014; 4, Choi et al. 2011; 5, Couto et al. 2015; 6, Galka et al. 2008; 7, Jang et al. 2014; 8, Lappann et al. 2013; 9, Lee et al. 2007; 10, Post et al. 2005; 11, Whitworth et al. 2015. See Chapter 4 Reference list.

^c Codes for bacterial species and strains used in studies: CJ = *Campylobacter jejuni* NCTC11168; EC = *Escherichia coli* DH5 α ; LP = *Legionella pneumophila* Philadelphia-1 strain JR32; MX = *Myxococcus xanthus* DK1622; NMB = *Neisseria meningitidis* serogroup B strain NMB (NMB-ACE1); NMST = *Neisseria meningitidis* unencapsulated mutants of strains MC58 (ST-74) and 2120 (ST-11); PAO1 = *Pseudomonas aeruginosa* PAO1; PA14 = *Pseudomonas aeruginosa* UCBPP-PA14; PAC1 = *Pseudomonas aeruginosa* clinical isolate 1; PAC2 = *Pseudomonas aeruginosa* clinical isolate 2; SE = *Salmonella enterica* Serovar Typhimurium 14028S (ATCC 14028); VC = *Vibrio cholerae* El Tor biotype strain C6706.

^d P = BLASTP, standard protein blast; Δ = Delta-BLAST.

^e Percent identical amino acids in aligned segment (high scoring sequence pair).

^f Percent positive amino acids in aligned segment (high scoring sequence pair).

^g Y = Protein detected in S⁰ is the best match for the OMV homolog in *C. tepidum*; N = Protein detected in S⁰ is not the best match for the OMV homolog in *C. tepidum*. (rank / total matched proteins in *C. tepidum*)

Table G.1 List of S⁰ proteins where homologs were found in proteomic studies of outer membrane vesicles

<i>C. tepidum</i> S ⁰ protein information				OMV protein information				BLAST stats					
Locus ID	Accession	Gene name	Description ^a	In WT S ⁰ ?	In C3 S ⁰ ?	Reference ^b	Species ^c	Accession	Type ^d	E-value	% ID ^e	% +S ^f	Best <i>C. tep</i> match? ^g
CT0018	NP_660924	<i>atpH</i>	ATP synthase F0F1 subunit delta	Y	N	4	PAO1	NP_254244.1	P	2.E-17	32	53	Y (1/1)
CT0020	NP_660926	<i>atpE</i>	ATP synthase F0 subunit C	Y	N	3	PA14	NP_254246.1	P	3.E-03	42	58	Y (1/1)
CT0031	NP_660937	<i>ftsA</i>	cell division protein FtsA	Y	N	3	PA14	NP_253098.1	P	2.E-86	37	62	Y (1/3)
						4	PAO1	NP_253098.1	P	2.E-86	37	62	Y (1/3)
CT0068	NP_660974		hemagglutinin-related protein (LomR)	Y	N	6	LP	WP_010946469.1	Δ	1.E-08	28	42	Y (1/4)
						10	NMB	AAD53279.1	P	5.E-06	36	42	Y (1/2)
CT0089	NP_660995	<i>clpB-2</i>	ATP-dependent Clp protease, ATP-binding subunit ClpB	Y	Y	3	PA14, PAC2	NP_253232.1	P	1.E-150	51	71	N (3/4)
						4	PAO1	NP_253232.1	P	1.E-150	51	71	N (3/4)
						7	CJ	WP_002852743.1	P	3.E-73	39	62	N (3/3)
CT0150	NP_661056	<i>nusG</i>	transcription antitermination protein NusG	Y	N	3	PA14	NP_252965.1	P	4.E-42	39	61	Y (1/1)
						7	CJ	YP_002343907.1	P	2.E-32	35	58	Y (1/1)
CT0153	NP_661059	<i>rplJ</i>	50S ribosomal protein L10	Y	N	9	EC	NP_418412.1	P	2.E-16	27	53	Y (1/1)
						2	SE	NP_463020.1	P	2.E-15	26	53	Y (1/1)
						3	PA14, PAC2	NP_252962.1	Δ	3.E-15	26	54	Y (1/1)
						4	PAO1	NP_252962.1	Δ	3.E-15	26	54	Y (1/1)

Table G.1 continued.

<i>C. tepidum</i> S ⁰ protein information				OMV protein information				BLAST stats					
Locus ID	Accession	Gene name	Description ^a	In WT S ⁰ ?	In C3 S ⁰ ?	Reference ^b	Species ^c	Accession	Type ^d	E-value	% ID ^e	% +S ^f	Best <i>C. tep</i> match? ^g
CT0154	NP_661060	<i>rplL</i>	50S ribosomal protein L7/L12	Y	N	9	EC	NP_418413.1	P	7.E-33	56	74	Y (1/1)
CT0155	NP_661061	<i>rpoB</i>	DNA-directed RNA polymerase subunit beta	Y	N	3	PA14, PAC1, PAC2	NP_252960.1	P	0.E+00	45	60	Y (1/1)
						4	PAO1	NP_252960.1	P	0.E+00	45	60	Y (1/1)
						5	PAO1	NP_252960.1	P	0.E+00	45	60	Y (1/1)
						7	CJ	WP_010891860.1	P	0.E+00	41	56	Y (1/1)
						9	EC	NP_418414.1	P	0.E+00	46	60	Y (1/1)
CT0156	NP_661062	<i>rpoC</i>	DNA-directed RNA polymerase subunit beta'	Y	N	3	PA14, PAC1, PAC2	NP_252959.1	P	0.E+00	46	64	Y (1/1)
						4	PAO1	NP_252959.1	P	0.E+00	46	64	Y (1/1)
						5	PAO1	NP_252959.1	P	0.E+00	46	64	Y (1/1)
						7	CJ	WP_002858508.1	P	0.E+00	47	64	Y (1/1)
						9	EC	NP_418415.1	P	0.E+00	46	64	Y (1/1)
CT0159	NP_661065	<i>efp</i>	elongation factor P	Y	N	3	PA14	NP_251541.1	P	4.E-26	35	52	Y (1/1)
CT0160	NP_661066	<i>hupB</i>	DNA-binding protein HU-beta	Y	Y	2	SE	NP_459447.1	P	9.E-32	61	73	Y (1/2)
						3	PA14	NP_250495.1	P	7.E-29	57	69	Y (1/2)
						4	PAO1	NP_250495.1	P	7.E-29	57	69	Y (1/2)
						5	PAO1	NP_250495.1	P	7.E-29	57	69	Y (1/2)

Table G.1 Continued.

<i>C. tepidum</i> S ⁰ protein information				OMV protein information				BLAST stats					
Locus ID	Accession	Gene name	Description ^a	In WT S ⁰ ?	In C3 S ⁰ ?	Reference ^b	Species ^c	Accession	Type ^d	E-value	% ID ^e	% +S ^f	Best <i>C. tep</i> match? ^g
CT0173	NP_661079	<i>serB</i>	phosphoserine phosphatase	Y	N	5	PAO1	NP_253647.1	P	0.E+00	61	78	Y (1/1)
CT0240	NP_661144	<i>nusA</i>	transcription elongation factor NusA	N	Y	3	PA14	NP_253433.1	P	1.E-44	30	52	Y (1/1)
						4	PAO1	NP_253433.1	P	1.E-44	30	52	Y (1/1)
CT0254	NP_661158	<i>ompH</i>	outer membrane protein OmpH	Y	N	6	LP	WP_010946255.1	Δ	1.E-07	24	49	Y (1/1)
						1	VC	NP_231882.1	Δ	1.E-06	28	49	Y (1/1)
						9	EC	NP_414720.1	Δ	5.E-05	25	45	Y (1/1)
CT0264	NP_661168	<i>rho</i>	transcription termination factor Rho	Y	N	4	PAO1	NP_253926.1	P	0.E+00	59	80	Y (1/1)
CT0288	NP_661192	<i>rpsA</i>	30S ribosomal protein S1	Y	N	9	EC	NP_415431.1	P	7.E-142	42	63	Y (1/1)
						3	PA14, PAC2	NP_251852.1	P	2.E-139	39	61	Y (1/1)
						4	PAO1	NP_251852.1	P	2.E-139	39	61	Y (1/1)
CT0295	NP_661199		DNA-binding protein HU-alpha, putative	N	Y	2	SE	NP_463039.1	P	3.E-18	34	61	N (1/2)
CT0302	NP_661206	<i>petC</i>	cytochrome b6-f complex, iron-sulfur subunit	Y	Y	7	CJ	WP_002852880.1	P	2.E-12	36	55	Y (1/2)
CT0303	NP_661207	<i>petB</i>	cytochrome b-c complex, cytochrome b subunit	Y	N	7	CJ	WP_002852758.1	P	7.E-46	32	52	Y (1/1)
						3	PA14	NP_253120.1	P	3.E-42	29	50	Y (1/1)
						4	PAO1	NP_253120.1	P	3.E-42	29	50	Y (1/1)
CT0350	NP_661254	<i>fabI</i>	enoyl-(acyl-carrier-protein) reductase	Y	Y	7	CJ	YP_002344783.1	P	2.E-36	33	53	Y (1/1)
						2	SE	NP_460659.1	P	2.E-34	31	52	Y (1/2)

Table G.1 Continued.

<i>C. tepidum</i> S ⁰ protein information				OMV protein information				BLAST stats					
Locus ID	Accession	Gene name	Description ^a	In WT S ⁰ ?	In C3 S ⁰ ?	Reference ^b	Species ^c	Accession	Type ^d	E-value	% ID ^e	% +s ^f	Best <i>C. tep</i> match? ^g
CT0529	NP_661429	<i>groES</i>	co-chaperonin GroES	Y	N	3	PA14	NP_253076.1	P	5.E-30	52	73	Y (1/1)
CT0530	NP_661430	<i>groEL</i>	chaperonin GroEL	Y	Y	1	VC	NP_232292.1	P	0.E+00	65	80	Y (1/1)
						2	SE	NP_463194.1	P	0.E+00	66	80	Y (1/1)
						3	PA14, PAC1, PAC2	NP_253075.1	P	0.E+00	66	82	Y (1/1)
						4	PAO1	NP_253075.1	P	0.E+00	66	82	Y (1/1)
						5	PAO1	NP_253075.1	P	0.E+00	66	82	Y (1/1)
						6	LP	WP_010946425.1	P	0.E+00	64	80	Y (1/1)
						7	CJ	WP_002858047.1	P	0.E+00	67	81	Y (1/1)
						8	NMST	NP_274966.1	P	0.E+00	65	80	Y (1/1)
						9	EC	NP_418567.1	P	0.E+00	66	81	Y (1/1)
CT0531	NP_661431		sensor histidine kinase/response regulator	Y	N	4	PAO1	NP_254171.1	P	1.E-14	30	48	N (5/7)
						5	PAO1	NP_254048.1	P	9.E-11	24	45	Y (3/6)
						4	PAO1	NP_249619.1	P	4.E-08	27	49	N (7/7)
						4	PAO1	NP_253184.1	P	3.E-06	24	42	N (2/2)
						4	PAO1	NP_251961.1	P	2.E-05	26	44	N (4/4)
CT0547	NP_661447	<i>mreB</i>	rod shape-determining protein MreB	Y	N	7	CJ	WP_010891850.1	P	4.E-106	48	72	Y (1/4)
						6	LP	WP_010946547.1	P	5.E-100	46	67	Y (1/3)
						4	PAO1	NP_253171.1	P	1.E-98	46	68	Y (1/3)

Table G.1 Continued.

<i>C. tepidum</i> S ⁰ protein information				OMV protein information				BLAST stats					
Locus ID	Accession	Gene name	Description ^a	In WT S ⁰ ?	In C3 S ⁰ ?	Reference ^b	Species ^c	Accession	Type ^d	E-value	% ID ^e	% +s ^f	Best <i>C. tep</i> match? ^g
CT0638	NP_661535		peptidoglycan-associated lipoprotein (PRK10802, Pal_lipo)	Y	N	1	VC	NP_231469.1	P	7.E-38	58	73	Y (1/2)
						9	EC	NP_415269.1	P	8.E-33	50	70	Y (1/2)
						3	PA14, PAC2	NP_249664.1	P	7.E-31	38	55	Y (1/2)
						4	PAO1	NP_249664.1	P	7.E-31	38	55	Y (1/2)
						5	PAO1	NP_249664.1	P	7.E-31	38	55	Y (1/2)
						7	CJ	WP_002851617.1	P	8.E-21	33	53	Y (1/1)
						3	PA14, PAC1, PAC2	NP_250468.1	P	3.E-20	43	57	N (2/2)
						4	PAO1	NP_250468.1	P	3.E-20	43	57	N (2/2)
						5	PAO1	NP_250468.1	P	3.E-20	43	57	N (2/2)
						1	VC	NP_231844.1	P	1.E-10	31	47	N (2/2)
CT0643	NP_661540	<i>dnaK</i>	molecular chaperone DnaK	Y	Y	3	PA14, PAC2	NP_253449.1	P	0.E+00	59	76	Y (1/1)
						4	PAO1	NP_253449.1	P	0.E+00	59	76	Y (1/1)
						6	LP	YP_096041.1	P	0.E+00	61	76	Y (1/1)
						8	NMST	NP_273598.1	P	0.E+00	58	74	Y (1/1)

Table G.1 Continued.

<i>C. tepidum</i> S ⁰ protein information				OMV protein information				BLAST stats					
Locus ID	Accession	Gene name	Description ^a	In WT S ⁰ ?	In C3 S ⁰ ?	Reference ^b	Species ^c	Accession	Type ^d	E-value	% ID ^e	% +S ^f	Best <i>C. tep</i> match? ^g
CT0670	NP_661566		ABC transporter, periplasmic substrate-binding protein	N	Y	7	CJ	WP_002857286.1	Δ	8.E-14	28	46	Y (1/1)
						2	SE	NP_462944.1	P	1.E-08	27	40	Y (1/1)
						8	NMST	NP_274051.1	P	3.E-03	28	41	Y (1/1)
CT0722	NP_661617	<i>metK</i>	S-adenosylmethionine synthetase	N	Y	6	LP	WP_010947738.1	P	6.E-148	57	71	Y (1/1)
						7	CJ	WP_002852836.1	P	9.E-84	41	57	Y (1/1)
CT0829	NP_661723	<i>htpG</i>	heat shock protein 90	Y	Y	3	PA14, PAC2	NP_250287.1	P	1.E-159	40	62	Y (1/1)
						4	PAO1	NP_250287.1	P	1.E-159	40	62	Y (1/1)
CT0893	NP_661786		uncharacterized protein CT0893 (Porin_5)	Y	N	5	PAO1	NP_249387.1	P	4.E-14	36	58	Y (1/1)
CT0895	NP_661788		phosphate ABC transporter, periplasmic phosphate-binding protein, putative	N	Y	11	MX	WP_011554775.1	P	8.E-48	36	56	Y (1/2)
CT0960	NP_661853	<i>purC</i>	phosphoribosylaminoimidazole-succinocarboxamide synthase	Y	Y	3	PA14, PAC2	NP_249704.1	P	3.E-73	49	64	Y (1/1)
						4	PAO1	NP_249704.1	P	3.E-73	49	64	Y (1/1)
CT1021	NP_661913	<i>soxB</i>	sulfur oxidation protein SoxBN	Y	Y	1	VC	NP_231805.1	P	6.E-14	27	41	Y (1/1)
CT1023	NP_661915		thioredoxin family thiol:disulfide interchange protein	N	Y	8	NMST	NP_273072.1	P	1.E-12	34	47	N (2/5)
						8	NMST	NP_274952.1	P	5.E-11	25	50	N (4/5)

Table G.1 Continued.

<i>C. tepidum</i> S ⁰ protein information				OMV protein information				BLAST stats					
Locus ID	Accession	Gene name	Description ^a	In WT S ⁰ ?	In C3 S ⁰ ?	Reference ^b	Species ^c	Accession	Type ^d	E-value	% ID ^e	% +S ^f	Best <i>C. tep</i> match? ^g
CT1053	NP_661944	<i>fbaA</i>	fructose-bisphosphate aldolase	N	Y	3	PA14, PAC2	NP_249246.1	P	2.E-86	43	61	Y (1/1)
CT1054	NP_661945	<i>prc</i>	carboxyl-terminal protease	Y	Y	5	PAO1	NP_251947.1	P	1.E-166	43	60	Y (1/3)
						9	EC	NP_416344.1	P	2.E-143	40	60	Y (1/3)
						8	NMST	NP_274351.1	P	4.E-29	29	47	N (3/3)
						10	NMB	AAF41707	P	4.E-29	29	47	N (3/3)
						3	PA14, PAC2	NP_253821.1	P	6.E-27	26	48	N (3/3)
						4	PAO1	NP_253821.1	P	6.E-27	26	48	N (3/3)
CT1170	NP_662061		uncharacterized protein CT1170 (SRPBCC)	Y	N	3	PAC2	NP_250270.1	P	6.E-30	31	53	Y (1/2)
CT1225	NP_662115		N-acetylmuramoyl-L-alanine amidase	Y	N	3	PA14	NP_249498.1	P	4.E-03	29	51	Y (1/2)
						4	PAO1	NP_249498.1	P	4.E-03	29	51	Y (1/2)
						5	PAO1	NP_249498.1	P	4.E-03	29	51	Y (1/2)
CT1239	NP_662127	<i>secA</i>	preprotein translocase subunit SecA	Y	Y	3	PA14, PAC2	NP_253093.1	P	0.E+00	41	56	Y (1/2)
						4	PAO1	NP_253093.1	P	0.E+00	41	56	Y (1/2)
						5	PAO1	NP_253093.1	P	0.E+00	41	56	Y (1/2)
						7	CJ	WP_002858134.1	P	3.E-175	48	66	Y (1/2)
CT1327	NP_662214		rubrerythrin	N	Y	7	CJ	WP_002853081.1	P	3.E-25	42	53	Y (1/1)

Table G.1 Continued.

<i>C. tepidum</i> S ⁰ protein information				OMV protein information				BLAST stats					
Locus ID	Accession	Gene name	Description ^a	In WT S ⁰ ?	In C3 S ⁰ ?	Reference ^b	Species ^c	Accession	Type ^d	E-value	% ID ^e	% +s ^f	Best <i>C. tep</i> match? ^g
CT1353	NP_662240		OmpA family protein (type_VI_ompA, OmpA_C-like)	Y	Y	3	PA14, NP_250468.1	PAC1, PAC2	P	7.E-27	47	64	Y (1/2)
						4	PAO1 NP_250468.1		P	7.E-27	47	64	Y (1/2)
						5	PAO1 NP_250468.1		P	7.E-27	47	64	Y (1/2)
						3	PA14, NP_252382.1	PAC2	P	1.E-25	42	61	Y (1/2)
						4	PAO1 NP_252382.1		P	1.E-25	42	61	Y (1/2)
						5	PAO1 NP_252382.1		P	1.E-25	42	61	Y (1/2)
						1	VC NP_231844.1		P	3.E-24	47	65	Y (1/2)
						3	PA14, NP_249810.1	PAC2	P	8.E-24	43	58	Y (1/2)
						5	PAO1 NP_249810.1		P	8.E-24	43	58	Y (1/2)
						4	PAO1 NP_251590.1		P	4.E-15	33	50	Y (1/2)
						5	PAO1 NP_251590.1		P	4.E-15	33	50	Y (1/2)
						3	PA14, NP_249664.1	PAC2	P	8.E-15	40	53	N (2/2)
						4	PAO1 NP_249664.1		P	8.E-15	40	53	N (2/2)
						5	PAO1 NP_249664.1		P	8.E-15	40	53	N (2/2)
						1	VC NP_231469.1		P	1.E-14	36	53	N (2/2)
						9	EC NP_415477.1		P	2.E-12	33	55	Y (1/2)
						2	SE NP_460044.1		P	4.E-11	31	53	Y (1/2)

Table G.1 Continued.

<i>C. tepidum</i> S ⁰ protein information				OMV protein information				BLAST stats					
Locus ID	Accession	Gene name	Description ^a	In WT S ⁰ ?	In C3 S ⁰ ?	Reference ^b	Species ^c	Accession	Type ^d	E-value	% ID ^e	% +S ^f	Best <i>C. tep</i> match? ^g
CT1361	NP_662248	<i>prsA</i>	ribose-phosphate pyrophosphokinase	Y	N	7	CJ	WP_002853293.1	P	2.E-118	57	73	Y (1/1)
						3	PA14, PAC2	NP_253359.1	P	7.E-113	53	73	Y (1/1)
						4	PAO1	NP_253359.1	P	7.E-113	53	73	Y (1/1)
						9	EC	NP_415725.1	P	4.E-110	52	73	Y (1/1)
CT1362	NP_662249	<i>ctc</i>	50S ribosomal protein L25 general stress protein	Y	N	3	PA14	NP_253360.1	P	1.E-18	32	53	Y (1/1)
CT1447	NP_662333		serine protease (degP_htrA_DO)	Y	Y	4	PAO1	NP_253360.1	P	1.E-18	32	53	Y (1/1)
						4	PAO1	NP_249457.1	P	2.E-104	41	58	Y (1/1)
						5	PAO1	NP_249457.1	P	2.E-104	41	58	Y (1/1)
						9	EC	NP_417701.1	P	1.E-91	38	55	Y (1/2)
						7	CJ	WP_002853235.1	P	2.E-89	38	56	Y (1/1)
						9	EC	NP_414703.1	P	8.E-89	38	56	Y (1/2)
CT1485	NP_662370	<i>grpE</i>	heat shock protein GrpE	Y	N	1	VC	NP_230217.1	P	4.E-86	41	59	Y (1/1)
						3	PA14	NP_253450.1	Δ	2.E-15	26	52	Y (1/1)
						2	SE	NP_461308.1	P	5.E-99	50	67	Y (1/1)
						3	PA14	NP_251802.1	P	7.E-95	51	64	Y (1/1)
CT1555	NP_662438	<i>accD</i>	acetyl-CoA carboxylase, carboxyl transferase subunit beta		Y	4	PAO1	NP_251802.1	P	7.E-95	51	64	Y (1/1)
CT1577	NP_662460	<i>frr</i>	ribosome recycling factor	Y	Y	3	PA14	NP_252343.1	P	2.E-49	43	64	Y (1/1)
CT1591	NP_662474	<i>ribBA</i>	3,4-dihydroxy-2-butanone 4-phosphate synthase	Y	N	7	CJ	WP_002852104.1	P	3.E-70	38	59	Y (1/1)

Table G.1 Continued.

<i>C. tepidum</i> S ⁰ protein information				OMV protein information				BLAST stats					
Locus ID	Accession	Gene name	Description ^a	In WT S ⁰ ?	In C3 S ⁰ ?	Reference ^b	Species ^c	Accession	Type ^d	E-value	% ID ^e	% +S ^f	Best <i>C. tep</i> match? ^g
CT1649	NP_662532	<i>pnp</i>	polynucleotide phosphorylase/polyadenylase	Y	Y	2	SE	NP_462195.1	P	0.E+00	49	65	Y (1/3)
						3	PA14	NP_253428.1	P	0.E+00	48	67	Y (1/2)
						4	PAO1	NP_253428.1	P	0.E+00	48	67	Y (1/2)
						6	LP	WP_010948458.1	P	0.E+00	48	65	Y (1/2)
						7	CJ	WP_002853182.1	P	1.E-170	41	59	Y (1/2)
CT1780	NP_662659	<i>tsf</i>	elongation factor Ts	Y	Y	3	PA14	NP_252345.1	P	3.E-54	39	58	Y (1/1)
						2	SE	NP_459222.1	P	3.E-49	38	58	Y (1/1)
						7	CJ	WP_002864836.1	P	2.E-44	30	49	Y (1/1)
CT1781	NP_662660	<i>rpsB</i>	30S ribosomal protein S2	Y	N	9	EC	NP_414711.1	P	2.E-87	55	71	Y (1/1)
						2	SE	NP_459221.1	P	5.E-87	55	71	Y (1/1)
						3	PA14, PAC2	NP_252346.1	P	6.E-87	53	71	Y (1/1)
						4	PAO1	NP_252346.1	P	6.E-87	53	71	Y (1/1)
						7	CJ	WP_002892710.1	P	5.E-86	54	70	Y (1/1)
CT1782	NP_662661	<i>rpsI</i>	30S ribosomal protein S9	Y	N	9	EC	NP_417697.1	P	3.E-34	52	69	Y (1/1)
						2	SE	NP_462254.1	P	4.E-34	52	68	Y (1/1)
						1	VC	NP_230222.1	P	1.E-31	51	66	Y (1/1)
						3	PA14, PAC2	NP_253122.1	P	1.E-31	49	68	Y (1/1)
						4	PAO1	NP_253122.1	P	1.E-31	49	68	Y (1/1)

Table G.1 Continued.

<i>C. tepidum</i> S ⁰ protein information				OMV protein information				BLAST stats					
Locus ID	Accession	Gene name	Description ^a	In WT S ⁰ ?	In C3 S ⁰ ?	Reference ^b	Species ^c	Accession	Type ^d	E-value	% ID ^e	% +S ^f	Best <i>C. tep</i> match? ^g
CT1785	NP_662664		ATP-binding Mrp/Nbp35 family protein (ParA, minD_arch)	Y	N	7	CJ	YP_002344975.1	P	6.E-79	38	57	Y (1/7)
						4	PAO1	NP_251934.1	P	3.E-04	22	43	N (2/3)
						6	LP	WP_010947451.1	Δ	3.E-04	25	41	N (5/12)
CT1833	NP_662712	<i>gatC</i>	aspartyl/glutamyl-tRNA amidotransferase subunit C	Y	N	7	CJ	WP_002858734.1	Δ	6.E-07	32	52	Y (1/1)
CT1921	NP_662798		cysteine synthase/cystathionine beta-synthase	Y	N	8	NMST	NP_273805.1	P	4.E-46	34	55	N (2/2)
						3	PA14	NP_251399.1	P	7.E-44	35	55	N (2/2)
CT1947	NP_662824	<i>ssb-I</i>	single-strand binding protein	Y	N	11	MX	WP_011551191.1	P	1.E-47	48	59	Y (1/2)
						3	PA14	NP_252922.1	P	2.E-43	46	61	Y (1/1)
CT1970	NP_662846		HSP20 family protein	Y	Y	4	PAO1	NP_251816.1	Δ	3.E-05	23	51	Y (1/1)
CT2001	NP_662877	<i>bcp-2</i>	bacterioferritin comigratory protein, thiol peroxidase	Y	N	8	NMST	NP_274952.1	P	1.E-11	26	52	N (3/5)
						3	PA14	NP_251222.1	P	1.E-09	33	48	N (2/3)
CT2032	NP_662907	<i>atpG</i>	ATP synthase F0F1 subunit gamma	N	Y	3	PA14	NP_254242.1	P	3.E-56	37	59	Y (1/1)
						4	PAO1	NP_254242.1	P	3.E-56	37	59	Y (1/1)
CT2033	NP_662908	<i>atpA</i>	ATP synthase F0F1 subunit alpha	Y	N	3	PA14, PAC2	NP_254243.1	P	0.E+00	55	74	Y (1/3)
						4	PAO1	NP_254243.1	P	0.E+00	55	74	Y (1/3)
						6	LP	WP_010948668.1	P	0.E+00	58	75	Y (1/3)
						7	CJ	WP_002851836.1	P	0.E+00	61	79	Y (1/3)
						8	NMST	NP_274930.1	P	0.E+00	58	74	Y (1/3)

Table G.1 Continued.

<i>C. tepidum</i> S ⁰ protein information				OMV protein information				BLAST stats					
Locus ID	Accession	Gene name	Description ^a	In WT S ⁰ ?	In C3 S ⁰ ?	Reference ^b	Species ^c	Accession	Type ^d	E-value	% ID ^e	% +S ^f	Best <i>C. tep</i> match? ^g
CT2047	NP_662922		AcrB/AcrD/AcrF family protein	Y	N	4	PAO1	NP_252509.1	Δ	1.E-05	22	48	Y (1/2)
CT2049	NP_662924		LipD protein, putative (type_I_sec_TolC)	Y	N	5	PAO1	WP_003089909.1	Δ	1.E-07	21	41	N (4/6)
						1	VC	NP_232066.1	Δ	6.E-07	19	38	Y (5/7)
						9	EC	NP_417507.2	Δ	2.E-06	21	38	N (4/7)
CT2129	NP_663003	<i>rplT</i>	50S ribosomal protein L20	Y	N	3	PA14,	NP_251431.1	P	3.E-41	58	73	Y (1/1)
							PAC2						
						4	PAO1	NP_251431.1	P	3.E-41	58	73	Y (1/1)
						2	SE	NP_460302.1	P	6.E-41	57	73	Y (1/3)
						9	EC	NP_416231.1	P	6.E-41	57	73	Y (1/2)
CT2144	NP_663018		outer surface protein, putative (LomR)	Y	Y	2	SE	NP_459304.1	P	9.E-10	29	42	Y (1/3)
						6	LP	WP_010946469.1	Δ	2.E-07	29	45	Y (2/4)
CT2161	NP_663035	<i>rplQ</i>	50S ribosomal protein L17	Y	N	2	SE	NP_462318.1	Δ	2.E-25	48	62	Y (1/1)
						9	EC	NP_417753.1	Δ	3.E-25	48	62	Y (1/1)
						3	PA14,	NP_252927.1	Δ	2.E-23	47	61	Y (1/1)
							PAC2						
						4	PAO1	NP_252927.1	Δ	2.E-23	47	61	Y (1/1)
CT2162	NP_663036	<i>rpoA</i>	DNA-directed RNA polymerase subunit alpha	Y	N	2	SE	NP_462319.1	P	3.E-72	38	60	Y (1/1)
						3	PA14,	NP_252928.1	P	7.E-71	39	59	Y (1/1)
							PAC2						
						4	PAO1	NP_252928.1	P	7.E-71	39	59	Y (1/1)
						7	CJ	YP_002344964.1	P	2.E-54	36	54	Y (1/1)

Table G.1 Continued.

<i>C. tepidum</i> S ⁰ protein information				OMV protein information				BLAST stats						
Locus		Gene	Description ^a	In WT S ⁰ ?		Reference ^b	Species ^c	Accession	Type ^d	E-value	ID ^e		+s ^f	Best <i>C. tep</i> match? ^g
ID	Accession	name		Y	N						%	%		
CT2175	NP_663049	<i>rpsH</i>	30S ribosomal protein S8	N	Y	2	SE	NP_462330.1	P	2.E-29	38	67	Y (1/1)	
CT2177	NP_663051	<i>rplE</i>	50S ribosomal protein L5	Y	N	9	EC	NP_417767.1	P	2.E-77	58	78	Y (1/1)	
						2	SE	NP_462332.1	P	6.E-77	58	78	Y (1/1)	
						1	VC	NP_232212.1	P	2.E-75	55	78	Y (1/1)	
						3	PA14, PAC2	NP_252941.1	P	1.E-67	51	75	Y (1/1)	
						4	PAO1	NP_252941.1	P	1.E-67	51	75	Y (1/1)	
						7	CJ	YP_002345061.1	P	8.E-62	46	74	Y (1/1)	
CT2182	NP_663056	<i>rplP</i>	50S ribosomal protein L16	Y	N	9	EC	NP_417772.1	P	5.E-57	61	80	Y (1/1)	
						2	SE	NP_462337.1	P	3.E-55	60	78	Y (1/1)	
						3	PA14, PAC2	NP_252946.1	P	7.E-53	56	74	Y (1/1)	
CT2186	NP_663060	<i>rplB</i>	50S ribosomal protein L2	Y	N	9	EC	NP_417776.1	P	8.E-105	58	72	Y (1/1)	
						2	SE	NP_462341.1	P	8.E-105	57	72	Y (1/1)	
						3	PA14	NP_252950.1	P	3.E-104	58	72	Y (1/1)	
						4	PAO1	NP_252950.1	P	3.E-104	58	72	Y (1/1)	
						1	VC	NP_232221.1	P	4.E-100	57	70	Y (1/1)	
						7	CJ	YP_002345070.1	P	7.E-97	57	70	Y (1/1)	
CT2190	NP_663064	<i>rpsJ</i>	30S ribosomal protein S10	N	Y	2	SE	NP_462345.1	P	4.E-35	49	77	Y (1/1)	
						3	PA14	NP_252954.1	P	1.E-33	48	77	Y (1/1)	

Table G.1 Continued.

<i>C. tepidum</i> S ⁰ protein information				OMV protein information				BLAST stats					
Locus ID	Accession	Gene name	Description ^a	In WT S ⁰ ?	In C3 S ⁰ ?	Reference ^b	Species ^c	Accession	Type ^d	E-value	% ID ^e	% +S ^f	Best <i>C. tep</i> match? ^g
CT2191	NP_663065	<i>tuf</i>	elongation factor Tu	Y	Y	1	VC	NP_229975.1	P	0.E+00	72	85	Y (1/5)
						3	PA14, PAC2	NP_252955.1	P	0.E+00	69	80	Y (1/6)
						4	PAO1	NP_252955.1	P	0.E+00	69	80	Y (1/6)
						5	PAO1	NP_252955.1	P	0.E+00	69	80	Y (1/6)
						7	CJ	WP_002855271.1	P	0.E+00	69	83	Y (1/6)
						9	EC	NP_418407.1	P	0.E+00	74	86	Y (1/6)
						10	NMB	AAF40583	P	0.E+00	70	83	Y (1/6)
CT2215	NP_663089	<i>gatB</i>	aspartyl/glutamyl-tRNA amidotransferase subunit B	Y	N	7	CJ	WP_002858123.1	P	5.E-169	50	68	Y (1/1)
CT2233	NP_663107		thiol:disulfide interchange protein, thioredoxin family protein	N	Y	8	NMST	NP_274376.1	P	2.E-168	49	67	Y (1/1)
						8	NMST	NP_273072.1	P	6.E-13	31	43	Y (1/5)
						8	NMST	NP_274952.1	P	8.E-13	29	52	N (2/5)
CT2234	NP_663108	<i>atpD-2</i>	ATP synthase F0F1 subunit beta	Y	N	7	CJ	WP_002852711.1	P	1.E-04	30	51	Y (1/3)
						3	PA14, PAC2	NP_254241.1	P	0.E+00	68	82	Y (1/3)
						4	PAO1	NP_254241.1	P	0.E+00	68	82	Y (1/3)
						6	LP	WP_010948666.1	P	0.E+00	70	83	Y (1/3)
						7	CJ	WP_002852005.1	P	0.E+00	70	84	Y (1/1)
						8	NMST	NP_274928.1	P	0.E+00	69	82	Y (1/3)

Table G.1 Continued.

<i>C. tepidum</i> S ⁰ protein information				OMV protein information				BLAST stats					
Locus ID	Accession	Gene name	Description ^a	In WT S ⁰ ?	In C3 S ⁰ ?	Reference ^b	Species ^c	Accession	Type ^d	E-value	% ID ^e	% +s ^f	Best <i>C. tep</i> match? ^g
CT2264	NP_663137	<i>surA</i>	peptidyl-prolyl cis-trans isomerase SurA	Y	N	9	EC	NP_414595.1	P	5.E-31	28	45	Y (1/4)
						3	PA14, PAC2	NP_249285.1	P	1.E-21	25	47	Y (1/2)
						4	PAO1	NP_249285.1	P	1.E-21	25	47	Y (1/2)
						1	VC	NP_230099.1	P	1.E-19	25	43	Y (1/4)
CT2281	NP_663152	<i>clpB-1</i>	ATP-dependent Clp protease, ATP-binding subunit ClpB	Y	Y	3	PA14, PAC2	NP_253232.1	P	4.E-166	57	75	N (2/4)
						4	PAO1	NP_253232.1	P	4.E-166	57	75	N (2/4)
						7	CJ	WP_002852743.1	P	5.E-78	47	66	N (2/3)

Table G.2 List of S⁰ proteins with no homologs in OMV proteomes.

Locus ID	Accession	Gene name	Description ^a	In WT S ⁰ ?	In C3 S ⁰ ?	No homolog in OMV bacteria = X
CT0027	NP_660933		uncharacterized protein CT0027	Y	N	X
CT0058	NP_660964		Hit family protein (PKCI_related)	N	Y	
CT0131	NP_661037		uncharacterized protein CT0131 (SDR_a8, yfcH)	Y	N	
CT0163	NP_661069		alpha oxoglutarate ferredoxin oxidoreductase, alpha subunit	N	Y	
CT0249	NP_661153		glutathione S-transferase	Y	N	
CT0291	NP_661195		uncharacterized protein CT0291	N	Y	X
CT0293	NP_661197	<i>apt</i>	adenine phosphoribosyltransferase	N	Y	
CT0312	NP_661216		DnaK suppressor protein	Y	Y	
CT0331	NP_661235	<i>pdxJ</i>	pyridoxine 5'-phosphate synthase	N	Y	
CT0563	NP_661463	<i>tyrS</i>	tyrosyl-tRNA synthetase	Y	N	
CT0607	NP_661507		uncharacterized protein CT0607 (YqeY)	Y	N	
CT0642	NP_661539		uncharacterized protein CT0642 (C_GCAxxG_C_C)	Y	N	X
CT0644	NP_661541		HSP20 family protein	Y	Y	
CT0760	NP_661655		Hit family protein (FHIT)	N	Y	
CT0785	NP_661680	<i>trx-1</i>	thioredoxin	N	Y	
CT0841	NP_661735	<i>trx-2</i>	thioredoxin	Y	Y	
CT0853	NP_661747	<i>dsrB-1</i>	sulfite reductase, dissimilatory-type, beta subunit	N	Y	
CT0857	NP_661751	<i>dsrH</i>	DsrH protein	N	Y	
CT0864	NP_661758	<i>aspB</i>	adenylylsulfate reductase, beta subunit	N	Y	
CT0903	NP_661796		transcriptional regulator (PhoU)	Y	N	
CT0941	NP_661834	<i>btuR</i>	cob(I)alamin adenosyltransferase	Y	N	
CT0980	NP_661873		ArsA ATPase	Y	N	

Table G.2 continued.

Locus ID	Accession	Gene name	Description ^a	In WT S ⁰ ?	In C3 S ⁰ ?	No homolog in OMV bacteria = X
CT0985	NP_661878		P-II family protein	N	Y	
CT1007	NP_661900		uncharacterized protein CT1007 (DsrE)	Y	N	X
CT1017	NP_661909	<i>soxY</i>	sulfur oxidation protein SoxY	N	Y	X
CT1018	NP_661910	<i>soxZ</i>	sulfur oxidation protein SoxZ	N	Y	X
CT1019	NP_661911	<i>soxA</i>	sulfur oxidation protein SoxA	N	Y	X
CT1133	NP_662024		uncharacterized protein CT1133 (Cas8c_I-C)	Y	Y	
CT1213	NP_662103		uncharacterized protein CT1213 (RmlK)	N	Y	
CT1215	NP_662105		thioredoxin	N	Y	
CT1297	NP_662185	<i>bchI</i>	magnesium-chelatase subunit I	Y	N	
CT1305	NP_662193		uncharacterized protein CT1305	N	Y	X
CT1309	NP_662197		uncharacterized protein CT1309 (Metal_resist)	Y	N	X
CT1320.1	AAY51681		uncharacterized protein CT1320.1	N	Y	X
CT1499	NP_662384	<i>fmoA</i>	bacteriochlorophyll A protein	Y	Y	X
CT1634	NP_662517		uncharacterized protein CT1634 (RaiA)	N	Y	
CT1742	NP_662622	<i>feoB-1</i>	ferrous iron transport protein B	Y	N	
CT1743	NP_662623	<i>feoA-1</i>	ferrous iron transport protein A	Y	Y	
CT1744	NP_662624		uncharacterized protein CT1744 (FeoA)	Y	N	X
CT1745	NP_662625		uncharacterized protein CT1745 (Phenol_MetA_deg)	Y	N	X
CT1804	NP_662683		uncharacterized protein CT1804	Y	Y	X
CT1867	NP_662744		uncharacterized protein CT1867 (SIMPL)	Y	N	
CT1888	NP_662765		SpoU rRNA methylase family protein	N	Y	
CT1897	NP_662774		uncharacterized protein CT1897 (MscS, MS_channel)	N	Y	
CT1898	NP_662775		protoporphyrinogen oxidase, putative	N	Y	
CT1939	NP_662816		ArsA ATPase	Y	N	
CT1942	NP_662819	<i>csmA</i>	chlorosome envelope protein A	Y	Y	X
CT1943	NP_662820	<i>csmC</i>	chlorosome envelope protein C	Y	Y	X

Table G.2 continued.

Locus ID	Accession	Gene name	Description ^a	In WT S ⁰ ?	In C3 S ⁰ ?	No homolog in OMV bacteria = X
CT1955	NP_662832		magnesium-chelatase, bacteriochlorophyll c-specific subunit	Y	Y	
CT1986	NP_662862		uncharacterized protein CT1986 (WD40)	Y	N	
CT2026	NP_662901		c-type cytochrome	Y	N	X
CT2054	NP_662929	<i>csmB</i>	chlorosome envelope protein B	Y	Y	X
CT2067	NP_662942		pentapeptide repeat-containing protein	Y	N	
CT2097	NP_662971		uncharacterized protein CT2097 (CxxC_CxxC_SSSS)	Y	N	
CT2101	NP_662975		uncharacterized protein CT2101 (DUF190)	Y	N	X
CT2131	NP_663005		uncharacterized protein CT2131	N	Y	X
CT2147	NP_663021		uncharacterized protein CT2147	Y	N	X
CT2151	NP_663025	<i>bchB</i>	light-independent protochlorophyllide reductase subunit B	Y	N	X
CT2160	NP_663034	<i>gidB</i>	16S rRNA methyltransferase GidB	Y	N	
CT2216	NP_663090		uncharacterized protein CT2216 (SYLF)	Y	Y	
CT2250	NP_663123	<i>dsrC-2</i>	sulfite reductase, dissimilatory-type, gamma subunit	N	Y	